THE GEOLOGY AND GEOCHEMISTRY OF THE MOUNT ELLIOTT COPPER-GOLD DEPOSIT, NORTHWEST QUEENSLAND

Samuel J M Garrett

A thesis submitted in partial fulfilment
of the the requirements for the degree of
Masters of Economic Geology

CODES

UNIVERSITY OF TASMANIA

DECEMBER 1992

ABSTRACT

A new resource of approximately two million tonnes at 4.2% Cu equivalent has been discovered beneath old workings of the Mount Elliott mine in northwest Queensland. Potentially economic copper and gold mineralisation occurs as massive chalcopyrite with pyrite and pyrrhotite hosted in breccia matrix and shallow-dipping calc-silicate+calcite veins which cross-cut the local stratigraphy. The en-echelon series of mineralised veins are constrained between two northwest-trending, steeply-dipping reverse faults.

The deposit occurs within a unit of brecciated and pervasively skarn-altered shales ("Elliott Beds") near to the top of the Kuridala Formation. Bleaching of the shales followed by Ca-F metasomatism and albite-hematite (red-rock) alteration formed an early ground-preparation event that enhanced brittle fracturing and brecciation of the shale. The advancing red-rock alteration is geochemically characterised by increasing Na_2O and Al_2O_3 contents and decreasing SiO_2 content (quartz dissolution). Brecciation was accompanied by pervasive, prograde skarn alteration consisting of coarse-grained diopside-hedenbergite, scapolite, sphene, apatite and calcite. Wholerock geochemical analysis of calc-silicate altered rocks reveals severe depletions in SiO_2, Na_2O and Al_2O_3 contents accompanied by markedly increased Fe_2O_3 content. Magnetite plus chalcopyrite, pyrrhotite and pyrite replaces the calc-silicate assemblage preferentially along the contact of calcite and clinopyroxene grains. Late, anhydrous retrograde alteration of the skarn comprises minor chlorite and epidote. Fracturing is the primary control on localisation of alteration in which hydrothermal fluids repeatedly utilised the same pathways during progressive stages of alteration.

The prograde skarn assemblage formed from a hot (450-650°C) saline (>10 wt % NaCl), weakly acidic and relatively oxidised magmatic fluid that was rich in CO_2 and depleted in total sulphur. At depth the granitic fluid homogenously mixed with a downward-convecting, low temperature, reduced and sulphur-rich fluid that had leached metals and sulphur from biogenic sulphides ($\delta^{34}S \approx -12‰$) in the black shale. The resulting hot (250-

350°C) sulphur and metal-rich hydrothermal fluid transported iron, copper and gold in solution as chloride complexes and, upon interaction with the calc-silicate+calcite gangue, precipitated sulphides ($\delta^{34}S$ = -5.7 to -3.6‰) in response to decreasing fO_2 and increasing pH conditions.

The unique style of high-grade massive copper-gold mineralisation and its genetic association with granite-derived fluids and localised thrusting suggests that repetitions of this deposit style elsewhere in the region are not unlikely.

ACKNOWLEDGEMENTS

The submission of this work completes the Masters of Economic Geology course which was sponsored by Cyprus Gold Australia Corporation. Senior geologists Dave Timms, Chris Torrey, Greg Kary, Bob Blakestad and Chris Dredge are gratefully acknowledged for their encouragement and support.

Many hours were spent discussing and arguing the geology of Mount Elliott with Gordon Maclean (geologist).

Technical assistance was received from Simon Stevens and Naomi (slide preparation), W. Jablonsky (CSL, microprobe), John Smith (CSL, sulphurisotope laboratory).

Although unable to visit the project area, my supervisor, Dr. Garry Davidson, gave great support with many suggestions and ideas and proof-reading this work. Many people have looked over core and outcrop and entertained ideas and suggestions as to the geology and genesis of Mount Elliott. I thank them all.

Finally, I wish to thank my mother, Barbara Garrett , for her tireless efforts in typing and compiling this report.

CONTENTS

LIST OF FIGURES

LIST OF PLATES

LIST OF TABLES

Chapter 1

INTRODUCTION

1.1 Background

The Mount Elliott copper-gold mineralisation and associated calc-silicate alteration is confined to a steeply-dipping breccia pipe within a unit of multiply deformed graphitic shales of the Kuridala Formation, locally termed the "Elliott Beds." Ore grade chalcopyrite-gold mineralisation is hosted in a series of shallowly-dipping, anastomosing calc-silicate+calcite veins which cross-cut the local geology. Discovered in the late 1890's, Mount Elliott quickly became the major copper producer in the Cloncurry region with both open cut and underground mining operations. Subsequent attempts to discover further ore lenses in the vicinity of the old workings were unsuccessful primarily due to inappropriate drill-hole spacings.

Previous studies of the geology of Mount Elliott have been severely hampered by the lack of outcrop in the immediate mine vicinity, incomplete and inaccurate mine records and descriptions, scarce drill core data, and the overall complexity of geology, alteration and mineralisation relationships associated with the deposit. The concept of structurally-controlled skarn alteration and mineralisation associated with a gabbroic/mafic/amphibolite intrusive is a consistent theme throughout all reports.

The deposit has strategic importance to the nearby Selwyn Cu-Au mine (a joint venture between Cyprus Gold Australia, Elders Resources and ARIMCO) which, facing declining ore reserves, will look to Mount Elliott to increase the productive mine life of the Selwyn operation. The unique style of high grade Cu-Au mineralisation at Mount Elliott will ensure its regional significance, particularly as its genetic association with granite-derived metasomatic fluids and localised thrusting suggest that repetitions of the deposit style elsewhere in the region are likely. The deposit style has international importance in that being a brecciated, skarn-hosted vein deposit, it does not conform to the general

classification of non-porphyry-associated Cu skarn, but rather, shares features characteristic to each of calcic Cu skarns, Fe skarns and gold skarns.

1.2 Aims of the Investigation

Recent drilling by Cyprus Gold beneath the old workings at Mount Elliott has significantly improved the geological data-base of the deposit to the extent that the three-dimensional extent and morphology of the ore is well defined and the surrounding alteration is successfully sub-divided into several mappable and paragenetically distinct units. Previously, all calc-silicate alteration was included within the term "DMS" (diopside-magnetite-scapolite) of Dimo (1975) and the newly discovered orebody represents a style of mineralisation not previously discussed. The primary aim of this thesis is to document the geology, alteration and mineralisation styles that characterise the Mount Elliott Cu-Au deposit. Significant emphasis is given to determining paragenetic and zoning relationships both within and between the alteration and mineralisation with a view to placing the deposit within a regional framework.

A preliminary study of the geochemistry of alteration types and mineralisation styles is presented in an attempt to understand the various chemical changes imposed on the rocks as a result of the evolving metasomatic processes. The conditions of alteration and mineralisation were assessed using sulphur isotopes determined from a broad range of mineralisation styles within the deposit, together with physical observations and comparison with studies of other similar deposit types. Understanding the physiochemical parameters (i.e., temperature, salinity, acidity, fO_2, etc.) of the hydrothermal fluid, its chemistry and the processes controlling the solution, transport and precipitation of components from the fluid is fundamental to formulating a general genetic model for the mineralisation at Mount Elliott based upon the documented features.

Features of the geology and geochemistry of the deposit considered relevant to assisting in the exploration of further deposits of similar type are presented in conclusion.

1.3 Location

The Mount Elliott Mine and prospect (ML 2454, ML 2736) is located approximately sixteen kilometres north of the Selwyn (formerly Starra) copper-gold mine in northwest Queensland. The original mine was operated from the nearby town of Selwyn with smelted ore railed north to Cloncurry (Figure 1.1).

Mount Elliott is approximately 375m. above sea level located in the central part of the Selwyn Ranges, an elongate dissected peneplain which forms a major west northwest-trending continental divide. The mine is situated on the drainage divide.

1.4 Scope of the Thesis

This work is based predominantly on the investigation of some fifty drill-holes located within the immediate mine vicinity with minor contributions from petrographic and electron microprobe investigations. A preliminary study of major and trace element geochemistry of alteration and mineralisation includes twenty-five wholerock samples of various alteration styles and lithologies, plus one wholerock sample each of pyrite, pyrrhotite and chalcopyrite taken from ore veins. A detailed sulphur isotope study is presented as part of this study and includes thirty samples of sulphide separates taken from ore veins, disseminated chalcopyrite in massive skarn, and biogenic sulphide in unaltered hangingwall shale. More detailed studies of the deposit geochemistry together with fluid inclusion and stable isotope work would greatly improve the understanding of chemical and physical processes controlling alteration and mineralisation at Mount Elliott.

A complicated structural history is inherent in the genesis of mineralisation at Mount Elliott. However, little emphasis is given to structure in this study. A proposed decline and associated mine workings through the deposit should reveal many hidden secrets. Further work on the structural controls on mineralisation is highly recommended.

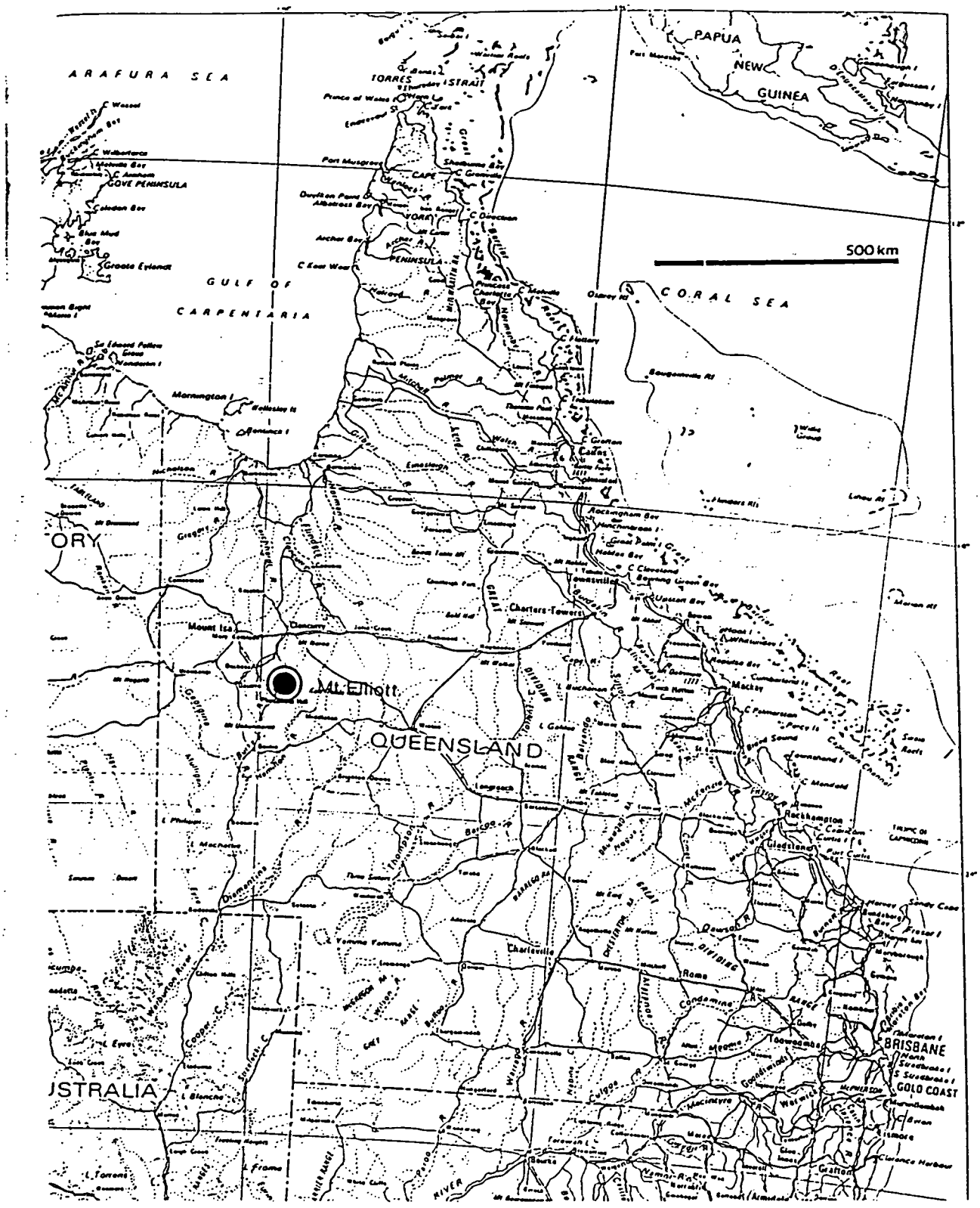

Figure 1.1: *Mount Elliott project location, northwest Queensland.*

1.5 Regional Geology

1.5.1 Regional Overview

The Mount Isa Inlier, northwest Queensland, occupies an area greater than 50,000 km^2 (Blake *et al. 1990*) and comprises variably deformed, Early to Middle Proterozoic sediments and intrusives that are host to several major copper and lead-zinc-silver orebodies, and numerous smaller deposits of copper, lead, zinc, silver, gold, uranium and cobalt.

The Mount Isa Inlier is broadly divided into three major, North - South trending, tectonic units (Carter *et al.* 1961; Blake, 1987): the Western Fold Belt, the Kalkadoon-Leichhardt Belt and the Eastern Fold Belt (Figure 1.2). Within this tectonic framework four major Proterozoic sequences are present (Figure 1.3). The oldest basement sequence, deformed and metamorphosed before 1875 Ma, is overlain by three younger sequences of Proterozoic volcano-sedimentary rocks, namely cover sequences 1, 2 and 3 (Blake, 1987).

Six major granite batholiths intrude the Proterozoic sequences and are identified as the Kalkadoon (~1860 Ma), Ewen (~1840 Ma), Wonga and Sybella batholiths (1670 -1740 Ma) outcropping in the Kalkadoon-Leichardt belt and Western Fold Belt, and the Williams and Naraku batholiths (~1500 Ma) of the Eastern Fold Belt. Three smaller granites in the Western Fold Belt (Blake *et al.* 1990) include the Yeldham Granite (~1820 Ma), Big Toby Granite (~1800 Ma) and the Weberra Granite (~1700 Ma).

At least four generations of mafic intrusions (E1 to E4) are recognised in the region, ranging in age from older than 1870 Ma to younger than 1500 Ma (Ellis and Wyborn, 1984). Most of the intrusions have been metamorphosed, metasomatised, and deformed to greenschist facies amphibolite or mafic schist. Structural features include sheared margins and boudinage-like terminations.

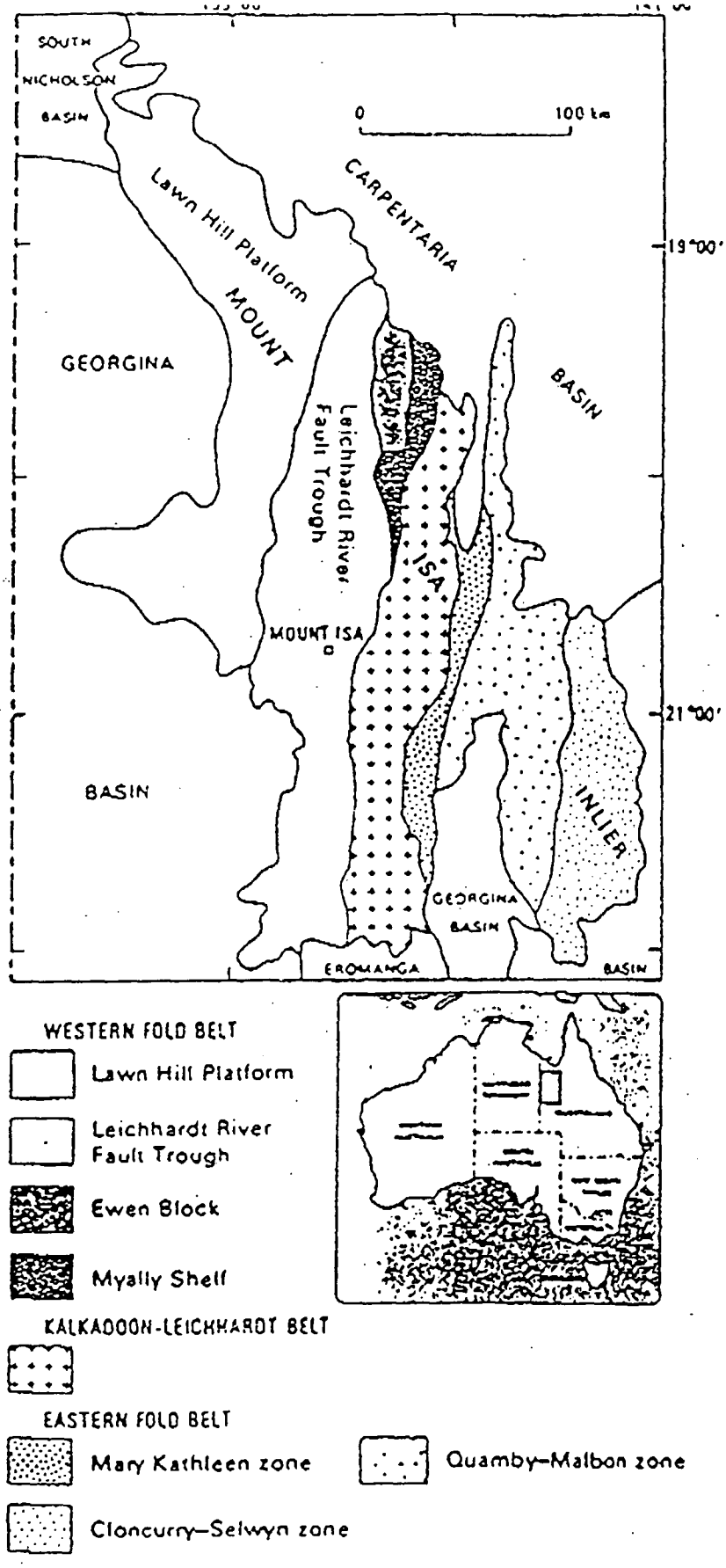

Figure 1.2: *Major tectonic units of the Mount Isa Inlier.*

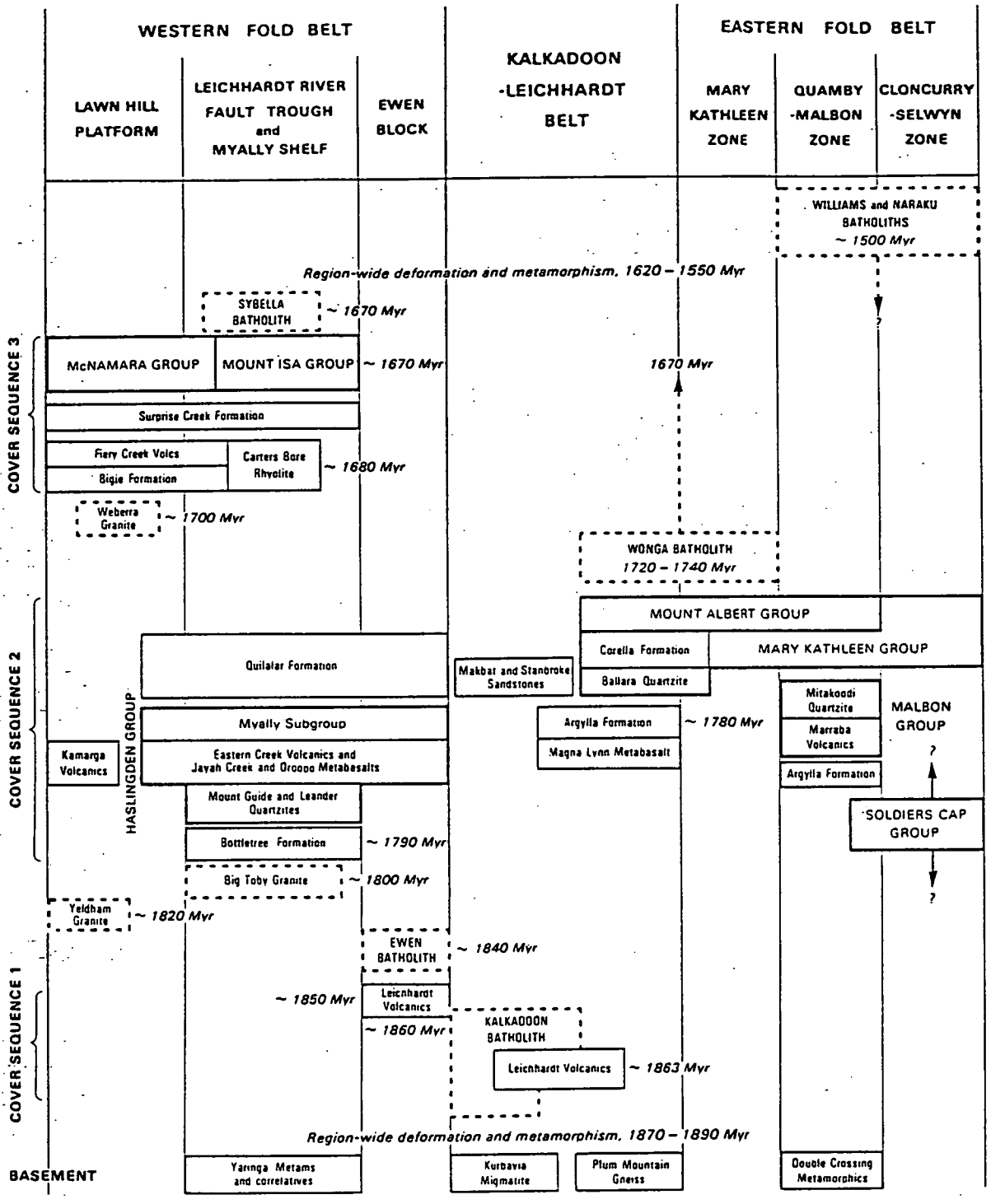

Figure 1.3: *Stratigraphic framework of the Mount Isa Inlier. From Blake et al. (1990)*

Two major orogenies characterised by widespread compressional deformation and regional metamorphism have affected rocks of the Mount Isa Inlier (Blake *et al.*. 1990). The older, less understood, event, correlated with the Barramundi Orogeny of Etheridge *et al.*. (1987) post-dates deposition of the basement sequence and pre-dates Cover Sequence 1 (i.e. 1890-1870 Ma). The younger compressional Isan Orogeny (Blake *et al.* 1990) post-dates deposition of the Mount Isa Group (Cover Sequence 3, 1670 Ma), and pre-dates emplacement of most of the Williams and Naraku batholiths at 1620 - 1550 Ma. The Isan Orogeny comprises three events consisting of initial moderate to large scale thrusting, folding, followed by major upright folding about north-trending axes (Blake *et al.* 1990). Brittle-ductile folding about upright northwest-trending axes was the final major deformation. Greenschist to upper amphibolite facies metamorphic assemblages prevail throughout the region.

The tectonic setting of the Mount Isa Inlier was modelled by early workers to be an evolving Andean-style continental margin to a palaeo-Australian plate (Plumb and Derrick, 1975; Glikson *et al.*. 1976; Wilson, 1978). Later workers proposed an intracontinental rift model for the Mount Isa Inlier (Derrick, 1982; Wyborn and Blake, 1982). The rifting model implicates extensional tectonics, however, does not account for the two compressional phases of deformation at ~1870 Ma and 1620-1550 Ma.

The Mount Isa Inlier contains a wide range of economic mineral deposit styles of which the shale-hosted stratiform Pb-Zn-Ag deposits of Mount Isa and Hilton, and the accompanying brecciated copper deposit at Mount Isa are the grandest examples. Other historically significant deposits of Cu, Pb, Zn, Ag, Au, Co, REE and U occur in the region. Recent spectacular discoveries of base metal mineralisation (Century, Cannington) have established the Mount Isa Inlier as perhaps the most significant base metal province in the world.

1.5.2 Eastern Fold Belt

1.5.2.1 Stratigraphy

The Mount Elliott Cu-Au deposit is hosted within graphitic shales and phyllites of cover Sequence 2 in the Eastern Fold Belt/Eastern Succession. Figure 1.3 illustrates that all stratigraphic units, except the Double Crossing Metamorphics, belong to cover Sequence 2 of the Eastern Fold Belt, which has been sub-divided into three tectonic elements (Blake, 1987); the Mary Kathleen Zone, Quamby-Malbon Zone and the Cloncurry-Selwyn Zone.

The oldest rocks, cropping out east of Cloncurry, belong to the Soldiers Cap Group (Figure 1.4) and dominantly comprise mica schist, quartzofeldspathic gneiss, metagreywacke, phyllite and amphibolite, with minor banded iron formation and calc-silicate units (Blake *et al*. 1984; Blake, 1987).

Westward, the Soldiers Cap Group is overlain with apparent conformity by mainly fine-grained sedimentary carbonates, siltstones and shales of the Mary Kathleen Group. The Mary Kathleen Group includes the Overhang Jaspilite and Answer Slate, the Kuridala, Doherty and Staveley Formations, the Agate Down Siltstone and Marimo Slate (Blake *et al*. 1984).

In the Selwyn region, the Kuridala Formation forms the base of the Mary Kathleen Group and is separated from calc-silicate rocks and breccias of the Doherty Formation to the east by the Williams batholith (Figure 1.4). The Kuridala Formation is a tightly folded package of moderately deep-water turbiditic sediments (schistose greywacke, siltstone and shale) derived from an easterly landmass (Blake *et al.* 1984). Quartzite, carbonaceous and pyritic slate, calc-silicate rocks and banded iron formations are also present. The thickness of this sequence is greater than 2000m, although neither the top nor the base of the Kuridala Formation are well established. Beardsmore *et al*. (1988) propose to remove the Kuridala

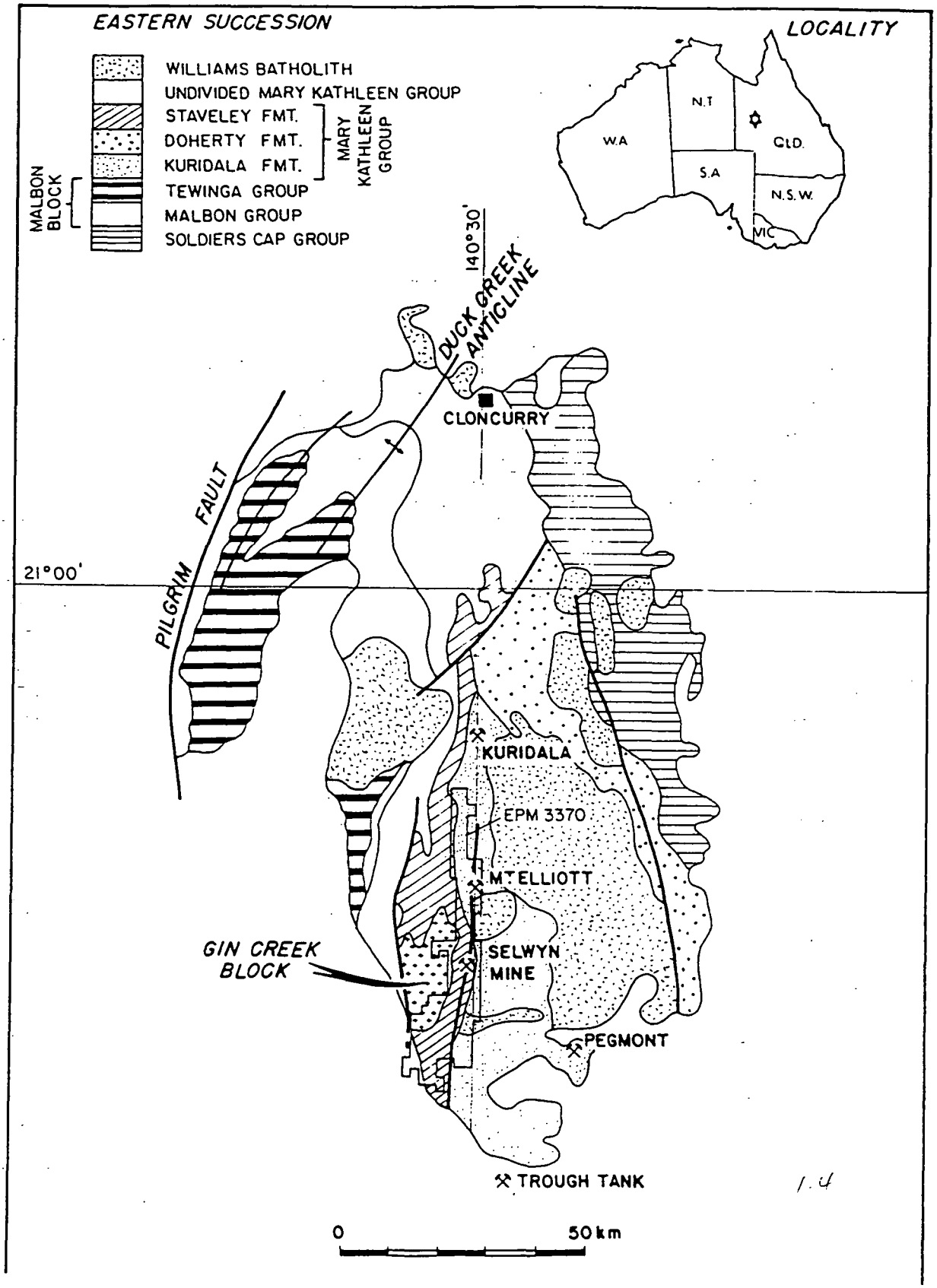

Figure 1.4: *Regional geology of the Eastern Fold Belt (Eastern Succession).*

Formation and incorporate the rocks into the Maronan Supergroup, a term encompassing a complex stratigraphy yet to be formally described.

Contact relationships with the Staveley Formation to the west are not clear. Most workers report the Staveley Formation to overlie the Kuridala Formation, with Beardsmore *et al*. (1988) defining the contact as the Mount Dore Fault zone. Davidson (1989) presents evidence favouring an unconformable relationship in the Starra area.

The Staveley Formation comprises a >2000m thick linear belt of well-bedded to brecciated calcareous, ferruginous, feldspathic, siliceous and micaceous sediments of possibly shallow-water origin (Blake, 1987; Davidson, 1989). The western margin is characterised by a 750m thick package of basic to acid lavas and epiclastics with intercalated massive ironstones and banded iron formations (Davidson, 1989). To the west the Staveley Formation is conformably overlain by the Agate Downs Siltstone and the Marimo Slate (Blake *et al*. 1984).

The Marraba Volcanics and Mitakoodi Quartzite of the Malbon Group are restricted to the Quamby-Malbon Zone conformably overlying the Argylla Formation. These units pass conformably into the Overhang Jaspilite of the Mary Kathleen Group and are correlated to overlay the Soldiers Cap Group.

The transition from volcano-sedimentary lithologies of the Malbon Group to sediments of the overlying Mary Kathleen Group is interpreted to represent the progression from rift phase to sag phase of an evolving extensional basin (Blake *et al*. 1990).

1.5.2.2 Intrusives

Emplacement of felsic intrusions such as the Williams Batholith, and several episodes of mafic intrusion has significantly influenced the geology, deformation and mineralisation of the Eastern Fold Belt. Early pre- to syntectonic plutons of the Williams Batholith include

the Blackeye, Cowie, Maramungee granites, parts of the Gin Creek Granite and several unnamed bodies (Blake *et al.* 1984). These granites are recrystallised and foliated concordantly with the surrounding host rocks, imparting a pale pink to grey, leucocratic, heterogeneous, non-porphyritic fabric (Blake, 1987). Table 1.1 lists the various granite bodies, their lithologies and intrusive relationships.

However, the bulk of the Williams Batholith consists of non-foliated medium to coarse grained, homogeneous pink granite and includes the Wimberu, Gin Creek, Mount Angelay, Mount Cobalt, Mount Dore, Saxby, Squirrel Hills and Yellow Waterhole Granites (Table 1.1). They consist of strained quartz and feldspar (oligoclase-microcline) with 5-15% biotite ± hornblende, clinopyroxene and up to 5% magnetite and sphene. Accessory phases include allanite, apatite, calcite, chlorite (after biotite), epidote, fluorite, muscovite, sericite, sulphides and zircon (Blake *et al.* 1984). Most granite of the Williams Batholith was probably emplaced at around 1500 Ma (Nisbet *et al* . 1983; Wyborn *et al* . 1988).

Sills, dykes and pod-like bodies of metadolerite and amphibolite are widespread in the Eastern Fold Belt. The mafic intrusives predate the major Isan folding and metamorphic event and are probably older than most phases of the Williams Batholith (Blake *et al.* 1984). East-trending dykes of unmetamorphosed dolerite up to 50m thick cutting granite are the youngest Proterozoic rocks in the Eastern Fold Belt.

1.5.2.3 Structure

At least three phases of folding have been recognised in the strongly deformed rocks of cover sequence 2 in the Cloncurry-Selwyn Zone (Blake, 1987). First and second generation folds are mostly tight to isoclinal and later folds generally open. Axial planes and associated cleavages and foliations are typically steep to vertical, with structural trends dominantly occupying a north-northwest to north-northeast orientation in the Selwyn region. Small to large scale refolded folds, basin-and-dome interference folds, and crenulated cleavages are common features (Blake, 1987).

Name of unit (reference to definition)	*Lithology*	*Relationships*
Foliated granites **Blackeye Granite** (Blake & others, 1981a)	Foliated leucocratic granodiorite and minor pegmatite	Intrudes Doherty Formation
Cowie Granite (Blake & others, 1981a)	Generally foliated biotite-bearing leucocratic granite, granodiorite, and tonalite: pegmatite	Intrudes Soldiers Cap Group and Doherty Formation: intruded by Squirrel Hills Granite.
Maramungee Granite (Blake & others, 1981a)	Generally foliated biotite-bearing leucocratic granite, granodiorite, and tonalite; pegmatite	Intrudes Soldiers Cap Group; cut by dolerite dyke
Non-foliated granites **Wimberu Granite** (Carter & others, 1961)	Commonly prophyritic granite and granodiorite containing biotite and/or hornblende ≠ clinopyroxene: subordinate finer-grained non-porphyritic biotite granite: minor aplite and pegmatite	Intrudes Argylla Formation. Marraba Volcanics, Mitakoodi Quartzite. Overhang Jaspilite. Answer Slate. Doherty Formation, Staverley Formation and metadolerite.
Gin Creek Granite (Blake & others, 1981a)	Partly porphyritic biotite granite: subordinate slightly foliated line to coarse leucogranite containing muscovite and tourmaline, and intensely foliated biotite granite with abundant inclusions mostly of gneiss and schist derived from the Double Crossing metamorphics; minor biotite microgranite, aplite, and greisen	Intrudes Double Crossing Metamorphics, Answer Slate, Staveley Formation, Kuridala Formation and metadolerite
Mount Angelay Granite (Blake & others, 1981a)	Partly porphyritic granite containing biotite and/or hornblende and/or clinopyroxene; minor leucogranite, porphyritic microgranite, contaminated grey granite, aplite, and pegmatite; xenoliths common near margins of granite	Intrudes Soldiers Cap Group and Doherty Formation; cut by dolerite dykes
Mount Cobalt Granite (Blake & others, 1981a)	Biotite granite and minor aplite	Intrudes Kuridala Formation and metadolerite
Mount Dore Granite (Blake & others, 1981a)	Biotite and hornblende-biotite granite, porphyritic in places: Minor microgranite, aplite, pegmatite and greisen	Intrudes Kuridala Formation and metadolerite
Saxby Granite (Blake & others, 1981a)	Biotite and hornblende-bearing granite: minor leucogranite, xenolithic diorite, monzonite, granodiorite, aplite and pegmatite	Intrudes Soldiers Cap Group, Doherty Formation, and metadolerite: cut by dolerite dykes
Squirrel Hills Granite (Blake & others, 1981a)	Commonly prophyritic granite containing hornblende and/or biotite and locally clinopyroxene; minor aplite, porphyritic microgranite, monzonite, and granoliorite; rare pegmatite	Intrudes Soldiers Cap Group and Kuridala, Doherty, and Staveley Formations, Cowie Granite, and metadolerite; cut by dolerite dykes
Yellow Waterhole Granite (Blake & others, 1981a)	Partly porphyritic biotite and hornblende-biotite granite: minor aplite	Intrudes Kuridala Foundation
Undivided granite	Foliated leucocratic tonalite and pegmatite; biotite granite: minor hornblende-biotite tonalite	Intrudes Soldiers Cap Group, Kuridala Formation, and Doherty Formation

TABLE 1.1: *Granites of the Williams Batholith. From Blake et al. (1984).*

Calc-silicate breccias in the Cloncurry-Selwyn Zone are thought to be tectonic in origin, forming after deposition of the Soldiers Cap and Mary Kathleen Groups and pre- to syn-emplacement of the Williams Batholith (Glikson, 1972; Blake *et al.* 1984).

The dominant structural-tectonic features in the Selwyn region include the Starra Shear, a major D1 extensional zone separating the Gin Creek Block (Switzer, 1987) from the less deformed Staveley Formation, and the Mount Dore Fault Zone, a 75 km-long, N-S trending fault within the Kuridala-Staveley Formations (Beardsmore, 1988; Beardsmore *et al.* 1988).

1.5.2.4 Metallogenesis of the Eastern Fold Belt

Several hundred small mines and occurrences of shear and fault-controlled vein-copper deposits occur in the district. The dominant host for these deposits are carbonaceous and pyritic shales, phyllites and calc-silicate rocks. A close spatial relationship to amphibolites is also common. Deposits of this type are typically of low tonnage and high grade with only the zones of oxidation and supergene enrichment being exploited in many cases. Besides copper, many deposits contain significant concentrations of gold, silver and less commonly, minor bismuth.

Beardsmore (1988) described shear and vein Cu-deposits as "Selwyn-style" ores, of which the early-mined mineralisation at Mount Elliott is included. Other examples in the area include the Swan Prospect (1 km west of Mount Elliott) comprising a large-tonnage, low-grade supergene-enriched Cu-Au-REE deposit hosted in brecciated calc-silicates of the Staveley Formation (Nyvlt, 1980), and the large, low-grade Mount Dore Cu-deposit hosted in brecciated black shales overthrust by the Mount Dore Granite (Ophel, 1980; Scott, 1986; Beardsmore, 1988).

Approximately 778 tonnes of metallic cobalt was extracted from shear zone-hosted cobalt mineralisation between metadolerites and shales of the Kuridala Formation at Mount Cobalt, 140 km south of Cloncurry. The mine remains as the most significant resource of cobalt in the region.

Recent discoveries of stratabound ironstone-hosted Cu-Au mineralisation at Starra and Trough Tank have realised a new deposit type for the region. At Starra ore-grade Cu-Au deposits, hosted in magnetite-hematite-quartz ironstone, are prefentially located in the hinge zones of steeply plunging post-D2 folds, and are interpreted by Laing *et al*. (1988) to represent metamorphic replacement of favourable lithologies followed by introduction of mineralising fluids into structurally prepared sites. Kary and Harley (1990) recognised the spatial relationship of large hangingwall amphibolites to mineralisation and proposed that these bodies represent the source of mineralising fluids. A lack of obvious fluid pathways and alteration in the hangingwall needs to be explained.

Clearly the most detailed and technically diverse investigation of the Starra Cu-Au area was carried out by Davidson (1989) who proposes a synsedimentary exhalative origin for the ironstones and sulphides, with later remobilisation concentrating sulphides and gold in hinge zones of D_2 folds.

1.6 Previous Studies of the Mount Elliott Mineralisation

In a report to Broken Hill South Limited, Sullivan (1951) recognised the lack of carbonate rocks in the area and suggested that "dolomitisation" of the sediments occurred as a result of igneous activity and subsequent metamorphism to a "lime silicate rock." The widespread occurrence of scapolite in the area led to the assumption that a local amphibolite body ("dyke") was responsible for the "dolomitisation" and later for the introduction of metals. Sullivan concluded that the basic dyke was unlikely to have contributed all of the Cu-Au, but acted as a channel-way for mineralising fluids rising from gabbroic bodies at depth.

Dimo (1975) presented a Master's thesis describing mineralisation in the Mount Elliott area as an example of late syn-to post-magmatic, pneumatolytic, contact metasomatic and exo-skarn style processes associated with gabbroic intrusives. The various alteration styles of Mount Elliott, ranging from coarse "pegmatitic veins" to pervasive alteration of "gabbroic" bodies were grouped by Dimo under the term "DMS" (diopside-magnetite-scapolite). The DMS alteration and associated mineralisation were interpreted as synchronous with intrusion of a gabbroic plug and predating emplacement of the Williams Batholith.

In a study of the geology and mineralisation of the nearby calc-silicate breccia-hosted Cu-Au-REE deposit at Swan (which has lithological similarities to Mount Elliott and is geophysically connected to it), Nyvlt (1980) concluded that amphibolites were not the source of mineralising fluids. Instead, local metasomatic remobilisation of metals from country rocks (that is, a sedimentary source) during a period of hydrothermal leaching was attributed to mineralisation.

Davidson (1989) and Davidson and Dixon (1992) analysed sulphides from Mount Elliott/Swan as part of a sulphur isotope study of various deposit styles throughout the Eastern Fold Belt.

I.7 History of Mining at Mount Elliott

Mineralisation was discovered at Mount Elliott in the late 1890's as a gossan outcrop of "dense, red, jaspery limonite with abundant oxide copper." The gossanous ore comprising cuprite and malachite with chrysacolla, atacamite and gold (Dimo, 1975) was contained within a N-S trending, steeply dipping crush zone produced by faulting and fracture-filling of cherty black shales (Sullivan, 1951).

The Mount Elliott Company was formed in London and commenced mining of the gossan in 1901 as a small open-cut operation. Production records for this early stage of mining are unclear, with grades from the gossan yielding an estimated 15% Cu and 3 g/t Au (Dimo,

1975). Production quickly expanded with the construction of a railway plus numerous shafts and a smelter. The orebody was developed on six main levels to a depth of 198m with ore reported to have averaged 12% Cu and 7.8 g/t Au, although copper grades decreased dramatically from 6% at four level (122m) to 2% at five level (168m). In an attempt to prolong the life of the Mount Elliott mine and smelting operations, a number of small mines in the district were purchased and their ores railed to Mount Elliott.

However, a lack of high grade ore coupled with falling copper prices and labour unrest saw both mining and smelting ceased by 1920; up to this time Mount Elliott had yielded an estimated 264,000 tonnes of ore averaging 9.3% Cu and 4 g/t Au. This includes 161,861 tonnes at 11.85% Cu and 6.4 g/t Au and 101,860 tonnes at 5.17% Cu and unknown gold grade (Nye and Rayner, 1941; Darlington, 1957). Most of the ore was won from the oxidised and supergene zones extending from surface to three level (87m), although exploration development had progressed to six level.

1.8 History of Exploration

Prior to 1952, exploration activity in the area was limited to surface mapping and examination of mine workings by the AGGSNA in 1936/37 (Nye and Rayner, 1941), plus a geological-geophysical (EM, SP) survey by the BMR in 1951/52. Since 1950, five companies have carried out mineral exploration programmes of the Mount Elliott mine and adjacent areas.

During 1952-1955 Broken Hill South Limited (BHS) conducted a six hole diamond drilling programme with the holes located in a circular pattern around the deposit, designed to intersect a pipe-like mineralised body (Sullivan, 1951; Dutton, 1952). Cross-sections are incomplete, some results and all drill cores have been lost.

Mount Isa Mines drilled three deep holes during 1955-1957 to test the potential at depth below, and along strike of the Mount Elliott workings. MIM-1 confirmed the extension of

low-grade mineralisation vertically beneath the old workings (Darlington, 1957). MIM relinquished their option in 1957.

In 1957, Rio Tinto Southern (RTS, now CRAE) carried out a geological mapping and geophysics programme incorporating EM, IP, SP and gravity surveys. In 1958, the BMR conducted a soil geochemistry survey of the geophysical anomalies revealing associated elevated copper grades. Two diamond holes were later drilled in the mine vicinity. Poor results prompted CRA to relinquish their ground, although the Mount Elliott Mine lease, ML 5094, was retained (Wade, 1958).

No further detailed exploration took place until Anaconda Australia farmed into the lease in 1970 and commenced a programme of geological mapping, drainage geochemistry and airborne magnetics (Dimo, 1971; Dimo, 1973). Regional mapping produced a good understanding of the local geology and structural features and included informally naming the mappable lithological units. In 1974 Union Miniere drilled a 625m deep hole to fulfil an option agreement. The hole was designed to test the Mount Elliott mineralised "pipe" and intersected only weak mineralisation, whereupon both Anaconda and Union Miniere relinquished their interest in the lease (Reeve, 1975).

Prior to Cyprus Minerals Australia Pty Ltd. purchasing the lease, the only other exploration activities occurred in 1980/81 with CRAE incorporating the area in an airborne magnetic and radiometric survey which identified the Mount Elliott magnetic anomaly. Since 1989 Cyprus has drilled 26 percussion holes and some 55 diamond holes to outline the present resource, which includes the discovery of a new shallow-dipping lens of high-grade copper-gold beneath the old workings. Down-hole missa-la-masse, EM and moving loop EM surveys have also been conducted.

Chapter 2

GEOLOGY OF THE MOUNT ELLIOTT AREA

Introduction

A structural complexity within the Kuridala Formation metasediments at Mount Elliott has localised mineralising fluids resulting in precipitation of skarn and sulphides. Previous mapping by Anaconda (1:2500) and recent detailed work by Cyprus (1:500) has identified the major lithological and structural features in the mine area. Rocks of the Kuridala Formation have been informally sub-divided into three units: The "Selwyn Beds," "Elliott Beds," and "Town Beds," (Figure 2.1) characterised on an outcrop scale by grain size and compositional variations (Reeve, 1975; Dimo, 1975). Outcrop in the area is good, except in the immediate mine vicinity where mine ruins plus slag and mullock obscure much of the geology. This chapter presents a detailed description and chronology of the geology and alteration of the deposit as determined from extensive investigation of diamond drill cores, with less emphasis on surface relationships, since bleaching, strong weathering and ancient mine workings have rendered identification of alteration types in outcrop difficult. Although mineralisation at Mount Elliott occurs solely within shales of the Elliott Beds, adjacent to the Town Beds contact, detailed logging of drill cores has permitted the delineation of distinct mappable alteration styles and textures. Recent diamond drilling reveals a broad progressive zonation of alteration styles comprising phyllitic shales, outer skarn carapace and massive calc-silicate-magnetite sulphide skarn.

2.2 Selwyn Beds

East of Mount Elliott, the Selwyn Beds form the base of the Kuridala Formation comprising a >600m thick unit of quartz siltstones, quartzite and minor shale. The sediments are

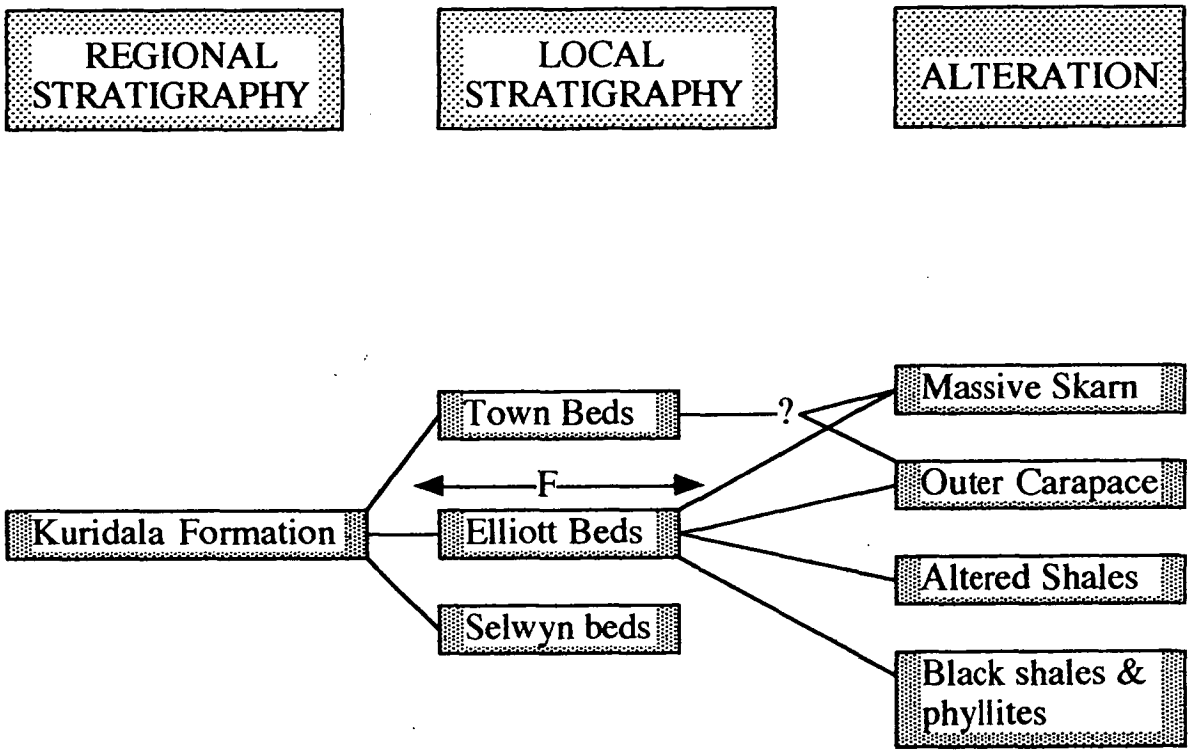

Figure 2.1: *Local stratigraphy and alteration at Mount Elliott*

strongly foliated grading to biotite-quartz augen schist (Dimo, 1975) and are intruded by the Williams Granite. Calcareous sediments and amphibolite units are absent.

2.3 Elliott Beds

The Elliott Beds conformably overlies the Selwyn Beds and is the host to the Mount Elliott Cu-Au mineralisation (Figure 2.1). The unit is approximately 150-175m thick (Dimo, 1975) and comprises thinly banded black to grey, fine grained, isoclinally folded, carbonaceous and pyritic shales and phyllites. Colour variations reflect variable mica contents with dark bands being typically biotite rich and paler bands quartz or muscovite-rich. Minor anhedral calcite is disseminated within quartz-rich bands.

Small quartz blows (< 30cm) occur sporadically throughout the carbonaceous shales and phyllites, parallel with the S_1 foliation. The veins are often folded, weakly deformed and cracked, with weak pyrite mineralisation healing hair-line fractures and also forming coarse (<0.5 cm), blebby aggregates. Andalusite-rich horizons, generally <1m wide, occur regularly throughout the Elliott Beds (Plate 2.1a), indicating a middle amphibolite facies grade metamorphism. The andalusite forms chaotic clusters of coarse grained, acicular, randomly orientated porphyroblasts that overprint the primary S_1 foliation, but are deformed by the S_2 crenulation cleavage (Plate 2.12b). Regionally, the andalusite is described as chiastolite, a variety typical of contact metamorphosed argillites (Deer *et al.* 1980).

The late, upright S_2 crenulation cleavage is not ubiquitous throughout the shales and phyllites, but tends to form in discrete, often regularly dispersed horizons and typically forms small-scale tight to open folding of the S_1 metamorphic banding. A wavy crenulation highlighted on planar surfaces of S_1 represents an intersection lineation between S_1 and the later crenulation cleavage, S_2. The structural terminologies reflect the foliations recorded locally at Mount Elliott and do not necessarily equate with regional observations.

Plate 2.1a: *Andalusite cluters in black shale (Elliott Beds).*

Plate 2.1b: *Crenulated pyrite-chalcopyrite vein in hanging wall shale - "Elliott Beds."*

Mineralistion in this unit is dominated by fine (<2-3mm) semi-continuous stratiform lenses of pyrite and pyrrhotite. The sulphide bands are sub-conformable to the primary foliation and may reflect the orientation of original bedding (ie, diagenetic sulphides). Iron-staining and limonite development along cleavage partings in the surface shale outcrops result from weathering of these sulphides (Plate 2.1b). Very finely disseminated pyrite and lesser pyrrhotite (flattened into the foliation) are ubiquitous. Fine, calcite ± pyrite-filled fractures (<1-2mm) appear to be a late feature cross-cutting all foliations.

2.3.1 Altered Shales and Phyllites

Towards the top of the Elliott Beds and along strike from the mine workings the rocks become weak to intensely fractured and partially to pervasively bleached. This is particularly evident in outcrop immediately south of the mine and represents the outermost envelope of alteration surrounding the Mount Elliott Cu-Au mineralisation. Peripheral alteration is manifested as <0.05m - <3.5m thick bleached, pale grey to cream-green siliceous zones within and adjacent to highly fractured rock (Plate 2.2a). The alteration generally obliterates the foliated fabric of the rock due to bleaching of biotite although in rare contradictory cases tight isoclinal folding is highlighted. Early scapolite (?) development in the bleached rock is manifested as a blotchy translucent yellowish-green texture, often associated with weak carbonate.

Alteration bands are intensely fractured. Pyrite and/or pyrrhotite typically heals the hairline fractures, but also forms fine disseminations and blebby aggregates. Larger veins of pyrite and/or pyrrhotite typically form selvages of chlorite and calcite marginal to the veins.

Purple fluorite is a common accessory phase in the bleached zones, forming blebby disseminations (<5-10mm) in siliceous bands and veins (Plate 2.2b). The occurrence of fluorite in the alteration package is consistent with a granite influence on the ore fluids.

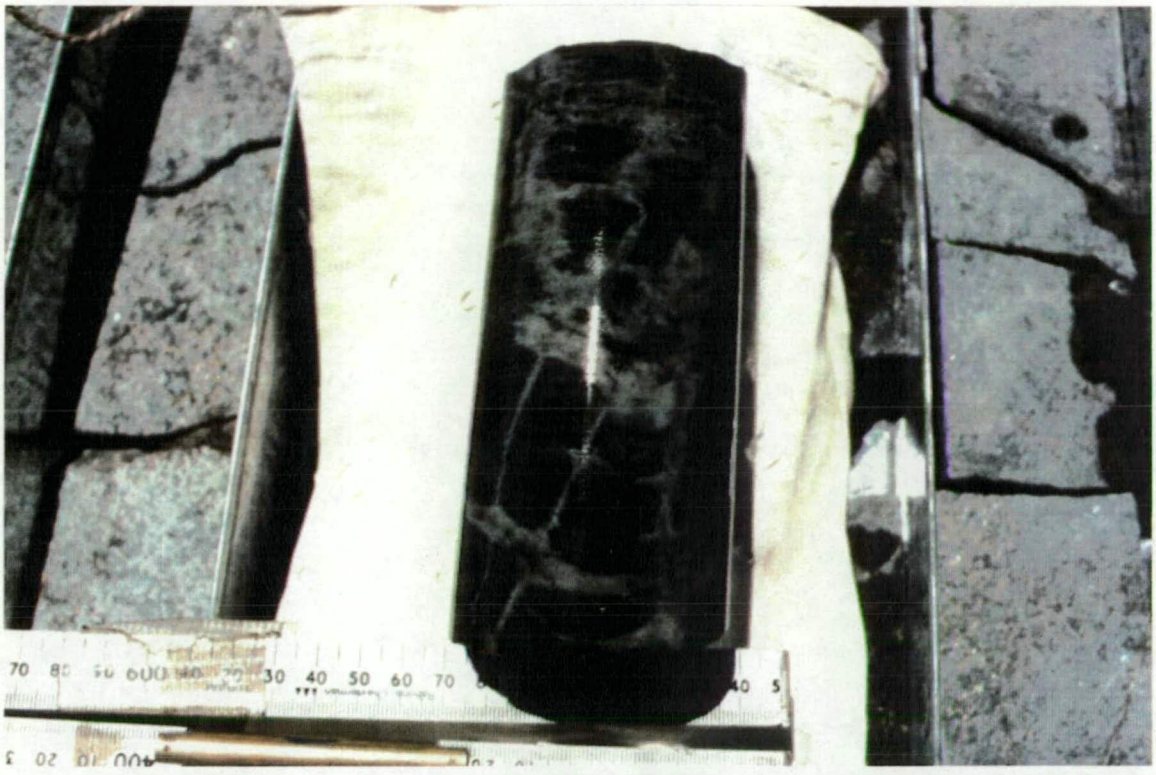

Plate 2.2a: *Fracture controlled infiltration alteration.*

Plate 2.2b: *Fluorite bleb in pyrite vein within bleached shale.*

Frequency and width of the siliceous bleached/altered units increases with depth towards the outer carapace.

The altered shales and phyllites are uncommonly interrupted by semi-conformable bands of green, medium grained, semi-crystalline to weakly foliated calc-silicate rock (granofels?). Calc-silicate alteration comprises dark green amphibole, feldspar (altering to scapolite), and calcite, and tends to exhibit biotite enrichment/replacement towards the margins. These rocks appear to have formed early as they are both foliated and overprinted by similar alteration features as the surrounding rocks.

2.3.2 Outer Skarn Carapace

The outer carapace forms a large cap (up to 100-150 m) surrounding the massive skarn body, consisting of a complex arrangement of brecciated, pervasively altered shales, supported in a matrix of coarsely crystalline calc-silicate-calcite-sulphide mineralisation (Figure 2.2). Brecciation is not usually evident in the outermost portion of the carapace which is initially characterised by the pervasively altered nature of the shales and weak introduction of pink albite-hematite into small veins and fractures with only minor diffusion into the shale. The altered shales are typically pale grey-brown to cream-white, fine grained and finely banded reflecting compositional variation related to alteration (Plate 2.3a). Albite-hematite alteration intensifies locally, ultimately destroying the shale cleavage and forming thin bands (<20-30cm) of massive, pink albite-hematite (Plate 2.3b).

With depth the altered shales are increasingly disrupted by thin to broad (typically <20-30cm, but up to 2m) 'veins' (matrix) of coarsely crystalline calc-silicate+calcite+sulphide, with brecciation evidenced by abrupt changes in core-axis-to-foliation angles on opposite sides of the veins (up to 90°). Altered shale clasts are typically angular, varying in size from up to 3m (top of the carapace) to less than 10cm at the base. The blocks are highly fractured

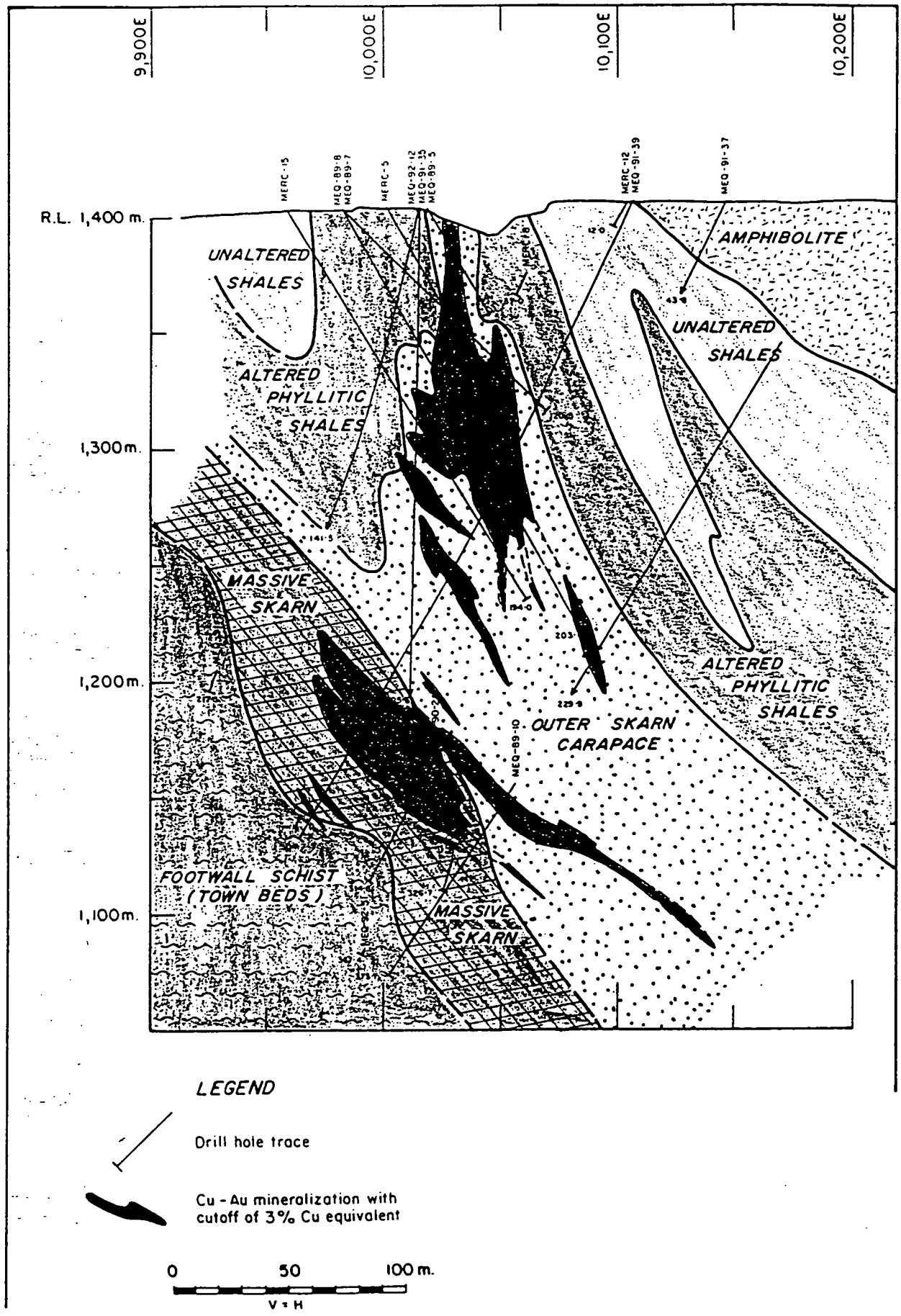

Figure 2.2: *Cross -section 9950N. Geology of the Mount Elliott deposit showing outline of mineralised zones.*

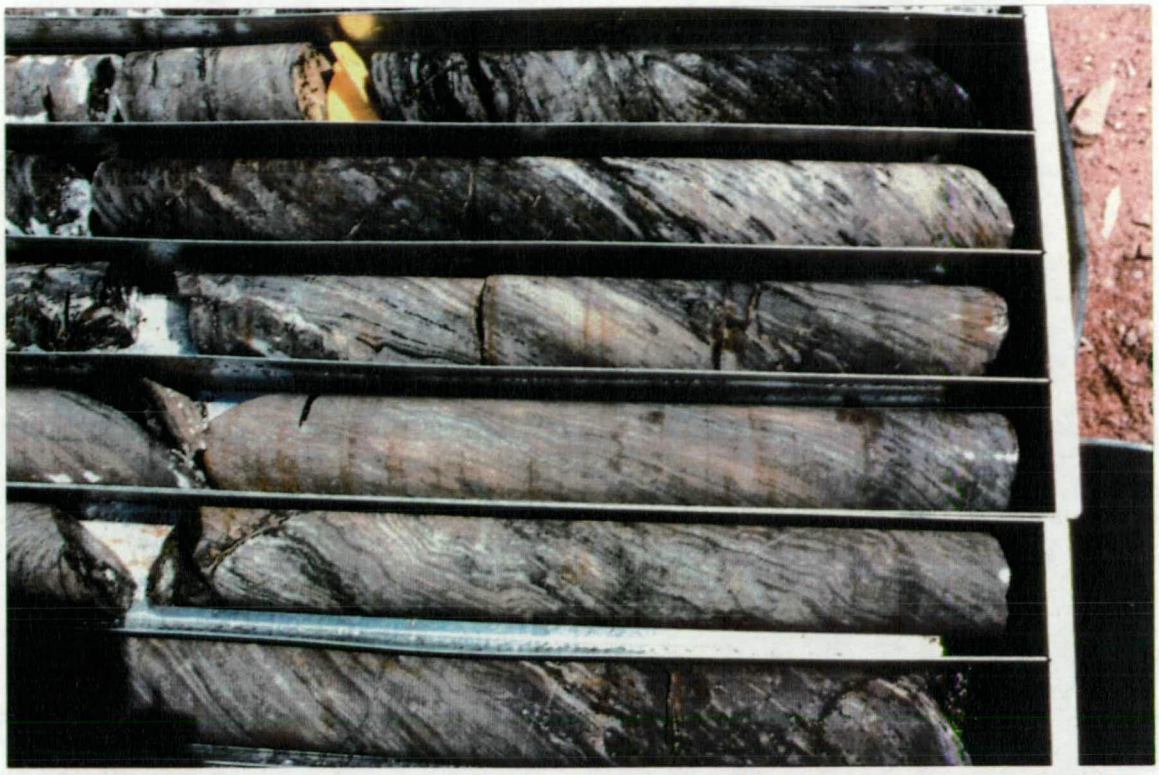

Plate 2.3a: *Pervasively altered shales of the outer carapace.*

Plate 2.3b: *Development of albite-hemate; (L-R) initially occupying small veins and fractures, gradually invading the shale along cleavage planes and ultimately forming bands of massive albite-hem.*

and altered by pink albite-hematite, green calc-silicate, and sulphide. Intensity of alteration broadly increases with depth, correlating with decreasing clast size and greater disorientation of the shale foliation to the breccia matrix (Plate 2.3c). Blocks of predominantly black, unaltered to poorly altered shale occur rarely within the outer carapace zone and are notably poorly fractured.

The matrix is not a breccia, but a network of pegmatitic veins which are typically zoned with coarse crystals of calc-silicate minerals (dominantly clinopyroxene, diopside-hedenbergite), developed on the 'vein' walls, infilled by coarse calcite and blebby sulphides (chalcopyrite-pyrrhotite-pyrite). Rarely, the veins incorporate rafts of altered shale (up to 10cm diameter).

Other calc-silicate phases commonly occurring in the 'veins' include scapolite and apatite. Coarse, bladed crystals of pale yellow-green scapolite are particularly common to veins higher in the carapace, often dominating over clinopyroxene (Plate 2.4). In the lower portion of the carapace, coarse blebby magnetite (<0.5-1.0cm) occurs commonly within the matrix-vein, typically associated with sulphide-calcite mineralisation. The introduction of magnetite is usually associated with the loss of pyrrhotite from the system, although the two may occur together over 1-2m. Vughs formed in the calc-silicate matrix are typically lined, or filled, with crystalline amethyst.

Margins of matrix-veins vary from being sharp to highly diffuse depending primarily upon the orientation of the shale foliation to the matrix-vein. Plate 2.5a shows a classic matrix-vein conformable to shale foliation and sharp contact, whereas the cross-cutting vein in Plate 2.5b exhibits strongly diffuse margins. Thus, individual 'veins' may be sharply bound on one side and highly diffuse on the other.

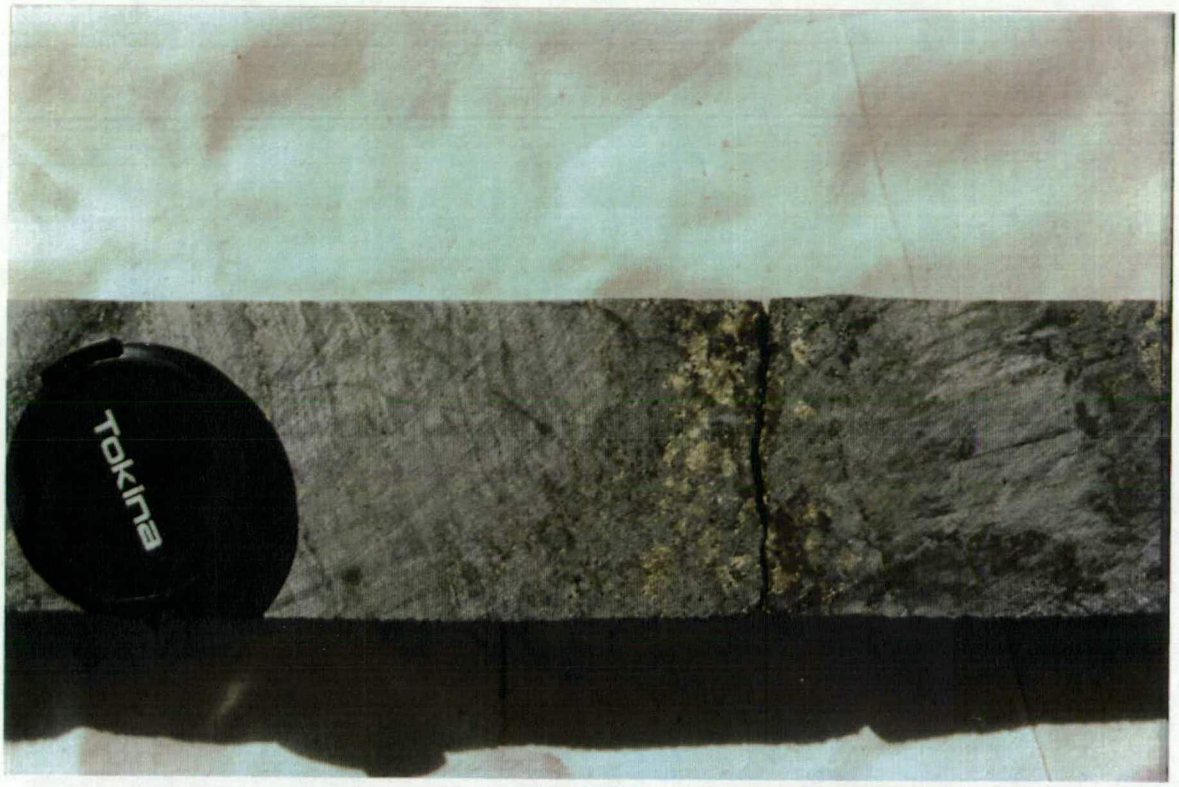

Plate 2.3c: *Brecciation of altered shale in outer carapace with coarse calc-silicate-calcite-sulphide matrix.*

Plate 2.4a: *Abundant scapolite crystallisation on vein walls and 'ripped crystals within calcite.*

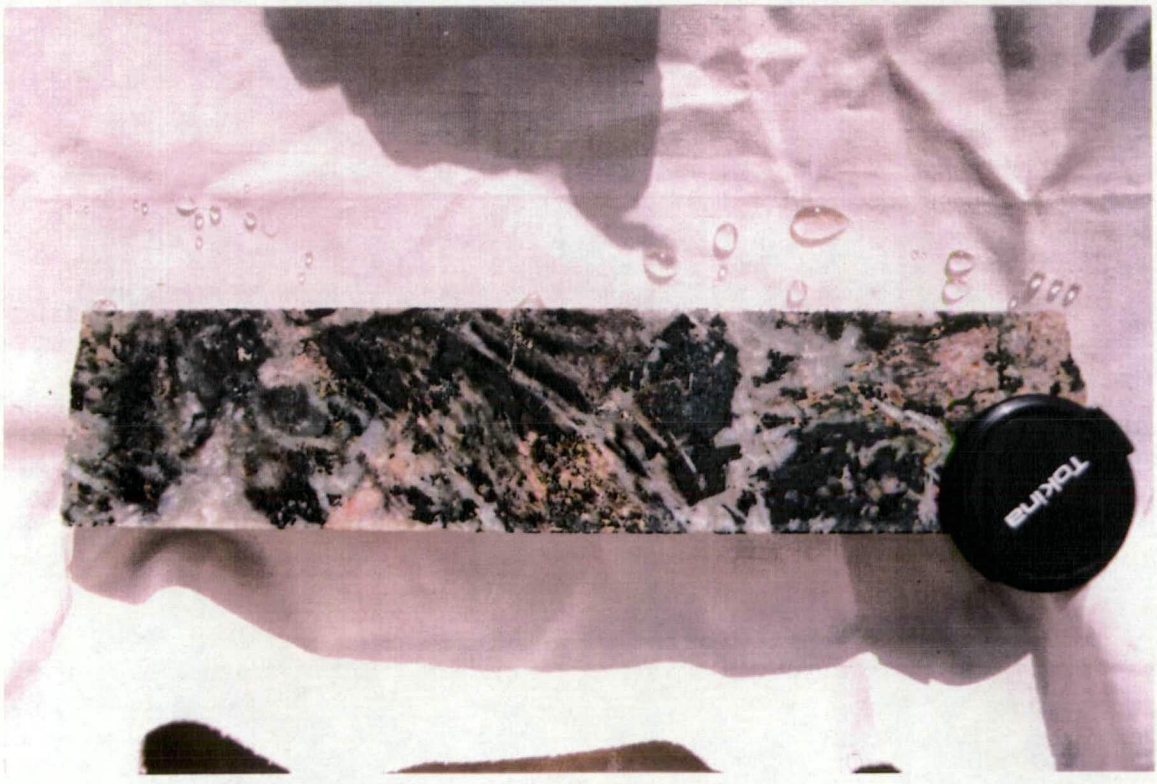

Plate 2.4b: *Chaotic brecciation with infilling matrix dominated by coarse bladed scapolite.*

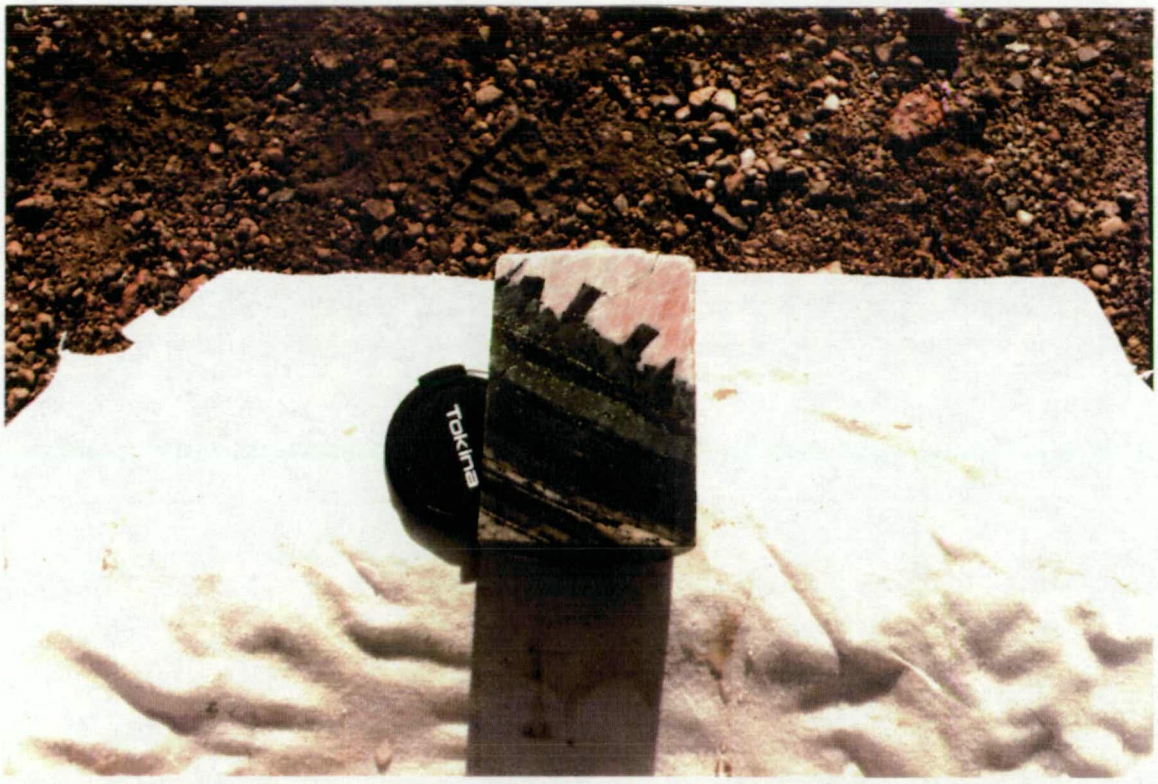

Plate 2.5a: *Sharply bound matrix-vein conformable to foliation.*

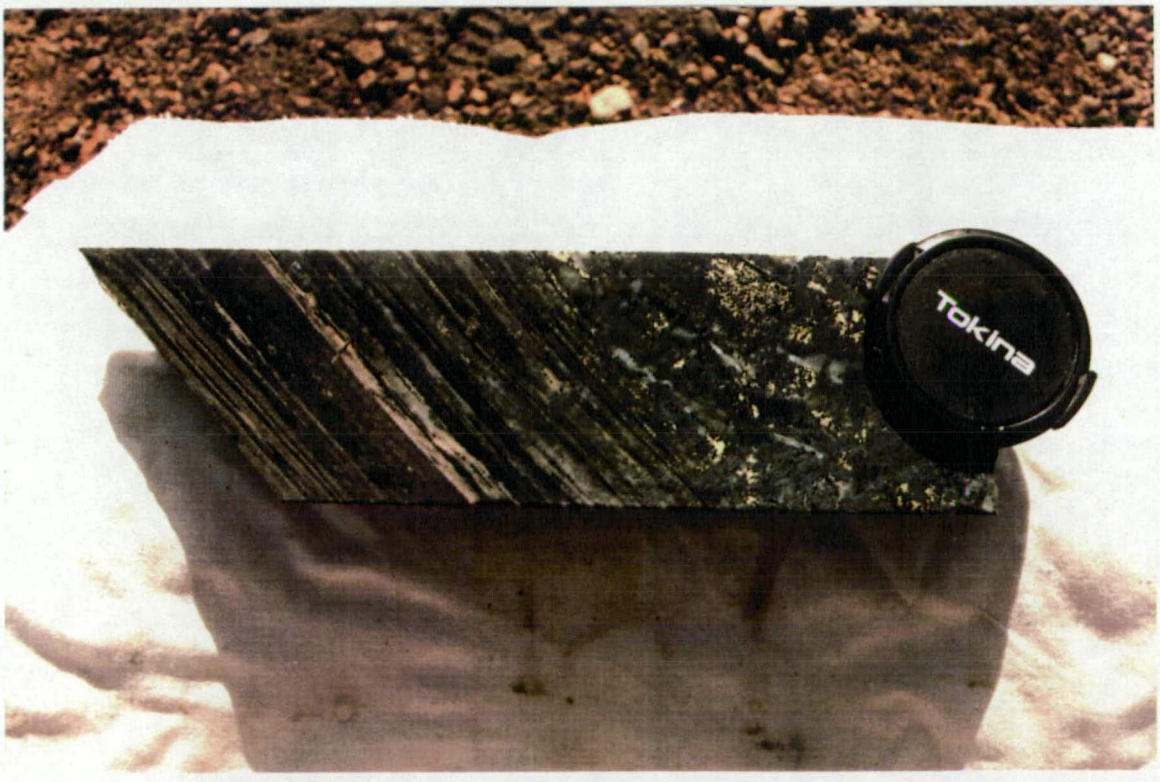

Plate 2.5b: *Matrix-vein cross-cutting the shale foliation and exhibiting diffuse margins due to infiltration alteration along cleavage planes.*

A second type of breccia occurs infrequently throughout the 'outer carapace.' It consists of small, rounded and embayed fragments of silicified rock within a fine grained chlorite-biotite rich matrix (Plate 2.6). Breccia fragments in Plate 2.6b appear to have been plucked from the host rock, implicating a tectonic fabric. However, relationships in Plate 2.6c indicate a pseudo-breccia fabric resulting from progressive replacement of a highly fractured rock. The highly embayed nature of most fragments supports this, although a combination of the two processes is likely.

A set of steeply-dipping widely-spaced, fine calcite-filled fractures/veins cross-cuts both the altered shale blocks and calc-silicate+calcite+sulphide cement.

2.3.3. Massive Skarn

The outer carapace passes both abruptly and gradationally to a unit of massive, semi-crystalline skarn (Figure 2.3) which is sub-divided according to grain size into 'medium grained skarn' and 'fine grained skarn.' Both the outer carapace and massive skarn are overprinted by a number of broad, shallowly-dipping, pegmatitic veins of calc-silicate-calcite ± magnetite that host significant sulphide mineralisation as chalcopyrite, pyrrhotite and pyrite.

2.3.3.1 Medium Grained Skarn

The massive skarn body forms the core of the alteration sequence and is dominated by a pink-green-black massive, medium-coarse grained, semi-crystalline, intensely altered rock locally termed 'medium grained skarn.' In it interlocking crystals of randomly orientated, sieve-textured albite-hematite are overprinted by prograde calc-silicate minerals; clinopyroxene, scapolite and amphibole, with accessory phases sphene and apatite. Retrograde calcite (± quartz-plagioclase), magnetite and sulphide (chalcopyrite-pyrite) occur

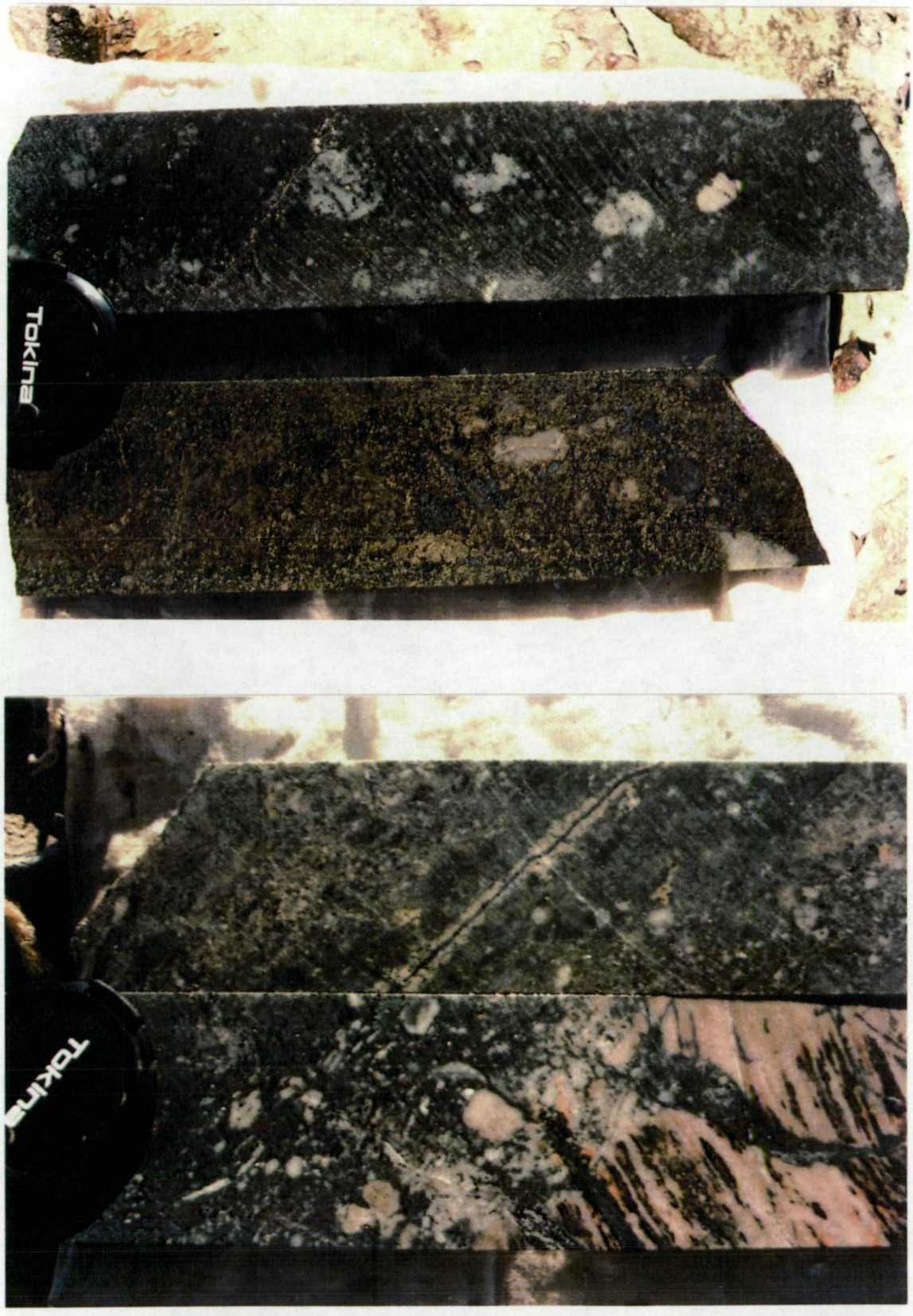

Plate 2.6a,b: *Breccia textures of siliceous fragments in fine grained chloritic matrix. Clasts exhibit rounded, embayed margins and possible evidence of pinching from vein (?) walls (b).*

Plate 2.6c: *Progressive replacement of a siliceous-altered rock. Initial invasion via a myriad of fine fractures results in rounded 'clasts' in a fine grained chloritic matrix.*

interstitial to and replacing the albite-hematite-calc-silicate assemblage and also occupying small common vughs (<1-2cm). Pyrrhotite is notably absent from the sulphide assemblage in this rock. Continuing replacement of the albite-hematite by calc-silicates and retrograde phases has delineated individual albite-hematite crystals, producing a characteristic semi-crystalline, pseudo (?)-intrusive texture (Plate 2.7a). The intensity of alteration varies considerably throughout the skarn and is best reflected by magnetite content (Plate 2.7b).

Remnants of the early brecciated shale protolith are often recognised by relicit foliation banding within the skarn (Plate 2.8) and as randomly oriented blocks of altered shale (generally <20-40cm, but up to 1-2m) in a massive skarn matrix. Such fragments typically exhibit massive skarn at their margins and in isolated patches internally, particularly along foliation planes. Fragments of coarse grained footwall schist incorporated in the skarn indicate that the skarn body, although apparently conformable, is not lithology-specific; transgressing the interpreted faulted contact between shale and schist.

A distinctive feature unique to the medium grained skarn is the development of a pseudo-breccia fabric when magnetite contents are moderate to high (>10-15% mag). Rounded 'clasts' of moderate to high sphericity and variable size (up to ~15cm dia) that are magnetite-poor and calc-silicate-rich relative to the enclosing semi-crystalline, magnetite-rich skarn matrix (Plate 2.9). 'Clasts' are often sulphide enriched (chalcopyrite ± pyrite). The origin of the fabric is not certain; however, replacement is favoured over a tectonic mechanism, because the fabric is not observed in less altered skarn and no evidence of relict foliation exists within the 'clasts.'

Thin fractures and veins (<5mm) filled with calcite, plus minor chalcopyrite are a late-stage feature cross-cutting the skarn.

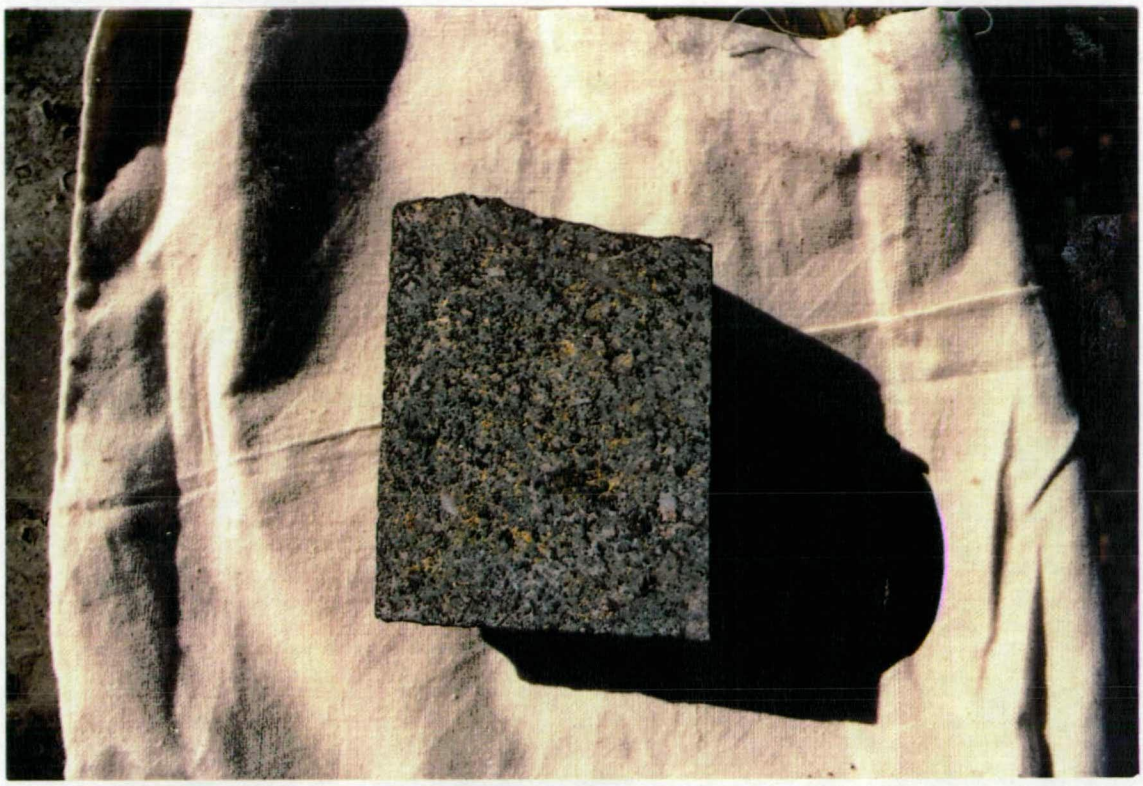

Plate 2.7a: *Typical medium grained skarn.*

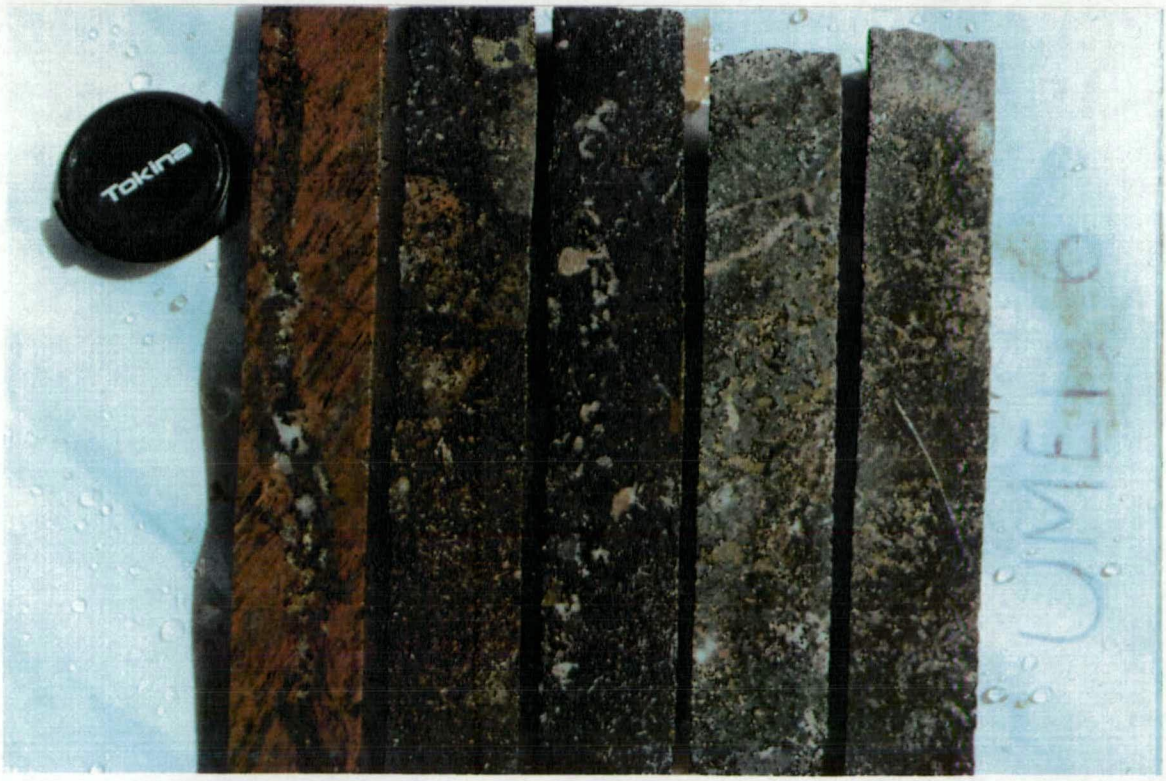

Plate 2.7b: *Variation of skarn fabrics with depth in a single intersection - UMED 6. Reflects local variation in alteration intensity.*

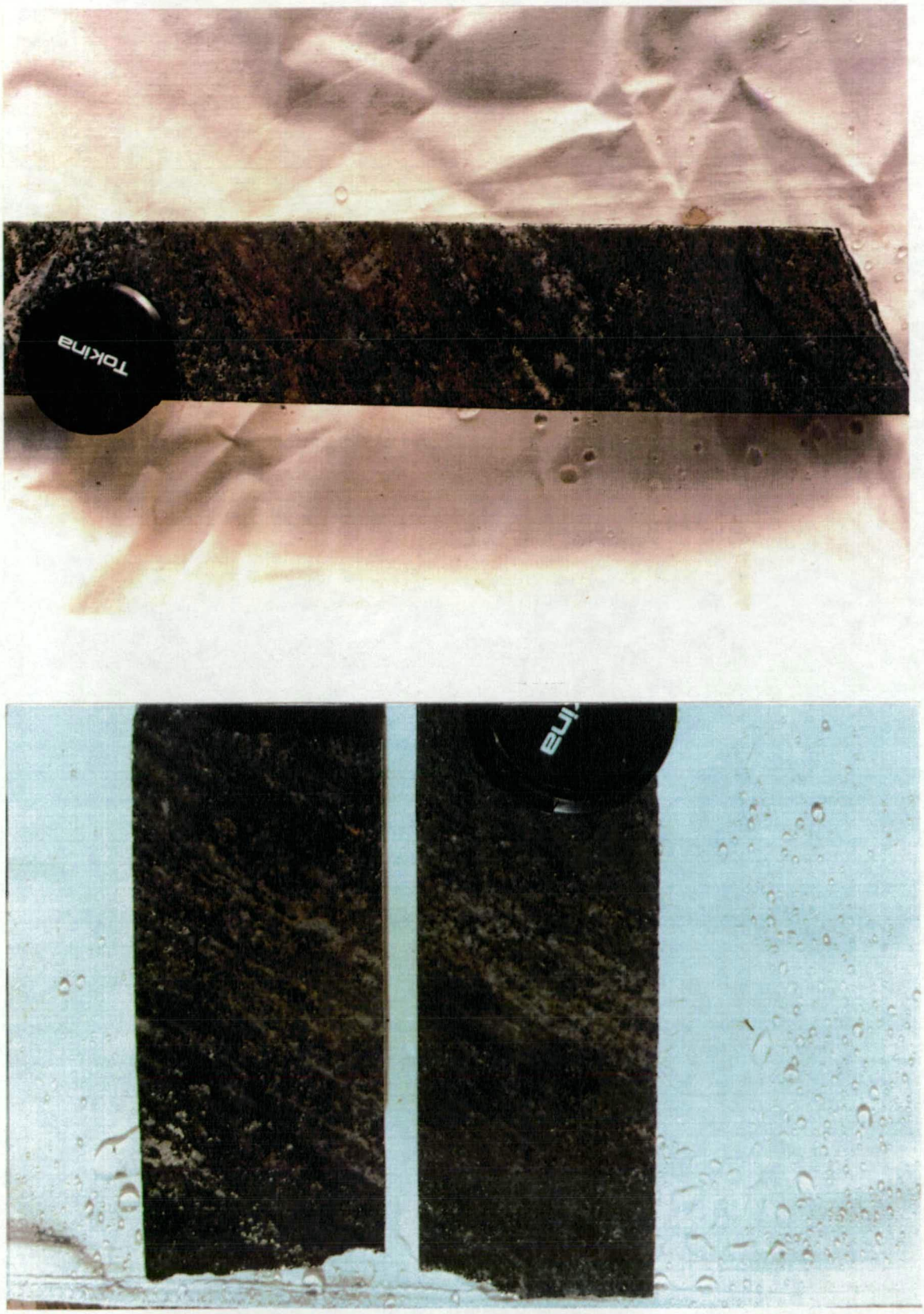

Plate 2.8: *Foliated fabrics in massive skarn - indicative of early shale protolith*

Plate 2.9: *Pseudo-breccia fabric in medium grained skarn. Rounded 'clasts' of calc-silicate-rich skarn enveloped by magnetite-rich skarn.*

2.3.3.2 Fine Grained Skarn

A dark green, massive, fine grained, equigranular calc-silicate+magnetite rock is intersected in several drill holes. In thin section the rock comprises porphyritic actinolite-plagioclase-biotite-sphene in a fine grained plagioclase-rich groundmass. The mafic minerals are typically replaced by chlorite with grain boundaries commonly embayed and corroded by calcite, however, the rock is notably calcite- and sulphide-poor relative to the enveloping medium grained skarn. Magnetite is common in this rock unit occurring as fine disseminations interstitial to the calc-silicates. Very rare sulphides include finely disseminated pyrite ± chalcopyrite.

The shape of this unit is unclear because continuity between sections is imperfect and original contacts with the shale are strongly overprinted by medium grained skarn alteration. The rock may represent an early intrusive phase (eg, dolerite-amphibolite) similar to the semi-conformable hangingwall amphibolite and is not considered to be the source of alteration and mineralising fluids, although it may have acted as a preferential pathway for such fluids. It is also cross-cut by pegmatitic calc-silicate+sulphide veins and late-stage, calcite-filled fractures and veinlets.

2.4 Town Beds

The Elliott Beds pass abruptly, with faulted contact, into a greenish-brown-grey-yellow, medium to coarse grained, intensely foliated unit of quartz-feldspar-biotite-garnet schist. Well developed banding occurs in places reflecting localised compositional and grain size variations. The schists are less resistant to weathering and erosion than the adjacent shales and characteristically occupy areas of low relief. A thin veneer of ubiquitous quartz float obscuring outcrop is derived from abundant small to large quartz "blows (<10-70cm)." The "blows" are often preserved as rootless fold hinges providing clear evidence for isoclinal

folding or transposition of the schists, not recognisable in the micaceous domains (Garrett *et al*. 1991).

The original contact with the Elliott Beds shale is overprinted by massive skarn alteration with the current skarn-schist contact typically defined by weak-moderate brecciation of the skarn (zones up to 30cm wide) accompanied by intense feldspathisation (pink albite-hematite) of the schist. However, several intersections display abrupt contacts with minimal leakage of albite-hematite along foliation planes and fractures in the schist (Plate 2.10a).

The schist is visually and petrographically differentiated from the overlying shale by its coarse grain size, mineralogy (garnet-staurolite-silliminite) and weaker susceptibility to metasomatic alteration. The presence of staurolite, tourmaline and andalusite indicates that the rocks have been regionally metamorphosed to middle amphibolite facies. Interestingly, the garnets are static growths exhibiting no rotation, pressure shadowing, or deformation of surrounding biotite, implicating a post-deformational timing. Compositions determined by electron microprobe analysis (Table 2.1) identify the footwall garnets as Mn-Fe-Al-rich spessartine-almandine end-members (Figure 2.3). Composition of biotites, plus staurolite and sillimanite are shown in Appendix 1.

Clusters of coarsely crystalline, randomly oriented pseudomorphs of andalusite occur in discrete bands throughout the schist and similarly overprint the foliation. At depths greater than 320-350m (down-hole), schist intersections typically include fine, ovoid to semi-ovoid disseminations (<1-2mm) of magnetite ± hematite aligned weakly with the foliation. Few grains are smeared along the foliation. The iron-oxide zones are generally broad (>5m) and tend to be sharply bound.

Retrograde chloritisation of biotite imparts a prominant green spotty fabric to the rock in places. Skarn alteration of the schist is common, although generally poorly developed and

Plate 2.10a: *Abrupt contact of FW Schist with massive skarn MEQ-48-247.4m.*

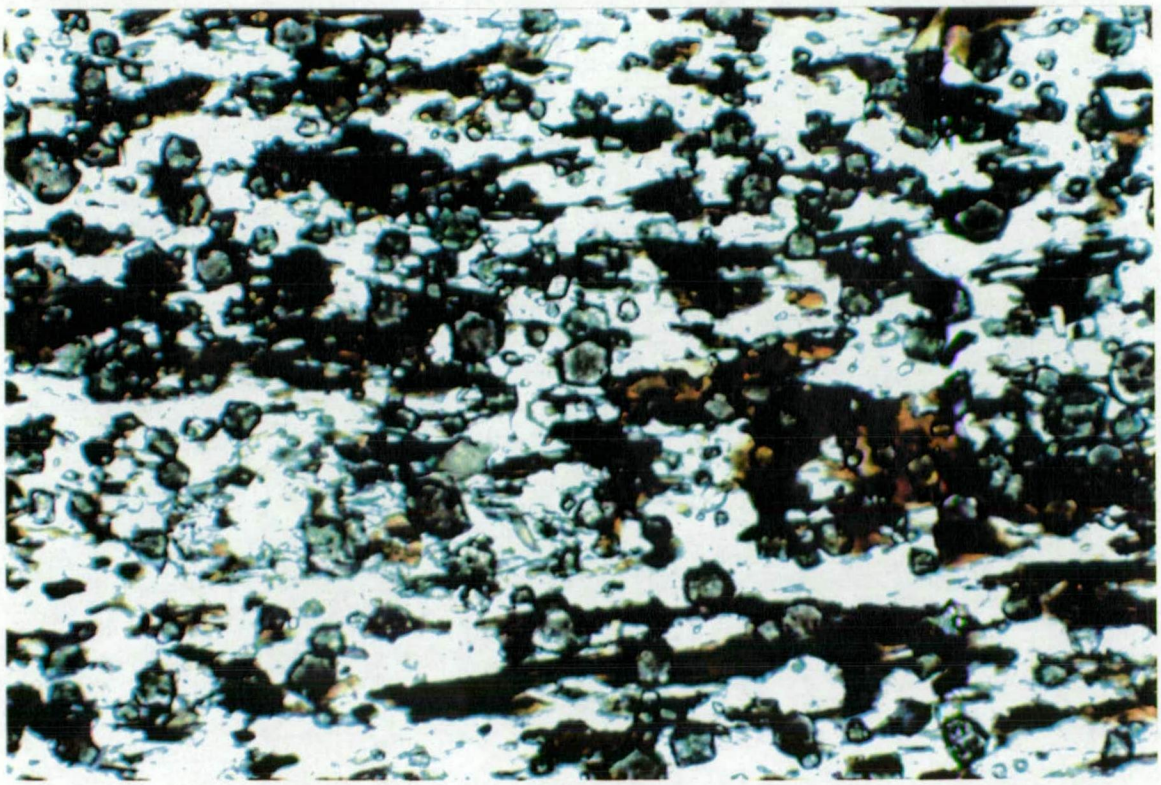

Plate 2.10b: *Photomicrograph (x10) illustrating hexagonal garnet overprinting the schistose fabric in the Footwall Schist. MEQ-14-280.3m.*

	1	2	3	4	5	6
S03	0.1602	0.0401	0.0000	0.0400	0.1401	0.0200
P205	0.0000	0.0424	0.0000	0.0000	0.0000	0.0000
Si02	36.0058	36.2648	36.7266	36.8649	37.1212	37.0124
Ti02	0.0267	0.0215	0.0531	0.0392	0.0000	0.0084
Al203	20.4458	20.6185	20.8828	20.9330	21.1117	21.2617
Cr203	0.0363	0.1246	0.0000	0.0283	0.0081	0.0364
Mg0	1.4408	1.6534	1.6859	1.5058	1.5389	1.7090
Ca0	2.1057	2.6194	1.8512	2.3949	2.5917	2.0516
Mn0	8.8593	5.7878	11.7996	12.0609	11.6481	12.9177
Fe0	28.8471	31.8992	25.5984	24.7624	25.2280	24.5625
Ni0	0.0588	0.0000	0.0000	0.1058	0.0000	0.0584
Ma20	0.0706	0.0106	0.0062	0.0255	0.0012	0.0137
K20	0.0000	0.0000	0.0513	0.0465	0.0340	0.0078
Cl	-	-	-	-	0.0496	0.0331
total	98.0572	99.0823	98.6552	98.8072	99.4614	99.6853
cations	24.0000	24.0000	24.0000	24.0000	24.0000	24.0000
	Cations based on 24 (0, Cl)					
Si	5.9699	5.9535	6.0212	6.0273	6.0201	6.0006
Al	3.9954	3.9891	4.0351	4.0336	4.0352	4.0626
Ca	0.3561	0.4607	0.3252	0.4195	0.4503	0.3564
Fe	4.0000	4.3792	3.5097	3.3858	3.4215	3.3303
Mn	1.2442	0.8047	1.6385	1.6702	1.6000	1.7739
Total	15.9982	16.0245	15.9610	15.9484	15.9246	15.9583
	Mole %					
Sp	154.0100	154.2980	153.9600	152.3400	152.8500	154.9600
Gr	47.2070	49.0952	47.3190	49.0510	49.9990	48.6780
Andr	64.0110	71.6566	56.7500	56.7100	58.2310	55.2800

Table 2.1: *Composition of garnets from Footwall Schist determined by electron microprobe analaysis . 1 - 2: MEQ-14-310.9m; 3 - 6: MEQ-14-280.3m.*

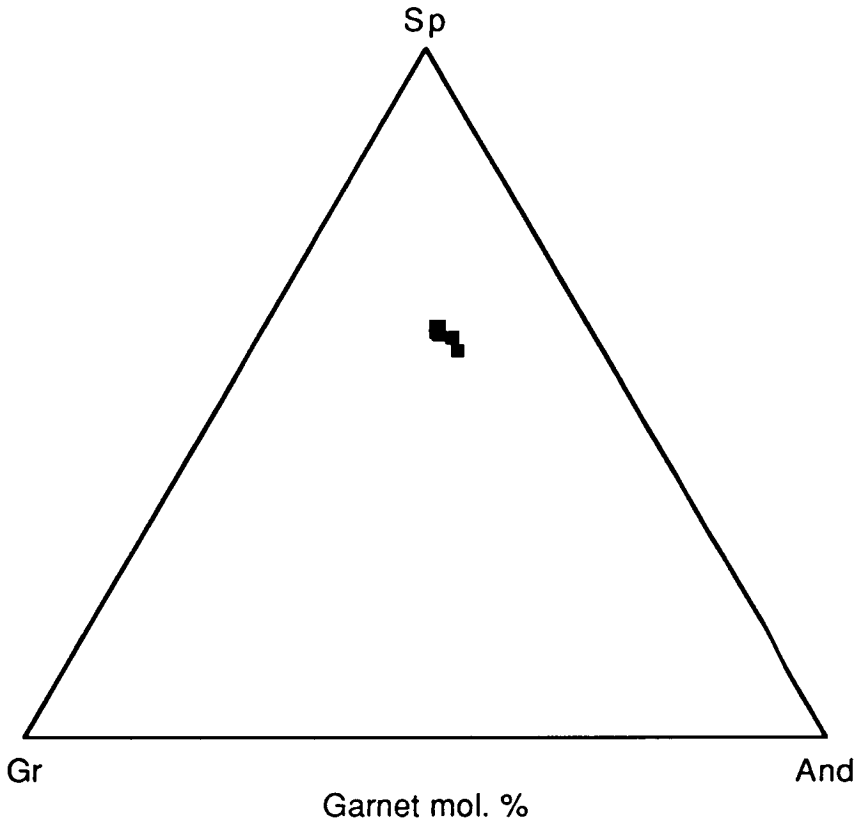

Figure 2.3: *Ternary plot of Footwall Schist garnet compositions (mol %).*

occurring where the rock fracturing is moderate to intense. Pink albite-hematite filled fractures, with limited infiltration of the local foliation (<5-10cm) is most common (Plate 2.11a), however, intermittent bands of calc-silicate-calcite-magnetite ± sulphide alteration increases towards the north (Plate 2.11b). Small bands of massive skarn (0.5 - 5.0m) are usually tightly constrained, displaying limited diffusion of calc-silicate alteration along foliation planes in the schist. Retrograde alteration of calc-silicate phases to chlorite and epidote, plus leaching of interstitial calcite, is more prevalent in the schist. Rarely, strong transgression of poorly altered schist to massive medium grained skarn (characteristic of alteration in the shale) can occur, particularly where fracturing and brecciation of the schist is more pronounced (Plate 2.11c). Unlike the shale, core-to-schistosity angles remain relatively consistent down-hole (±20°) providing little evidence for large scale brecciation necessary for the development of extensive replacement skarn alteration.

Several strongly mineralised calc-silicate veins (0.3-1.3m) comprising massive chalcopyrite ± pyrite, magnetite cross-cut the Town Beds with lesser veins (<5cm) of calc-silicate-sulphide-magnetite being common throughout several intersections.

The Town Beds mark the top of the Kuridala Formation at Mount Elliott and are overlain to the southwest by metasediments and massive/banded calc-silicates of the Staveley Formation.

2.5 Structure

A complex structural history at Mount Elliott, evidenced by at least three phases of deformation related to orogenic and intrusive events, has culminated in the localisation of vein-hosted chalcopyrite ± Au mineralisation within structurally prepared sites.

Plate 2.11a: *Fracture-controlled albite-hematite alteration in Town Beds schist.*

Plate 2.11b: *Mineralised calc-silicate veins cross-cutting the Footwall Schist with weak dispersion of alteration into the foliation.*

Plate 2.11c: *Progressive development of massive skarn within the Footwall Schist illustrating brecciation and early overprinting of the schistose fabric by albite-hematite.*

Tokina
Tokina
Tokina

Within the 'Elliott Beds' a penetrative axial planar cleavage (S_1) formed by tight isoclinal folding of the original bedding (S_0) is superimposed on S_0 and generally strikes northwest to north-northwest dipping steeply (50-80°) east. Fold hinges are difficult to locate and are not discernible in the 'Town Schist' due to its uniformity.

Deformation of S_1 is easily recognisable forming larger, southeast-trending moderately plunging (30° - 50°) open folds, with amplitudes up to 100m (Garrett *et al.1991*). A change to northwest plunges in the mine vicinity may be attributed to strain variation parallel to the axial plane (R. Keele, pers.comm., 1991) rather than an overprinting folding episode (Sullivan, 1951). The D_2 folds are accompanied by a steeply dipping axial planar crenulation cleavage (S_2) that is displayed in drill core as a low amplitude and wavelength crenulation lineation (L_2) in the plane of S_1. In thin section the S_2 crenulation cleavage is emphasised by a strong re-alignment of biotite grains (Plate 2.12a). The D_2 deformation event clearly post-dates deposition of lamellae sulphides in the shale (pre-S_1), evidenced by coarse clotting of sulphides where the S_2 cleavage intersects the sulphide bands, and is later than the post-S_1, andalusite-forming metamorphic event (Plate 2.12b).

Dimo (1975) reports small-scale crenulation folding of the S_2 crenulation cleavage only within the 'Town Beds' schist.

Faulting has truncated D_2 folds within the 'Elliott Beds' at their western contact with the 'Town Beds', thus dating fault movement as post-S_2 (Garrett *et al.* 1991). A strong metamorphic textural contrast across the fault, with similar metamorphic grade, implies significant displacement (oblique dip-slip). In outcrop to the south of Mount Elliott mine, the fault is invaded by small, intensely weathered granular bodies (intrusive?) that also cross-cut the adjacent rock. At depth the fault is obscured by massive skarn alteration. Reverse faults are evident in outcrop immediately south of the mine.

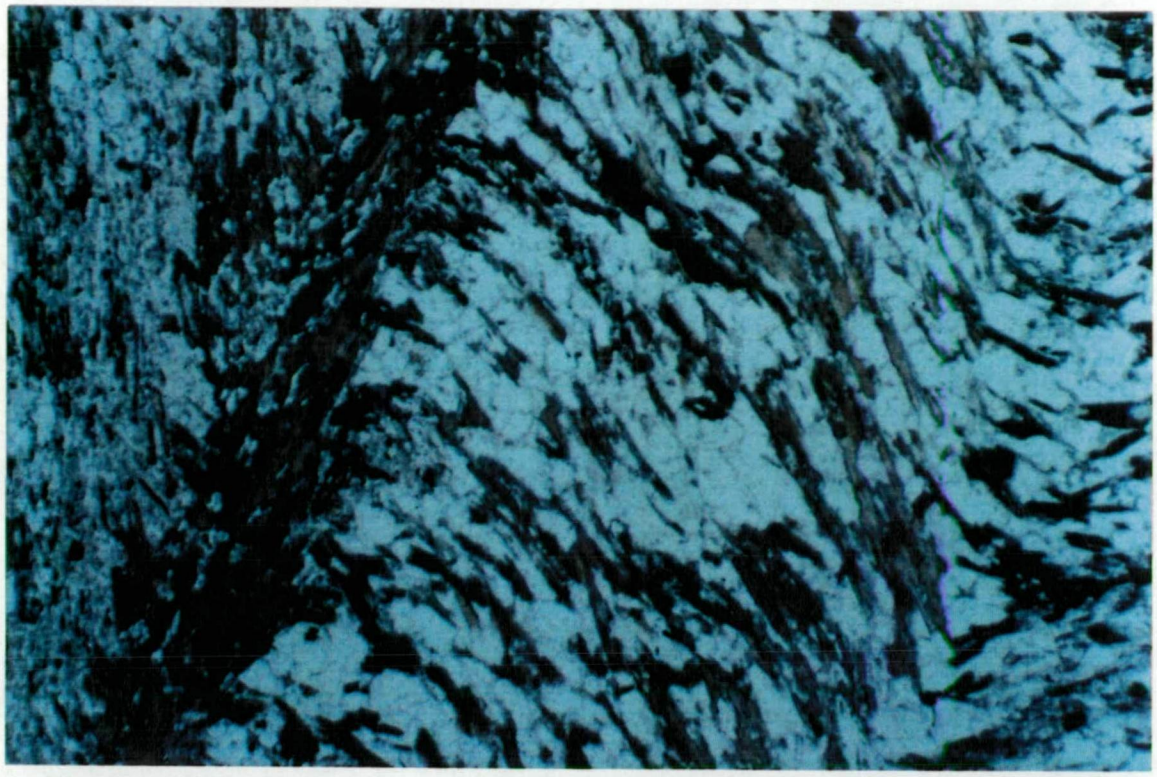

Plate 2.12a: *Photomicrograph (x2.5) showing re-alignment of S_1 biotite grains to form the steeply dipping S_2 crenulation cleavage. MEQ-19-279.7m.*

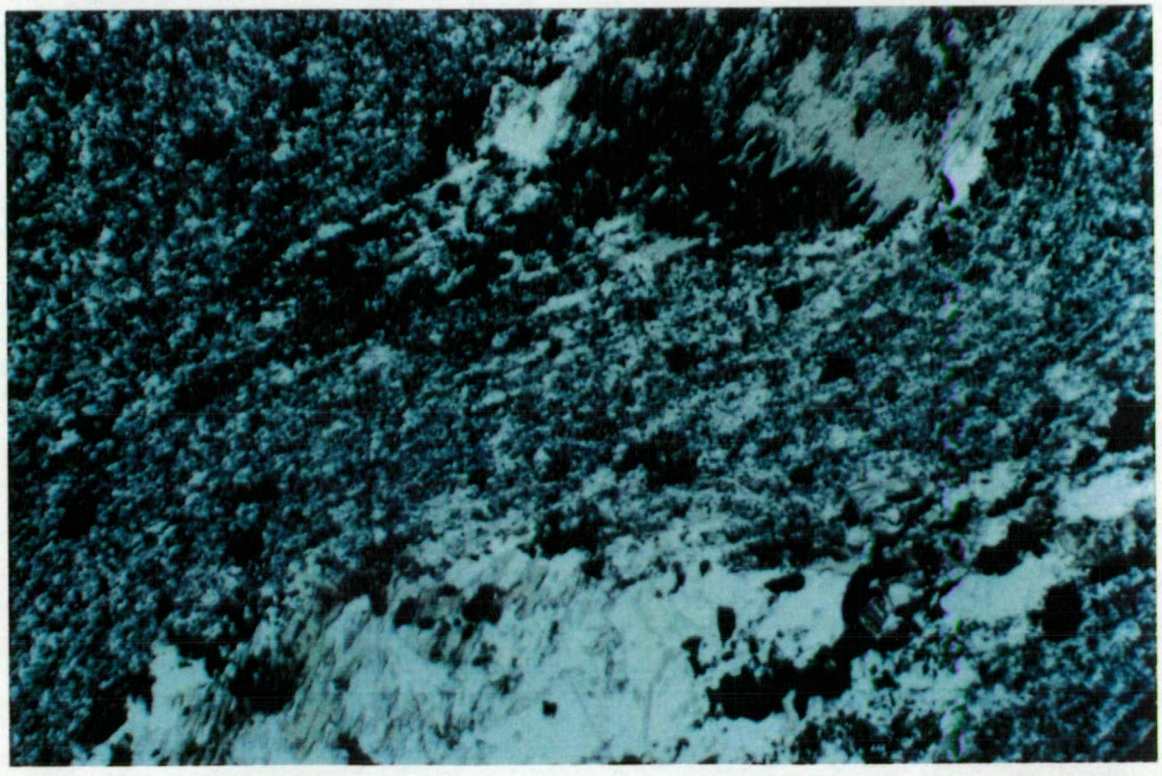

Plate 2.12b: *Photomicrograph (x2.5) of post-S_1 andalusite prophyroblast deformed by S_2 crenulation cleavage. MEQ-22-111.9m.*

Immediately west of the Mount Elliott mine both the fault and accompanying rock units are open flexure folded anticlinally about a north-northeast axis (Garrett *et al.* 1991). The massive skarn alteration is concentrated in the nose and southern limb of the flexure and appears to pinch out along the western limb. However, no evidence of deformational textures related to folding are discerned in the massive skarn, thus implicating a post-flexure age to the alteration event. Albite-hematite and calc-silicate overprinting and invading both the S_1 and S_2 cleavages clearly dates the alteration as post-S_2 (Plate 2.13a).

Alteration at Mount Elliott may have formed over a broad time interval with bleaching, Ca-metasomatism and albite-hematite alteration perhaps forming an early ground-preparation event that enhanced brittle fracturing and brecciation of the shale. Brecciation was followed by calc-silicate-calcite-sulphide alteration. Rotation of both the S_1 and S_2 cleavages in clasts of shale within the breccia dates brecciation as post-S_2, however, its relationship to alteration and flexure-folding is less clear.

The shallowly east-dipping mineralised veins exist as the only recognisable event deforming the alteration (and brecciation?). The cross-cutting pegmatitic veins are undeformed and as such represent the latest event in the area. Numerous low-angle, east-dipping reverse faults are observed in outcrop in the mine vicinity and may represent the surface expression of the mineralised veins at depth (Plate 2.13b). Thrust surfaces are typically gossanous and limonitic and prior to discovery of the lower lenses were not considered significant to ore deposition (Sullivan, 1951).

The en-echelon series of shallow-dipping mineralised veins are constrained between two northwest-trending, steeply-dipping faults; the flexure-folded footwall fault to the west and a 15m wide crush zone to the east (Figure 2.4). The latter includes the discovery gossan and was considered by early workers to host the sulphide mineralisation at Mount Elliott.

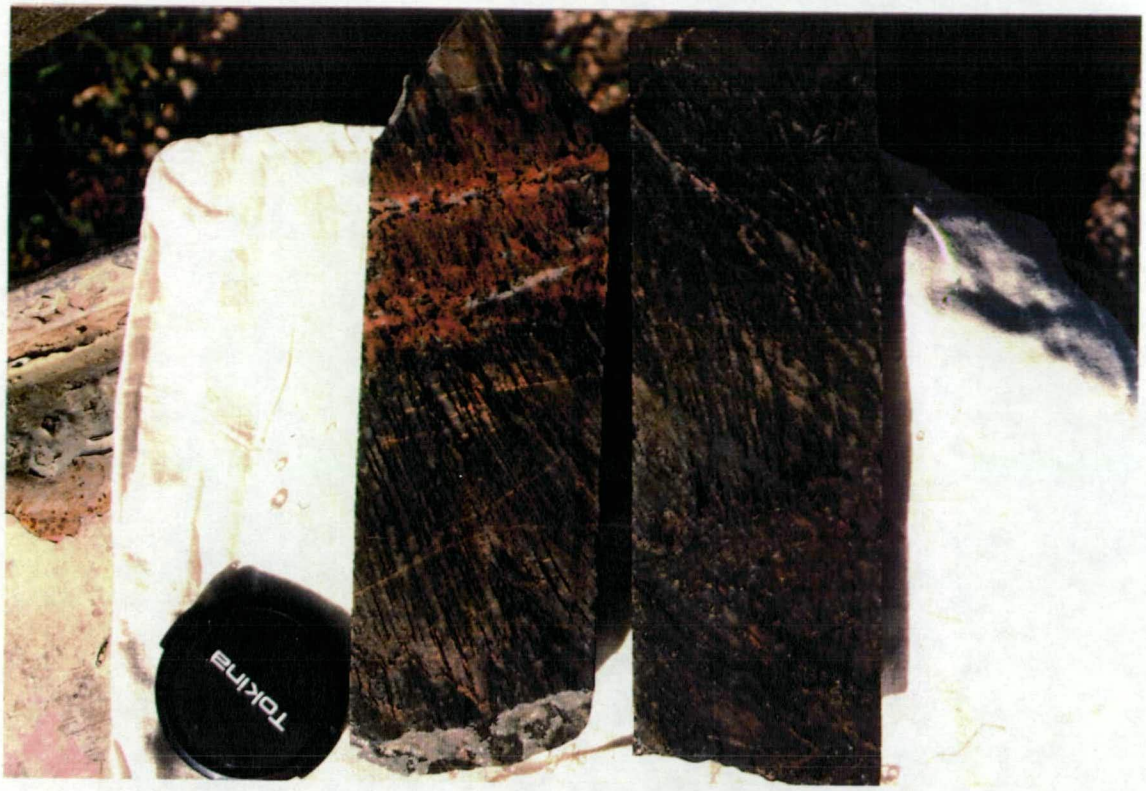

Plate 2.13a: *Early pink albite-hematite plus green calc-silicate alteration cross-cutting & invading both the S_1 and S_2 cleavage planes.*

Plate 2.13b: *Low angle thrust surface in outcropping shale immediately south of Mount Elliott open cut showing limonite alteration at base.*

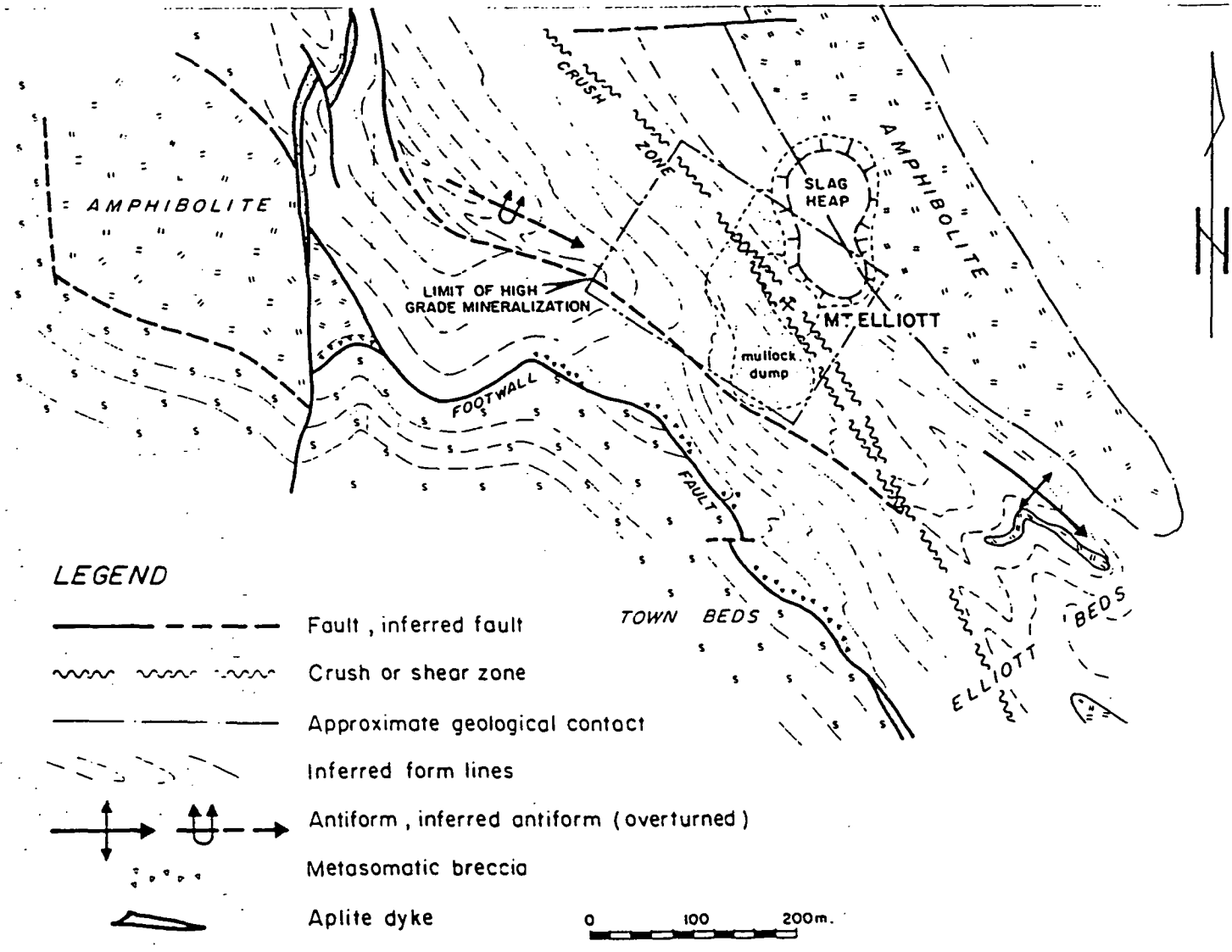

Figure 2.4: *Major structures and surface geology of the Mount Elliott area.*

2.6 Intrusives

Massive amphibolitic bodies are common throughout the Kuridala and Staveley formations. However, their origins and the significance of their close spatial relationship to several mineralised occurrences is poorly understood. Dimo (1975) distinguished four types of amphibolite in the area based on texture, shape and concordance with surrounding sediments, with all types being virtually identical mineralogically.

The Mount Elliott hangingwall amphibolite crops out poorly as a blocky elongate body, subparallel to the enclosing schistosity (Figure 2.4). The amphibolite is a dark green, medium to coarse-grained, equigranular, holocrystalline hornblende-scapolite (after feldspar) biotite-rich rock, with minor chlorite, epidote, quartz and magnetite. Weak metasomatic alteration of scapolite to red albite-hematite, and hornblende to chlorite-epidote occurs throughout. Disseminated sulphides (pyrite and chalcopyrite) interstitial to the calc-silicate phases are rare. The basal contact with the underlying shales, revealed only in percussion chip samples, exhibits minor shearing and silicification (or possibly hornfelsing) into the shale.

The western margin of the Mount Dore granite outcrops approximately 1 km east and 7 km south of the Mount Elliott mine, comprising a well differentiated unit of medium to coarse grained, leucocratic, pink to grey granite and adamellite (Dimo, 1975). Porphyritic orthoclase in a groundmass of granular microcline oligoclose, quartz, hornblende, biotite and accessory apatite-sphene-magnetite (Dimo, 1975).

A granitic influence imparted on the local geology of Mount Elliott is evidenced by the occurrence of large veins (>30cm) of granitic "buck" quartz ± hematite, smaller veins of pegmatitic feldspar and tourmaline, and numerous randomly orientated, strongly discordant dykes and plugs of acid to intermediate composition. The latter are typically pink-white,

very hard, blocky-jointed albite-rich rocks with locally abundant K-feldspar, and fine carbonate in the groundmass interstitial to albite (Dimo, 1975). The dykes are mapped as aplite and typically display weak to moderate chilled margins.

Chapter 3

ALTERATION

3.1 Introduction

Limited bleaching and iron staining of outcropping shales at Mount Elliott provides few clues to the extent, intensity and character of alteration related to the deeply buried copper mineralisation. Diamond drilling beneath the old workings reveals a broad zonation of mappable alteration textures and lithologies; however, complex wallrock alteration and veining relationships has rendered earlier interpretations of the geology complicated and poorly defined. The complexity of skarn morphology and mineralogy at Mount Elliott is characteristic of skarn deposits, caused by host rock lithology and depth of emplacement, as well as the chemistry of the hydrothermal fluids which may change as the system evolves (McMillan *et al.* 1990). This work aims to improve on previous geological interpretations by identifying the physical mechanisms responsible for alteration and characterising the various styles and parageneses of alteration events. Detailed investigation of diamond drill core from some 50 holes forms the dominant component of this study, together with petrography, electron microprobe and whole-rock geochemical analysis.

3.2 Mechanisms of Alteration

The spatial association of alteration mineralogies and textures with zones of intensely fractured and brecciated rock clearly indicates that fracturing is the primary control on localisation of alteration. That is, brittle fracturing and brecciation of the host shale during structural adjustments (ground preparation) has acted to rapidly increase the permeability of the rock, facilitating the introduction of hydrothermal fluids, possibly derived from a crystallising magma at depth. The ability of the fluid to be transported long distances to interact with the shales is a function of pressure and temperature gradients.

The interaction of components in the fluid with reactive minerals in the host rock acts to alter the host rock via infiltration metasomatism (Einaudi *et al.* 1981). The resulting metasomatic reactions, unlike metamorphic ones, produce changes in the amounts of nonvolatile components (e.g., Ca, Fe, Si) in the rock (Einaudi *et al.* 1981). The theory of infiltration metasomatism and diffusion is a difficult one and attempts to successfully model the thermodynamics of metasomatic mineral formation during mass transport by infiltration (e.g., Golubev, 1983; Guy, 1984) typically fail in their complexity. For these reasons the concept is perhaps best appreciated visually at a handspecimen or outcrop scale.

At Mount Elliott the diffusive/infiltrating character of the alteration occurred along cleavage-bedding planes, emanating from a network of fractures and veins (Plate 3.1b). The occurrence of narrow, well defined zones of extreme alteration within fresher rock, together with obvious over-printing relationships, suggests that hydrothermal fluids repeatedly utilised the same pathways during progressive alteration. This is a feature common to a broad range of hydrothermal deposits (Barrett and MacLean, 1991). An important result of the infiltration models is that no gradients occur in the composition of the fluid within zones and infinite gradients in the fluid composition exist at zonal fronts (as opposed to reaction/diffusion skarns where diffusion occurs in response to concentration gradients and no infinite gradients occur at zone boundaries). Hence, the resulting alteration sequence displays abrupt zonal boundaries and the composition of minerals within zones remains constant (Einaudi *et al.* 1981).

Later retrograde alteration occurs as a result of hydration of prograde skarn (to minerals such as chlorite and epidote) plus infilling of vughs and cavities with lower temperature phases (400-200°C) such as calcite, magnetite and sulphide. This process may be effected by either insitu cooling of the hydrothermal magmatic fluid or via interaction with a descending, cool meteoric fluid. At Mount Elliott the former is considered to be the dominant retrograde alteration process.

Plate 3.1a: *Early bleaching and Ca-metasomatism of black shales (Elliott Beds). Dark bands biotite-rich, pale bands quartz carbonate.*

Plate 3.1b: *Paragenetic sequence of infiltration metasomatic alteration in the outer carapace. Bleached shale overprinted by pink albite (hem) along fractures, followed by green clinopyroxene (diop-hed) and rare sulphide.*

Plate 3.1c: *Photomicrograph (x2.5) of calc-silicate banding in outer carapace. Anhedral form suggests replacement of blebby calcite-rich horizons. MEQ-25-232.3m.*

Tokina
Tokina

3.3 Alteration Paragenesis, Geochemistry and Zoning

3.3.1 The Outer Carapace

The paragenesis of alteration within the outer carapace is best illustrated in Plate 3.1. Early Ca-metasomatism of the shales typically produces a thinly banded rock comprising pale quartz-rich bands plus quartz-rich bands with interstitial anhedral calcite (± fluorite), interspersed with darker biotite-rich bands with quartz and rare carbonate (Plate 3.1a). The fluorite occurs in fine calcite-filled fractures and as rare to common fine disseminations within the shale. A possible formation reaction is:

$$CaC0_3 + 2HF \text{ <-> } CaF_2 + H_2C0_3$$

Calcite was added metasomatically since it is not present in primary shale and carbonate concentrations decrease away from fractures.

The outer carapace is characterised by the introduction of orange-pink hematitic albite within fractures and fine veinlets (eg. Plate 3.1b). The albite noteably forms thin to broad (<10cm) selvages of massive alteration adjacent to fractures and also persists along cleavage planes normal to the fractures. The ability of the albite to destroy the shale foliation has significant implications to later discussion of the origin of the massive skarn.

Calc-silicate alteration, dominated by dark green clinopyroxene, overprints albite and typically utilises the fractures occupied by albite (Plate 3.1b). From the fractures the calc-silicate invades the shale foliation with alteration fronts characteristically extending further from the fracture than the albite alteration. In thin section, the blebby, anhedral calc-silicate mineralisation is developed in discrete bands (Plate 3.1c.) and is interpreted to represent alteration after calcite;

$$CaC0_3 + (Mg,Fe)^{2+} + 2SiO_2 + 2H_20 \text{ <-> } Ca(Mg,Fe)Si_20_6 + 4H^+ + H_2CO_3$$

Lesser calc-silicate phases identified with this stage of alteration include sphene ($CaTiSiO_5$) and scapolite $(Na, Ca, K)_4 Al_3(Al, Si)_3Si_6O_{24}(Cl, CO_3, SO_4, OH)$. Fluorite is noticably reduced to absent in calc-silicate altered rocks. Towards the fractures and veinlets the calc-silicate phases increase in both grain size and concentration, but remain anhedral in form. Finally, the calc-silicates may be overprinted by late-stage retrograde calcite and sulphide mineralisation occupying the core of fractures and veins, with weak-moderate infiltration of the shale foliation. Within the shale, sulphides (dominantly pyrite ± pyrrhotite) generally form on the margins of clinopyroxene and calcite grains.

Hence the paragenetic sequence of alteration assemblages, as defined in Plate 3.1b. is interpreted as follows;

bleaching->Ca metasomatism + F->albite-hematite->calc-silicate->Calcite-sulphide ± mag

producing a cream-pink-green-brown colour-banded rock characteristic of the outer carapace. Note that biotite-rich bands remain relatively unaltered. At depth, towards the base of the carapace, magnetite begins to occur with calcite and sulphides in the retrograde assemblage, generally at the expense of pyrrhotite.

Interestingly, the albite, or red-rock alteration, is not part of the pegmatitic breccia matrix-vein assemblage of calc-silicate+calcite+sulphide, suggesting it is associated with an earlier fracturing event. Susequent brecciation might have reactivated the existing fracture network thus allowing calc-silicate (± calcite-sulphide) to invade the fractures and adjacent country rock. However, an early calc-silicate mineralisation event prior to brecciation, is also likely.

Increased fracturing and brecciation with depth facilitated greater fluid access to a larger surface area of reactible rock resulting in increased alteration intensity and a progressive destruction of the shale fabric (Plate 3.2). As alteration of the shale intensifies massive crystalline development of albite and clinopyroxene can be recognised within the shale

Plate 3.2: *Progressive alteration in the outer carapace from (L-R) early fracturing to ultimately massive coarse grained skarn. The speciments are arranged according to paragenetic alteration intensity and not in special sequence.*

proximal to fluid pathways, until ultimately an albite-clinopyroxene-rich rock of massive fabric is developed (Plate 3.2). Small blocks of massive skarn (<1-2m) are not uncommon in the outer carapace, particularly near the contact with the massive skarn, and are typically less developed than the main body of massive skarn (ie., weak development of retrograde alteration).

Locally this alteration sequence does not form a progressive zoned pattern, but rather is patchy and irregular, reflecting the necessary fracture/vein-infiltration-diffusion control on alteration. On a deposit scale, however, zoning of alteration mineralogies and textures is clearly evident (ie., from bleached shales -> brecciated/veined altered shales -> massive skarn).

3.3.2 Massive Skarn

Alteration in the medium grained skarn unit, the core of the alteration system at Mount Elliott, differs from that in the enveloping carapace only in terms of intensity and texture. Mineralogies and paragenesis remain the same. Remnant pods of prograde skarn comprises predominantly massive interlocking sieve-textured laths of medium to coarse grained albite. The prominent orange-red colour of the albite, pale brown in thin section, is attributed to an ubiquitous dusting of very fine hematite. Microprobe compositions of albites are given in Table 3.1.

Where least abundant clinopyroxene occurs along fine fractures in the albite rock, but as abundance increases a characteristic pervasive spotty fabric develops. Large anhedral clusters of calc-silicate grains progressively overprint the albite fabric. In detail, advancement of the alteration is blocked at albite crystal junctions which has acted to delineate individual albite grains within the enclosing skarn (Plate 3.3a). Calcite and K-feldspar, in apparent equilibrium with the calc-silicate, occupies interstices between albite crystals and internally replaces the albite, and further highlights individual albite crystals

	1	2	3	4	5	6	7
SO3	0.0213	0.1510	0.0000	0.0000	0.0000	0.0649	0.1081
P205	0.0606	0.0000	0.0000	0.0021	0.0404	0.0404	0.0331
Si02	65.8815	68.6192	65.6441	68.1270	67.3072	67.7301	67.8900
Ti02	0.0129	0.0206	0.0000	0.0050	0.0183	0.0046	0.0184
Al203	18.6510	19.1135	20.6410	19.1271	20.0470	19.8933	19.3837
Cr203	0.0000	0.0046	0.0000	0.0000	0.0634	0.0000	0.0182
Mg0	0.2206	0.0054	0.0128	0.0000	0.0344	0.0021	0.5693
Ca0	0.1646	0.1754	2.1650	0.2471	0.5073	0.3069	0.1579
Mno	0.0000	0.0347	0.0193	0.0000	0.0000	0.0000	0.0784
Fe0	0.7188	0.0532	0.1028	0.0841	0.9065	0.1612	0.5682
Ni0	0.0000	0.0000	0.0343	0.0000	0.0000	0.0609	0.0000
Na20	8.5300	11.0098	10.1635	11.1526	10.8425	11.0646	10.9326
K20	3.9969	0.0671	0.1106	0.0432	0.1245	0.0114	0.0395
Cl	0.0000	0.0212	0.0432	0.0000	0.0355	0.0000	0.0089
total	98.2583	99.2709	98.9974	98.7862	99.8805	99.3403	99.8041
cations	24.0000	24.0000	24.0000	24.0000	24.0000	24.0000	24.0000

1 MEQ-14-243.1
2 MEQ-14-212.3
3 "
4 "
5 MEQ-14-267.8
6 MEQ-14-270.0
7 "

Table 3.1: *Electron microprobe composition of medium grained skarn albites.*

(Plate 3.3b). Continuing replacement of the albite by calc-silicates, calcite-K-feldspar and later retrograde phases produces a pseudo-igneous texture (Plate 2.7).

Dark green clinopyroxene clearly dominates the prograde calc-silicate assemblage and is associated with scapolite, sphene, and rare apatite [$Ca_5(F,Cl)(PO_4)_3$]. A ternary plot of clinopyroxene compositions (Table 3.2, Figure 3.1) shows them to form in the diopside-hedenbergite solid solution series typical of prograde anhydrous alteration in calcic Cu-Fe-Au skarn deposits (McMillan *et al.* 1990). The occurrence of scapolite in the skarn and its abundance in the outer carapace suggests a significant Na-Cl metasomatic event coeval with "cpx"(1) mineralisation. Compositions of scapolite, sphene and apatite, plus calcite and K-feldspar, are given in Appendix 1. Although bands of spessartine-almandine are common throughout the footwall schist, skarn alteration at Mount Elliott is unique for its lack of garnet, a mineral characteristically associated with all styles of mineralised and unmineralised skarn deposits. Rare crystals of pink-brown garnet (possibly after apatite because of their crystal form) have been recognised in pegmatite matrix-veins in the outer carapace, usually rimming bladed "cpx" crystals.

Retrograde alteration, probably formed by insitu cooling of the hydrothermal magmatic fluid, is ubiquitous throughout the medium grained skarn unit. Magnetite overprints all prograde phases and clearly precedes the introduction of sulphides, occurring as blebby disseminations and infilling or rimming small vughs. Sulphides (dominantly chalcopyrite plus pyrite) commonly infill fractures in magnetite but typically occur interstitial to and replacing the prograde albite+calc-silicate assemblage. Vugh fillings of sulphide are also common and usually associated with magnetite and calcite.

Late stage retrograde alteration by hydrous phases is dominated by chlorite which attacks all calc-silicate minerals (preferentially scapolite) and commonly infills fractures in magnetite

(1) "cpx" represents a member of the diopside-hedenbergite solid solution.

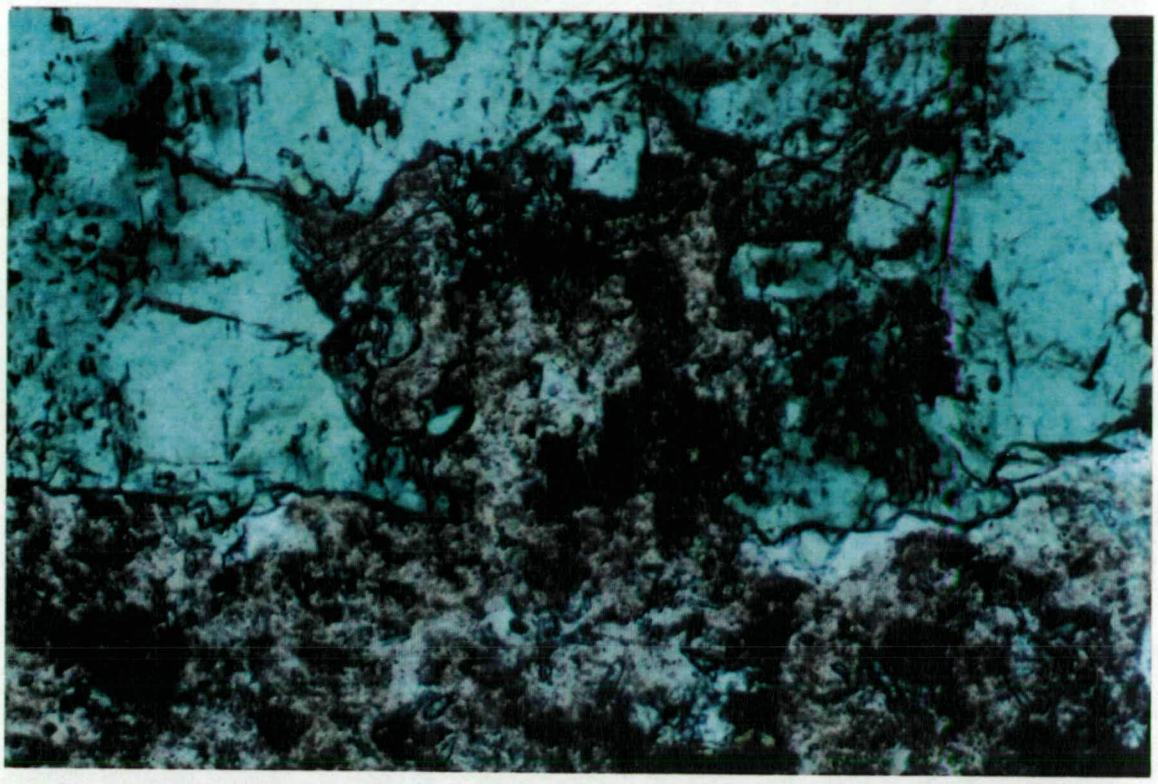

Plate 3.3a: *Photomicrograph (x10) showing replacement of sieve-textured albite by "cpx" (green). MEQ-14-270m.*

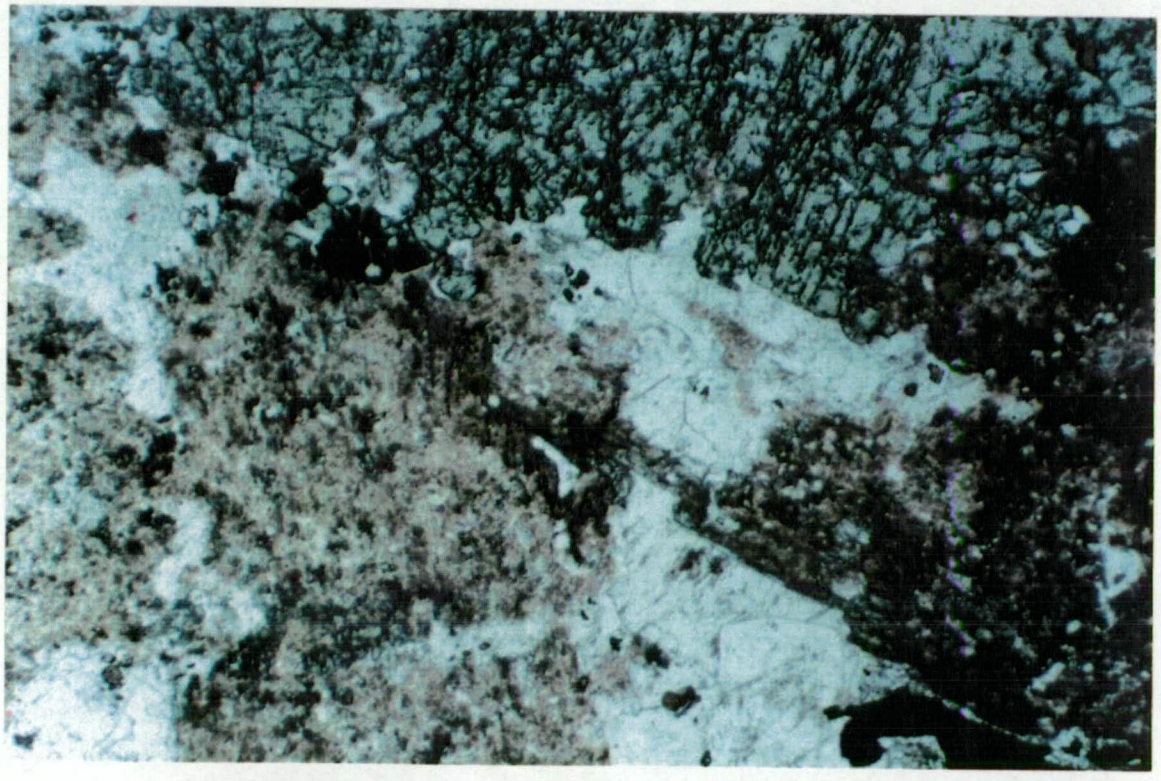

Plate 3.3b: *Photomicrograph (x5) of Cpx-Ca-K-feld replacement of albite, MEQ-16-290.4m.*

	1	2	3	4	5	6	7	8	9	10	11	12	13	14	15
S03	0.0201	0.0000	0.0202	0.0000	0.0810	0.0000	0.0000	0.0202	0.0000	0.1653	0.0000	0.0000	0.0407	0.0407	0.0204
P205	0.3102	0.4894	0.4422	0.4796	0.4759	0.4265	0.2237	0.4154	0.4356	0.2624	0.2365	0.4290	0.4118	0.4645	0.4233
Si02	51.4579	52.3740	52.3441	52.8509	52.7107	53.1042	53.7170	52.7693	53.1544	54.6190	53.4138	52.5158	52.3494	52.7369	52.7746
Ti02	0.0358	0.0893	0.0514	0.0364	0.0515	0.0091	0.0400	0.0000	0.0000	0.0000	0.0000	0.0167	0.0654	0.0152	0.0563
Al203	0.6665	1.0580	1.0133	0.2364	0.9159	0.2375	0.6339	0.3166	0.2616	0.8688	0.6532	0.5873	0.9532	0.6884	0.7932
Cr203	0.0532	0.0000	0.0000	0.0000	0.0000	0.0486	0.0000	0.0000	0.0000	0.0307	0.0000	0.0354	0.0000	0.0089	0.0089
Mg0	10.7590	11.2865	11.2052	12.1265	11.5755	12.0608	12.5862	11.9895	12.3915	16.6442	12.4591	12.3181	11.5756	11.9274	11.8026
Ca0	22.6101	19.4655	18.9336	20.0518	19.4532	19.7330	11.3066	20.5777	20.4408	10.6843	10.7621	19.3300	19.1768	19.8647	19.5934
Mn0	0.1526	0.1222	0.0215	0.0704	0.0736	0.1052	0.2349	0.1719	0.2817	0.1159	0.0925	0.1138	0.0896	0.1912	0.0332
Fe0	11.2092	10.4133	10.4735	9.8293	10.2990	9.5853	17.1789	10.5065	9.3486	11.7232	17.7699	9.8495	10.7500	9.9493	10.3278
Ni0	0.0225	0.0000	0.0037	0.0000	0.0000	0.0000	0.0818	0.0149	0.0265	0.0000	0.0560	0.0263	0.1201	0.0338	0.0000
Na20	0.9987	0.9456	0.9419	0.4121	0.8845	0.5061	0.0988	0.7915	0.6214	0.5053	0.1166	0.8287	0.9141	0.8185	0.9251
K20	0.0000	0.0088	0.0078	0.0118	0.0000	0.0000	0.0404	0.0020	0.0000	0.1480	0.5850	0.0246	0.0000	0.0000	0.0000
Cl	0.0066	0.0167	0.0335	-	0.0084	-	0.0084	-	-	0.0512	0.1100	-	-	0.0084	0.0337
total	98.3009	96.2655	95.4844	96.1053	96.5273	95.8204	96.1490	97.5786	96.9618	95.8068	95.7035	96.0754	96.4466	96.7461	96.7850
cations	24.0000	24.0000	24.0000	24.0000	24.0000	24.0000	24.0000	24.0000	24.0000	24.0000	24.0000	24.0000	24.0000	24.0000	24.0000

Cations based on 24 (0,Cl)

Cations based on 24 (0,Cl)

Si	7.9330	8.0980	8.1440	8.1610	8.1120	8.2060	8.3320	8.0840	8.1390	8.2690	8.3340	8.1160	8.0900	8.1050	8.1107
Fe	1.4450	1.3470	1.3630	1.2690	1.3260	1.2390	2.2290	1.3470	1.1970	1.4840	2.3190	1.2730	1.3890	1.2790	1.3270
Mn	0.0200	0.0160	0.0030	0.0090	0.0100	0.0140	0.0310	0.0220	0.0370	0.0150	0.0120	0.0150	0.0117	0.0250	0.0040
Mg	2.4720	2.6010	2.5990	2.7910	2.6550	2.7780	2.9100	2.7380	2.8280	3.7560	2.8980	2.8380	2.6670	2.7350	2.7040
Ca	3.7350	3.2250	3.1562	3.3170	3.2080	3.2670	1.8790	3.3530	1.7330	1.7990	3.2010	3.2010	3.1750	3.2710	3.2260
Total	16.0800	15.8390	15.8030	15.7830	15.8180	15.7610	15.5790	15.9200	15.8450	15.6450	15.5680	15.8690	15.0620	15.8520	15.8570

Mole %

Mole %

Table 3.2: *Electromicroprobe compositions of clinopyroxenes from medium grained skarn. 1-5: MEQ-10-285.6 6-10: MEQ-14-223.0 MEQ-14-267.8 MEQ-14-270.0*

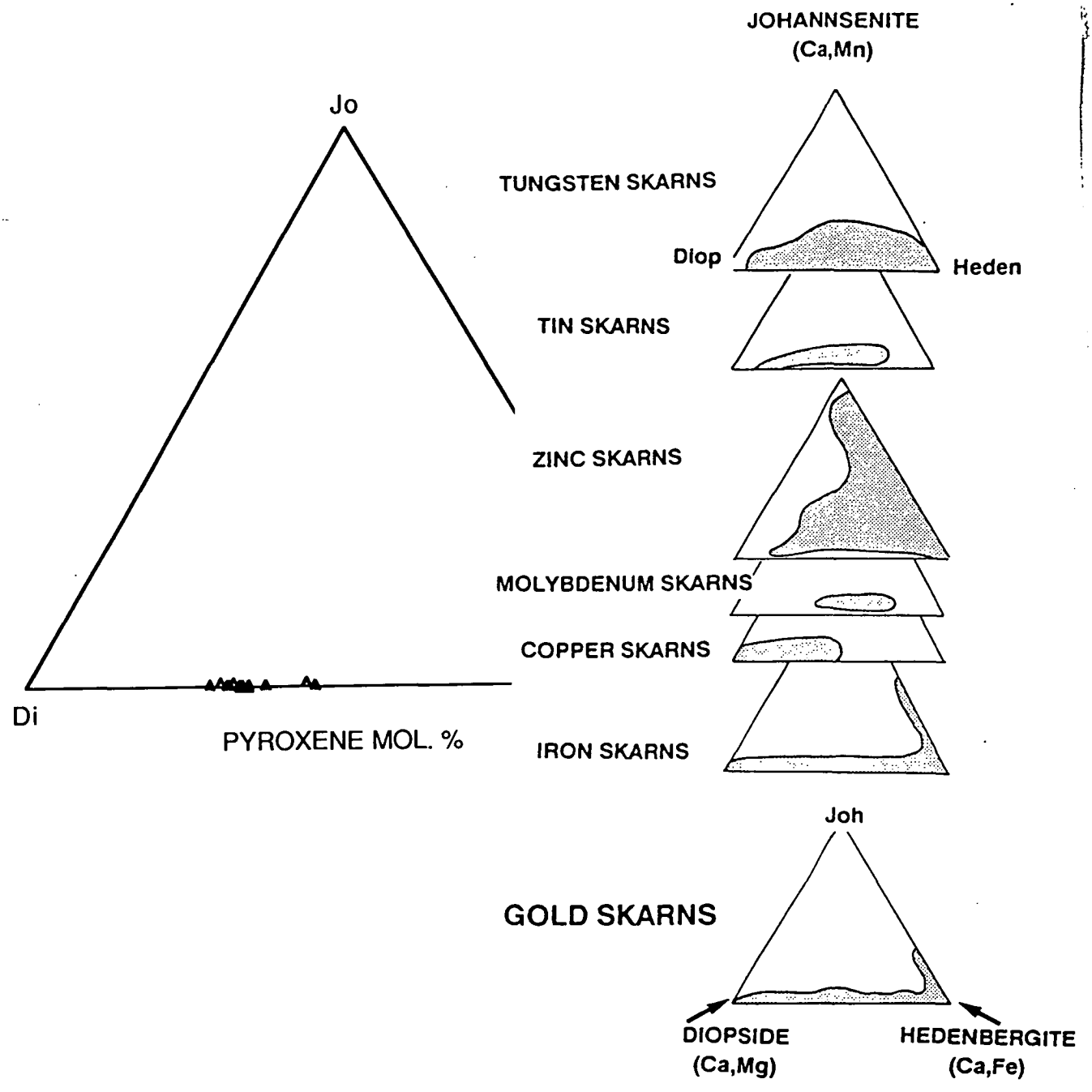

Figure 3.1: *Ternary plot of clinopyroxene compositions.*

(Plate 3.4a). Epidote is less frequent, usually forming large aggregates replacing calc-silicate phases (Plate 3.4b).

In summary, a paragenesis of alteration for the medium grained skarn is:

albite-hematite -> calc-silicate-calcite-K-feld -> magnetite-calcite-sulphide (±chl-epi).

Although the intensity of alteration varies considerably throughout the massive skarn, a broad zonation is evident and best reflected by magnetite concentration. At the top of the skarn (pink-green albite-cpx rock) a notable lack of magnetite (<5%), associated with weak Cu-mineralisation and absence of pseudo-breccia fabric, grades to <20-40% magnetite at the base of the skarn (green-black ± pink, albite poor, calc-silicate-magnetite-rich rock). The magnetite content also tends to increase at depth with the deepest holes intersecting ironstone-grade magnetite skarn (>50-60% magnetite) in places.

3.4 Geochemistry of Alteration.

A suite of twenty-two drill core samples representing various lithologies and alteration stages was selected and analysed for a range of major, trace and rare earth elements. The samples were prepared and analysed commercially by Australian Laboratory Services (ALS) in Brisbane. Results are shown in Table 3.3 and field descriptions of each sample are given in Appendix 2. For consistency, samples were taken from the same drill hole where possible, and are arranged in order of increasing alteration intensity.

3.4.1. Whole Rock Geochemistry - Major Elements

Geochemical features of the metasomatic rocks at Mount Elliott generally reflect the variable overprinting of bleaching, albitization, calc-silicate development and magnetite-sulphide mineralisation. The major geochemical expression of bleaching in the altered shales unit is

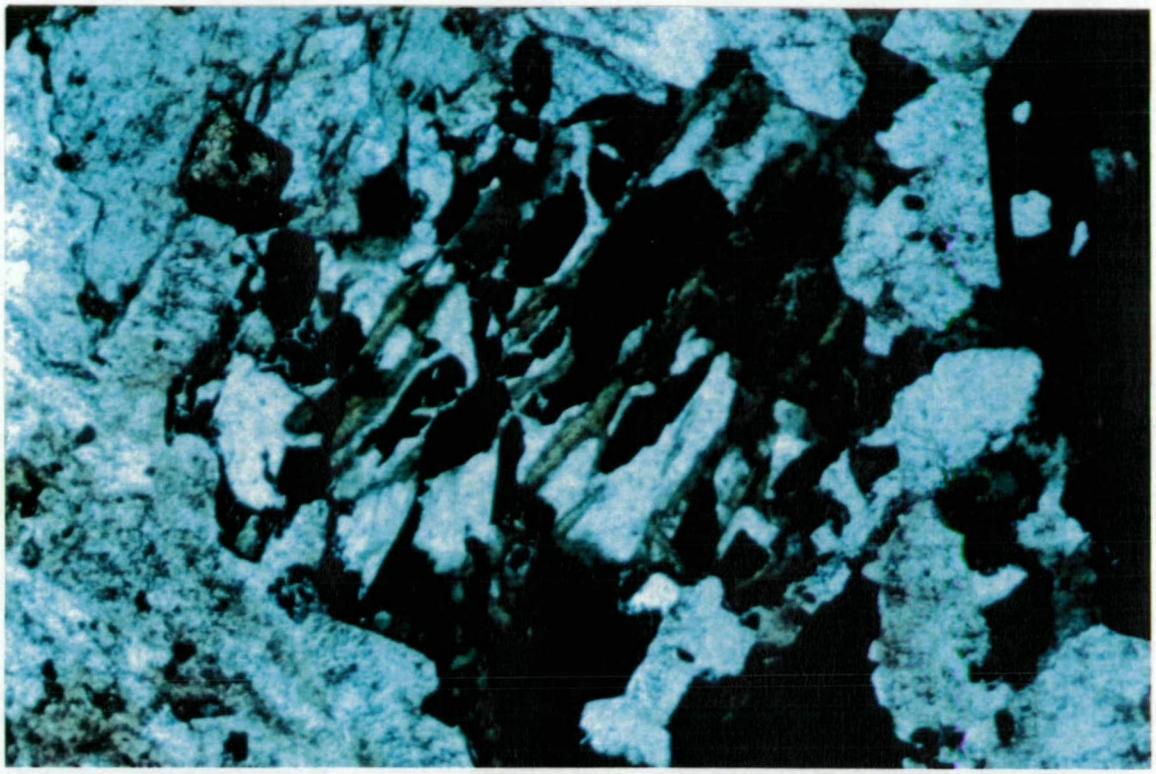

Plate 3.4a: *Photomicrograph (x5) showing fractured magnetite infilled by calcite-chlorite. MEQ-14-260m.*

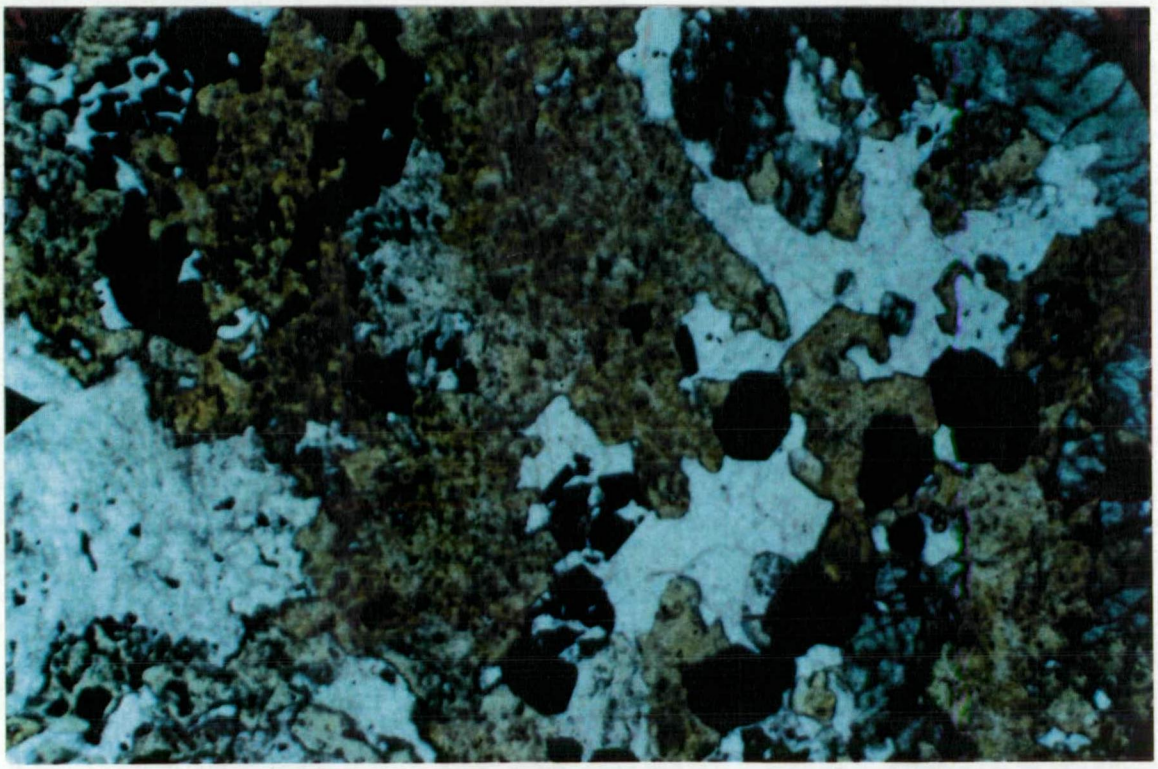

Plate 3.4b: *Photomicrograph (x2.5) of epidote alteration (yellow) replacing cpx (green) MEQ-21-273.8m.*

	400704	400711	400721	400706	400707	400708	400709	400710	400723	400712	400713	400715	400716	400717	400720	400727	400725	400726	400728	400714	400705	DET.LIMIT
Si02(%)	69.00	65.20	50.60	66.00	58.60	66.40	68.30	66.60	72.60	65.00	63.30	66.10	53.80	56.70	7.15	17.50	63.40	58.50	46.40	49.00	50.60	0.01
Al203(%)	16.30	15.30	13.60	15.80	18.40	14.90	14.50	15.10	12.80	15.90	16.10	16.30	17.10	14.20	0.06	4.34	19.00	18.90	12.90	13.80	0.99	0.01
Fe203(%)	1.39	1.85	10.30	1.17	1.33	0.83	1.04	0.97	1.31	2.71	4.81	1.96	7.38	5.60	55.50	70.80	8.20	8.88	17.40	14.40	14.70	0.01
Ca0(%)	0.98	3.36	10.10	3.50	2.93	3.00	3.28	3.59	2.98	1.84	3.38	2.05	7.62	9.17	4.37	3.21	0.44	1.07	9.24	10.80	21.80	0.01
Mg0(%)	1.64	3.30	3.76	2.35	3.51	2.69	2.64	2.84	1.46	2.51	2.26	2.38	3.16	3.59	0.86	2.00	1.87	1.53	6.26	6.41	10.40	0.01
Ti02(%)	0.54	0.69	0.57	0.60	0.72	0.60	0.57	0.58	0.52	0.68	0.68	0.77	0.77	0.47	0.02	0.36	0.87	0.78	1.69	1.56	0.02	0.01
Na20(%)	8.69	3.37	5.23	6.64	4.11	4.60	5.35	4.83	5.20	5.21	6.50	5.26	5.64	7.44	0.08	1.25	0.74	5.38	4.23	1.99	0.74	0.01
K20(%)	0.26	3.19	1.15	1.87	5.99	2.62	2.29	3.86	1.23	5.37	2.33	4.23	2.33	1.67	0.00	0.45	4.32	3.26	1.28	1.05	0.02	0.01
P205(%)	0.22	0.05	0.06	0.13	0.13	0.08	0.09	0.09	0.07	0.03	0.03	0.04	0.02	0.03	0.18	0.02	0.04	0.03	0.02	0.02	0.08	0.01
Mn0(%)	0.01	0.00	0.06	0.01	0.00	0.00	0.00	0.00	0.02	0.00	0.03	0.01	0.04	0.05	0.02	0.01	0.21	0.06	0.12	0.26	0.15	0.01
Ba0(%)	0.00	0.03	0.02	0.02	0.06	0.03	0.02	0.04	0.00	0.06	0.03	0.06	0.03	0.03	0.00	0.02	0.10	0.08	0.02	0.00	0.00	0.01
Zr02(%)	0.03	0.03	0.01	0.03	0.03	0.03	0.03	0.03	0.00	0.03	0.03	0.02	0.02	0.02	0.00	0.00	0.00	0.00	0.00	0.02	0.01	0.01
L.0.I(%)	1.05	3.86	1.18	1.71	4.09	4.45	1.98	1.45	0.66	0.91	0.66	1.00	0.83	0.76	19.90	1.50	1.81	1.67	0.59	0.87	0.15	0.01
Cu (ppm)	80.00	180.00	8750.00	115.00	300.00	120.00	140.00	100.00	2900.00	510.00	3850.00	310.00	4250.00	990.00	9850.00	6050.00	210.00	2750.00	210.00	140.00	3950.00	5.00
Zn (ppm)	30.00	0.00	15.00	15.00	60.00	35.00	5.00	25.00	10.00	5.00	20.00	15.00	10.00	5.00	45.00	30.00	80.00	20.00	15.00	75.00	20.00	5.00
Ag (ppm)	<1	<1	<1	<1	<1	<1	<1	<1	<1	<1	<1	<1	<1	<1	<1	<1	<1	<1	<1	<1	<1	1.00
As (ppm)	9.00	11.00	12.00	6.00	9.00	10.00	9.00	9.00	7.00	8.00	9.00	9.00	10.00	11.00	18.00	12.00	8.00	9.00	17.00	22.00	15.00	1.00
Bi (ppm)	<5	<5	<5	<5	<5	<5	<5	<5	<5	<5	<5	<5	<5	<5	10.00	<5	<5	<5	<5	<5	<5	5.00
Sb (ppm)	<5	<5	<5	<5	<5	<5	<5	<5	<5	<5	<5	<5	<5	<5	<5	<5	<5	<5	<5	<5	<5	5.00
Mo (ppm)	60.00	5.00	0.00	35.00	15.00	15.00	20.00	20.00	10.00	5.00	5.00	15.00	5.00	0.00	5.00	5.00	0.00	25.00	0.00	0.00	0.00	5.00
Co (ppm)	0.00	0.00	20.00	0.00	10.00	0.00	0.00	0.00	10.00	15.00	30.00	20.00	45.00	15.00	1050.00	230.00	20.00	15.00	35.00	35.00	55.00	5.00
Ni (ppm)	0.00	10.00	15.00	0.00	10.00	55.00	10.00	10.00	5.00	25.00	20.00	25.00	45.00	10.00	490.00	170.00	45.00	40.00	50.00	60.00	20.00	5.00
Sr (ppm)	0.00	40.00	60.00	40.00	30.00	40.00	50.00	40.00	30.00	20.00	30.00	20.00	60.00	50.00	10.00	20.00	10.00	40.00	100.00	70.00	10.00	10.00
V (ppm)	90.00	90.00	110.00	130.00	150.00	110.00	130.00	120.00	100.00	90.00	100.00	120.00	90.00	40.00	10.00	350.00	70.00	60.00	350.00	310.00	70.00	10.00
Se (ppb)	100.00	300.00	0.00	0.00	200.00	0.00	100.00	150.00	0.00	600.00	100.00	950.00	400.00	50.00	33500.00	3600.00	0.00	50.00	250.00	400.00	250.00	50.00
Te (ppb)	50.00	0.00	0.00	0.00	0.00	0.00	50.00	0.00	0.00	0.00	0.00	0.00	0.00	0.00	4800.00	450.00	0.00	150.00	0.00	0.00	0.00	50.00
Sn (ppm)	<5	<5	10.00	<5	<5	<5	<5	<5	<5	<5	<5	<5	<5	<5	<5	<5	<5	<5	<5	<5	<5	5.00
W (ppm)	<10	<10	<10	<10	<10	<10	<10	<10	<10	<10	<10	<10	<10	<10	<10	<10	<10	<10	<10	<10	<10	10.00
Pd (ppm)	<0.01	<0.01	<0.01	<0.01	<0.01	<0.01	<0.01	<0.01	<0.01	<0.01	<0.01	<0.01	<0.01	<0.01	<0.01	<0.01	<0.01	<0.01	<0.01	<0.01	<0.01	10.00
Au (ppm)	0.00	0.00	0.42	0.02	0.00	0.00	0.00	0.00	0.00	0.06	0.11	0.00	0.37	0.00	1.95	2.02	0.00	0.12	0.00	0.00	0.42	0.01
F (ppm)	510.00	1320.00	120.00	9440.00	1570.00	1220.00	2430.00	3140.00	2530.00	1150.00	830.00	1270.00	280.00	90.00	150.00	100.00	550.00	370.00	300.00	360.00	60.00	20.00
Hg (ppb)	<50	<50	<50	<50	<50	<50	<50	<50	<50	<50	<50	<50	<50	<50	<50	<50	<50	<50	<50	<50	<50	50.00
Rb (ppm)	20.00	156.00	56.00	84.00	136.00	144.00	112.00	168.00	60.00	1680.00	88.00	176.00	78.00	18.00	14.00	34.00	218.00	158.00	86.00	50.00	6.00	2.00
Y (ppm)	12.00	14.00	6.00	12.00	16.00	12.00	12.00	14.00	10.00	12.00	14.00	12.00	16.00	20.00	0.00	0.00	16.00	14.00	4.00	4.00	0.00	2.00
Nb (ppm)	10.00	14.00	6.00	12.00	16.00	12.00	12.00	12.00	10.00	12.00	14.00	10.00	16.00	20.00	0.00	0.00	16.00	16.00	4.00	4.00	0.00	2.00
U (ppm)	32.00	0.00	0.00	28.00	16.00	12.00	20.00	20.00	8.00	4.00	12.00	8.00	12.00	4.00	0.00	0.00	0.00	8.00	0.00	0.00	0.00	4.00
Th (ppm)	12.00	12.00	8.00	12.00	12.00	12.00	12.00	12.00	8.00	8.00	12.00	8.00	12.00	0.00	8.00	0.00	16.00	20.00	0.00	0.00	0.00	4.00

ALTERED SHALES:

400707	MEQ-46-112.3	unaltered shale
400721	MEQ-50-84.6	unaltered shale
400711	MEQ-46-135.5	unaltered shale
400708	MEQ-46-121.2	weak altered shale
400706	MEQ-46-112.5	bleached shale
400704	MEQ-46-57.7	bleached shale
400709	MEQ-46-121.3	bleached si shale
400710	MEQ-46-121.4	bleached c/s shale

OUTER CARAPACE BANDED SHALES

400723	MEQ-50-131.4	qtz-ca altered shale
400715	MEQ-46-180.6	alb-ca no cpx
400712	MEQ-46-143.2	alb-ca qtz no cpx
400713	MEQ-46-163.4	alb±qtz-ca Minor cpx
400716	MEQ-46-208.2	alb+ cpx

MEDIUM GRAINED SKARN

400717	MEQ-46-214.5	60% albite No mag
400720	MEQ-46-234.9	40-50% albite <10% mag
400727	MEQ-46-271.1	<30% albite 30% cpx 30% mag

FW SCHIST

400725	MEQ-16-319.2	unaltered FW schist
400726	MEQ-16-314.6	albite FW schist

FINE SKARN

400728	MEQ-21-265.4	Fine grained skarn

HW SKARN

400714	MEQ-46-163.8	Hangingwall skarn - similar to above
400705	MEQ-46-105.8	Coarse clinopyroxene

Table 3.3: *Wholerock compositions of drill core samples of various alteration stages and lithologies at Mount Elliott.*

an increase in SiO_2 with a corresponding decrease in L.O.I. (graphite). K_2O content decreases whereas CaO is somewhat erratic, although generally increasing.

Alteration of banded shales in the outer carapace is characterised by the introduction of albite, and later by calc-silicates (predominantly "cpx"). Albite mineralisation is evidenced by an initial increase in Na_2O content associated with increasing Al_2O_3 and decreasing SiO_2 (quartz dissolution). Late replacement of albite by calc-silicate alteration acts to reduce Na_2O and increase Fe_2O_3, MgO and CaO. A possible genetic link between albitization and quartz dissolution has been recognised for albite-rich, silica-depleted metasomatic rocks in northeast Queensland (Charoy and Pollard, 1989) which has important implications for massive albite development in previously thinly banded rocks at Mount Elliott. As observed in the shales of the outer carapace, Na-metasomatism of the Town Beds is almost completely accommodated by SiO_2 depletion. Here also, the massive albitization overprints a previously strongly schistose fabric.

Overprinting of albite by calc-silicate plus magnetite and sulphides in the massive medium grained skarn is reflected in severe depletions of SiO_2, Na_2O and Al_2O_3 accompanied by markedly increasing Fe_2O_3 content. CaO content is also significantly reduced in the magnetite-sulphide zone.

The wholerock geochemistry of a sample of fine grained skarn is remarkably similar to that of foliated calc-silicate-rich rock (skarn) sampled in the hangingwall shale. Both rock types are strongly depleted in SiO_2 content and enriched in Fe_2O_3, CaO and MgO and TiO_2, reflecting calc-silicate dominant mineralogies. Trace and rare earth element geochemistry are also similar with depleted Cu contents and anomalous Co, V and Se concentrations. Slightly higher Na_2O and Sr contents and lower SiO_2 in the fine grained skarn is attributed to higher albite and/or scapolite concentrations.

3.4.2 Trace and Rare Earth Elements

Elevated concentrations of the metals Cu, Co, Ni and Au are clearly related to late-stage sulphide mineralisation. As expected, anomalous Au exhibits a positive correlation with Cu hosted in chalcopyrite (Figure 3.2). Co shows a strong positive correlation with Ni. A similar trend for Ni and Fe_2O_3 suggests that both Ni and Co occur as trace elements in pyrrhotite and pyrite (Figure 3.3).

Surprisingly high concentrations of Se and Te were detected in samples of well developed massive skarn. Although the highest anomalies correlate with high Cu values, and both Se and Te are considered possible complexing ligands for transporting metal ions, anomalous Se contents in outer carapace samples do not neccessarily correlate with Cu. Anomalous concentrations of Ag, Bi, Sb, Sn and W were not detected.

Clearly the most important trace element trend, in terms of exploration significance, is that of fluorine, which displays a strong antipathetic relationship with Fe_2O_3 (Figure 3.4). Fluorite, concentrated in bleached shales distal to the Cu-Au mineralisation is progressively overprinted with depth by the advancing skarn alteration (reflected by increasing iron concentration). Remobilisation of F ahead of the advancing iron front is also probable. The result is a high grade fluorine halo, several hundred metres wide, enveloping the copper deposit.

Rare earth elements exhibit little variation at the detection limits given. Rb contents broadly correlate with F (Figure 3.4) suggesting its complexing and transport by a F-rich fluid.

3.5 Discussion - The Protolith Problem

Significant controversy remains as to the origin of the massive, medium grained skarn, primarily as a result of its coarse grained porphyritic texture. Proponents of the intrusive-

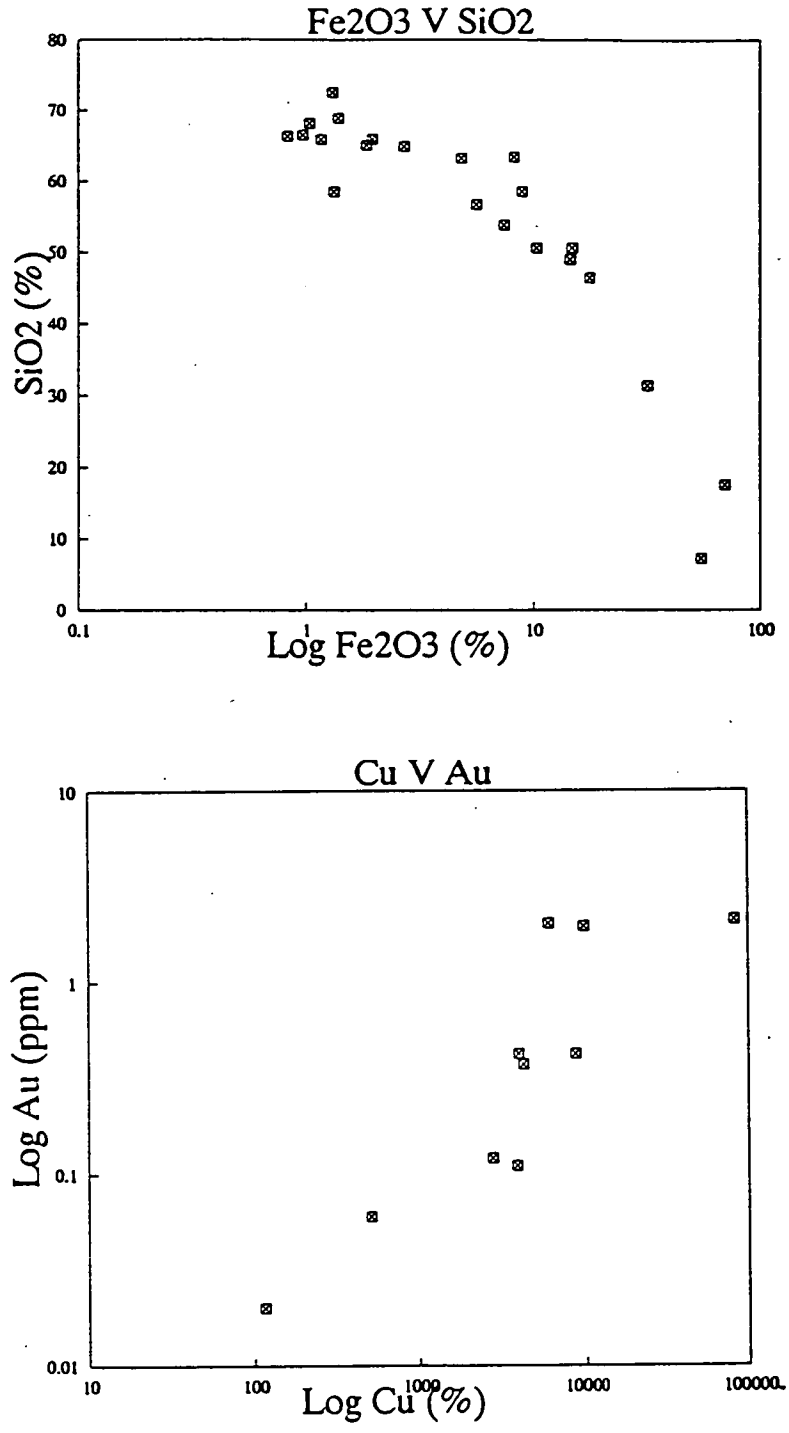

Figure 3.2: *Element correlation plots; (a). $Si0_2$ v log Fe_20_3 and (b). log Au v Log Cu*

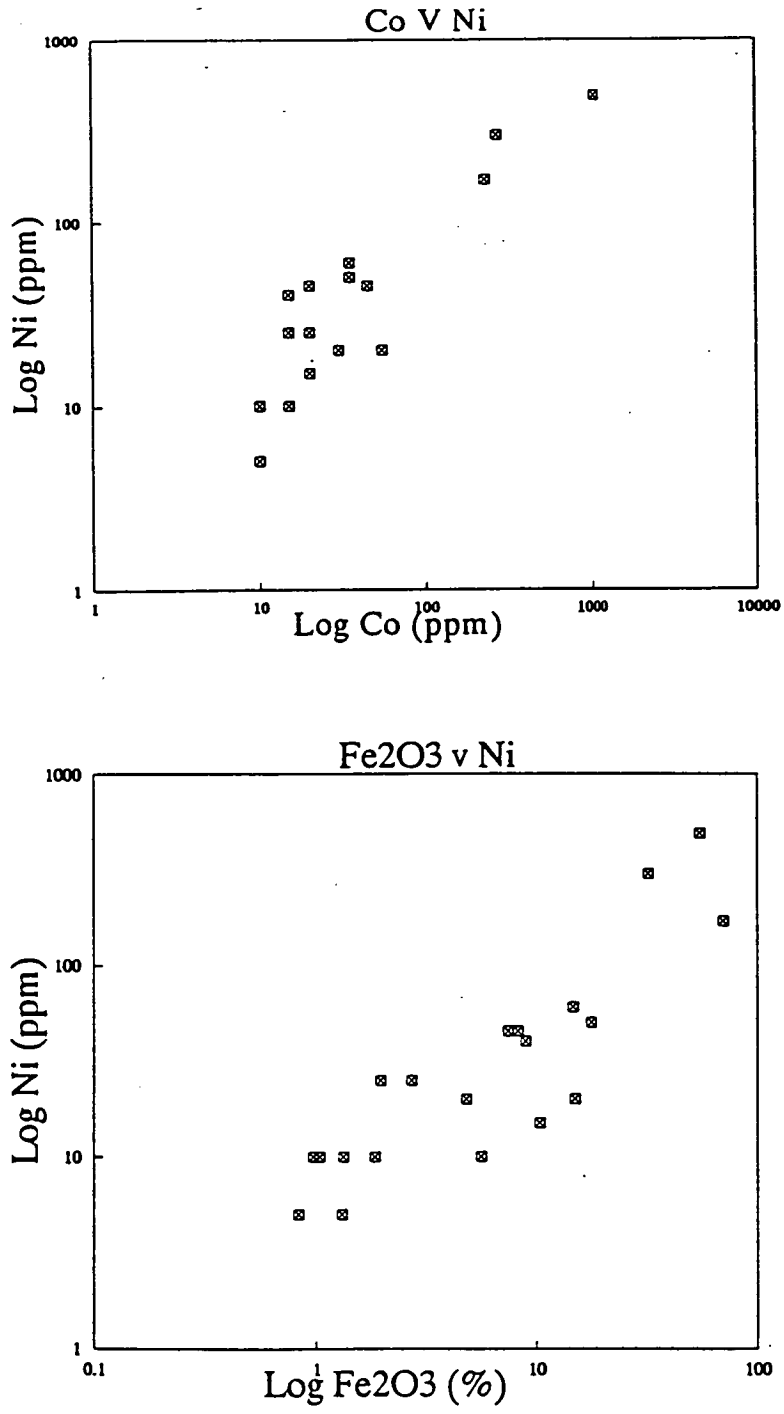

Figure 3.3: *Element correlation plots for (a). Log Ni v log Co, and (b). Log Ni v log Fe_2O_3.*

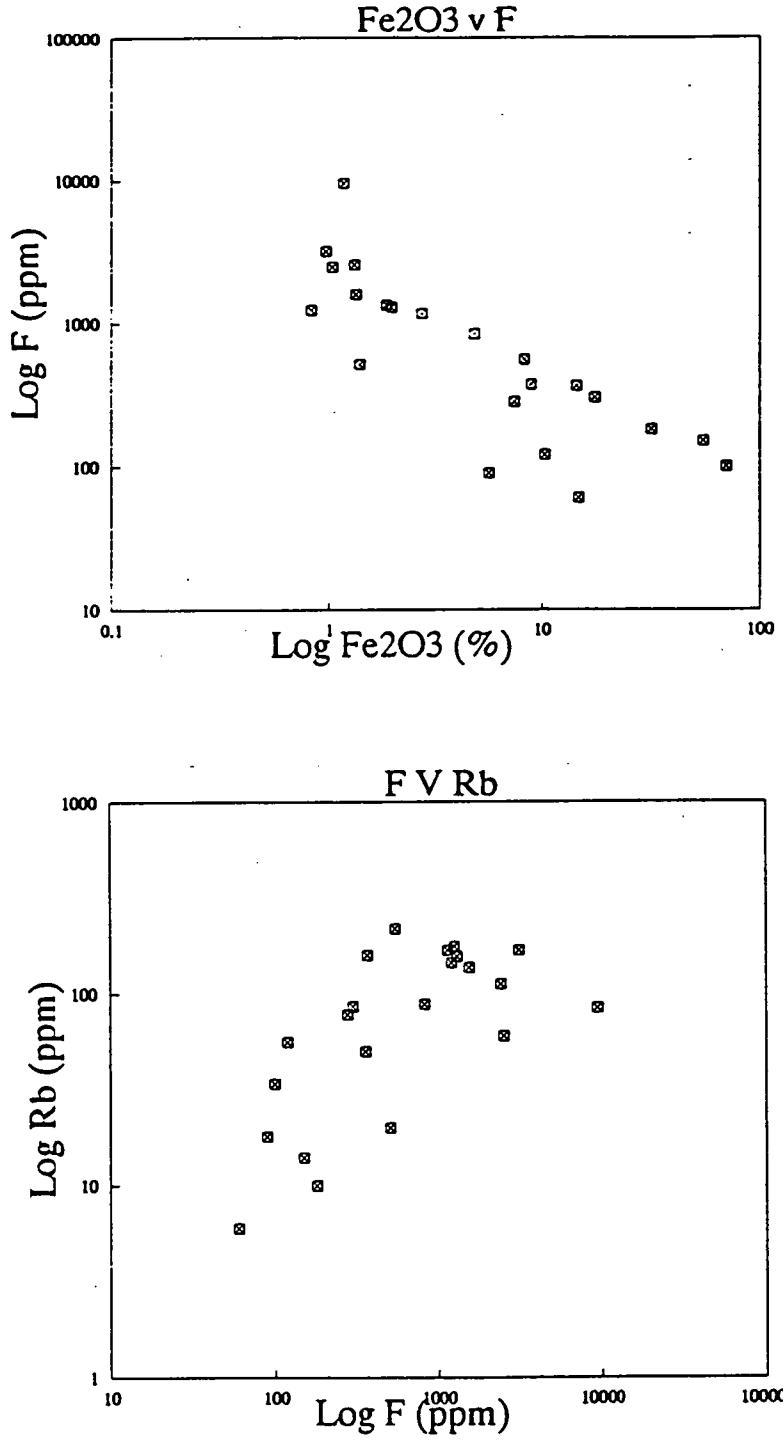

Figure 3.4: *Element correlation plots. (a) Log F v Fe_2O_3, and (b) Log Rb v log F.*

endoskarn idea (typically with little knowledge of the geology) give scant regard to textures observable in the surrounding rocks. This work has shown that albitization, invading via a myriad of fractures and veinlets, ultimately acted to destroy foliation fabrics within both the outer carapace and the footwall schist. Overprinting of the albite-rich rock by calc-silicate alteration enhances individual albite grains to ultimately produce a feldspar-phyric, porphyry-like rock. Plate 3.2 provides an excellent example of this process hand-specimen scale within the outer carapace. Here, relict foliation banding in breccia fragments of extensively altered shale is clearly discernible. What is less obvious, however, is that on the margins of these fragments isolated patches of massive skarn are developed exhibiting pseudo-porphyritic textures indistinguishable from those observed in the medium grained skarn unit. It is not difficult to envisage this process operating at a larger scale to produce the core skarn.

Within the massive skarn, relict foliation/banding and randomly oriented blocks of altered shale provide rare evidence of an earlier shale protolith (Plate 2.8). Several intersections of a fine grained, calc-silicate-rich rock (fine grained skarn) within the medium grained skarn provide some evidence for an earlier mafic intrusive or amphibolite. However, grain-for-grain replacement (endoskarn) of this lithology to produce the massive skarn is not considered likely because of its fine grained nature relative to the enclosing medium-coarse grained alteration. Geochemical evidence against the fine grained skarn as the protolith includes:-

1. The unit is geochemically very similar to other skarns in the hangingwall which are spatially unrelated to the alteration.

2. This study has shown that albitization results in SiO_2 depletion. However, the least altered, albite-rich massive skarn is significantly enriched in SiO_2 relative to the fine grained skarn sample.

3. The iron content of intrusions is inversely proportional to the iron content of calc-silicate minerals in associated skarn (Meinert, 1984).

   Total Fe in skarn clinopyroxenes ranges 10-17%, compared with 17.4% total Fe in the fine grained skarn sample.

4. Korobeynikov (1982) indicates that metasomatic skarn pyroxenes contain two to three times more gold than igneous pyroxene. A sample of pegmatitic pyroxene from a metasomatic vein contains 0.42 ppm Au. No Au was detected above detection in the fine grained skarn, although individual pyroxenes were not probed.

Features favouring the fine grained skarn as the protolith to massive skarn alteration include:-

1. Its spatial position.

2. Meinert (1984) has shown that the presence of an igneous protolith for calcic iron skarn deposits is clearly distinguishable as an Al, Mg, Ti and V signature in calc-silicate minerals. The fine grained skarn has elevated concentrations of all these elements and individual calc-silicate minerals in the skarn are enriched in particular elements: Al-scapolite, Mg-"cpx", Ti-sphene. Vanadium was not analysed in individual phases; however, the wholerock V content of a sample of intensely altered skarn is comparable to that in the fine grained skarn. (Table 3). Results are not conclusive.

3. Although Cu-rich skarn deposits are typically associated with diorite to quartz monzonite stocks, studies of calcic iron and Fe-Cu skarns (Meinert, 1984; Eugster and Chou, 1979; Hellingwerf, 1987) suggest that associated plutons are generally more mafic.

However, the field evidence and majority of geochemical evidence points to the banded shales being the favourable protolith to the massive, medium grained skarn alteration. Overprinting of foliated fabrics in metasedimentary rocks by massive metasomatic alteration is not uncommon in the region. The best known perhaps occurs fifteen kilometres south of Mount Elliott at Starra, where an extensive horizon of magnetite-hematite-quartz ironstone, up to 30m thick, hosts several Cu-Au lenses. Here, iron metasomatism and subsequent deformations have all but obliterated any evidence of the original exhalatives/metasediments within the ironstone horizon.

Chapter 4

MINERALISATION

4.1 Introduction

Several spatially and temporally distinct types of sulphide mineralisation are recognised in drill core at Mount Elliott. These styles are not typical of those associated with classical skarn deposits, in which massive sulphides are hosted in pure limestones or impure carbonate rocks and volcanics. Instead, recent exploration at Mount Elliott reveals that potentially ore-grade Cu-Au mineralisation is hosted in shallowly dipping pegmatitic veins of calc-silicate+calcite that cross-cut the local geology. Little is known about the ore recovered during the early mining operations and as such is not considered here in detail. The deposit was originally expressed at surface as a jasparoidal gossan containing cuprite, malachite, chrysacolla, atacamite and gold. The main ore body beneath the gossan was mined as a pipe-like feature comprising tenorite, chrysacolla, cuprite, malachite and chalcocite with average grades of 12% Cu (Meinert, 1987). Evidence from surrounding mullock dumps suggests that the rich sulphide ore taken beneath the oxide zone includes chalcopyrite-pyrrhotite-pyrite and associated pegmatitic calc-silicate calcite gangue hosted in veins and breccia matrix.

4.2 Morphology of the Deposit

The Mount Elliott Cu-Au deposit is divided into three spatially distinct zones (Figure 4.1). The upper zone includes the previously worked Mount Elliott mine, is semi-elliptical in plan and is tightly constrained by the outer carapace breccia-pipe (Figure 4.2). The ore body has an inverted cone shape, comprising dominantly breccia matrix-veins with extensive infiltration of sulphides into the altered host rock. Thin tentacles of calc-silicate vein-hosted

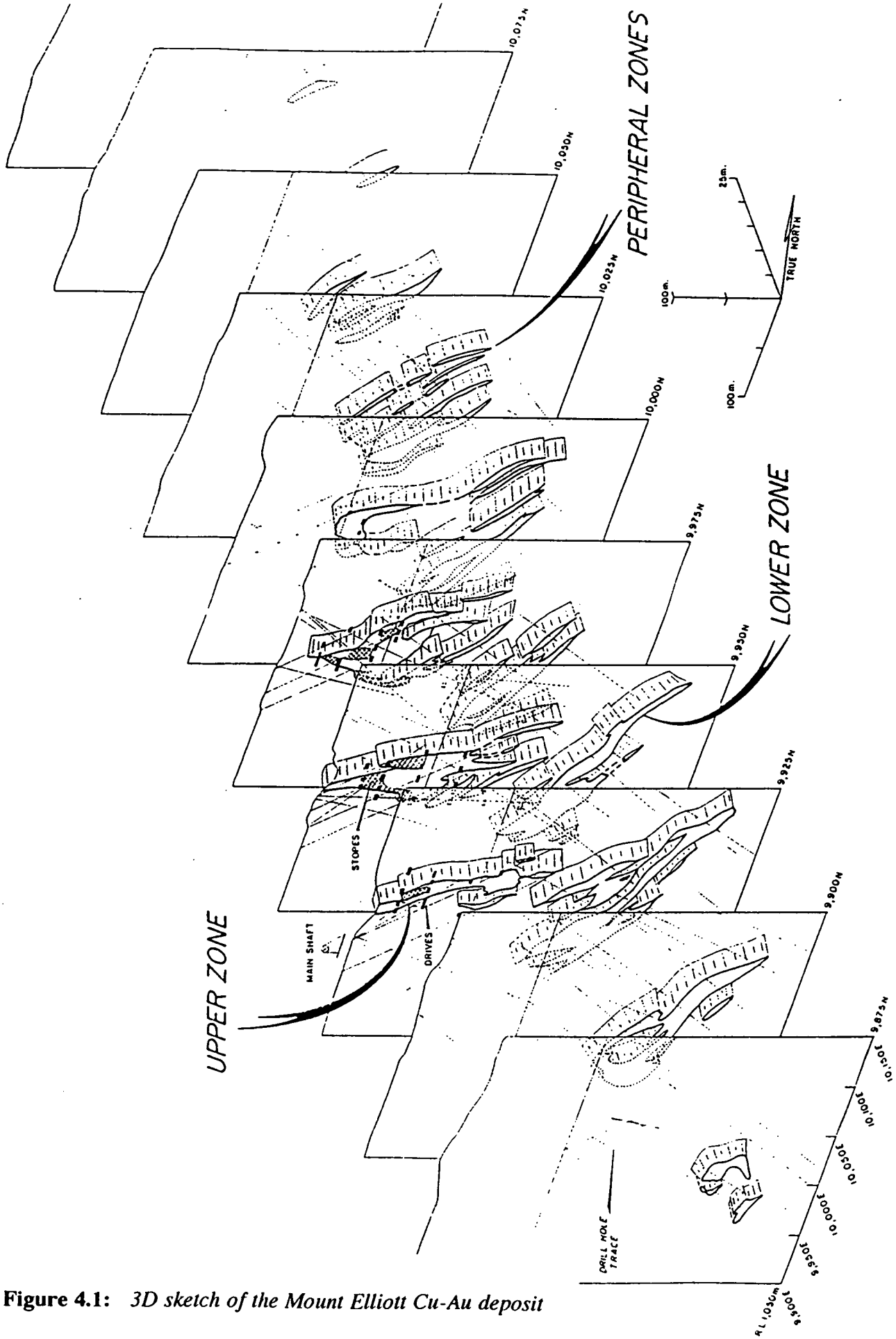

Figure 4.1: *3D sketch of the Mount Elliott Cu-Au deposit*

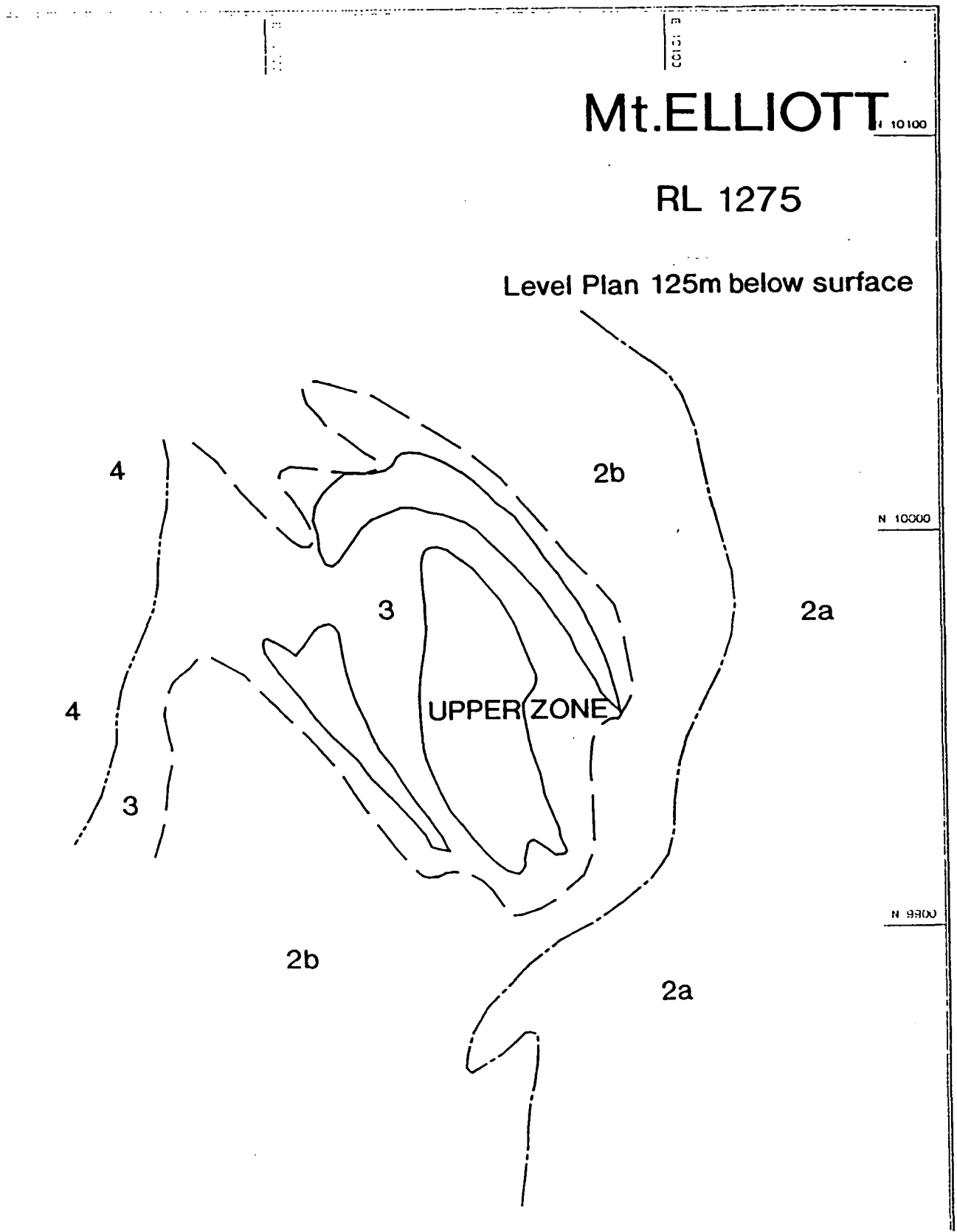

Figure 4.2: *Level plan RL1275, Mount Elliott. Scale 1:1000.*
2a - black shale; 2b - altered shale; 3 - outer carapace; 4 - massive skarn
Dark lines - 3% Cu equivalent outline.

mineralisation extend downwards from the base of the upper zone, possibly connecting with the vein system beneath.

The lower zone is a set of anastomosing calc-silicate-calcite-sulphide veins (as opposed to stacked lenses) dipping 45-50° NE with a strike length of about 150m. The deposit is abruptly terminated at its southern boundary and pinches out to the north where the alteration approaches a major NE-trending fold hinge (Figure 4.3). Individual true sections outlining mineralised zones at 3% Cu-equivalent(2) cut off grade are given in Appendix 3. A number of thin veins dipping more steeply than the main system have been intersected at the northern end of the deposit. More drilling is required to determine the full extent and continuity of these peripheral veins. Figure 4.3 illustrates how well the mineralisation is accommodated within the outer carapace breccia-pipe which tends to balloon outwards with increasing depth. Similarly the halo of bleached shales surrounding the deposit tends to broaden with depth.

The total estimated resource for the Mount Elliott deposit is currently 2 million tonnes at 4.2% Cu equivalent. Within the 3% cut-off contour the metal grades tend to be highly erratic, particularly in the upper zone where mineralisation is breccia-controlled and this is reflected in the severely skewed data for frequency distribution plots of copper and gold grades from both zones (Appendix 4). On a tonnage and grade classification plot (Figure 4.4) Mount Elliott is unarguably associated with the field of non-porphyry associated Cu skarns.

4.3 Styles of Mineralisation

4.3.1 Stratiform Pyrite-Pyrrhotite

The earliest phase of sulphide deposition are thin, stratiform lamellae (<2-3mm) of pyrite and/or pyrrhotite within unaltered shales and phyllites of the Elliott Beds. The semi-

(2) Where Cu-equiv = Cu + 0.8 Au

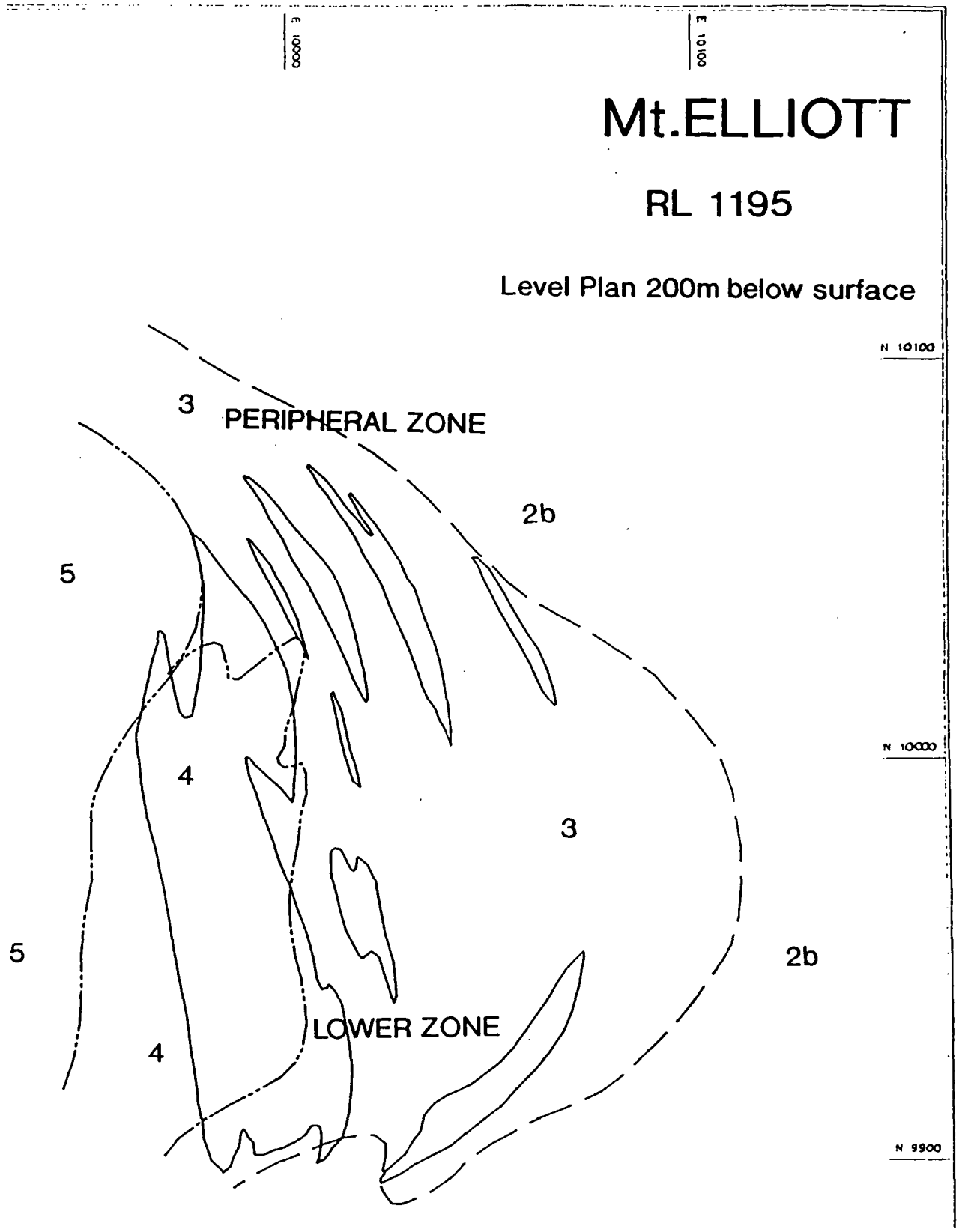

Figure 4.3: *Level plan RL1195.*
2b - altered shale; 3 - outer carapace; 4 - massive skarn; 5 - footwall schist; black solid line - 3% Cu equivalent outline.

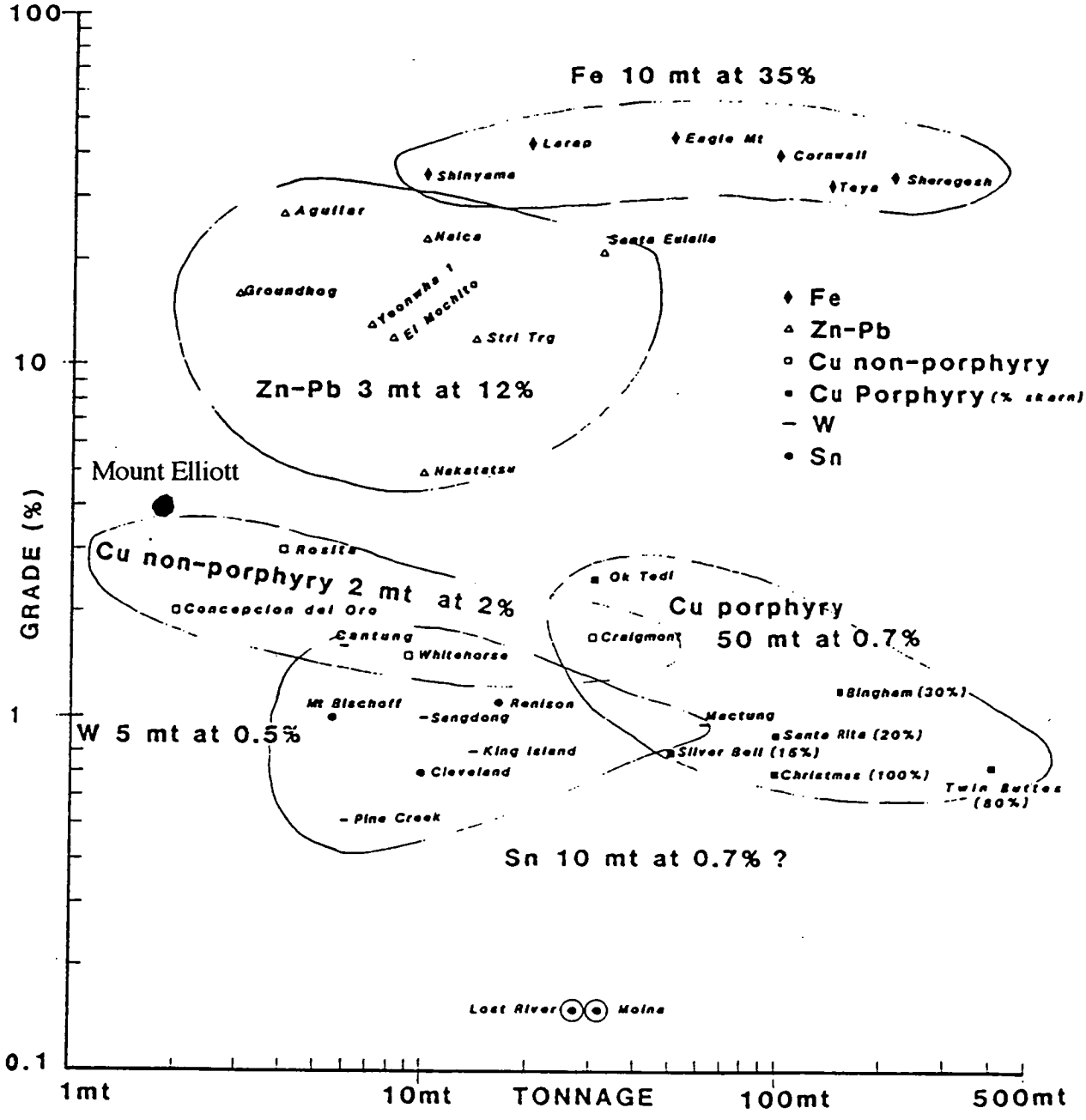

Figure 4.4: *Tonnage v grade deposit-classification plot. Mount Elliott closely associates with non-porphyry copper skarns. From Morrison 1980.*

continuous bands are common throughout the rock and represent a potentially significant source of leachable metals (broad thicknesses of up to 10-20% pyrite - pyrrhotite of this nature are reported in old core holes drilled in the area). Finely disseminated pyrite and pyrrhotite are also ubiquitous throughout the shales. Bleaching in altered shales correlates with a loss of iron sulphides, possibly due to remobilisation into veins and fractures.

4.3.2 Fracture-controlled Mineralisation - Outer Carapace

Fracturing imparts a major control on localisation of sulphide mineralisation within the outer carapace, particularly in the outer unbrecciated portion. Here, pyrrhotite, chalcopyrite and pyrite invade as veinlets and ultimately infiltrate the altered shale foliation. (Plate 4.1). Calc-silicate matrix-veins at the top of the carapace are commonly scapolite-rich with coarse bladed crystals of scapolite growing normal to the vein walls. Here calcite is less common in the veins, and pyrrhotite dominates over chalcopyrite (Plate 4.2a). With depth, clinopyroxene and chalcopyrite become increasingly dominant (Plate 4.2b). Initially, sulphides are deposited interstitial to the calc-silicate phases and at the calc-silicate+calcite interface. With continuing sulphide development the calc-silicate phases are overprinted, and weak to moderate diffusion of sulphides into the altered host shale is evident. Sulphide content within the matrix-vein network varies considerably from virtually absent to total sulphide replacement, producing highly erratic copper grades throughout the outer carapace.

4.3.3 Low-grade Interstitial Sulphide - Medium Grained Skarn

Low-grade disseminated chalcopyrite mineralisation is ubiquitous throughout the medium-grained skarn. Chalcopyrite and lesser pyrite is interstitial to, and replacing, calc-silicate alteration phases (Plate 4.3a). Chalcopyrite invades fractures in magnetite. Small vughs (<5-10mm) common throughout the skarn are typically infilled with magnetite-calcite-chalcopyrite ± pyrite; the sulphides appear to replace calcite. Large vughs filled with

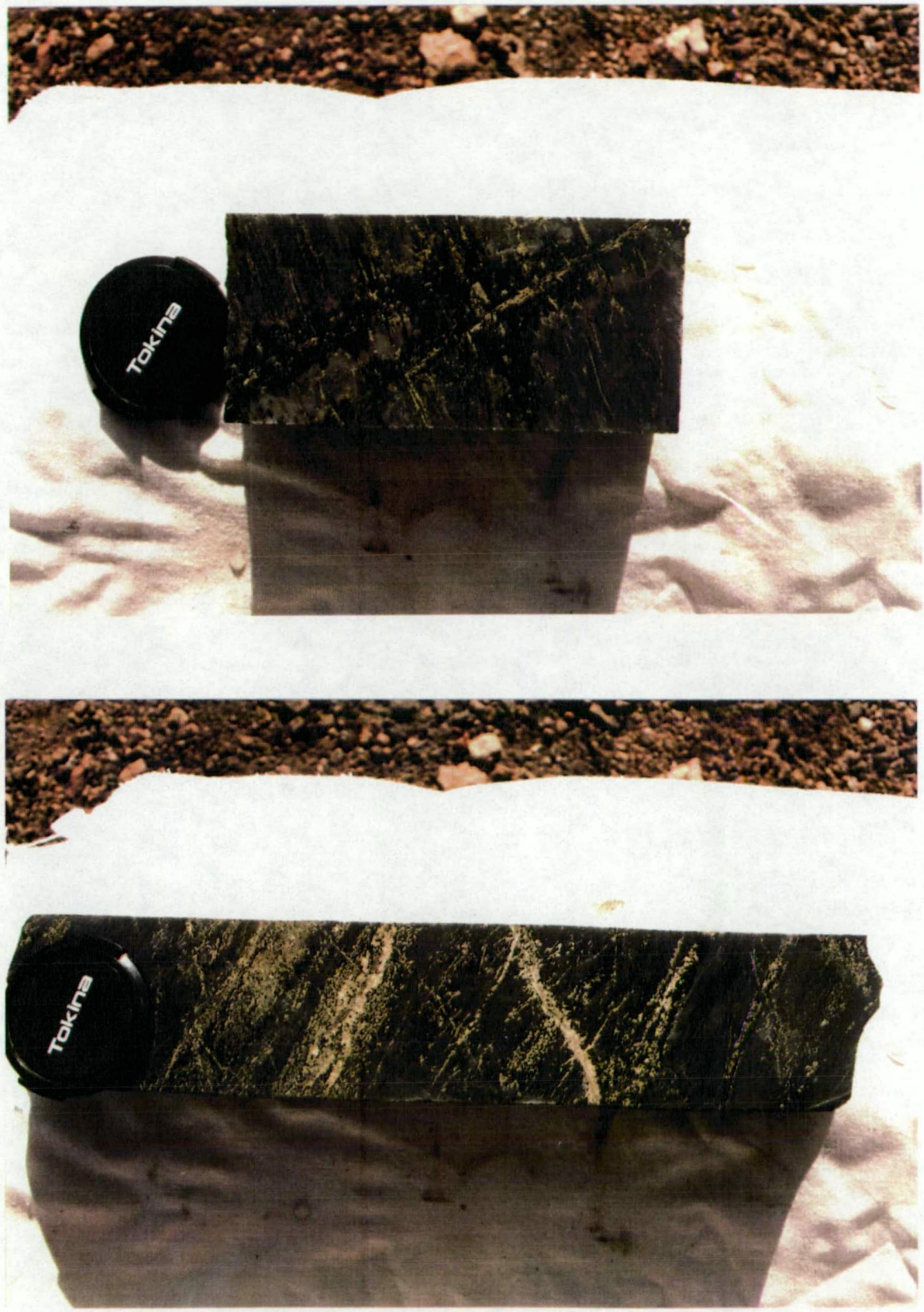

Plate 4.1: *Fracture-controlled sulphide mineralisation in altered shales of the outer carapace. Top: MEQ-46-98m Bottom: MEQ-46-90.4m.*

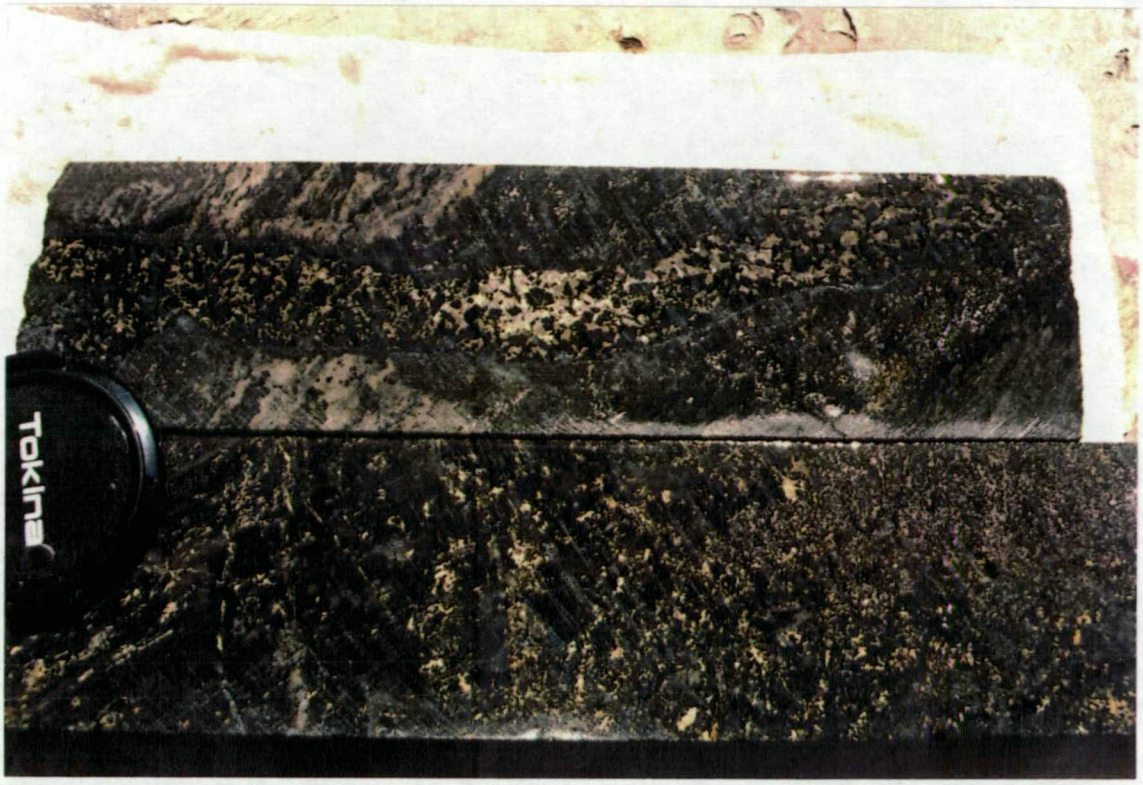

Plate 4.2a: *Scapolite-pyrrhotite rich veins and alteration in outer carapace breccia.*

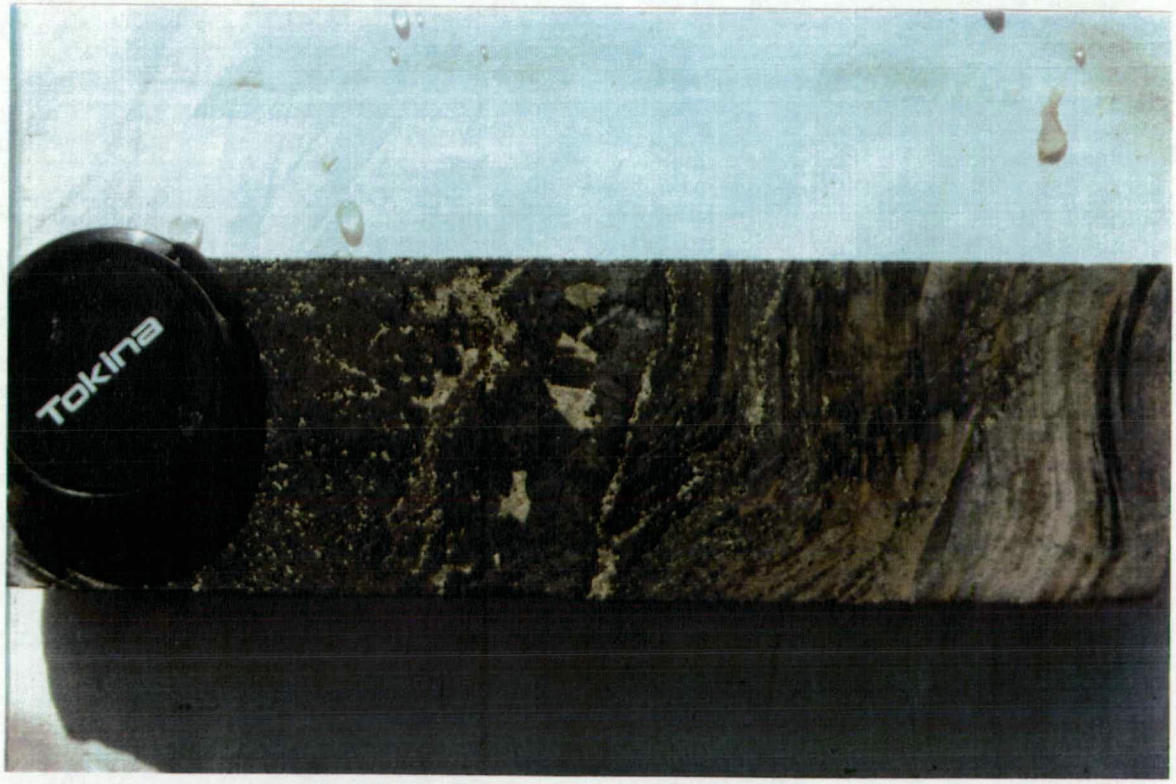

Plate 4.2b: *Clinopyroxene-chalcopyrite rich vein and alteration in outer carapace breccia. Note internal replacement of chalcopyrite by pyrrhotite.*

chalcopyrite are rare (Plate 4.3 b). The medium grained skarn is characteristically pyrrhotite-absent which may reflect fundamental differences in geochemical parameters of the early mineralising fluid.

4.3.4 Sub-economic Pegmatite-hosted Cu-Au Mineralisation

High grade chalcopyrite-gold-pyrrhotite-pyrite mineralisation is associated with calc-silicate-calcite ± magnetite gangue hosted in a series of anastomosing pegmatite veins that abruptly cross-cut the geology. Gangue components in the veins are predominantly dark green, coarsely crystalline clinopyroxene ("cpx") infilled with coarse pink calcite. Minor calc-silicate phases include scapolite, apatite and sphene. Unlike the matrix-veins of the outer carapace, clinopyroxene development is not restricted to pegmatitic growths on vein walls but also forms abundant crystal growths within the calcite 'matrix,' resulting in generally higher sulphide contents (Plate 4.4 a). That is, the reactable surface area of clinopyroxene-calcite, apparently a favourable site for sulphide development, is greatly increased.

Sulphide content and gangue textures vary markedly within veins, primarily as a function of diop-hed growth and sulphide availability (Plate 4.4 b). Vein textures vary from open vein style to clusters of "cpx" crystals enclosing pockets of calcite in an ophitic-like texture. Like the breccia matrix-veins, sulphide contents vary from absent to massive replacement of the clinopyroxene-calcite gangue.

The veins cross-cut both the massive skarn alteration and altered shales of the outer carapace; several smaller, less continuous bodies have been discovered in the footwall Town Beds schist. Despite this, the gangue mineralogies and sulphide species remain the same across lithology/alteration boundaries with the notable exception of magnetite introduction at depth, coinciding with loss of pyrrhotite, a non lithology-specific feature.

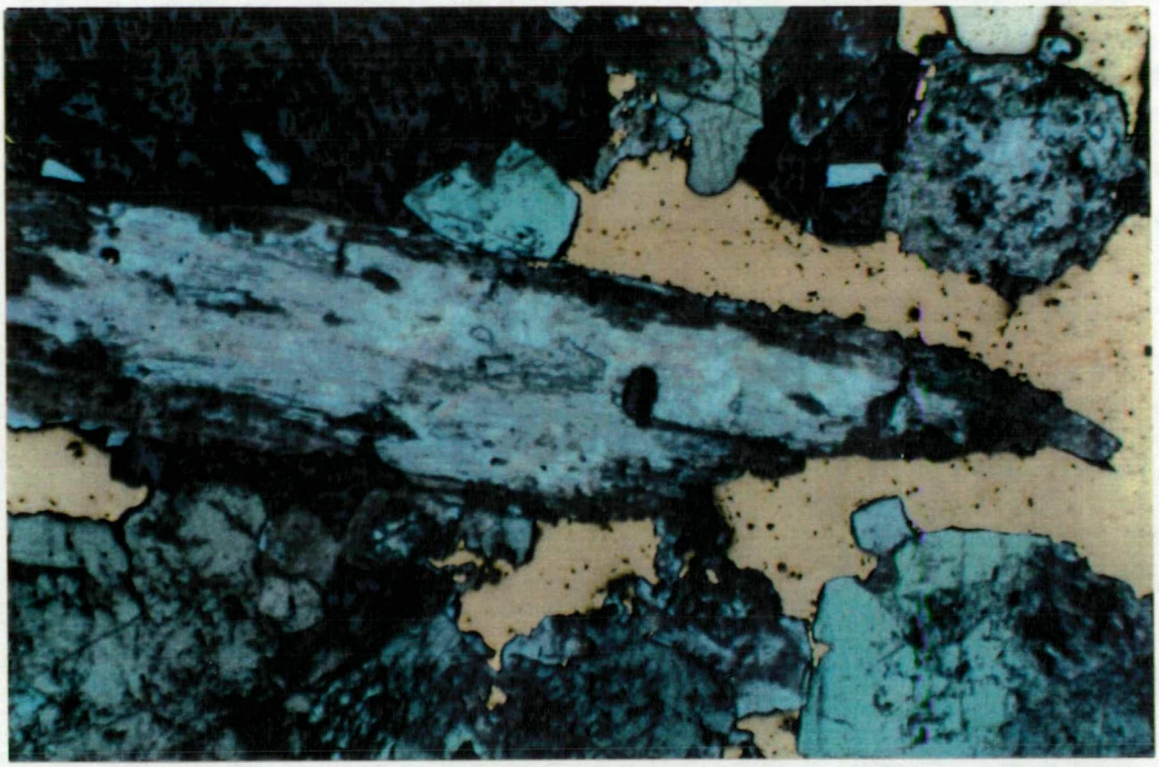

Plate 4.3a: *Photomicrograph (x2.5) plane light/reflected light showing chalcopyrite mineralisation overprinting prograde albite and clinc pyroxene in medium grained skarn. MEQ-19-301m.*

Plate 4.3b: *Large vugh in medium grained skarn alteration invaded by chalcopyrite MEQ-48-192.8m.*

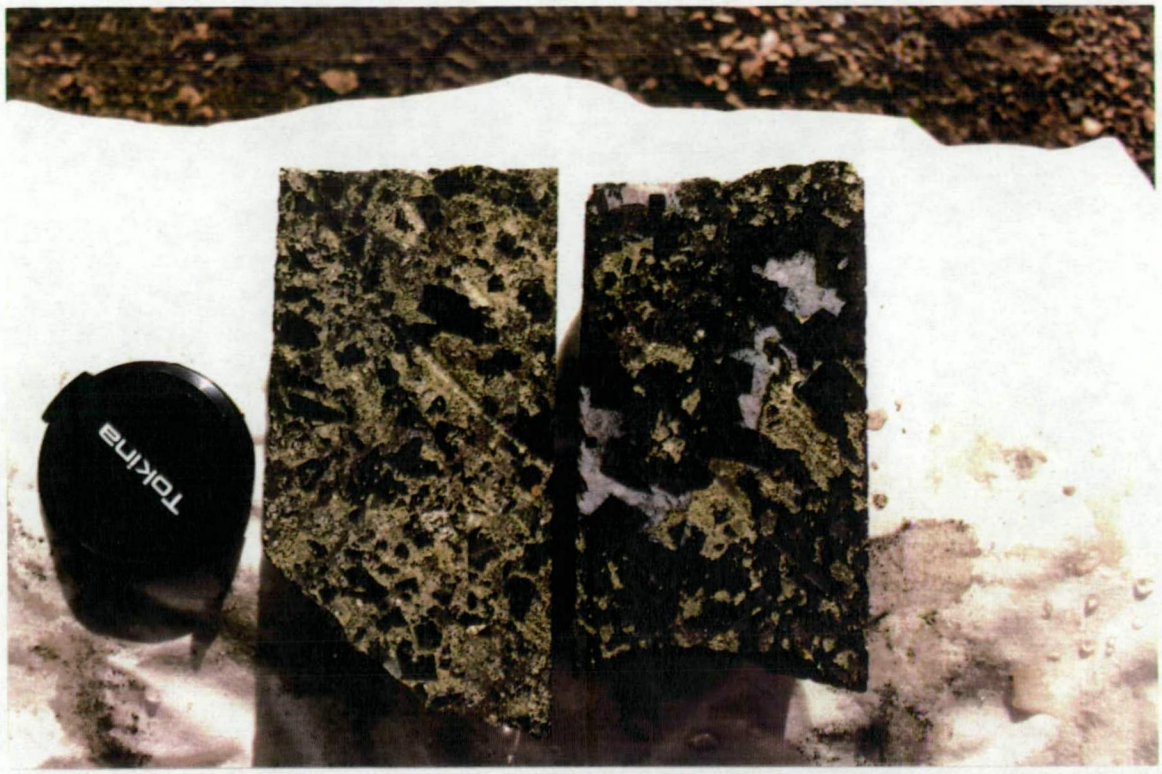

Plate 4.4a: *Clinopyroxene-calcite vein with chalcopyrite mineralisation initially in the calcite 'matrix' and along diop-hed crystal boundaries (right) followed by pervasive replacement of the calc-silicate (left).*

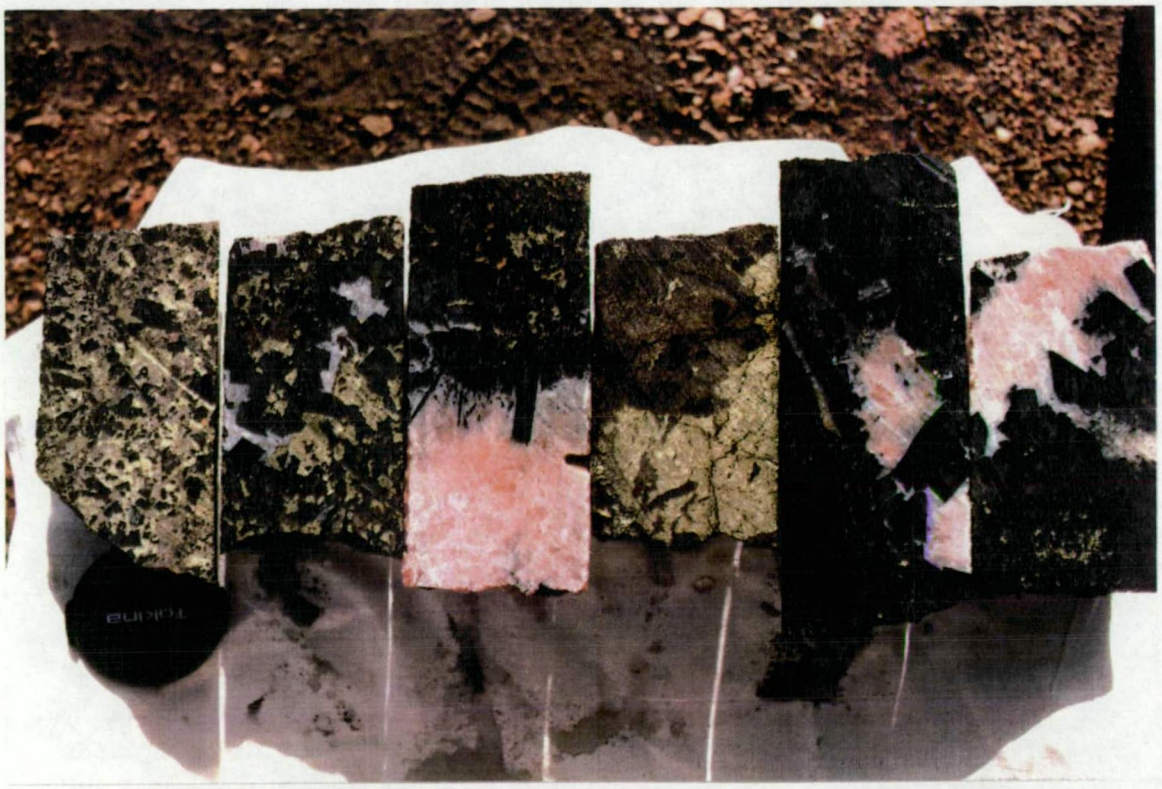

Plate 4.4b: *Variable gangue textures and sulphide contents within mineralised veins. MEQ-48, 230.75-239.7m.*

4.4 Zoning and Paragenesis

A broad zonation of sulphide species at Mount Elliott is clearly evident and generally reflects the paragenetic sequence of sulphide mineralisation.

Pyrite is ubiquitous in the deposit, replaced by both chalcopyrite and pyrrhotite (surrounding grains and invading fractures). Within the massive skarn, chalcopyrite invades fractures in magnetite, although magnetite deposition coeval with chalcopyrite is also likely. However, the relationship between chalcopyrite and pyrrhotite is more difficult to assess with the majority of field evidence suggesting pyrrhotite replacement of chalcopyrite, although locally the reverse may hold. In the outer carapace, veins of chalcopyrite will commonly have a core of pyrrhotite (Plate 4.5a). Here, chalcopyrite rimming the vein with diffusion into the adjacent wallrock (bereft of pyrrhotite) implies pyrrhotite replacing chalcopyrite. In sulphide-rich pegmatite veins, pyrrhotite typically envelops the chalcopyrite, invading from the outside inwards, whereas it readily invades fractures in pyrite replacing from the inside outwards (Plate 4.5b).

Hence the paragenesis of sulphide mineralisation is interpreted as;

pyrite -> chalcopyrite -> pyrrhotite

This is reflected in several mineralised veins that exhibit variation from early gangue-dominant veins with pyrite through to chalcopyrite-clinopyroxene-rich veins to pyrrhotite-rich veins with minor gangue (Plate 4.6a). A consequence of this is that the later phase progresses further out into the country rock than the phase it replaces, which defines a general sulphide zonation that can be recognised in most drill-holes as (from top-bottom);

po -> po-cpy -> cpy-po ± mag -> cpy-mag -> mag-cpy -> mag

where pyrite occurs at all levels (Plate 4.6b).

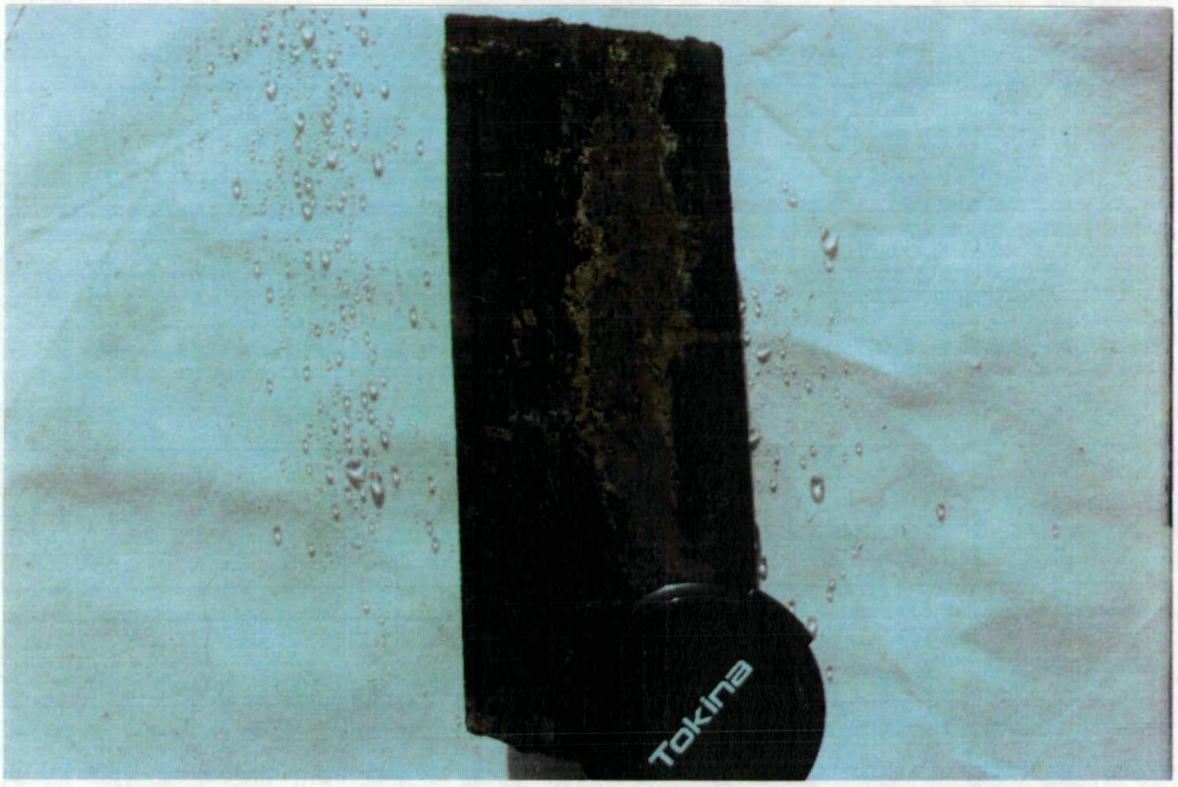

Plate 4.5a: *Interior of chalcopyrite vein invaded by pyrrhotite implies pyrrhotite replaces chalcopyrite . Outer carapace. MEQ-38-301.8m.*

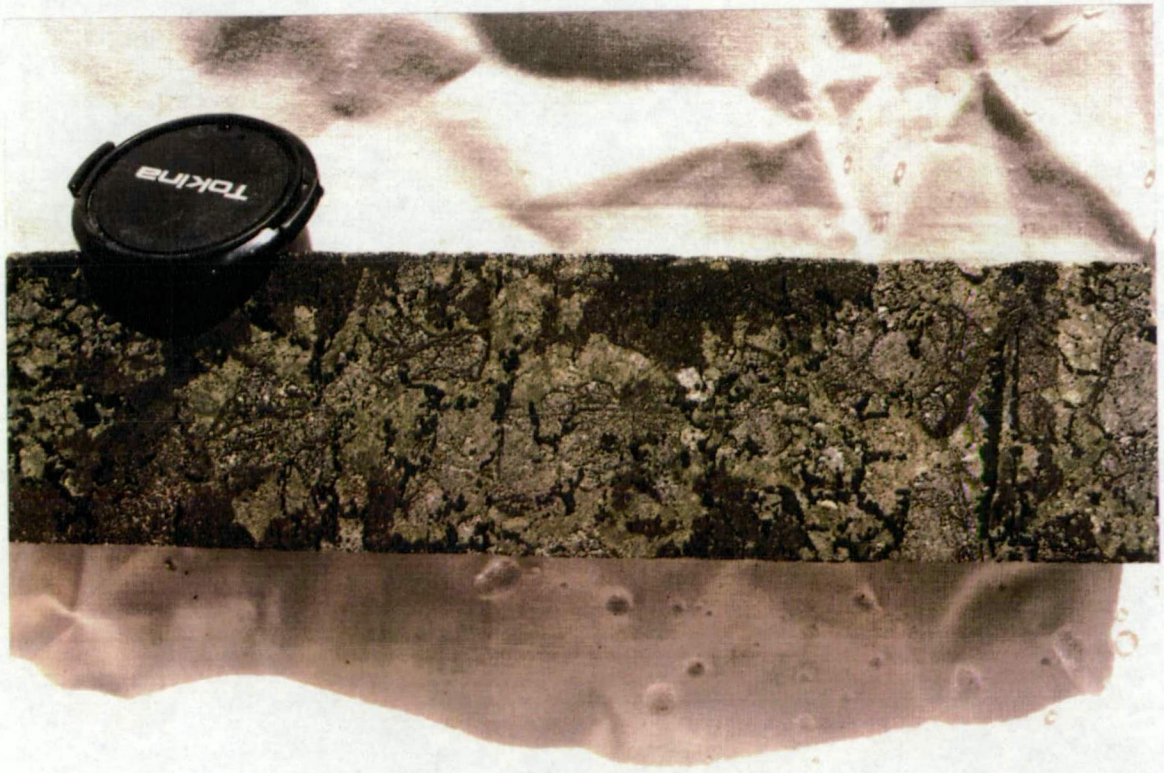

Plate 4.5b: *Massive sulphide replacement of calc-silicate-calcite gangue. Pyrrhotite invades pyrite fractures and envelops chalcopyrite. MEQ-48-219.5*

Plate 4.6a: *Paragenetic sequence of mineralised vein formation (L-R) calc-silicate-pyrite vein to chalcopyrite-clinopyroxene vein to pyrrhotite-rich vein with minor calc-silicate gangue. MEQ-38, 308.2-314.5m.*

Plate 4.6b: *Sulphide zonation through the deposit (from L-R; top to bottom) po ->po-cpy->cpy-po->cpy-mag±po->mag-cpy->mag, MEQ-38.*

4.5 Trace Element Geochemistry

A whole-rock sample of each of massive pyrrhotite, pyrite and chalcopyrite was analysed for a range of trace elements in an attempt to characterise their trace element geochemistry and to identify any elements suitable as potential pathfinders for exploration of further Mount Elliott style mineralisation in the area. The significance of this is emphasised by the lack of anomalous copper and gold geochemistry in rock chips and soils overlying the Mount Elliott deposit. The samples were prepared and analysed commercially by Australian Laboratory Services in Brisbane using a range of ICP, XRF and fire assay techniques. Results are shown in Table 4.1 and sample descriptions provided in Appendix 2. Pyrite and chalcopyrite grains in the medium grained skarn were probed for a smaller range of trace elements (Appendix 1).

The results indicate that pyrrhotite is highly anomalous in Cu, Co, Ni, Se and Te and weakly anomalous in Zn. The Cu may be attributed to relict chalcopyrite (and possibly the Zn), however, the Co, Ni, Se and Te are considered characteristic of the pyrrhotite. Although Ni and Co isomorphously replace iron in the pyrrhotite crystal lattice (Tvalchrelidze and Chichinazem, 1985) and pyrrhotite occurs in abundance in many skarn deposits, relatively few studies have documented anomalous cobalt contents (Ray *et al.*. 1988; Hellingwerf, 1987; Meinert, 1984; Einaudi *et al.* 1981; Vidal *et al.* 1990) and elevated nickel contents are rarer (Ochiai, 1987; McMillan *et al.* 1990). Cobalt enrichment is typically associated with calcic iron-rich skarns, occurring usually as separate phases such as cobaltite, erythrite or Co-Ni sulfarsenides (Beddoe-Stephens *et al.* 1987). Nickel and cobalt minerals are closely associated with pyrrhotite and chalcopyrite in the Tengumari Cu Skarn Deposit, Japan (Haruna *et al.* 1990). Enriched selenium and cobalt are reported in magnetite-rich replacement deposits at Tennant Creek (Wedekind *et al.* 1988). More recently, however, studies of precious metal gold skarns has shown them to be characteristically enriched in Te, Co and Ni, plus a wide range of other trace elements (Ettlinger and Ray, 1988; Ettlinger *et al.* 1990; Meinert, 1989; Theodore *et al.* 1930).

	400718 Pyrrhotite	400722 Pyrite	400724 Chalcopyrite	Det. limit
Cu (ppm)	2050.00	210.00	32.50%	5.00
Zn (ppm)	80.00	5.00	460.00	5.00
Ag (ppm)	<1	<1	7.00	1.00
As (ppm)	<1	<1	8.00	1.00
Bi (ppm)	<5	<5	<5	5.00
Sb (ppm)	<5	<5	<5	5.00
Mo (ppm)	<5	<5	5.00	5.00
CO (ppm)	1350.00	10.00	90.00	5.00
Ni (ppm)	2000.00	15.00	90.00	5.00
V (ppm)	<10	70.00	10.00	10.00
Se (ppb)	55000.00	300.00	<50	50.00
Te (ppb)	5000.00	150.00	50.00	50.00
Sn (ppb)	<5	<5	25.00	5.00
W (ppm)	<10	<10	<10	10.00
Ba (ppm)	20.00	710.00	40.00	10.00
Pd (ppm)	<0.01	<0.01	<0.01	0.01
Au (ppm)	0.04	<0.01	1.97	<0.01
Hg (ppb)	<50	<50	150.00	50.00

Table 4.1: *Trace element analyses of samples of massive pyrrhotite, pyrite and chalcopyrite.*

The pyrite sample exhibits anomalous V and Ba. Elevated concentrations of Zn and Au were detected in massive chalcopyrite together with weakly anomalous Ag, As, Sn and Hg. Weak Co and Ni enrichment in the chalcopyrite might be attributed to small pyrrhotite inclusions, although the relationship is not clear. Anomalous Sn is a remarkable result, but it may reflect regional geochemical enrichment given that Kary and Harley (1990) report elevated Sn contents in Cu-rich ironstones at Starra. Data for mercury in skarn deposits is very rare with a single report of up to 43 ppb Hg detected in chalcopyrite veins from a porphyry-Cu associated skarn deposit at Mines Gaspe, Quebec (Allcock, 1982). Results from this study (including probe data) suggest that Hg levels at Mount Elliott are relatively high. Gold is an important by-product of many Cu-skarns, including Mount Elliott. The similar crystal chemistry of Au and Cu suggests that Au might easily be accommodated in the chalcopyrite lattice (Garrett, 1989) and as such is not unexpected in a free state at Mount Elliott.

The data suggests that a number of trace elements have potential for use as geochemical pathfinders for Mount Elliott style mineralisation including, Co, Ni, Se, Te and Ba, although above-background Co concentrations characteristic of this region may diminish its effectiveness.

4.6 Gold Mineralisation and Geochemistry

Assay data of Mount Elliott drill cores clearly illustrate that gold grades exhibit a strong positive linear relationship to copper grades (Figure 4.5) which implicates chalcopyrite as the likely host for the majority of gold mineralisation at Mount Elliott. Analysis of samples of massive chalcopyrite, pyrrhotite and pyrite confirm this with chalcopyrite yielding 1.97 ppm Au and pyrrhotite 0.04 ppm Au. No gold was detected in pyrite (Table 4.1). Interestingly, a sample of massive pegmatitic clinopyroxene taken from a poorly mineralised vein in the outer carapace assayed 0.42 ppm Au (Table 3.3) suggesting that minor quantities of gold are hosted in the calc-silicate gangue.

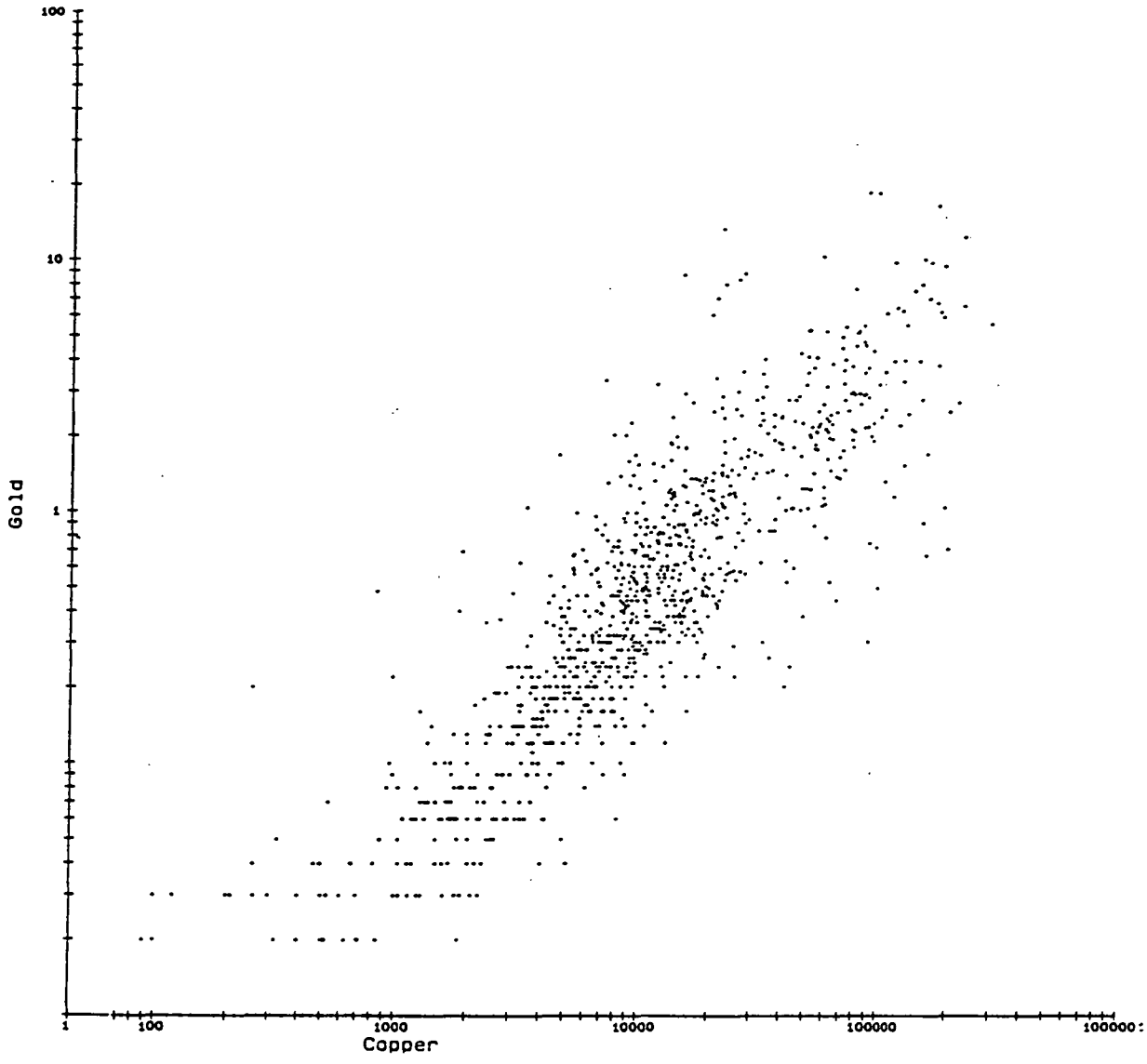

Figure 4.5: *log Au v log Cu assay grades for Mount Elliott core samples.*

Despite these results, however, no gold has been observed during visual and microscopic investigations of chalcopyrite grains from Mount Elliott core samples. Studies of gold geochemistry (Mironov *et al.* 1986; Garrett, 1989; Wilson *et al.* 1990) have shown that the higher solubility of gold in chalcopyrite than in pyrrhotite can be explained by gold's preference to form a substitutional solid solution series with Cu as opposed to Fe. That is, the similar crystal and chemical properties of Au and Cu (gold and copper are in the same group in the periodic table, have the same crystal structure and similar atomic radii, and have virtually unlimited isomorphous miscibility) result in gold being able to be accommodated in the crystal structure of chalcopyrite, but in pyrite or pyrrhotite it can only form as microscopic inclusions along crystal grain boundaries or imperfections in the sulphide lattice.

Coarse gold was detected, however, in a single thin section sample of a highly anomalous vein where it occurs associated with chalcopyrite invading intensely fractured pyrite. It also occurs at the pyrite-calc-silicate boundary, and as free gold along grain boundaries in calc-silicate adjacent to the pyrite (Plate 4.7). Electron microprobe compositions of a number of grains (Table 4.2) reveals that they are Au-rich (ave. 913 fine) with no detectable trace concentrations of Hg, Bi, or Cu, although this is likely due to the poor sensitivity of the instrument. Gold and silver compositions display a classic antipathetic trend characteristic of the Au-Ag solid solution series (Figure 4.6). A BiTeS mineral was probed (composition undetermined) abutting a large gold grain (Plate 4.7c). Although not particularly important at Mount Elliott, the significance of anomalous bismuth relates to deposit classification and exploration since relatively few deposit studies report anomalous Bi, and since it is principally associated with gold, or gold-rich skarn deposits. Bismuth and Bi-Te minerals are identified in skarn deposits from a broad range of geological environments across the globe, including; Au skarn in Australia (Red Dome: Torrey *et al.* 1986; Ewers *et al.* 1987), the Nickel Plate and Fortitude Au-skarns in Canada (Ray *et al.* 1987; Ray *et al.* 1988; Ettlinger and Ray, 1988; Ettlinger and Meinert, 1991) and the McCoy Au skarn (Nevada: Brooks *et al.* 1989); Au-Bi-Cu replacement bodies/skarn at Tennant Creek (Wedekind *et al.* 1988) and in Canada (Brown and Nesbitt, 1984; Brown

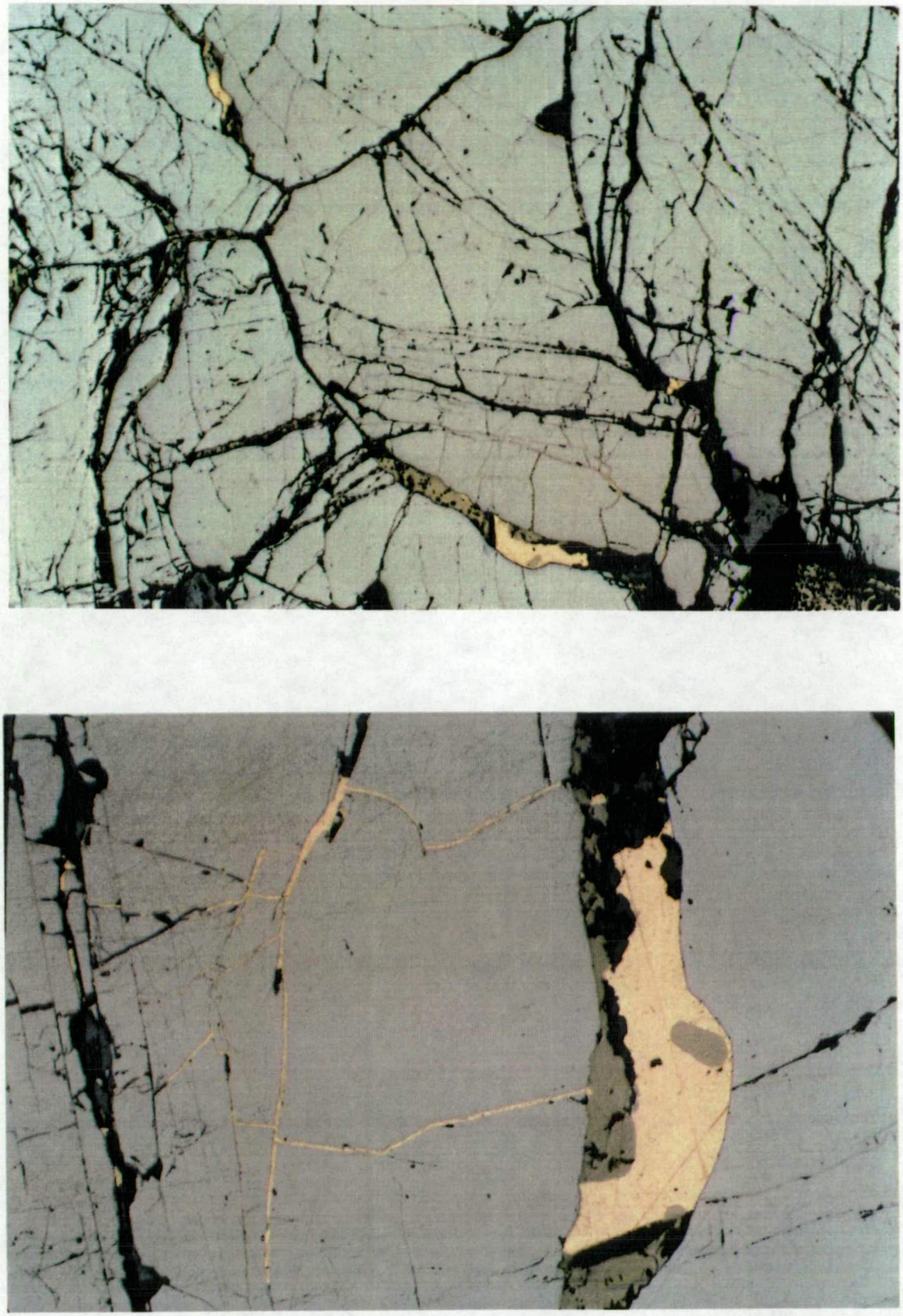

Plate 4.7 a,b: *Photomicrograph of coarse gold associated with chalcopyrite (olive green) invading highly fractured pyrite. MEQ-15-259.6m.*

Plate 4.7c: *Photomicrograph of coarse gold and associated Bi-Te-S mineral (blue-grey) in fractured pyrite. MEQ-15-259.6m.*

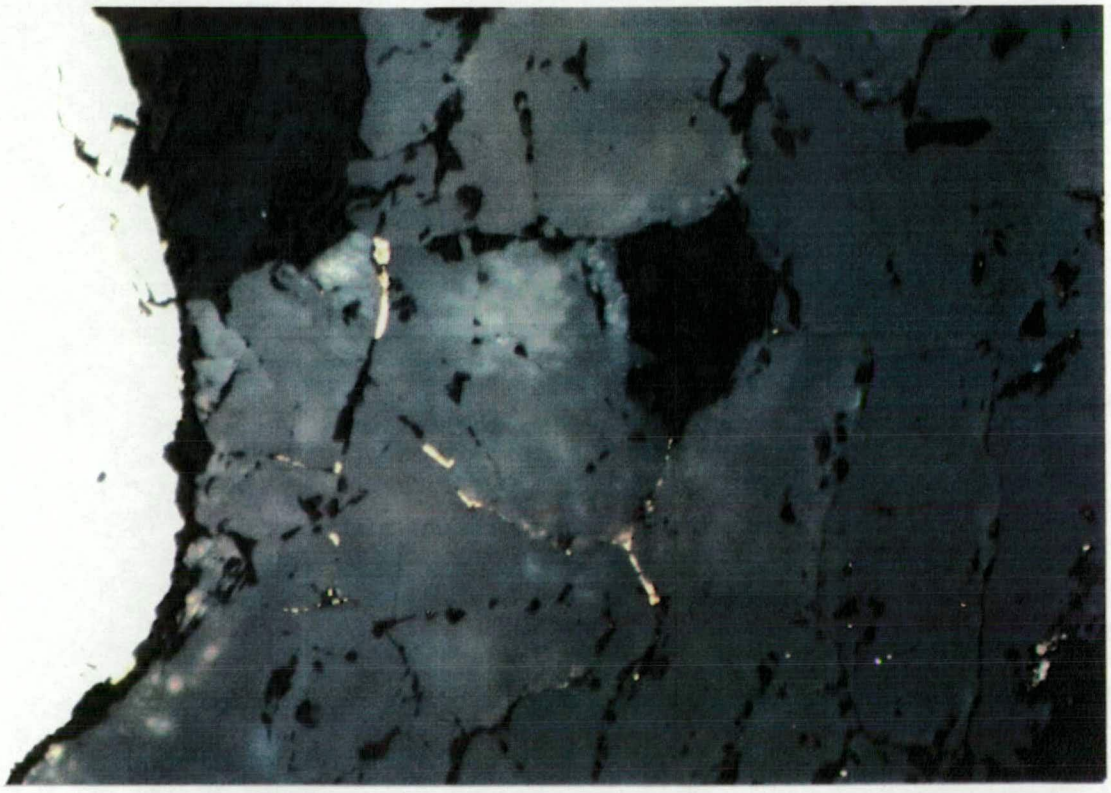

Plate 4.7d: *Photomicrograph of coarse gold hosted along calc-silicate grain boundaries. MEQ-15-259.6m.*

	1	2	3	4	5	6	7	8
Au	90.896	92.322	90.387	92.683	89.760	87.741	89.108	78.837
Ag	8.246	7.476	9.157	6.376	7.895	10.258	10.685	7.423
Hg	0.000	0.000	0.000	0.000	0.000	0.000	0.000	0.000
total	99.014	99.798	99.544	99.059	97.655	97.999	99.793	86.260
Finenes	917	925	908	936	919	895	893	914

Table 4.2: *Compositions of gold grains determined by electron microprobe analysis.*

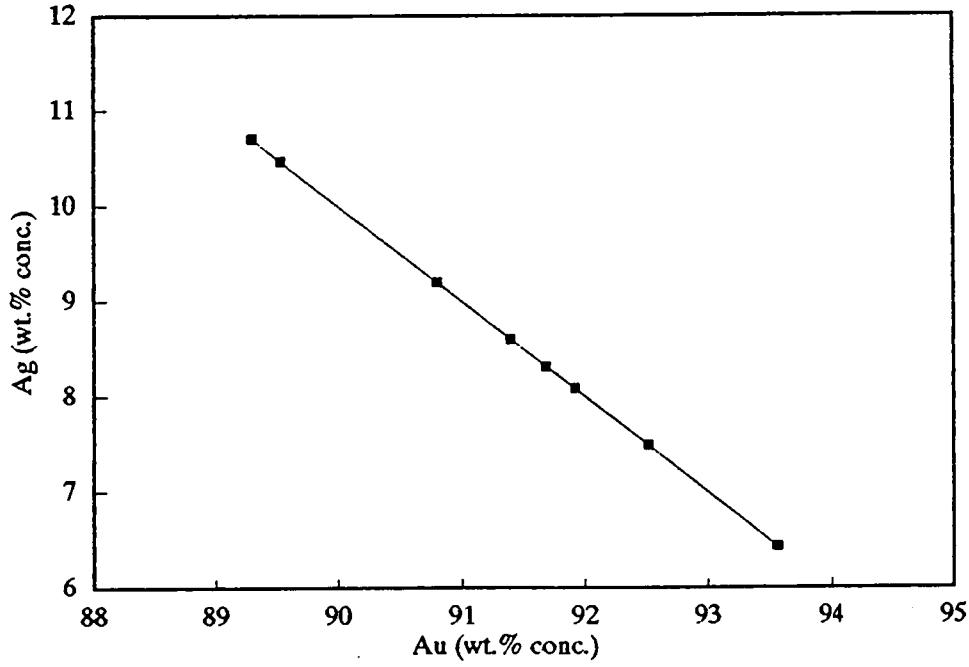

Figure 4.6: *Plot of Au v Ag compositions of gold grains, determined by electron microprobe analysis.*

and Nesbitt, 1987); Cu-Au skarn in Siberia (Ettlinger and Meinert, 1991) and Cu-Fe ± Au skarn at Concepcion del Oro, Mexico (Buseck, 1966). Other skarn deposit types with documented anomalous Bi contents but not associated with Au include; breccia pipe Cu-skarn (Atkinson *et al.* 1982) and porphyry Cu-associated Cu-Mo skarn (Allcock, 1982). The potential of Bi as an exploration pathfinder appears limited for the Mount Elliott area since no anomalous Bi was detected in a suite of wholerock samples, although the sensitivity of analysis (at 5 ppm detection limit) may not be appropriate.

The coarse, visible gold and accompanying metals are clearly remobilised, although the enclosing pyrite is not considered a likely source. Pyroxenes are significant gold carriers in many intrusive rock types and Korobeynikov (1982) has shown that metasomatic pyroxenes of calcic skarns typically have gold contents 2-3 times that of pyroxenes in the parent granitoid intrusions. However, very high gold contents in pyroxene would be necessary to develop coarse gold on calc-silicate crystal boundaries, as in Plate 4.7d, and also implies significant mobilisation of Au in the hydrothermal fluid prior to the introduction of Cu. Therefore it is considered more likely that the gold was remobilised from nearby chalcopyrite grains.

4.7 Timing of Mineralisation

The absence of hematitic albite from the vein skarn assemblage and the similarity in textures between the ore veins and breccia matrix-veins strongly suggests that filling of the flat-lying, cross-cutting veins with crystalline calc-silicate gangue post-dates brecciation. Rotated S_1 and S_2 cleavages in adjacent blocks indicates that brecciation post-dates the S_2 cleavage event. Filling of the veins by calcite followed, evidenced by broken crystals of scapolite suspended in calcite and calcite infilling fractures and imperfections in clinopyroxene crystals. Clinopyroxene continued to grow in the ore veins contemporaneous with calcite precipitation.

Sulphide is principally hosted in calcite preferentially in contact with "cpx". The commonly embayed, anhedral form of sulphide blebs enclosed by calcite does suggest that sulphide precipitation was broadly coeval with calcite filling of the veins. Generally poor gold grades associated with clinopyroxene-rich, sulphide-poor veins suggest it is unlikely that Au, originally hosted in calc-silicate gangue, was relocated into chalcopyrite during replacement, but rather was introduced later with the chalcopyrite.

The coarsely crystalline, undeformed nature of the mineralised veins cross-cutting the stratigraphy and early alteration at Mount Elliott suggests they represent the last event to actively affect the geology of the area.

Chapter 5

CONDITIONS OF ALTERATION AND MINERALISATION

5.1 Introduction

This chapter characterises the geochemical parameters of the ore-forming fluid using sulphur isotopes, phase-relationships mineralogy, ore textures and comparisons with studies of other skarn deposits (e.g., fluid inclusions). Certain features readily observable in hand specimen at Mount Elliott (including the presence of fluorine, gangue mineralogies, the absence of hematite and the magnetite-pyrrhotite relationship) can be used to place realistic constraints on fluid parameters such as source, composition, temperatures and oxygen fugacity. Thermodynamic modelling has not been attempted.

5.2 Sulphur Isotopes

Thirty sulphide separates were obtained from drill core samples of Mount Elliott ore and host rock by hand drilling. SO_2 gas was extracted by the method of Robinson and Kusabe (1975) and analysed in a VG Micromass spectrometer at the Central Science Laboratory of the University of Tasmania. The samples were calibrated against standard galena from Broken Hill ($\delta^{34}S = 3.4‰$) and Tullah, Tasmania ($\delta^{34}S = 15.2‰$), and CIG cylinder gas ($\delta^{34}S = 0.7‰$).

Results for all standards were reproducible within 0.1‰. Detailed results for the Mount Elliott samples are presented in Table 5.1 and sample descriptions are given in Appendix 5.

The data shows that sulphides associated with the ore mineralisation event are very highly constrained (range -5.7 to -3.6‰) and differ markedly from a single sample of shale-hosted lamellae pyrite ($\delta^{34}S = -12.7‰$, Figure 5.1). Although this sample is not statistically significant, its large variation from a separate population of highly consistent data suggests

UNIT	SAMPLE LOCATION	SULPHIDE	$\delta^{34}S_{CDT}$
Unaltered Shale	MEQ-16-184.6	Pyrite	-12.7
Outer Carapace Vein	MEQ-10-213.8	Pyrrhotite	- 4.6
	MEQ-10-285.6	Chalcopyrite	- 5.4
	"	Pyrrhotite	- 5.3
	MEQ-11-302.6	Chalcopyrite	- 4.3
	MEQ-12-241.2	Pyrite	- 3.6
	MEQ-14-221.8	Pyrite	- 5.1
	MEQ-14-233.0	Pyrite	- 4.7
	"	Chalcopyrite	- 5.0
	MEQ-14-243.1	Chalcopyrite	- 5.4
	MEQ-14-242.5	Chalcopyrite	- 5.6
	"	Pyrite	- 5.6
	MEQ-15-241.1	Chalcopyrite	- 5.4
	"	Pyrite	- 5.0
	MEQ-21-232.1	Chalcopyrite	- 5.6
	"	Pyrite	- 5.5
	MEQ-22-164.6	Chalcopyrite	- 4.6
	"	Pyrrhotite	- 5.3
	MEQ-22-171.9	Pyrrhotite	- 5.1
Medium Grained Skarn	MEQ-11-373.7	Chalcopyrite	- 4.7
	MEQ-14-270	Chalcopyrite	- 5.1
	MEQ-10-315.8	Chalcopyrite	- 5.1
	"	Pyrite	- 5.0
	MEQ-25-281.8	Pyrite	- 5.5
Coarse Veins (Lower Zone)	MEQ-14-267.8	Chalcopyrite	- 5.7
	MEQ-22-243.4	Chalcopyrite	- 5.3
	"	Pyrrhotite	- 5.3
Footwall Schist	MEQ-14-310.9	Chalcopyrite	- 5.4
	MEQ-18-319.4	Chalcopyrite	- 3.7

	~	Mean ‰	S.D ‰	Range‰
All sulphides	30	- 5.3	1.5	-12.7 to - 3.6
All pyrite	9	- 5.7	2.4	-12.7 to - 3.6
All Chalcopyrite	15	- 5.1	0.6	- 5.7 to - 3.7
All pyrrhotite	6	- 5.1	0.3	- 5.3 to - 4.6

TABLE 5.1: *$\delta^{34}S$ derived from sulphide separates samples from Mount Elliott cores statistical data*

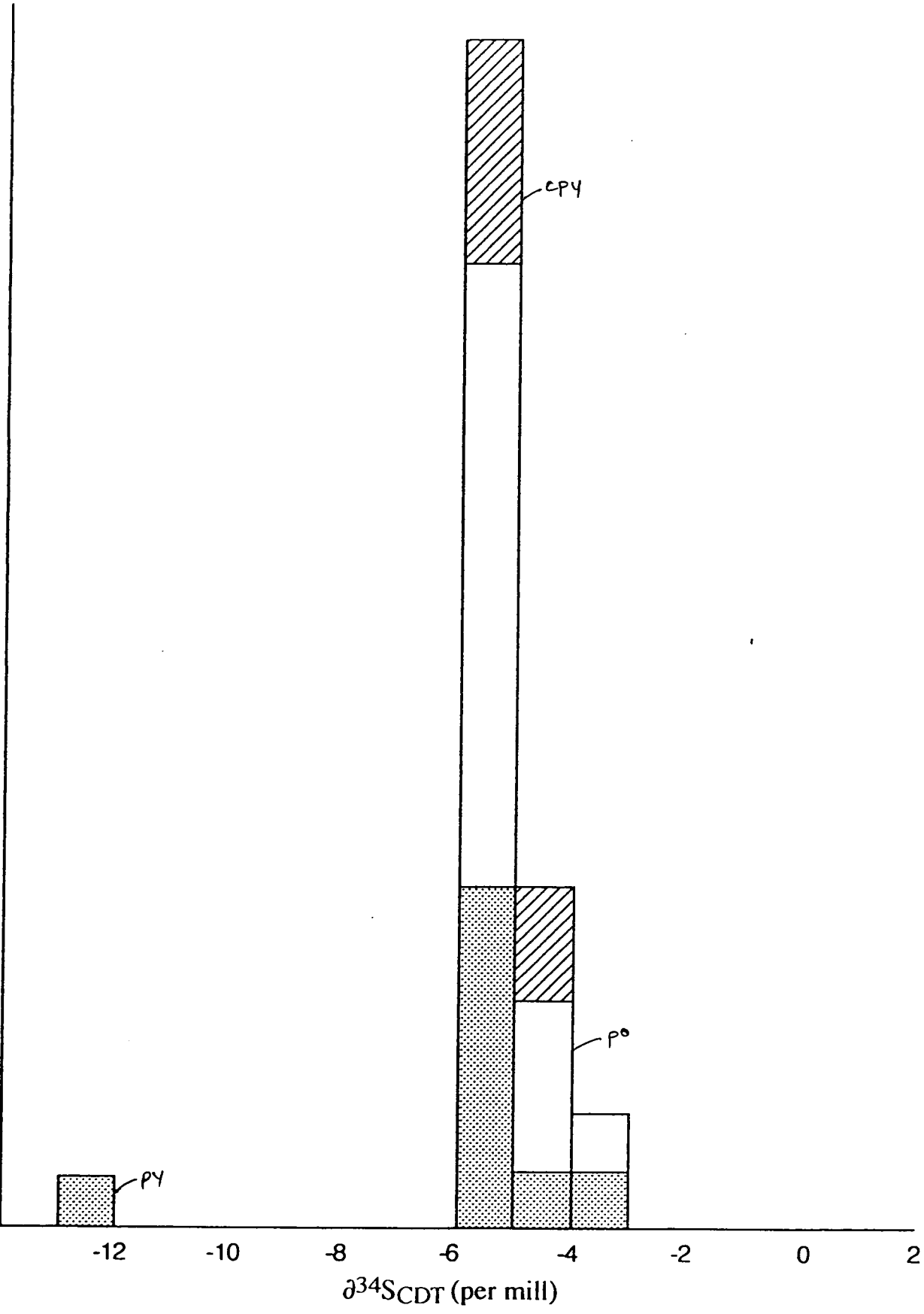

Figure 5.1: *Sulphur isotope date for Mount Elliott samples. Early shale-ho sted syngenetic pyrite exhibits a strong negative value relative to ore-related sulphides.*

that the value is real and can be interpreted to represent a substantially different mineralisation history for that sample. Within the larger population related to ore deposition, sulphides sampled in contact with each other exhibit a consistent trend of $\delta^{34}S_{po} \leq \delta^{34}S_{cpy}$ and $\delta^{34}S_{cpy} \leq \delta^{34}S_{py}$ which is compatible with the observed sulphide paragenesis of py -> cpy -> po and hence reflects an evolving system with the sulphides in relative isotopic disequilibrium.

The narrow range of $\delta^{34}S$ for sulphides from mineralised veins in this study implicates a single homogenous fluid source, or may be indicative of highly efficient mixing of two fluids from different sources. Mount Elliott and the nearby Swan prospect have recently been incorporated in a regional S-isotope study (Davidson and Dixon, 1992) with values equally constrained between -6.5 and -4.9‰ (ave. -5.6‰, 7 samples). Epigenetic sulphide from deposits closer to the Williams Batholith (e.g., Mount Dore, Hampden) were interpreted to be derived from exsolving granite fluids. Without the benefit of a $\delta^{34}S$ signature of pyrite shale the authors concluded that igneous sulphur present in fluids circulating granite bodies was fault channelled into pyritic shales of the Kuridala Formation where progressive mixing with biogenically derived sulphur resulted in the fluids acquiring locally homogeneous sediment-buffered $\delta^{34}S$ values in the range -10 to +10‰.

Studies of Cu ± Au skarns and replacement ores in different geological environments are also consistent with other magmatic or magmatic and host-rock sulphur sources. Magmatically-derived sulphur is implicated in the deposition of Au-Bi-Cu bodies at Tennant Creek with $\delta^{34}S$ values of 0-5‰ (Wedekind *et al.* 1989, Wedekind, 1988). Results from the Monterrosas Cu-Fe skarn in Peru ($\delta^{34}S$ = 2.7 to 3.3‰, Vidal *et al.* 1990) and the Tomboy-Minnie Au skarn, Canada ($\delta^{34}S$ + 2.7 to 4.7‰, Theodore *et al.* 1930) also suggest a magmatic sulphur source. A mixing of magmatic and country rock-derived sulphur at the Red Dome Au skarn, NE Queensland, is evidenced by values ranging from -0.8 to -4.4 ‰ (Ewers and Sun, 1988). Two spatially distinct orebodies in the Craigmont

Cu-Fe skarn were derived from separate sulphur sources (Morrison, 1980). Sulphide from the No. 1 orebody ($\delta^{34}S$ = 0.4 to -3.0‰) is interpreted to be magmatic-derived, whilst that from the distal No. 2 orebody has a biogenic source ($\delta^{34}S$ = -8.5 to -4.4‰).

Hence, with the new Mount Elliott data corroborated by sulphur sources deduced for Cu-Au skarns in general, it is proposed that interaction between a granitic-derived fluid ($\delta^{34}S$ + 0 to 4 ‰) and biogenic sulphur hosted in carbonaceous shales of the Kuridala Formation ($\delta^{34}S$ = 12 to -10‰) resulted in a highly constrained homogenous mixture with $\delta^{34}S$ values in the range of -6 to -3‰. A highly efficient mechanism of fluid interaction must have been involved. Intense hydraulic fracturing of a brittle, sulphide-rich hornfels/shale would provide the high permeabilities necessary and hence fluid access to a large surface area of leachable rock.

5.3 The Early Skarn-forming Fluid

The solubility of minerals in the ore-forming hydrothermal fluid is the key factor governing the processes of mineral transport, deposition and replacement that are intrinsic to the formation of hydrothermal ore deposits (Holland and Malinin, 1979) although determining the precise physiochemical conditions (e.g., T pH, fO_2, ΣS, ΣCl) of the fluid is a fundamental problem to understanding these processes. Therefore, in the absence of fluid inclusion data and thermodynamic model estimations, assumptions and conclusions about the hydrothermal fluid are necessarily derived from physical observations of Mount Elliott cores together with comparisons and extrapolations with studies of fluid conditions from similar hydrothermal systems.

Fluid inclusion studies of various deposits indicate that prograde skarn assemblages are formed from hot (450-650°C), relatively saline (>10 wt % NaCl equiv.) metasomatising fluids of magmatic origin (Vidal *et al.* 1990; Ochiai, 1987; Connelly *et al.* 1983; Brown and Nesbitt, 1984; Haruna *et al.* 1990). However, Kwak (1986) suggests that both distance

from source, and time, induce temperature and salinity gradients where skarn occurring proximal to the source are formed at high temperature (400-600° C), whilst those distal to the source are deposited at lower temperature (210-350°C). Calc-silicate assemblages can form at relatively low temperatures: Zierenberg and Shanks (1988) demonstrated that a magnetite-hematite-pyroxene equilibrium assemblage (313-346°C) formed in metalliferous sediment in the Red Sea by convecting hot brines. However, the pyroxene-scapolite assemblage common at Mount Elliott is probably indicative of a high temperature (450-650°C) metasomatic fluid (Baranov*et al.* 1985; Einaudi *et al.* 1981).

The prograde alteration at Mount Elliott indicates that the fluid was rich in calcium (all calc-silicates), Fe and Mg ("cpx"), Na (albite and scapolite), Cl (scapolite), and contained significant P (apatite) and Ti (sphene). The absence of sulphides (pyrite, chalcopyrite, pyrrhotite) associated with the pre-economic skarn suggests low total sulphur content (ΣS) and together with the absence of magnetite, is indicative of moderate to high oxygen fugacity conditions (Kish and Stein, 1989). Application of phase equilibria and fluid inclusion data to observed skarn assemblages (similar to Mount Elliott) of the Bwana and Maria Cu-skarns yielded calculated log fO_2 values between -18.5 and -17.0 (Connelly and Bowman, 1984). Oxidised assemblages are typically associated with magnetite-bearing intrusives (Brown and Nesbitt, 1987) implying that fO_2 and hence the phase assemblage are controlled externally by the redox characteristics of the magma and its derived fluid. Phosphorous is more likely to migrate with carbonate fluid phases (Dernov-Pegarev and Malinin, 1985) and, together with the abundance of calcium, suggests that the fluid was probably CO_2-rich.

The acidity of the early metasomatic fluid is difficult to determine. However, the common occurrence of K-feldspar in the skarn alteration assemblage and the absence of muscovite suggests that the pH is at least above the muscovite/K-feldspar buffer and thus the fluid pH is likely to range between weakly acidic and weakly alkaline. Carbonate deposition in other gold-rich skarns is interpreted to be derived from high temperature (450-650°) weakly acidic

solutions (e.g., Beddoe-Stephens *et al.* 1987). The replacement of quartz and calcite by infiltration metasomatism of shales in the outer carapace to form diopside-hedenbergite can be written as (Korzhinskiy, 1985);

$$2SiO_2 + 2CaCO_3 + (Mg,Fe)Cl_2 <=> Ca(Mg,Fe)Si_2O_6 + CaCl_2 + 2CO_2$$

which is independent of pH. Hence, acidity was not a controlling factor on calc-silicate mineralisation in the early fluid. The coarse crystalline growth of "cpx" enveloped by massive calcite in veins of the outer carapace, and in the cross-cutting mineralised veins suggests calcite precipitated in equilibrium with clinopyroxene. The solubility of calcite is controlled by T, P and X_{CO_2}, where X_{CO_2} of calcite exhibits the unique property of decreasing solubility with increasing temperature or increasing solubility with increasing pressure (Fein and Walther, 1987). However, the coarse crystalline vein textures suggest that both temperature and pressure were constant over a significant period and so calcite precipitated in response to changing X_{CO_2} conditions. With increasing X_{CO_2} calcite solubility is shown to increase to a maximum of X_{CO_2} = 0.02 to 0.05 at 2 kbars and 400-550°C (Fein and Walther, 1987) which corresponds with the estimated high temperature of the fluid.

The introduction of magnetite to the skarn assemblage at Mount Elliott characterises an intermediary phase between calc-silicate skarn development (prograde) and sulphide deposition (retrograde). However, magnetite locally post-dates the calc-silicate assemblage on a deposit-scale. Precipitation of magnetite from a fluid evolving from the base of the system may be contemporaneous with calc-silicate development higher in the system. This is evidenced by zoning of magnetite concentrations, a feature of many Fe-rich Cu-skarns (Vidal *et al.* 1990).

The mobilisation of Fe in high temperature aqueous solution is generally regarded as a function of chlorine concentration, although transport by H_2S, CO_2 and HF complexes is also considered likely where their concentrations are high (Dymkin *et al.* 1984; Purtov *et al.*

1989; Eugster and Chou, 1979). High temperatures transport (>600°C) is favoured as the $FeCl_2$ complex (Eugster and Chou, 1979);

$$Fe_3O_4 + 6HCl_{(aq)} + H_{2(g)} <=> 3FeCl_{2(aq)} + 4H_2O_{(aq)}$$

where HCl content ([HCl] > 10^{-3} mol/l) strongly enhances the solubility of magnetite. The mechanism of magnetite deposition is less consistent, however, with Eugster and Chou (1979) modelling a temperature dependence for Cornwall-type magnetite deposits. Iron is acquired at depth by convecting supercritical aqueous chloride solutions (600-670°C) and magnetite is deposited at the low temperature end of the cell (<500°C). Other workers report that magnetite deposition in calcic skarn is not related to temperature but occurs by neutralisation of acid solutions due to reaction of the fluid with calc-silicates (Stenina *et al.* 1979; Dymkin *et al.* 1984; Purtov *et al.* 1989);

$$Fe_3O_4 + 6H^+ + 6Cl^- <=> 3FeCl_2 + 3H_2O_{(l)} + {}^1/_2O_{2(g)}$$

The latter process is more consistent with observed phase relationships at Mount Elliott although decreasing temperature at the time of magnetite deposition is highly likely.

5.4 Transport and Deposition of Sulphides

Although a lack of experimental studies of sulphide solubility in systems buffered by common skarn calc-silicates is evident, most studies recognise that sulphide deposition usually takes place after the main period of skarn growth, as a consequence of decreasing temperature, local oxidation - reduction reactions, or neutralisation of the fluid at a marble contact (Einaudi *et al.* 1981). The introduction of sulphides at Mount Elliott indicates that significant changes took place in fluid conditions and composition, in particular in fO_2, temperature and $a_{H2S}(\Sigma S)$. An approximation of the evolving fluid path in the Fe-S-O system is illustrated in a plot of $\log fO_2$ vs pH (Figure 5.2).At high temperatures (>300-350°C) the stability of magnetite at relatively high ΣS (Wedekind *et al.* 1988) suggests that the entering fluids were initially in equilibrium with magnetite (A) and relatively reduced (at least below the hematite-magnetite buffer).

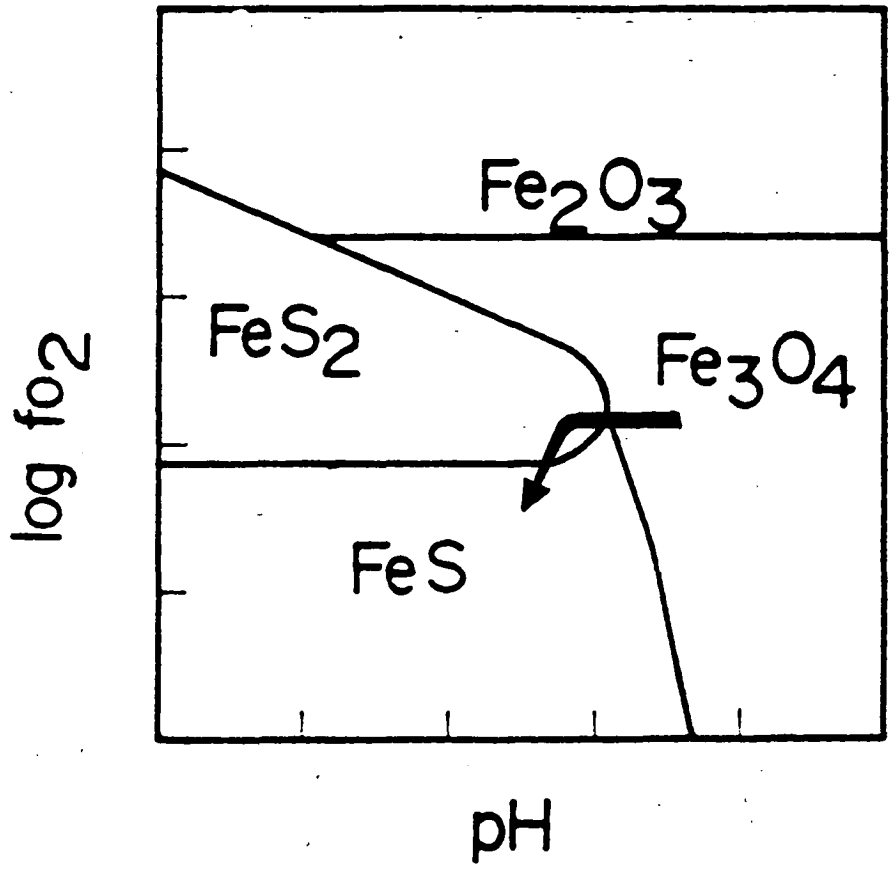

Figure 5.2: *fO_2-pH diagram of Fe-S-O phases showing path of mineralising fluid*

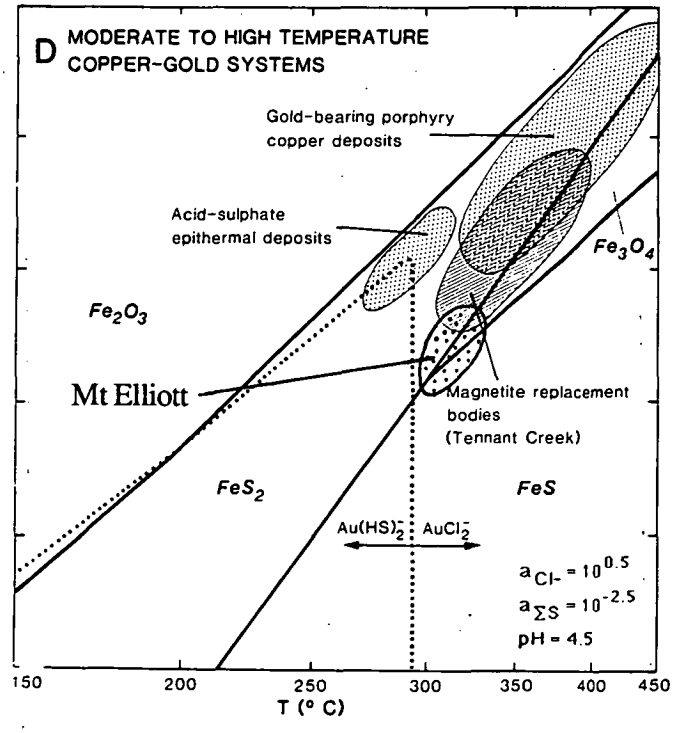

modified after Huston and Large (1989)

Figure 5.3: *Field of gold deposition in log f02-T space for Mount Elliott fluids compared with other moderate-high temperature Cu-Au systems.*

Whereas the oxidised nature of the early fluid was controlled by the intruding magma, the reduced character of the later mineralising fluid is influenced by the host rocks, whose reducing capacity is related to the presence of carbon and absence of hematite and gypsum. Reduced host rocks typically result in high pyrrhotite/pyrite ratios and the dominance of magnetite as the iron oxide phase (McMillan *et al.* 1990) which are characteristic features of the mineralisation at Mount Elliott.

From the magnetite field the fluid evolved into equilibrium with pyrrhotite (D), where the deposition/replacement process moved with increasing fluid pH from an early H_2S-poor environment (mag-py) to a later H_2S-rich environment (C;py-po±mag) at relatively constant fO_2. The very poor ability of pyrrhotite to form in equilibrium with magnetite indicates that the fluid was not buffered along the pyrrhotite-magnetite boundary, but rather passed instantaneously through (or below) the py-po-mag triple point, possibly in response to decreasing fO_2. Co-precipitation of chalcopyrite and pyrrhotite (at least in part) from a single hydrothermal solution is indicative of a mineralisation temperature of <325°C since the chalcopyrite-pyrrhotite assemblage is only stable below 325°C and 2 kbars (Haruna *et al.* 1990). Estimations of mineralisation temperatures from fluid inclusions range from 300-500°C for Cu ore in Au-Bi-Cu replacement bodies at Tennant Creek (Wedekind *et al.* 1988) and Canada (Brown and Nesbitt, 1987).

Deposition of sulphides from chloride complexes in relatively hot (250-350°C) aqueous solutions is favoured by increasing a_{H_2S}, decreasing fO_2, dilution (decreasing a_{Cl^-}), increasing pH and decreasing temperature (Barnes, 1979) all of which are consistent with the observations of the Mount Elliott system. Several workers on Cu skarns suggest that much of the ferrous ion necessary for crystallisation of sulphides was derived from the clinopyroxene with H_2S and Cu contributed by the fluid (Haruna *et al.* 1990; Brown and Nesbitt, 1987);

$$CaFeSi_2O_6 + H_2S + 2H^+ \Leftrightarrow FeS + Ca^{2+} + 2SiO_{2(aq)} + 2H_2O$$

$$CaFeSi_2O_6 + 2H_2S_{(aq)} + Cu^+ + H^+ \Leftrightarrow CuFeS_2 + Ca^{2+} + 2SiO_{2(aq)} + 2H_2O + {}^1/_2H_2$$

which implies that the later fluids were not in equilibrium with existing minerals. These equations are consistent with Mount Elliott mineralisation textures, where sulphides readily invade and replace the calc-silicate phases.

5.5 Gold transport and deposition

In high temperature hydrothermal systems, gold can be transported as either a chloride complex, $AuCl^-_2$, or as a bisulphide complex, $Au(HS)^-_2$, with deposition from solution controlled by temperature, pH, and fO_2. The mechanism of solution and precipitation of these complexes from the hydrothermal fluid are significantly different (Zaw, 1991);

$$4\,Au + 8\,H_2S + 0_2 <=> 4\,Au(HS)^-_2 + 2H_20 + 4H^+$$

$$4\,Au + 8Cl^- + 4H^+ + 0_2 <=> 4\,AuCl^-_2 + 2H_20$$

Hence a decrease in fO_2 will decrease the solubility of gold as either complex, whereas an increase in pH will cause an increase in $Au(HS)^-_2$ solubility, but decrease the solubility of $AuCl^-_2$. Similarly, an increase in a_{H_2S} will produce an increase in the solubility of gold as $Au(HS)^-_2$, but will not affect the stability of $AuCl^-_2$.

Studies of gold skarns report that the base metals were transported as chloride complexes at relatively high temperatures (>300°C) in promixal parts of the system, whereas the gold was transported mainly as the bisulphide complex in relatively lower temperature fluids (<300°C) and deposited in distal parts of the system (Meinert, 1989; Theodore *et al.* 1930; Myers, 1985). In Au-Bi-Cu replacement bodies at Tennant Creek, the gold was interpreted to be transported in high temperature, high salinity fluids as a chloride complex (Wedekind *et al.* 1988). The iron content of calc-silicate minerals in Canadian iron skarns is correlated with extremely high salinities (<50 wt % NaCl) to suggest that the chlorine content of metasomatic solutions may be the dominant control on the transport of both iron and gold

(Meinert, 1984). In volcanogenic hydrothermal systems, Huston and Large (1989) have shown that the $Au(HS)^-_2$ complex is only important in the pyrite stability field at relatively low temperature (<250°C) whereas gold transport by Cl^- ligands is not restricted by iron mineral equilibria and is most significant in the hematite, magnetite and pyrite fields at high temperature (>300°C).

The strong correlation of gold to copper at Mount Elliott suggests that the Au was transported with Cu as a chloride complex, $AuCl^-_2$, in high temperature (300-350°C), relatively reduced fluids, and was deposited with chalcopyrite in response to decreasing fO_2 and increasing pH conditions. The fluid path and field of gold deposition is shown in log fO_2-T space (Figure 5.3) with other moderate to high temperature copper-gold systems. Further work is necessary to evaluate the potential of gold to be accumulate initially in calc-silicates (e.g., Korobeynikov, 1982; Beddoe-Stephens *et al.* 1987) with later remobilisation into the lattice of chalcopyrite during replacement. The potential of Te and Se complexes to transport gold in solution has been considered in gold deposits where their concentration is high (Romberger, 1986) but are not considered significant in the Mount Elliott system.

5.6 Model of Fluid Evolution at Mount Elliott

Intrusion of a granitic body at depth acted to fracture brittle rocks such as the Elliott Beds shale. Expulsion of an initial low-temperature, halogen-rich, oxidised fluid from the intrusion invaded the fractured shale resulting in bleaching, F-Ca-metasomatism and extensive quartz± hematite veining. Continued fracturing by localised fluid over-pressuring enhanced the high permeability of the bleached shale permitting an invading hot, oxidised, Na-rich fluid to extensively albitise fractures and adjacent wallrock. Where fracturing was particularly intense (surrounding a less brittle amphibolite body) progressive infiltration of the fluid ultimately resulted in a massive overprint of the shale foliation and amphibolite textures by albite-hematite and accompanying quartz-calcite-K-feldspar.

Continued structural adjustments and localised thrusting along the Mount Dore thrust zone culminated in massive brecciation and vein development at Mount Elliott. The breccia was invaded by a very hot (450-650°C), high salinity, relatively oxidised magmatic fluid that was probably CO_2-rich and contained low total sulphur $\delta^{34}S$ = -0 to 2‰). The metasomatising fluid infilled the breccia and enclosing fracture system. Infiltration prograde-skarn alteration of the massive albite rock and shale ensued. Matrix textures indicate that the breccia was kept open by high fluid pressures allowing pegmatitic growth of calc-silicate minerals and calcite infill between the shale blocks.

At depth the hot metasomatic magmatic fluid interacted with, and homogenously mixed with a downward-convecting, low temperature, reduced, sulphur-rich fluid that had leached metals and sulphur from diagenetic sulphides in the shales ($\delta^{34}S$ = -12 to -10 ‰). The anomalous Ni and Co in pyrrhotite may be derived from this fluid, released during the partial breakdown of biotite (Nagaytsev, 1988) and subsequent migration into the fluid. The resulting hot (250-350°C) sulphur and metal-rich hydrothermal fluid interacted with the calc-silicate-calcite±magnetite skarn alteration and precipitated sulphides ($\delta^{34}S$ = -5.7 to -3.6‰) in response to decreasing fO_2 and increasing pH conditions (Figure 5.4).

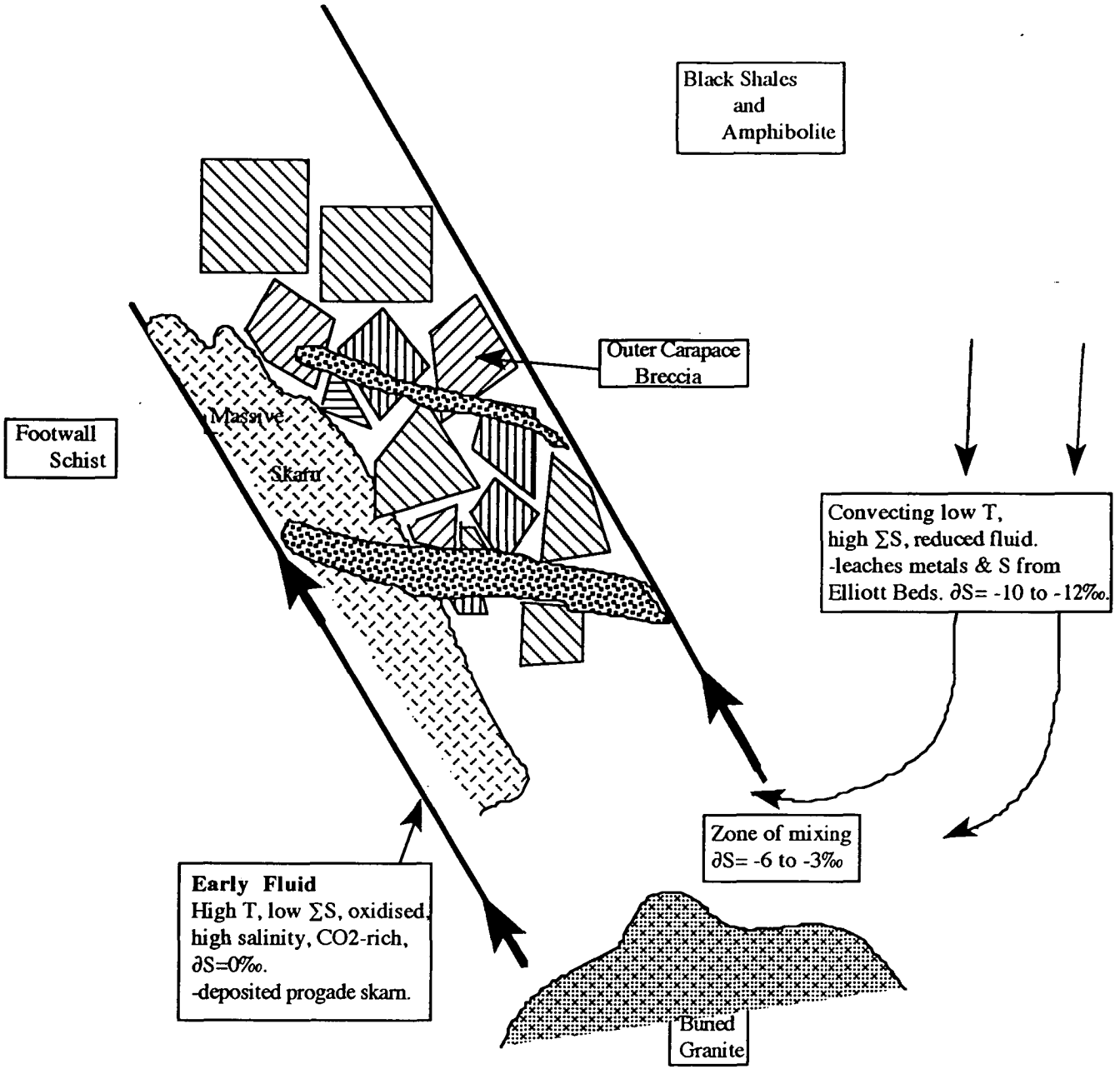

Figure 5.4: *Model of fluid evolution and alteration-mineralisation at Mount Elliott.*

Chapter 6

THE MOUNT ELLIOTT CU-AU DEPOSIT - A DISCUSSION

6.1 Classification of Mount Elliott-Style Mineralisation

Using the modern scheme of skarn classification (Einaudi *et al.* 1981) based upon the dominant calc-silicate mineral assemblages ("cpx", scapolite, opatite and sphene) and the dominant economic metals (copper-gold) Mount Elliott is characterised as a calcic Cu-Au skarn deposit. On grade/tonnage date (2 million tonnes at 4.2% Cu Equiv.) the deposit is within the field of small non-porphyry associated Cu-skarns. However, labelling the mineralisation at Mount Elliott as a skarn deposit raises some academic questions since the mineralisation of economic importance is hosted in pegmatitic veins that cross-cut earlier-formed skarn alteration. The orebody is a fracture-controlled vein deposit within a complex fault belt characterised by en-echelon fractures and massive brecciation. Extensive infiltration of hydrothermal fluids into the fractured host shale has produced intense coarse grained skarn alteration that encloses the set of mineralised veins and is open to the north, south and at depth. Although concentrated in veins, the mineralisation is clearly hosted in skarn. The mineralogical (and possibly genetic) similarity between the vein gangue and the wallrock skarn alteration suggests that classifying the mineralisation as a calcic skarn-hosted Cu-Au vein deposit is consistent with the observed physio-chemical features of the style of alteration and mineralisation at Mount Elliott.

6.2 Genesis of the Deposit

The concentration of sulphides in a series of pegmatitic calc-silicate veins within the Elliott Beds was controlled by two principal features; fluid-metal source and transport, and structure.

6.2.1 Fluid-metal Source and Transport

Work from this study suggests that an early, hot (>450°C), relatively oxidised and weakly acidic magmatic-derived fluid deposited calc-silicate skarn in fractured shales and phyllites of the Elliott Beds. The fluid was probably CO_2-rich, contained low total sulphur and was rich in calcium. Within the Kuridala Formation, Mount Elliott is highly anomalous in calcium. The close proximity of the deposit to the calcium-rich Staveley Formation and its juxtaposition to the Swan deposit, a mineralogically similar skarn within the Staveley Formation suggests that the calcium could have been leached from the Staveley Formation and redeposited at Mount Elliott. This implies either the presence of an unknown body of Williams Granite west of Mount Elliott beneath the Staveley Formation, or a large block of Staveley Formation incorporated in the Kuridala Formation.

Evidence from sulphur isotopes taken from sulphide samples throughout the deposit indicates that the hot granitic fluid ($\delta^{34}S \approx 0‰$) interacted with a circulating, cooler (<350°C), reduced fluid that had leached metals and sulphur from diagenetic sulphides in the shales ($\delta^{34}S$ = -12 to -10‰). Homogenous mixing of the two fluids, facilitated by high porosity in the fractured shale resulted in lightly constrained isotope values for the ore-related sulphides ($\delta^{34}S$ = -5.7 to -3.6‰). The metals were transported as chloride complexes and precipitated as sulphides in response to decreasing $f02$ and increasing pH conditions.

Other features consistent with a granite derived fluid source include a fluorine-enriched geochemical halo distal to the main body of mineralisation (grades up to 1%F), cross-cutting tourmaline-feldspar pegmatites and quartz veins, and discordant aplite dykes.

6.2.2 Structural Controls

The youngest deformation in the Mount Elliott vicinity involves east-west crustal shortening and thickening of the Elliott Beds controlled by reverse faulting. The presence of oxidised, low angle thrust features in outcrop at Mount Elliott indicates that development of the calc-silicate+chalcopyrite vein system at depth is related to this last phase of deformation and reactivation of the high-angle reverse faults.

No distinct cross-cutting relationship between the mineralised veins and the steeper faults is evident implying a general contemporaneity between development of the vein sets and reactivation of the high-angle thrusts. Movement on the thrust surfaces resulted in fracturing and ultimately brecciation of the brittle black shale unit, allowing influx of hydrothermal fluids via a mechanism similar to the 'flats-fault vein' model described for mesothermal gold-quartz deposits (Sibson *et al.* 1988, Sibson 1989). However, unlike the episodal pulsing of mineralising fluids involved in the above model, the very coarse crystal growth and absence of crack-seal textures in veins at Mount Elliott suggests that vein precipitation occurred under prolonged conditions of constant temperature and pressure with fluid pressure > lithostatic pressure. A structural model for mineralised vein development at Mount Elliott is illustrated in Figure 6.1.

FIGURE 6.1: *Structural model for mineralised vein development.*

6.3 Timing of Mineralisation

Mount Elliott shares features common to other deposits in the area which may be used to place the deposit within a regional context. The albite-hematite alteration is ubiquitous throughout the region associated with copper mineralisation. At Starra, extensive 'red-rock' alteration occurs in footwall metasediments and is overprinted by magnetite-hematite-sulphide mineralisation. This early phase of alteration is also prominent in skarn at Swan, but is only weakly developed in carbonate-poor shales at Mount Dore, and is attributed to an initial expulsion of fluid related to intrusion of the Williams Batholith.

Calc-silicate and calcite mineralisation, characteristic of the Mount Elliott style of mineralisation, is repeated at Swan although virtually absent at Mount Dore. This may be related to Mount Dore's close proximity to the granite within the Kuridala Formation and hence the fluids inability to leach carbonate from the Staveley Formation.

Numerous secondary copper deposits hosted in fractured black shales occupy a similar stratigraphic position to Mount Elliott at the top of the Kuridala Formation and a similar spatial association to the Williams Batholith and the Mount Dore fault zone.

Hence the Mount Elliott deposit is directly related to emplacement of the Williams Batholith (syn- to early post-intrusion) with mineralisation synchronous with other deposits in the region. Variations in deposit styles have resulted from differing structural domains and local variation in the geochemistry of hostrock lithologies.

6.4 Applications to Future Exploration

The genetic association of Mount Elliott-style mineralisation with granite-derived fluids and localised thrusting suggests that repetitions of this deposit type elsewhere in the region is likely. For example, to the north of Mount Elliott at Kuridala, the Hampden Cu-Au deposit (although associated with quartz veining - possibly a lower temperature end-member) exhibits several structural and geochemical similarities to Mount Elliott. These include low-angle mineralised veins bound by steeper structures and anomalous fluorine geochemistry in the hangingwall.

However, the poor surface expression of the flat-lying mineralised veins and depressed surface geochemical anomalies suggests that, in the absence of near-surface secondary enrichment, exploration by conventional copper and gold geochemistry is likely to be unsuccessful. The presence of a fluorine-enriched halo surrounding the deposit suggests that fluorine may be more successful as a geochemical path-finder for this style of mineralisation. Other trace elements with potential use as path-finders include nickel, selenium, tellurium, barium and possibly cobalt.

Detailed field mapping targeting localised bleaching of shales and structural features is essential. Significant structural features include;

- localised thickening of shale sequences and associated steep reverse faulting
- low-angle thrusting, possibly with oxidised and bleached fault planes
- large scale brecciation and breccia pipe features (possibly preferentially located in the hinges of D_2 folds)

- faults which cross-cut the Staveley Formation and are terminated in the Kuridala Formation (e.g., the Swan-Mount Elliott trend).

An improved understanding of the structural controls on Mount Elliott should significantly enhance future exploration programmes. A proposed decline through the deposit will greatly assist here.

The high magnetite and pyrrhotite content at Mount Elliott produces a strong magnetic signature that is partially obscured by the adjacent amphibolite body and the overlying slag dump. Electro-magnetic surveys also produce distinct anomalies associated with the massive sulphide. Little is known about the gravimetric signature over Mount Elliott. However, this study recommends the acquisition of gravity data for the region in an attempt to detect the presence of shallow-buried granite bodies that might have acted as preferential fluid sources which focussed hydrothermal fluids into cross-cutting structures.

Massive skarn and outer carapace alteration is open to depth beneath Mount Elliott which suggests that repetition of the flat-lying mineralised vein system at depth is possible.

REFERENCES

Aleksandrov, S. M., 1985. Metasomatic Changes in Carbonate Rocks at Contacts with Basic and Ultrabasic Intrusions. Translated from Geokhimiya, No. 8. p.1218-1232.

Allcock, J. B., 1982. Skarn and Porphyry Copper Mineralization at Mines Gaspe, Murdochville, Quebec. Economic Geology, v. 77, p.971-999.

Atkinson, W. W., Jr., Kaczmarowski, J. H., and Erickson, A. J., Jr., 1982. Geology of a Skarn-Breccia Orebody at the Victoria mine, Elko County, Nevada: Econ. Geol. v. 77, p.899-918.

Baranov, E. N., Grinenko, L. N. and Pavlov, G. P., 1985. Pyrite Sulfur-Isotope Compositions in Ural Skarn-Magnetite Deposits. Translated from Geokhimiya, No. 12, p.1713-1722.

Barnes, H. L., 1979. Solubilities of ore minerals: *in* Geochemistry of Hydrothermal Ore Deposits; H. L. Barnes (ed). p.405-460.

Barrett, T. J. and MacLean, W. H., 1991. Chemical, Mass, and Oxygen Isotope Changes During Extreme Hydrothermal Alteration of an Archean Rhyolite, Noranda, Quebec. Economic Geology, v. 86. p.406-414.

Beardsmore, T. J., 1986. Aspects of the geology and mineralisation in the Selwyn region: a preliminary report. Unpubl. report to Cyprus Minerals, Mount Isa, 155p.

Beardsmore, T. J., 1988. The Selwyn-Style Cu-Au Deposits in the Mount Isa Block - A late Orogenic, Granite and Deformation-Related Style. Abstracts, Geological Society of Australia, Ninth Australia Geological Convention: p.55-58.

Beardsmore, T. J., Newberry, S. P. and Laing, W. P., 1988. The Maranoan Supergroup: an inferred early volcano-sedimentary rift sequence in the Mount Isa Inlier and its implications for ensialic rifting in the Middle Proterozoic of northwest Queensland. Precambrian Res., 40/41: p.487-507.

Beddoe-Stephens, B., Shepherd, T. J., Bowles, J. F. W. and Brook, M., 1987. Gold mineralization and skarn development near Maura Sipongi, West Sumatra, Indonesia: Econ. Geol. v. 82, p.1732-1749.

Blake, D. H., 1987. Geology of the Mount Isa Inlier and environs, Queensland and Northern Territory. Bureau of Mineral Resources, Geology and Geophysics. Bulletin 225. p.5-61.

Blake, D. H., Bultitude, R. J., Donchak, P. J. T., Wyborn, L. A. I., and Hone, I.G., 1984. Geology of the Duchess-Urandangi region, Mount Isa Inlier, Queensland. Bureau of Mineral Resources, Geology and Geophysics. Bulletin 219. p.38-65.

Blake, D. H., Etheridge, M. A., Page, R. W., Stewart, A. J., Williams, P. R. and Wyborn, L. A. I., 1990. Mount Isa Inlier - Regional Geology and Mineralisation, *in* Geology of the Mineral Deposits of Australia and Papua New Guinea (Ed. F. E. Hughs), p.915-925. (The Australian Institute of Mining and Metallurgy: Melbourne).

Bohlke, J. K., 1989. Comparison of metasomatic reactions between a common CO_2-rich vein fluid and diverse wall rocks, intensive variables, mass transfers and Au mineralization at Alleghany, California. Econ. Geol. v. 84 (2), p.291-327.

Brooks, J. W., Meinert, L. D., Kuyper, B. A., Lane, M.L. and Pettit, P. M., 1989. Mineralogy and petrology of the McCoy gold skarn, Lander County, Nevada [abs.]: Geol. Soc. America Abstracts with Programmes. v. 21, p.59-60.

Brown, I. J. and Nesbitt, B. E., 1984. Gold-bismuth-copper skarn mineralisation in the Marn Skarn, Dawson City, Yukon [abstr.]: *in* The Geological Society of America; 97th Annual Meeting, Abstracts with Programmes - Geol. Soc. Amer., v. 16 (6), p.456.

Brown, I. J. and Nesbitt, B. E., 1987. Gold-Copper-Bismuth mineralization in hedenbergitic skarn, Tombstone Mountains, Yukon. Canadian Journal of Earth Sciences, v. 24 (12), p.2362-2372.

Buseck, P. R., 1966. Contact metasomatism and ore deposition: Concepcion Del Oro, Mexico: Econ. Geol., v. 61. p.97-136.

Cameron, D. E. and Garmoe, W. J., 1983. Distribution of gold in skarn ores of the Carr Fork Mine, Tooele, Utah [abs.]: Geol. Soc. America Abstracts with Programmes, v. 15, p.299.

Carter, E. K., Brooks, J. H. and Walker, K. R., 1961. The Precambrian Mineral Belt of North-Western Queensland, Bur. Miner. Resour. Geol. Geophys. Aust. Bull. 51.

Charoy, B. and Pollard, P. J., 1989. Albite-rich, silica depleted metasomatic rocks at Emuford, Northeast Queensland: Mineralogical, Geochemical, and Fluid Inclusion Constraints on Hydrothermal Evolution and Tin Mineralization. Econ. Geol., v. 84 (7), p.1850-1874.

Connelly, M. P., Bowman, J. R. and Whelan, J. A., 1983. Petrologic and Fluid Inclusion Studies of the Bwana and Maria Copper Skarns, Rocky Range, SW Utah. Geol. Soc. America Abstracts with Programmes v. 15, p.299.

Connelly, M. P. and Bowman, J. R., 1984. Petrologic and fluid inclusion studies of copper skarns, Rocky Range, SW Utah [abstr.]: *in* The Geological Society of America, 97th Annual Meeting, Abstracts with Programmes - Geol. Soc. Amer., 16 (6), p.476.

Darlington, R. E., 1957. Mount Elliott Mine, Selwyn, Queensland. Mount Isa Mines Ltd. Company Report. p.2.

Davidson, G. J. and Dixon, G.H., 1992. Two sulphur isotope provinces deduced from ores in the Mount Isa Eastern Succession, Australia. Mineral. Deposita 27, p.30-41.

Davidson, G. J., 1989. Starra and Trough Tank: Iron-Formation-Hosted-Gold-Copper Deposits of North-West Queensland, Australia. University of Tasmania: unpublished Ph.D. thesis.

Deer, W. A., Howie, R. A., Zussman, J., 1980. An introduction to the Rock Forming Minerals. Longman Group Ltd., London, 528 p.

Dernov-Pegarev, V. F.and Malinin, S. D., 1985. The Solubility of Apatite in Aqueous Alkali-Carbonate Solutions at 300, 400 and 500°C. Academy of Sciences of the USSR. Translated from Geokhimiya, No. 8. p.1196-1205.

Derrick, G. M., 1982. A Proterozoic rift zone at Mount Isa, Queensland, and implications for mineralization. BMR Jour. Aust. Geol. Geophys., v. 9, p.19-32.

Dimo, G., 1971. Final Report, Authority to Prospect 698m. (Selwyn). Anaconda Australia Ltd Company Report. 1 p.

Dimo, G., 1973. Report on Mount Elliott Cu-Prospect, Northwest Queensland. Anaconda Australia Inc. Company Report. 4 p.

Dimo, G., 1975. Precambrian Geology and Copper Mineralization of the Mount Elliott Area. M.Sc. Thesis University of Queensland p1-12.

Dutton, A. H., 1952. Report on the Mount Elliott Mine, Cloncurry District. Broken Hill South Limited Company Report. 1 p.

Dymkin, A. M., Purtov, V. K., and Yatluk, G. M., 1984. Transport of iron in high-temperature hydrothermal solutions. International Geology Review, v. 26 (10), p.1180-1184.

Einaudi, M. T., Meinert, L. D. and Newberry, R. J., 1981. Skarn Deposits. Economic Geology, 75th Anniversary Volume. p.317-391.

Ellis, D. J. and Wyborn, L. A. I., 1984. Petrology and geochemistry of Proterozoic dolerites from the Mount Isa Inlier. BMR Jour. Aust. Geol. Geophys., v. 9, p.19-32.

Etheridge, M. A., Rutland, R. W. R. and Wyborn, L. A. I., 1987. Orogenesis and tectonic process in the Early to Middle Proterozoic of northern Australia, in Proterozoic Lithosphere Evolution, Geodynamics Series 17 (Ed. A. Kroner), p.131-147 (American Geophysical Union; and Geological Society of America: Washington, D.C.).

Ettlinger, A. D. and Ray, G. E., 1988. Gold-Enriched Skarn Deposits of British Columbia. Geological Fieldwork Paper for British Columbia Ministry of Energy, Mines and Peroleum Resources. p.264-279.

Ettlinger, A.D. and Meinert, L. D., 1991. Copper-gold skarn mineralization at the Veselyi Mine, Siniukhinskoe District, Siberia, USSR. Econ. Geol. & Bull of Soc. Econ. Geologists, 86 (1), p.185-194.

Eugster, H. P. and Chou, I-Ming, 1979. A model for the Deposition of Cornwall-type Magnetite Deposits. Economic Geology, v. 74, p.763-774.

Ewers, G. R. and Sun, S. S., 1988. Genesis of the Red Dome Gold Skarn Deposit, Northeast Queensland. p.218-232.

Ewers, G. R., Torry, C. E. and Erceg, M. M., 1987. The Red Dome Gold Deposit.

Fein, J. B. and Walther, J. V., 1987. Calcite solubility in supercritical $C0_2$-H_20 fluids. Geochimica et Cosmochimica Acta, 51 (6), p.1665-1673.

Garrett, S. J. M., 1989. The Geology and Gold Drainage Geochemistry of the Lewis River Volcanics: Elliott Bay, Southwest Tasmania. Thesis for B.Sc. with Hons. 163 p.

Garrett, S. J. M., Stephens, M. and White, P., 1991. Report on Mount Elliott, Prefeasibility Study. Cyprus Gold Australia Company Report. p.7-25

Glikson, A. T., Derrick, G. M., Wilson, I. H. and Hill, R. M., 1976. Tectonic evolution and crustal setting of the middle Proterozoic Leichhardt River Fault Trough, Mount Isa Region, northwestern Queensland, BMR Jour. Aust. Geol. Geophys., V. 1, p.115-129.

Glikson, A. T., 1972. Structural setting and origin of Proterozoic calc-silicate megabreccias, Cloncurry region, northwestern Queensland. Jour. of the Geol. Soc. of Aust., Vol. 19, Pt. 1, p.53-63.

Golubev, V. S., 1983. Thermodynamics of metasomatic mineral formation at mobile geochemical barriers during mass transport by infiltration. Geochemistry International, 20 (5), p.111-117.

Guy, B., 1984. Contribution to the theory of infiltration metasomatic zoning, the formation of sharp fronts, a geochemical model. Bulletin de Mineralogie, 107 (1), p.93-105.

Harnish, D. E., and Brown, P. E., 1986. Petrogenesis of the Casseus Cu-Fe Skarn, Terre Neuve District, Haiti; *in* Mineral Deposits of Northern Alaska, Econ. Geol., v. 81 (7), p.1801-1807.

Haruna, M., Ueno, H. and Ohmoto, H., 1990. Development of skarn-type ores at the Tengumori Copper Deposit of the Kamaishi Mine, Iwate Prefecture, Northeastern Japan: Mining Geology, 40 [4(222)], p.223-243. (Japanese Journal).

Hellingwerf, R. H., 1987. Formation of sulphide deposits and its relation to sodic and potassic alteration of Proterozoic metabasites in the Saxa rift basin, Bergslagen, Sweden. Mineralium Deposita, 22 (1), p.53-63.

Holland, H. D. and Malinin, S. G., 1979. The Solubility and Occurrence of Non-Ore Minerals *in* Geochemistry of Hydrothermal Ore Deposits: second edition; Barnes, H. L. (ed). John Wiley and Sons, New York. p.461.

Huston, D. L., and Large, R. R., 1989. A Chemical Model for the Concentration of Gold in Volcanogenic Massive Sulphide Deposits. Ore Geology Reviews, v. 4, p.171-200.

Kary, G. L. and Harley, R. A., 1990. Selwyn Gold-Copper Deposits, in Geology of the Mineral Deposits of Australia and Papua New Guinea (Ed. F. E. Hughes). The Australasian Institute of Mining and Minerallurgy, Melbourne. p.955-960.

Kish, S. A. and Stein, H. J., 1989. Past Acadian metasomatic origin for copper-bearing vein deposits of the Virgilina District, North Carolina and Virginia. Econ. Geol. & Bull of Soc. of Econ. Geologists, v. 84 (7), p.1903-1920.

Korobeynikov, A. F., 1982. Gold in pyroxenes in intrusive and contact-metasomatic rocks. Geochemistry International 19 (2), p.13-24.

Korzhinskiy, M. A., 1985. Diopside-Wollastonite Equilibrium in a Supercritical Chloride Fluid. Academy of Sciences of the USSR. Translated from Geokhimiya, No. 10. p.1430-1440.

Kwak, T. A. P., 1986. Fluid inclusions in skarns (carbonate replacement deposits). Journals of Metamorphic Geology, 4 (4), p.363-384.

Laing, W. P., Rubenach, M., and Switzer, C. K., 1987. The Starra gold-copper deposit - syndeformational metamorphic mineralisation localised in a folded early regional zone of decollement. Ninth Aust. Geol. Soc. Conf. Abs., Brisbane, Qld. Geol. Soc. Aust. Abs. 21:229.

Lowell, G. R., Bizzio, R. R., Vierrether, C. B., and Noll, P. D., Jr., 1986. An unusual scapolite-bearing skarn assemblage from southeastern Missouri; [abstr.]: *in* The Geological Society of America , Southeastern section, 35th Annual Meeting; South-Central Section, 20th Annual Meeting, Abstracts with Programmes - Geo. Soc. Amer., 18 (3), p.252.

Luzgin, B.N., 1988. Intrusions and skarns of the Inskoy iron-ore deposit: International Geological Review v. 30 (4), p.459-466.

McMillan, W. J., MacIntyre, D. G., Nelson, J. L., Hoy, T., Nixon, G. T., Hammack, J. L., Panteleyev, A., Ray, G. E., Webster, I. C. L., 1990. Evolutionary Model of Skarn Formation *in* Ore Deposits, Tectonics and Metallogeny in the Canadian Cordillera. Association Geologique du Canada short course notes. p. 7.4 - 7.54.

Malone, D. H. and Brown, P. E., 1990. Precious metal mineralization of the Meme Contact Skarn, Terra Neuve District, Haiti, S.A.: *in* Geol. Soc. of Amer., North Central Section, 24th Annual Meeting, Abstracts with Programmes - Geol. Soc. of America, v. 22 (5), p.39.

Meinert, L. D., 1984. Mineralogy and petrology of iron skarns in Western British Columbia, Canada; *in* A second issue devoted to Canadian mineral deposits (Wolf, W. J., et. al.), Econ. Geol., v. 79 (5), p.869-882.

Meinert, L. D., 1987 (a). Skarn zonation and fluid evolution in the Groundhog Mine, Central mining district, New Mexico: Econ. Geol., v. 82 (3), p.523-545.

Meinert, L. D., 1987 (b). Gold in Skarn Deposits - A Preliminary Overview. 7th Quadrennial IAGOD Symposium, Stuttgart. p.1-18.

Meinert, L.D., 1988. Gold and Silver in Skarn Deposits. Bicentennial Gold 88. p.614-616.

Meinert, L. D., 1989. Gold Skarn Deposits - Geology and Exploration Criteria. Econ. Geol. Monograph 6, Gold 88 Proceedings. p.537-552.

Michaylov, D. A. and Krylova, M. D., 1978. Comparison of composition of chinopyroxenes from Precambrian magnesian skarns with pyroxenes from metamorphic rocks. Geochemistry International, 15 (3), p.47-55.

Mironov, A. G., Geletiy, V. F., Nesterova, I. N. and Tsepin, A. I, 1986. A Radioisotope Study of the Traces of Gold in Sulfides andMagnetite. Translated from Geokhimiya, No. 5: p.703-715.

Mizuta, T., and Scott, S. D., 1988. Speedometry of chalcopyrite and pyrrhotite exsolution in sphalerite from some skarn deposits [Abstr.] *in* Geol. Soc. of Amer. 1988, Centennial Celebration, Abstracts with Programmes - Geol. Soc. of Amer., 20 (7) p.94.

Morrison, G. W., 1980. Stratigraphic control of Cu-Fe skarn ore distribution and genesis at Cragimont, British Columbia. The Canadian Mining and Metallurgical Bulletin.

Morrison, G. W., 1992. Ore Deposition and Environments. Skarn Deposits. Course notes, James Cook University of North Queensland. p.9.

Myers, G. L., 1985. Gold distribution in the Fe-Cu-Au skarns of the Kasaan Pensinsula, Southeast Alaska [abstr.]: *in* The Geological Society of America, Cordilleran Section, 81st Annual Meeting, Abstracts with Programmes - Geol. Soc. Amer., 17 (6), p.397.

Nagaytsev, Y. V., 1988. The mobilisation of ore elements in the course of metamorphic reactions and processes. International Geology Review 30 (6), p.1084-1091.

Nisbet, B. W., 1983. A brief study of the relationship between metamorphism, mineralisation and structure in the Selwyn region, northwest Queensland. Unpubl. BMR Report.

Nisbet, B. W., Devlin, S. P. and Joyce, P. J., 1983. Geology and suggested genesis of cobalt-tungsten mineralization at Mount Cobalt, northwestern Queensland. Proc Australas. Inst. Min. Metall., v. 287, p.9-17.

Nye, ., and Rayner, ., 1941.

Nyvlt, J. A., 1980. Aspects of Metasomatic Alteration, Mineralization and Geochemistry at the Swan Copper Prospect, Northwest Queensland. B.Sc. Hon. Thesis, University of Sydney.

Ochiai, K., 1987. A reaction model relating skarn zones and ore formation at the Nippo Copper ore deposit, Kamaishi Mine, northeastern Japan. Econ. Geol. v. 82 (4), p.1001-1018.

Oliver, N. H. S., Holcombe, R. J., Hill, E. J. and Pearson, P. J., 1991. Tectono-metamorpic evolution of the Mary Kathleen Fold Belt, northwest Queensland: A reflection of mantle plume processes. Australian Journal of Earth Sciences, v. 38. p.425-455.

Ophel, M. A., 1980. Mineralogy and geochemistry of a copper-bearing breccia zone, Mount Dore, northwest Queensland. Unpubl. Hons. thesis, University of Sydney.

Percival, T.J., Radtke, A. S. and Bagy, W. C., 1990. Relationships among carbonate-replacement gold deposits, gold skarns and intrusive rocks, Bau Mining District, Sarawak, Malaysia: *in* Mining Geology, 40 [1(219)], p.1-16.

Plumb, K. A. and Derrick, G. M., 1975. Geology of Proterozoic rocks of the Kimberley to Mount Isa Region, *in* Economic Geology of Australia and Papua New Guinea. Vol. 1 Metals (Ed. C. L. Knight), p.217-252. (The Australian Institute of Mining and Metallurgy: Melbourne).

Purtov, V. K., Kholodnov, V. V., Anfilogov, V. N. and Nechkin, G. S., 1989. The role of chlorine in the formation of magnetite skarns. International Geology Review, 31, p.63-71.

Ray, G. E., Dawson, G. L. and Simpson, R., 1987. The Geology and Controls of Skarn Mineralisation in the Hedley Gold Camp, Southern British Columbia. British Columbia Ministry of Energy, Mines and Petroleum Resources, Geological Fieldwork, p.65-79.

Ray, G. E., Dawson, G. L. and Simpson, R., 1988. Geology, Geochemistry and Metallogenic Zoning in the Hedley Gold-Skarn Camp. British Columbia Ministry of Energy, Mines and Petroleum Resosurces, Geological Fieldwork, p.59-79.

Ray, G. E., Ettlinger, A. D. and Meinert, L. D., 1990. Gold Skarns: Their distribution, characteristics and problems in classification. Geological Fieldwork Paper for British Columbia Geological Survey Branch, p.237-246.

Reeve, E. J., 1975. Report on Mount Elliott Project, Northwest Queensland. Union Miniere Development and Mining Corporation Limited Company Report. 3 p.

Robinson, B. W. and Kusabe, M., 1975. Quantitative preparation of SO_2 for $^{34}S/^{32}S$ analyses, from sulphides by combustion with cuprous oxide. Anal. Chem. v. 47, p.1179-1181.

Romberger, S. B., 1986. The Solution Chemistry of Gold applied to the Origins of Hydrothermal Deposits, *in* Clark, L. M. (ed.) Gold in the Western Shield, Canadian Inst. Mining and Metallurgy Special vol. 38, p.168-186.

Scott, K. M.,1986. Geochemistry and Mineralogy of Metasediments, Mount Dore Copper Deposit. Geol. Soc. of Australia. V. 15, p.175-176.

Sibson, R. H., 1989. Structure Mechanics and Fluid Flow in the Quasi-Plastic Fault Regime *in* Structure and Mechanics of Fault Zones in Relation to Fault-Hosted Mineralization. Richard H. Sibson (ed), Course Notes, Australian Mineral Foundation. p.47-66.

Sibson, R. H., Robert, F. and Poulsen, K. H., 1988. High angle reverse faults, fluid-pressure cycling and mesothermal gold-quartz deposits. Geology v. 16, p.551-555.

Stenina, N. G., Mazurov, M. P., and Titov, A. T., 1979. Mechanism of magnetite deposition in calcareous skarn: Doklady of the Academy of Sciences of the USSR, Earth Science Section, 249 (1-6), p.149-152.

Sullivan, C. J., 1951. The Mount Elliott Mine - Selwyn, Queensland. Company Report for Broken Hill South. 6p.

Switzer, C. K., 1987. Implications of high strain for regional structural geometry and control on gold mineralisation in the Selwyn region, northwestern Queensland. Unpubl. Hons. Thesis. James Cook University.

Taylor, G. R., 1983. Copper and Gold in skarn at Brown's Creek, Blayney, NSW. Journal of the Geological Society of Australia, 30 (4), p.431-442.

Theodore, T. G., Orris, G. J., Hammarstrom, J. M. and Bliss, J. D., 1930. Gold Bearing Skarns. U.S. Geological Survey Bulletin, p.1-61.

Tomson, I. N., Polyakova, O. P., Polokhov, V. P. and Mityushkin, N. T., 1989. Metallogenic significance of carbon metasomatism. International Geology Review, 31, p.1055-1062.

Torrey, C. E., Karjalainen, H., Joyce, P. J., Erceg, M. and Stevens, M., 1986. Geology and Mineralisation of the Red Dome (Mungana) Gold Skarn Deposit, North Queensland. Proceedins of Gold '86 Sympsoium, Toronto (ed. A. James Macdonald). P.504-517.

Tvalchrelidze, A. G., and Chichinazem M. K., 1985. Features of the pyrrhotite in pyritic stratiform and vein ores in black schists. International Geology Review, 27 (4), p.492-499.

Vidal, C. E., Injoque-Espinoza, J., Sidder, G. B. and Mukasa, S. B., 1990. Amphibolitic Cu-Fe skarn deposits in the central coast of Peru. Econ. Geol. and Bull of the Soc. of Economic Geologists, 85 (7), p.1447-1461.

Wade, M. L., 1958. Mount Elliott Cu Mine, Selwyn, Northwest Queensland. Rio-Tinto Australia Exploration Pty Ltd Company Report. p.1.

Walshe, J. L., 1986. A six component chloride solid solution model and the conditions of chloride formation in hydrothermal and geothermal systems. Econ. Geol. v. 81, p.681-703.

Wedekind, M. R., 1988. Petrology, Sulphur Isotopes and Geochemistry of the Warrego Gold-Bismuth-Copper Mine, Tennant Creek, Northern Territory. Bicentennial Gold 88, p. 489-491.

Wedekind, M. R., Large, R. R., Zaw, K., Horvath, H. and Gulson, B., 1988. The Composition and Source of Ore Depositing Fluids in the Tennant Creek Goldfield. Bicentennial Gold 88, p.492-494.

Wedekind, M. R., Large, R. R. and Williams, B. T., 1989. Controls on High-Grade Gold Mineralization at Tennant Creek, Northern Territory, Australia. p.168-179.

Whittle, A. W. G., 1978. Mount Elliott: Mineralogical Report for Amoco. Appendix 20. p.1-4

Wilson, G. C., Rucklidge, J. C. and Kilius, L. R., 1990. Sulphide gold content of skarn mineralization at Rossland, British Columbia. Econ. Geol. & Bull of the Soc. of Econ. Geologists. 85 (6), p.1253-59.

Wilson, I. H., 1978. Volcanism on a Proterozoic continental margin in northwestern Queensland. Precambrian Res., v. 1, p.205-235.

Wyborn, L. A. I., Page, R. W. and McCulloch, M. T., 1988. Petrology, geochronology and isotope geochemistry of the post-1820 Ma granites of the Mount Isa Inlier: mechanism for the generation of Proterozoic anorogenic granites. Precambrian Res., 40/41, p.509-541.

Wyborn, L. A. I. and Blake, D. H., 1982. Re-assessment of the tectonic setting of the Mount Isa Inlier in the light of new field, petrographic and geochemical data (abstract), BMR Jour. Aust. Geol. Geophys. v. 8, p.53-69.

Zaw, K., 1991. The Effect of Devonian Metamorphism and Metasomatism on the Mineralogy and Geochemnistry of the Cambrian VMS Deposits in the Rosebery-Hercules District, Western Tasmania. Doctor of Philosophy Thesis, University of Tasmania. p.11.16-11.25.

Zierenberg, R. A. and Shanks, III, W. C., 1988. Isotopic Studies of Epigenetic Features in Metalliferous Sediment, Atlantis II Deep, Red Sea. Canadian Mineralogist: v. 26. p.737-753.

APPENDIX 1

ELECTRON MICROPROBE COMPOSITIONS OF

SKARN PHASES AND SULPHIDES

	1	2	3	4	5
S03	0.0000	0.0000	0.0836	0.0000	0.0000
P205	0.0000	0.0000	0.0695	0.0000	0.0000
Si02	63.9155	64.2102	66.7542	64.4716	64.2897
Ti02	0.0000	0.0000	0.2495	0.0000	0.0000
Al203	17.7945	17.6682	17.5598	18.4784	18.5991
Cr203	0.0364	0.2280	0.0316	0.0454	0.0000
Mg0	0.0222	0.0000	0.3374	0.0000	0.0000
Ca0	0.0000	0.0000	0.0000	0.0000	0.0163
Mn0	0.0000	0.1344	0.0000	0.0000	0.0302
Fe0	0.1722	0.0920	1.0781	0.1997	0.0293
Ni0	0.0000	0.0000	0.0000	0.0000	0.0942
Na20	0.1322	0.1897	1.5589	0.2136	0.1964
K20	16.8996	16.9512	11.8854	16.3541	16.2896
Cl	0.0017	0.0034	0.0947	0.0086	0.0257
Total	98.9741	99.2711	99.6812	99.7694	99.5647
Cations	24.0000	24.0000	24.0000	24.0000	24.0000

1 MEQ-14-243.1
2 "
3 MEQ-14-280.3
4 MEQ-14-243.1
5 "

	1	2	3	4	5	6
S03	0.2074	0.0399	0.0399	0.0000	0.0400	0.0000
P205	0.0293	0.0000	0.0000	0.0170	0.0142	0.0379
Si02	36.3916	34.5909	34.7395	34.2014	34.7245	34.8962
Ti02	0.0996	2.8713	2.7964	2.3148	2.0763	2.0895
Al203	19.0626	18.1724	18.6036	19.5685	18.4001	18.4683
Cr203	0.0172	0.0671	0.0379	0.0883	0.0000	0.0971
Mg0	15.2738	7.2893	6.9562	7.0274	8.9777	9.0029
Ca0	0.1168	0.0000	0.0276	0.0475	0.0144	0.0399
Mn0	0.0740	0.2733	0.2036	0.2085	0.3123	0.3388
Fe0	13.7262	21.4834	20.4840	20.5787	19.4342	19.8397
Ni0	0.0225	0.0000	0.0551	0.0589	0.0258	0.0258
Na20	0.0250	0.1049	0.1128	0.3049	0.1446	0.1326
K20	2.7167	9.1852	9.2513	9.1917	9.5238	9.2352
Cl	0.0205	0.7592	0.7269	0.6286	0.6379	0.6714
Total	87.7787	94.6657	93.8708	94.0942	94.3258	94.7238
Cations	24.0000	24.0000	24.0000	24.0000	24.0000	24.0000

1 MEQ-14-212.3

2 - 6 MEQ-14-280.3

	1	2	3	4	5	6	7
S03	0.0000	0.0000	0.0340	0.0000	0.0358	0.0000	0.1534
P205	0.7932	0.9703	0.8823	0.9467	0.7611	0.9411	0.8641
Si02	0.4998	2.5812	0.0195	0.0858	6.1332	0.0148	0.1920
Ti02	0.0000	0.0000	0.0323	0.0159	0.0186	0.0000	0.0528
Al203	0.2118	0.9405	0.0000	0.0253	2.0544	0.0000	0.0608
Cr203	0.0000	0.0000	0.0000	0.0000	0.0133	0.0000	0.0000
Mg0	0.0000	0.0000	0.1800	0.0007	3.0407	0.2511	0.0000
Ca0	55.8977	60.9995	58.7302	51.5809	41.0962	51.9578	48.6467
Mn0	0.0000	0.0019	0.2552	0.0804	0.0025	0.1687	0.0000
Fe0	0.9382	0.7339	0.3514	0.3267	5.3853	0.2952	0.1240
Ni0	0.0000	0.0000	0.0000	0.0218	0.0877	0.0000	0.0000
Na20	0.0118	0.0570	0.0188	0.0000	0.0226	0.0000	0.0465
K20	0.0039	0.0118	0.0050	0.0087	0.0180	0.0087	0.0048
Cl	0.0114	0.0144	0.0284	0.0212	-	0.0071	0.1001
Total	58.3678	66.3073	60.5306	53.1093	58.6693	53.6429	50.2226
Cations	24.0000	24.0000	24.0000	24.0000	24.0000	24.0000	24.0000

1 MEQ-14-243.1
2 "
3 "
4 MEQ-14-223.0
5 "
6 MEQ-14-243.1
7 MEQ-14-267.8

Appendix 1 - Scapolite

	1	2	3	4	5	6	7	8	9	10	11	12
S03	0.0000	0.2100	0.0000	0.0418	0.0000	0.1460	0.0000	0.1261	0.1262	0.2105	0.0000	0.0386
P205	0.1039	0.0495	0.0000	0.1035	0.1180	0.0000	0.0640	0.0620	0.0811	0.0711	0.5430	42.1894
Si02	58.1656	58.4532	57.1646	55.6005	55.5264	55.5982	58.6027	58.3916	58.8640	58.8181	30.6383	0.2270
Ti02	0.0026	0.0000	0.0222	0.0000	0.0001	0.0291	0.0000	0.0107	0.0000	0.0000	38.4144	0.0000
Al203	19.9957	20.2367	20.1040	20.0493	22.0748	22.2069	21.1111	21.0585	21.1266	21.2919	0.3671	0.0100
Cr203	0.0091	0.0045	0.0271	0.0045	0.0000	0.0091	0.0542	0.0000	0.0000	0.0000	0.0091	0.0273
Mg0	0.0000	0.0000	0.4361	0.4152	0.0000	0.0000	0.0000	0.0034	0.0000	0.0000	0.0000	0.0000
Ca0	4.5700	4.2325	4.4390	4.4801	7.5661	7.2032	4.1376	3.9634	4.0963	4.0021	28.9132	46.9006
Mn0	0.0000	0.0000	0.0688	0.0000	0.0000	0.0000	0.0369	0.0218	0.0436	0.0990	0.0000	0.0470
Fe0	0.1177	0.1280	2.2539	2.2235	0.0085	0.0290	0.2339	0.1875	0.1256	0.0826	0.2964	0.0839
Ni0	0.0000	0.0114	0.0000	0.0000	0.0000	0.0000	0.0377	0.0000	0.0604	0.0755	0.0184	0.0000
Na20	10.7273	10.2888	9.4028	9.2916	9.3385	9.3616	10.2741	10.3825	10.6400	10.3892	0.0069	0.0750
K20	1.1094	1.0528	0.9783	0.9915	0.8288	0.9404	1.0952	1.2515	1.1182	1.1499	0.0000	0.0000
Cl	3.5719	3.6401	3.5028	3.3804	3.1808	3.4678	3.3892	3.5020	3.5568	3.2805	0.0139	0.0217
Total	97.5672	97.4862	97.6091	95.8193	97.9244	98.2088	98.2719	98.1708	99.0364	98.7301	99.2175	89.7668
Cations	24.0000	24.0000	24.0000	24.0000	24.0000	24.0000	24.0000	24.0000	24.0000	24.0000	24.0000	24.0000

1 MEQ-14-243.1

2 "

3 MEQ-14-242.5

4 "

5 MEQ-21-260.

6 "

7 MEQ-14-223.0

8 "

9 MEQ-14-243.1

10 "

11 Sphene MEQ-21-260.1

12 Apatite MEQ-14-270.0

Appendix 1 - Pyrite

	1	2	3	4	5	6	7	8	9	10
S	51.907	52.548	52.497	52.273	52.814	52.726	52.593	53.013	53.358	52.478
Mn	0.000	0.005	0.000	0.008	0.002	0.000	0.000	0.000	0.014	0.005
Fe	47.020	47.011	46.383	46.735	46.557	46.058	45.182	44.600	45.409	45.860
Cu	0.000	0.012	0.000	0.008	0.033	0.026	0.014	0.004	0.000	0.000
Zn	0.000	0.018	0.000	0.009	0.028	0.000	0.000	0.000	0.010	0.000
Ag	0.000	0.046	0.008	0.000	0.023	0.006	0.004	0.000	0.000	0.001
Hg	0.748	0.079	0.256	0.118	0.197	0.024	0.077	0.035	0.000	0.000
Se	0.003	0.008	0.016	0.006	0.014	0.008	0.000	0.000	0.005	0.000
Total	99.679	99.726	99.160	99.157	99.668	98.847	97.871	97.653	98.796	98.344

1	MEQ-15-259.6	6	MEQ-14-221.3
2	"	7	"
3	"	8	Pontifex-G
4	"	9	"
5	"	10	"

	1	2	3	4	5	6	7
S	33.373	33.960	33.404	34.074	34.119	34.404	34.299
Mn	0.000	0.009	0.000	0.000	0.000	0.000	0.000
Fe	30.079	30.107	30.346	29.417	29.372	29.312	29.541
Cu	34.185	34.433	34.072	31.218	31.225	31.162	32.429
Zn	0.000	0.005	0.000	0.190	0.030	0.016	0.000
Ag	0.000	0.000	0.009	0.045	0.000	0.012	0.014
Hg	0.365	0.000	0.461	0.000	0.000	0.000	0.000
Se	0.000	0.000	0.005	0.027	0.009	0.020	0.006
Total	98.001	98.514	98.297	94.971	94.755	94.925	96.288

1	MEQ-15-259.6
2	"
3	"
4	MEQ-14-310.9
5	"
6	Pontifex-G
7	"

A P P E N D I X 2

WHOLEROCK GEOCHEM SAMPLES

SAMPLE DESCRIPTION

400704 MEQ-46-57m.

- White bleached shale fairly monotonous but extensively fractured.
- Contains rare sulphides pyrite and no discernible carbonate.
- Relict banding persists.
- The rock is surrounded by black grey, highly fractured and pyritic shales, also with no discernible carbonate.
- Similar samples of bleached shale are sulphide-rich (pyrite-pyrrhotite ± chalcopyrite) and commonly contain purple fluorite along fracture planes.

4004705 MEQ-46-105.8m.

- Massive, coarse grained, dark green clinopyrozene crystals occupying vugh/vein in outer carapace.
- Contains minor calcite and sulphide (cpy-py).
- The rock is surrounded by intensely metasomatised shales and coarse veins/breccia cementing calc-silicate-calcite-sulphide veins.

400706 MEQ-46-112.15m.

- Comprises a portion of bleached/altered shales.
- Forms the outer margin of pervasive alteration, passing into black, unaltered shale.
- The rock is yellowy-cream colour with minor disseminated sulphides (cpy-po) and possible disseminated flecks of fluorite.
- Minor carbonate alteration was detected in small nodules/veins.
- The outer edge of the altered zone against the unaltered shale is

marked by a soft green mineral -- sericite? (breakdown of feldspar).

4004707 MEQ-46-112.3m.

- This rock comprises a piece of unaltered shale immediately adjacent to the above altered sample.
- Black, fine grained shale transected by very fine cracks/fractures which contain disseminated pyrite plus minor carbonate.

The following three samples represent a progression away from a cross-cutting mineralised (weakly) vein. FOR COMPARISON.

400708 MEQ-46-121.2m.

- Black, fine grained, poorly altered to unaltered shale.
- Very minor carbonate was discerned.
- Rare, disseminated sulphides occur throughout.
- Occurs at the immediate margin of the advancing alteration front.

400709 MEQ-46-121.3m.

- Intermediate sample comprising an early pale cream grey silicic-carbonate alteration being progressively overprinted (on the vein side) by a pale yellowy-green, coarse, nodular calc-silicate? phase (2-4 mm).
- Carbonate was common in this rock.
- Sulphide is rare.

400710 MEQ-46-121.4m.

- Immediately adjacent to the vein, this rock comprises coarse, sub-hedral crystals of calc-silicate (?) aligned along the cleavage, yellowy-green in colour with interstitial brown matrix.

- Carbonate also rare.

* -> This suggests the $CaCO_3$ is added early as the first phase, then consumed to produce the calc-silicates?

400711 MEQ-46-135.5m.

- Comprises a unit of monotonous, black, fine-grained shale with abundant very fine grained disseminated py ±po
- The rock is part of a block of conspicuously unaltered shale in the outer carapace.
- The unit is only weakly fractured and devoid of carbonate which may explain its poor susceptibility to alteration.

400712 MEQ-46-143.2m.

- Pale, pink-cream to pale brown to dark brown, fine grained, compositionally banded and altered shale.
- Minor fine disseminated sulphides occur along bedding/cleavage planes.
- Alteration is dominantly silicic-qtz and alb/hem, with carbonate common in pale-whitish bands.
- Thin dark layers either remnant biotite or late added biotite.
- The rock is cut by a thin (2-3mm) vein of cpy-carb -> later than the alteration (not sampled).

400713 MEQ-46-163.4m.

- Pale pink to cream-white and pale green plus grey-brown, compositionally banded, intensely altered shale.
- Pink layers -- alb/hem rich.
- Dark brown layers -- biotite rich.

- Pale layers -- si-carbonate rich with overprinting pale green clinopyroxene and sulphide (py-cpy) development. Cpx-rich areas do not comprise carbonate.

400714 MEQ-46-163.8m.

- Dark green/black, medium grained, massive to poorly foliated calc-silicate-rich rock. HW skarn.
- Possible intrusive -> dolerite dyke now wholly metasomatised.
- Comprises dominantly cpx (or amphibole) plus feldspar - minor magnetite.
- The rock does not contain carbonate but is cut by fine veinlets of qtz-carb which in turn are cut by pegmatitic skarn veins.

* -> Possibly suggests that these are very early skarns or intrusives?

400715 MEQ-46-180.6m

- Pale cream to pale pink and red-pink and pale greeny brown, compositionally banded, intensely altered shale.
- Pale bands are carbonate-rich.
- Fractures of pale-pink alb/hem cut the rock with alteration seeping along the foliation.
- Fluopriteoccurs at the intersection of one alb/hem crack and pale carbonaceous band. (Fluorite occurs throughout the band).
- Minor fine grained pyrite is disseminated throughout.
- Darker bands possibly remnant bio.

400716 MEQ-46-208.2m.

- Red, green and grey compositionally banded, intensely altered shale.

- Grey carbonaceous bands are overprinted by pink alb/hem bands and green cpx bands.
- Alteration appears to be derived from nearby pegmatitic vein (off-hole).
- Remnant bio-rich bands -> 30-40% and are carbonaceous.

-> Shale -> carb -> alb/hem -> cpx/sulphide

- Fine dissemintion of cpy confined dominantly to cpx-rich bands.
- The rock is cut by late, fine fractures filled with mag-py.

-> Early massive skarn development.

400717 MEQ-46-214.5

- Pink and green, medium grained, massive, blotchy-textured skarn.
- Comprises ~60% pink albite/hem with ~40% overgrowths of green clinopyroxene.
- Clinopyroxone is typically surrounded by halo of calcite (+ plag?).
- Minor epidote mineralisation after cpx.
- Rare diseminated sulphide - cpy.
- No discernible magnetite -> suggests that this is early stage massive skarn.
- This rock forms part of a progressive replacement package within the outer carapace of shale -> massive skarn.

400718 MEQ-16-221.8m.

- Massive pyrrhotite.
- Relict chalcopyrite <2-3%
- From part of a coarse grained stkarn/vein system at contact of massive skarn and outer carapace.

400719 MEQ-46-227.4m.

- Coarse grained skarn comprising massive, very coarse intergrowths of clinopyroxene (60-70%) with interstitial anhedral masses of chalcopyrite and pyrrhotite (30-40%).
- Pyrrhotite replaces chalcopyrite.
- Minor carbonate (<2-3%).
- Rare magnetite (<2-3%).
- Central core of a pegmatitic mineralised vein/skarn (as 15).

400722 MEQ-46-232.1m.

- Massive pyrite in coarse grained skarn with rounded, blebby magnetite (<5%). and anhedral masses of calcite (<5%).
- Minor relict silicate phases remain (<2-3%).

400720 MEQ-46-234.9m.

- Green-red-black fine to medium grained skarn comprising pink albite-hem (40-50%), overprinted by green clinopyroxene + carbonate (40-50%) and magnetite (<10%) - Chalcopyrite (<2-3%).
- The skarn is more advanced than sample (14).

400721 MEQ-50-84.6m.

- Monotonous black shale.
- HW lithology.
- Fine grained, finely banded -> banding probably reflects qtz-rich -> bio rich units.
- Poorly fractured.
- Surrounding shales are intensely fracured with abundant qtz-py ± carb. veining.

400723 MEQ-50-131.4m.

- Pale cream-grey fine grained qtz-carb altered shale.
- Most foliation fabric has been destroyed.
- Carbonate very common.
- Overprinted by fine sulphide veinlets (chalcopyrite) and possible fluorite.
- Pale green tint to the rock in places is possible weak calc-silicate development or sericite (after break down of biotite).
- Occurs at the base of a slope.
- Surrounding rocks are similar with fluorite common.

400724 MEQ-48-176.5m.

- Massive chalcopyrite in core of vein.
- Outer carapace mineralisation.
- Vein bordered by cpx.
- Minor carbonate.
- Sample has thin fractures of qtz-carb through it.

400725 MEQ-16-319.2m

- FW schist.
- Pale-grey, brown, green, medium grained, strongly foliated schist.
- Qtz-feld-bio-gnt + staur/sill? dominant.
- Fresh-looking, unaltered.
- No discernible carbonate.

4005726 MEQ-16-319.6m.

- FW schist as above.
- Overprinted by 3cm.wide vein of pink alb/hem + smoky brown turbid mineral and trace sulphide-cpy.

- No apparent remnant minerals (eg. garnet. However, this is not clear).
- Alteration proceeds from the vein out into the schist along foliation planes.
- Trace carbonate.

400727 MEQ-50-271.1

- Magnetite-rich medium grained skarn.
- Comprises ~30% magnetite overprinting cpx (30%) and lathic, disorientated crystals of pale green to pink alb/hem (replacing scapolite?) 30%.
- <10% sulphide py-cpy.
- < 5% carbonate.

400728 MEQ-21-265.4m.

- Fine grained skarn/dolerite?
- Dark green/black, fine equant grained massive rock with semi-crystalline texture.
- The rock is intensely altered comprising dominantly cpx (or amph?)-feldspar (or/and scapolite?)-magnetite.
- Very rare carbonate and sulphides.
- Rock is cut by a thin vein of sulphide - not sampled.

-> This rock may be metasomatised dolerite dyke that has not suffered intense veining and alteration (possibly due to poor porosity?).

APPENDIX 3

TRUE SECTIONS

FOR GEOLOGY AND MINERALISATION,

MOUNT ELLIOTT

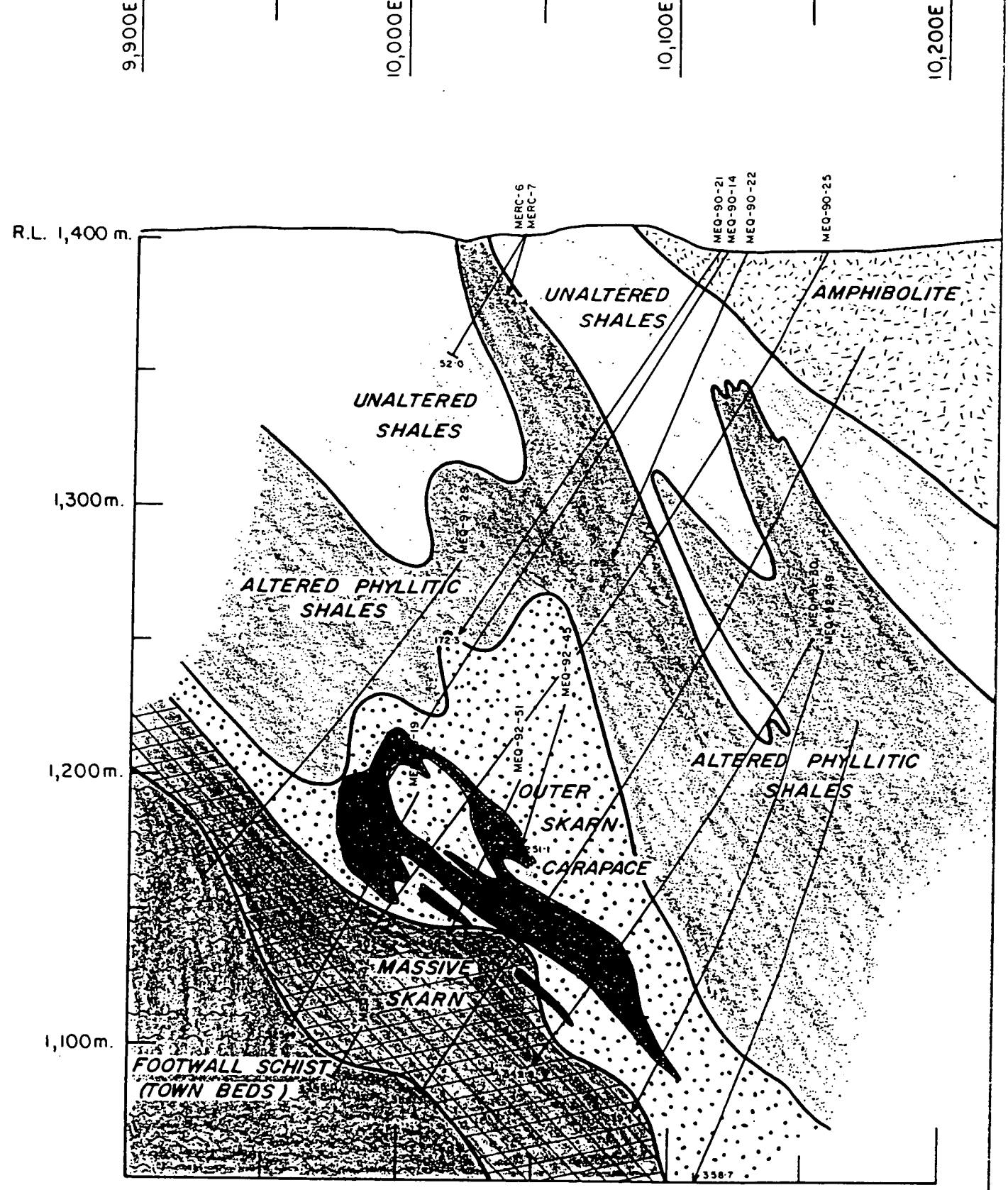

LEGEND

Drill hole trace

Cu - Au mineralization with cutoff of 3% Cu equivalent

0 50 100 m.

V = H

CYPRUS
Gold Australia Corporation

EPM 3370 SELWYN

Mt ELLIOTT MINERALIZATION
(CUTOFF - 3% Cu EQUIVALENT)

TRUE SECTION 9,900N

LOCATED ON	Mt MERLIN 1:100 000 SHEET			
COMPILED	S.GARRETT	MAY 92	SCALE 1:2000	FIG
DRAWN	K.J.CORRIE	MAY 92	SHEET 1 of 1	
REVISED			DWG No -	

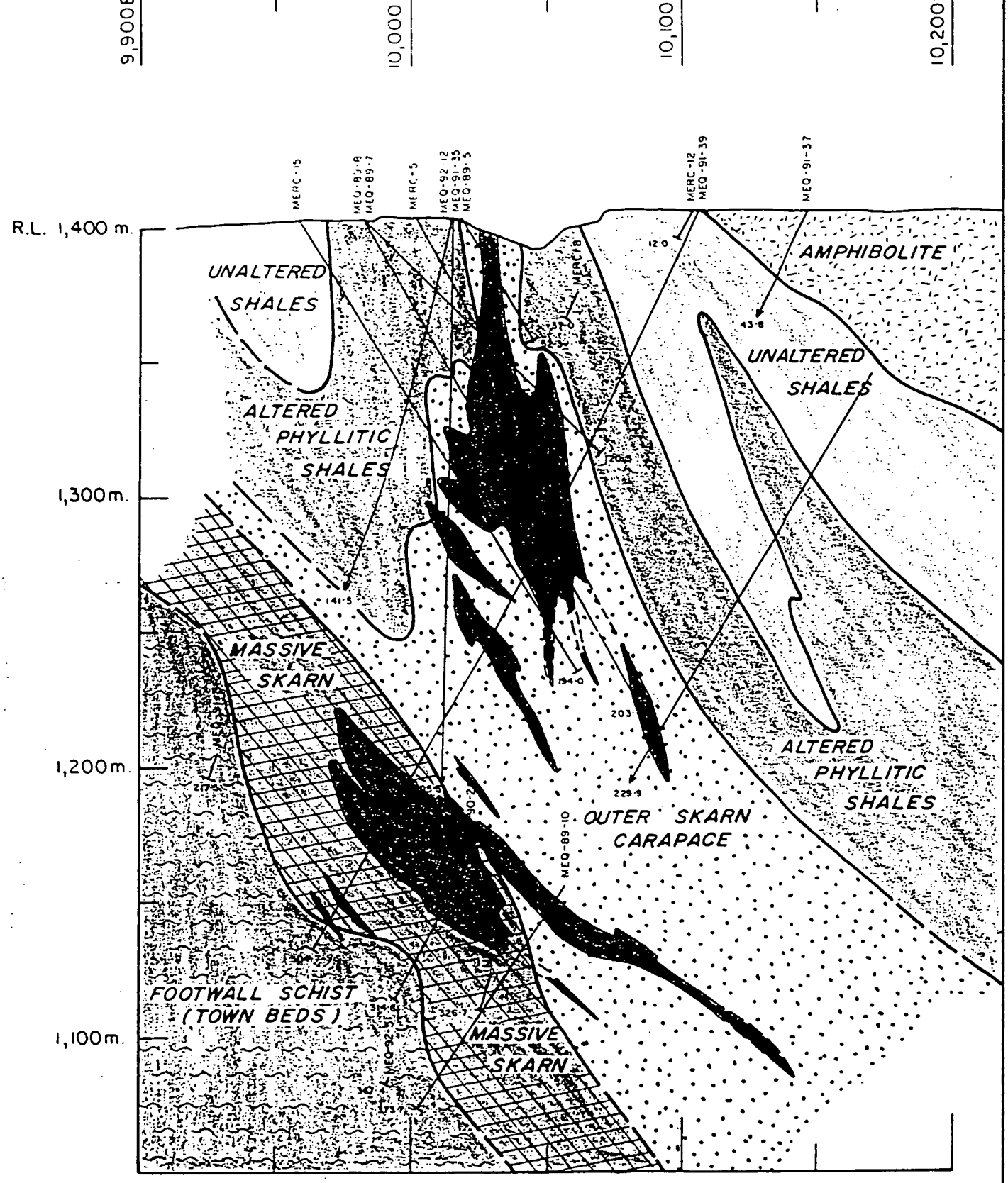

LEGEND

Drill hole trace

Cu - Au mineralization with cutoff of 3% Cu equivalent

0 50 100 m.

V = H

CYPRUS
Gold Australia Corporation

EPM 3370 SELWYN

MT ELLIOTT MINERALIZATION
(CUTOFF - 3% Cu EQUIVALENT)

TRUE SECTION 9,950N

LOCATED ON	Mt MERLIN 1:100,000 SHEET			
COMPILED	S.GARRETT	MAY 92	SCALE 1:2000	FIG
DRAWN	K.J.CORRIE	MAY 92	SHEET 1 of 1	
REVISED			DWG No -	

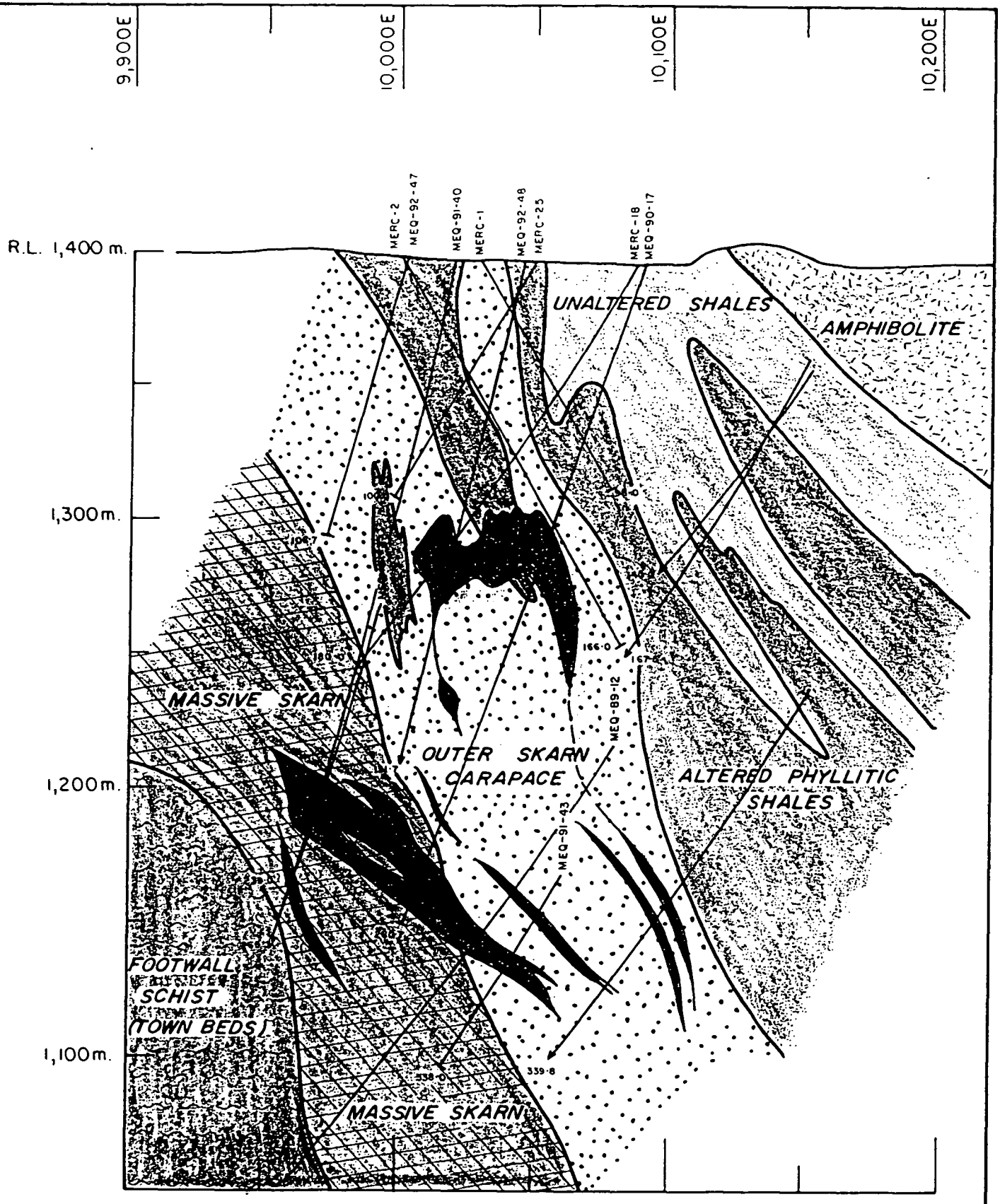

LEGEND

Drill hole trace

Cu - Au mineralization with cutoff of 3% Cu equivalent

0 50 100 m.

V = H

CYPRUS
Gold Australia Corporation

EPM 3370 SELWYN

MT ELLIOTT MINERALIZATION
(CUTOFF - 3% Cu EQUIVALENT)

TRUE SECTION 10,000N

LOCATED ON	MT MERLIN 1:100,000 SHEET			
COMPILED	S.GARRETT	MAY 92	SCALE 1:2000	FIG
DRAWN	K.J.CORRIE	MAY 92	SHEET 1 of 1	
REVISED			DWG NO -	

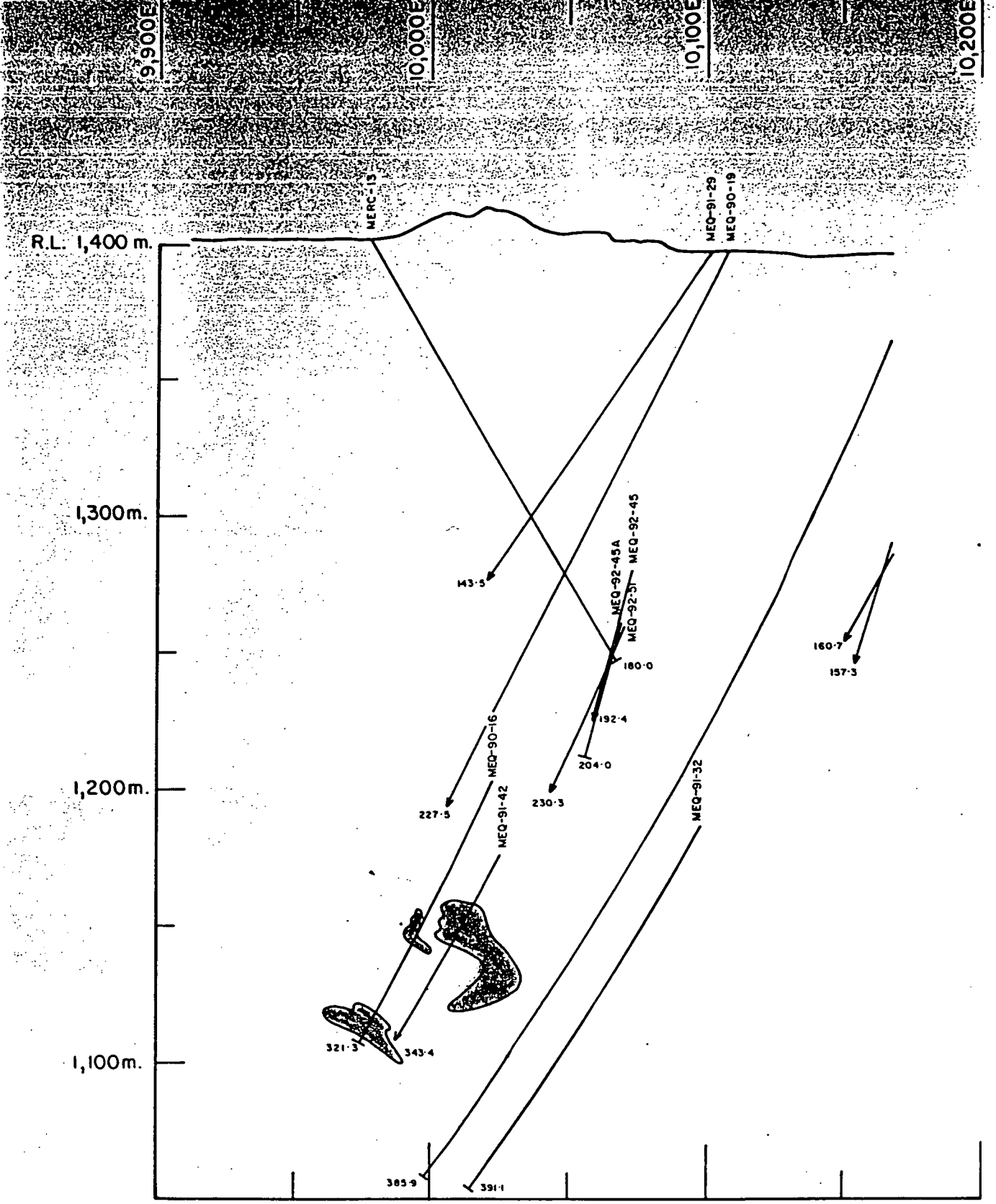

LEGEND

Drill hole trace

Cu - Au mineralization with cutoff of 3% Cu equivalent

0 50 100 m.

V = H

CYPRUS
Gold Australia Corporation

EPM 3370 SELWYN

MT ELLIOTT MINERALIZATION

(CUTOFF - 3% Cu EQUIVALENT)

TRUE SECTION 9,875N

LOCATED ON	MT MERLIN 1 100,000 SHEET		
COMPILED	S.GARRETT	MAY 92	SCALE 1:2000
DRAWN	K.J.CORRIE	MAY 92	SHEET 1 of 1
REVISED			DWG NO

FIG

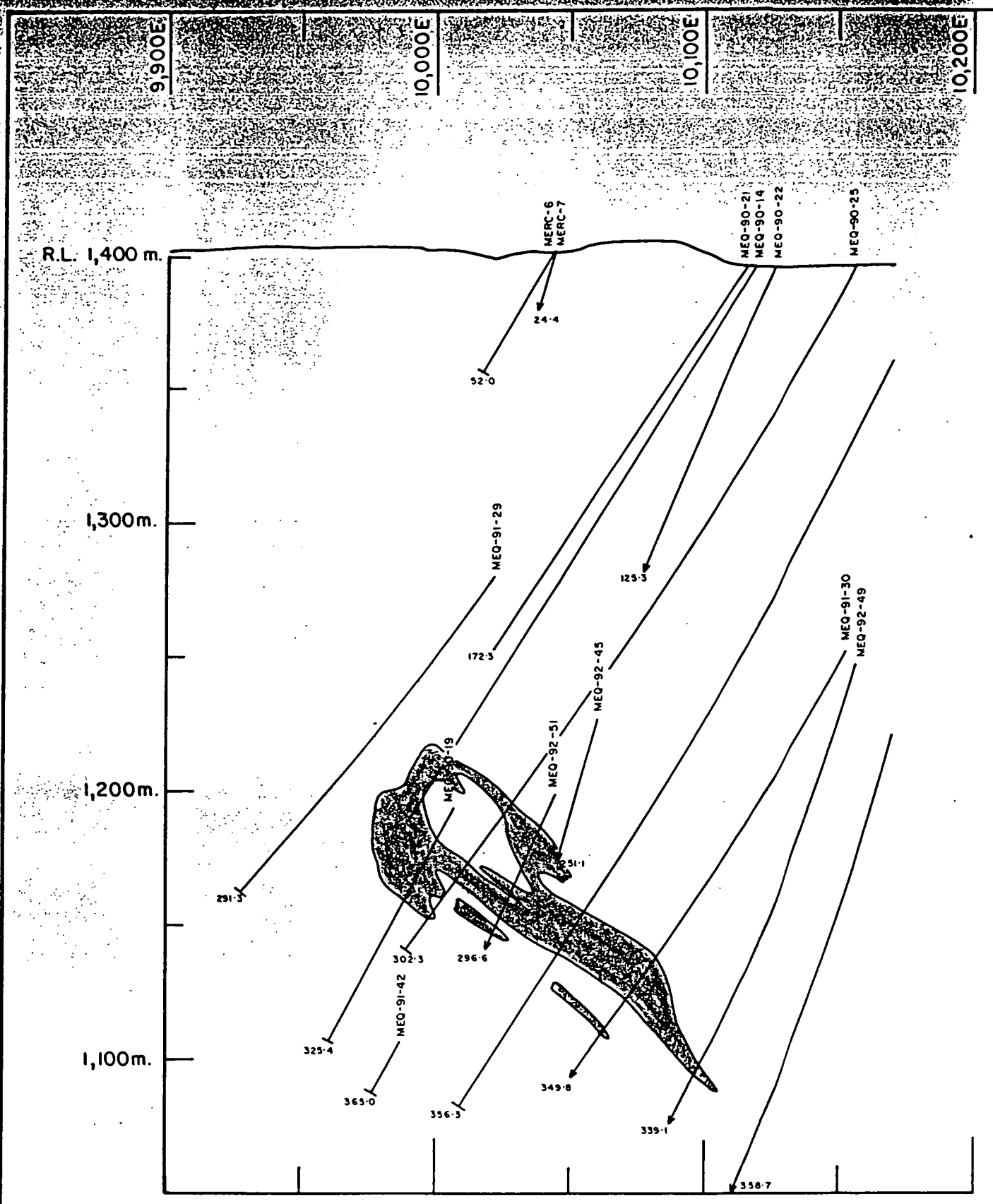

LEGEND

Drill hole trace

Cu - Au mineralization with cutoff of 3% Cu equivalent

0 50 100 m.

V = H

CYPRUS
Gold Australia Corporation

EPM 3370 SELWYN

Mt ELLIOTT MINERALIZATION
(CUTOFF - 3% Cu EQUIVALENT)

TRUE SECTION 9,900N

LOCATED ON	Mt MERLIN 1 100,000 SHEET		
COMPILED	S.GARRETT	MAY 92	SCALE 1:2000
DRAWN	K.J.CORRIE	MAY 92	SHEET 1 of 1
REVISED			DWG No

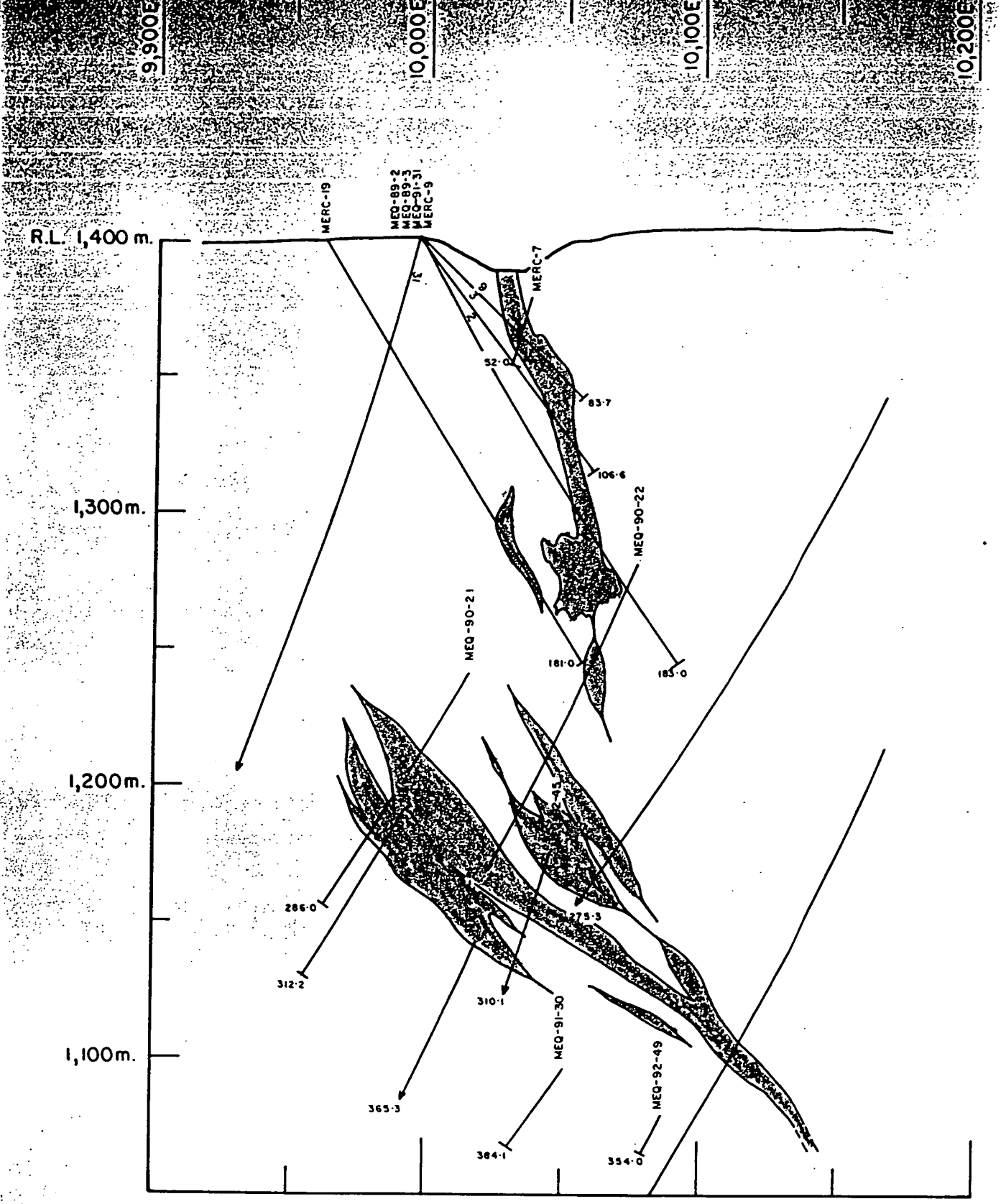

LEGEND

Drill hole trace

Cu - Au mineralization with cutoff of 3% Cu equivalent

0 50 100 m.

V = H

CYPRUS
Gold Australia Corporation

EPM 3370 SELWYN

MT ELLIOTT MINERALIZATION
(CUTOFF - 3% Cu EQUIVALENT)

TRUE SECTION 9,925N

LOCATED ON MT MERLIN 1 100,000 SHEET				
COMPILED	S.GARRETT	MAY 92	SCALE 1:2000	FIG
DRAWN	K.J.CORRIE	MAY 92	SHEET 1 of 1	
REVISED			DWG NO -	

9,900 10,000 10,100 10,200

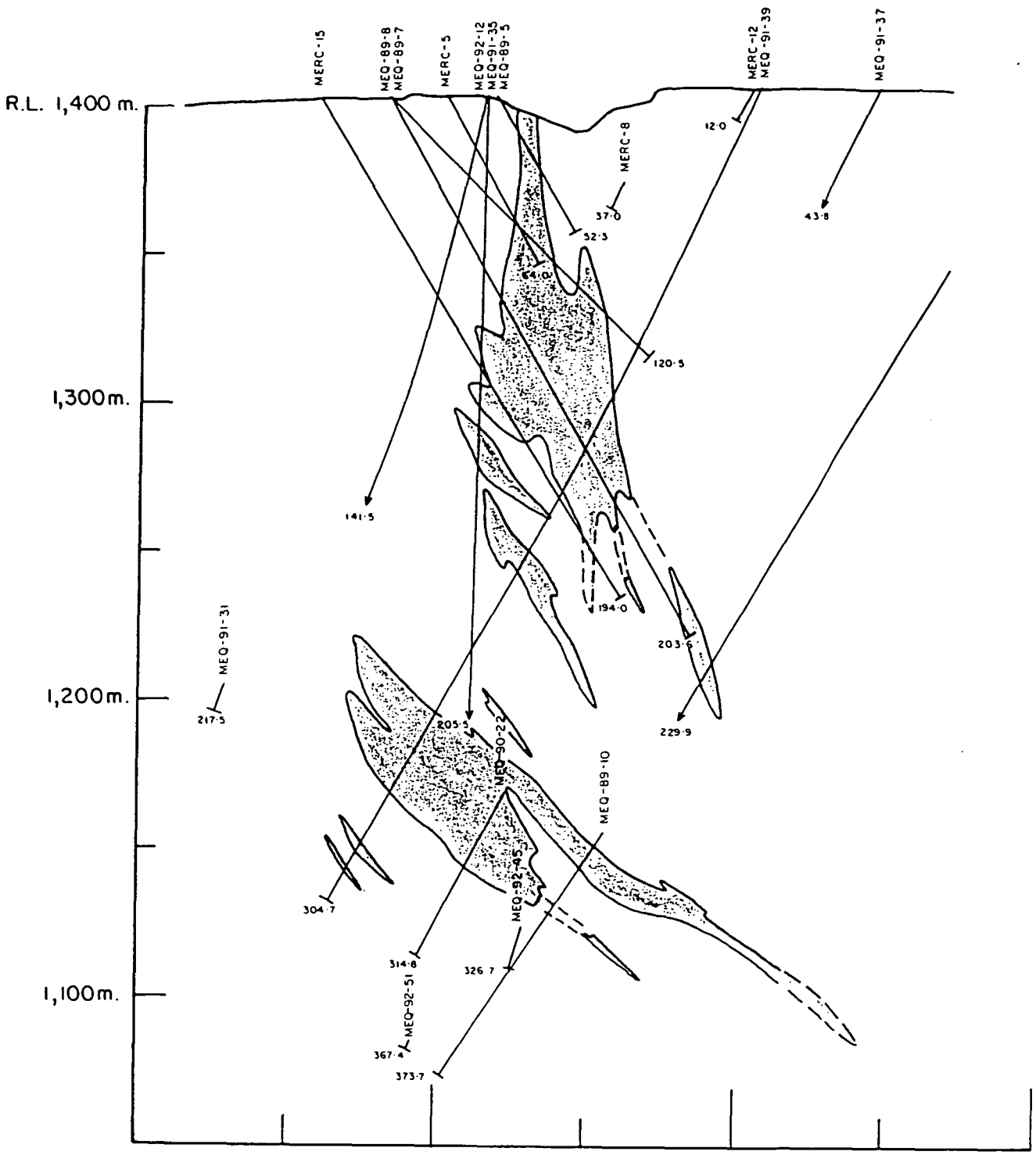

LEGEND

Drill hole trace

Cu - Au mineralization with cutoff of 3% Cu equivalent

0 50 100 m.

V = H

CYPRUS
Gold Australia Corporation

EPM 3370 SELWYN

MT ELLIOTT MINERALIZATION

(CUTOFF - 3% Cu EQUIVALENT)

TRUE SECTION 9,950N

LOCATED ON	MT MERLIN 1:100 000 SHEET			
COMPILED	S.GARRETT	MAY 92	SCALE 1:2000	FIG
DRAWN	K.J.CORRIE	MAY 92	SHEET 1 of 1	
REVISED			DWG NO -	

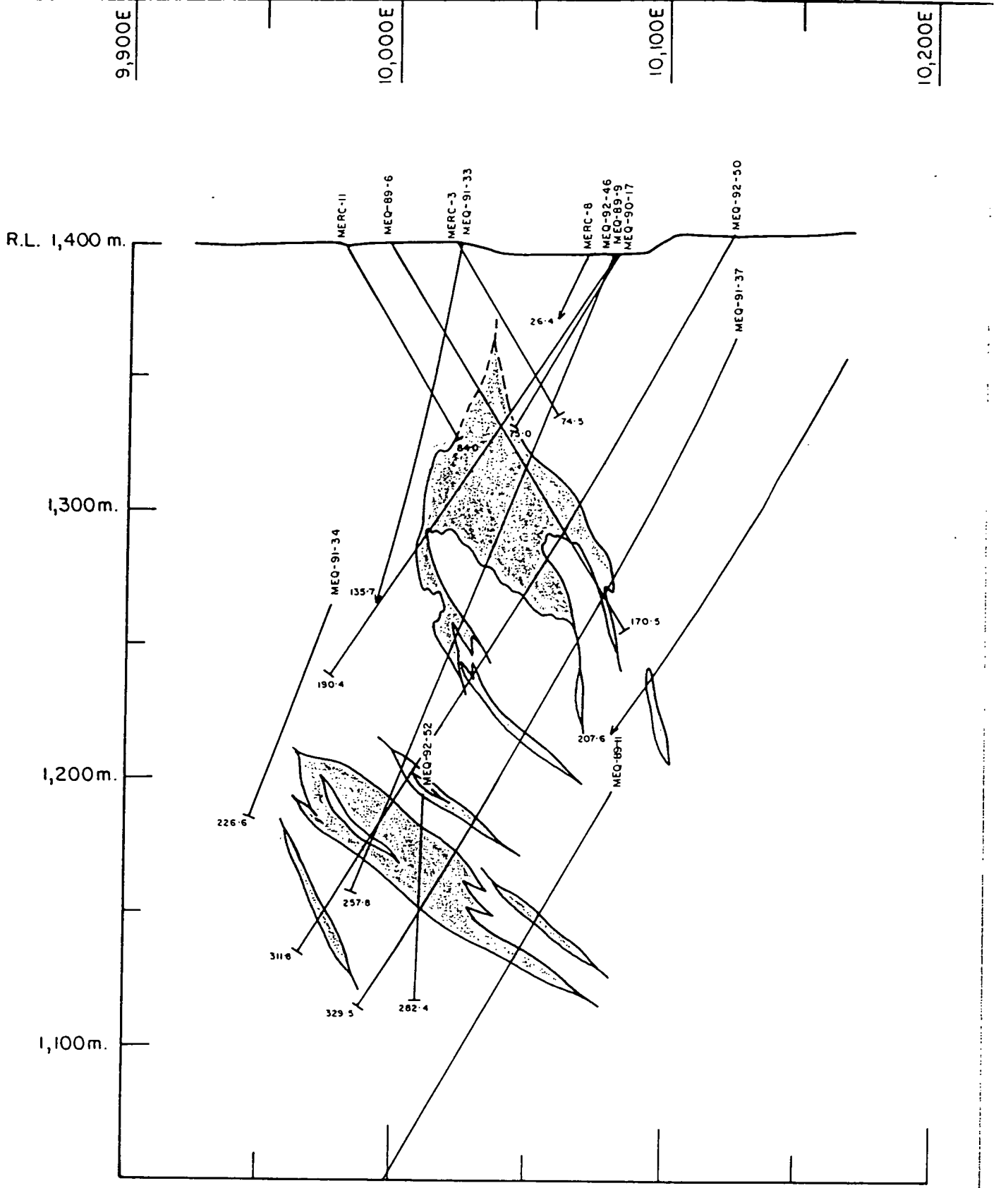

LEGEND

Drill hole trace

Cu - Au mineralization with cutoff of 3% Cu equivalent

0 50 100 m.

V = H

CYPRUS
Gold Australia Corporation

EPM 3370 SELWYN

MT ELLIOTT MINERALIZATION
(CUTOFF - 3% Cu EQUIVALENT)

TRUE SECTION 9,975N

LOCATED ON MT MERLIN 1:100 000 SHEET				
COMPILED	S.GARRETT	MAY 92	SCALE 1:2000	FIG
DRAWN	K.J.CORRIE	MAY 92	SHEET 1 of 1	
REVISED			DWG NO -	

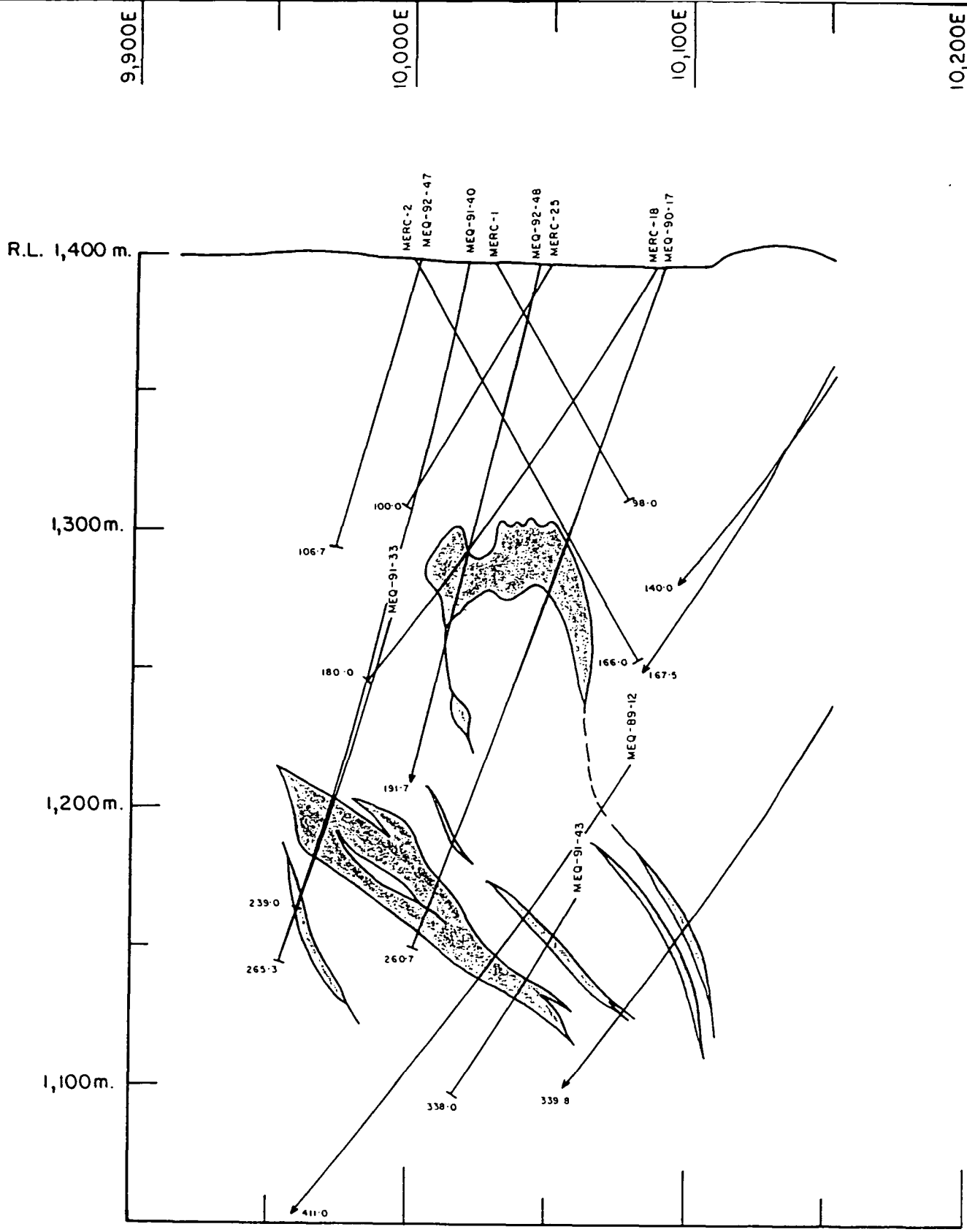

LEGEND

Drill hole trace

Cu - Au mineralization with cutoff of 3% Cu equivalent

0 50 100 m.

V = H

CYPRUS
Gold Australia Corporation

EPM 3370 SELWYN

MT ELLIOTT MINERALIZATION

(CUTOFF - 3% Cu EQUIVALENT)

TRUE SECTION 10,000N

LOCATED ON	MT MERLIN 1:100,000 SHEET		
COMPILED	S.GARRETT	MAY 92	SCALE 1:2000
DRAWN	K.J.CORRIE	MAY 92	SHEET 1 of 1
REVISED			DWG NO -

FIG

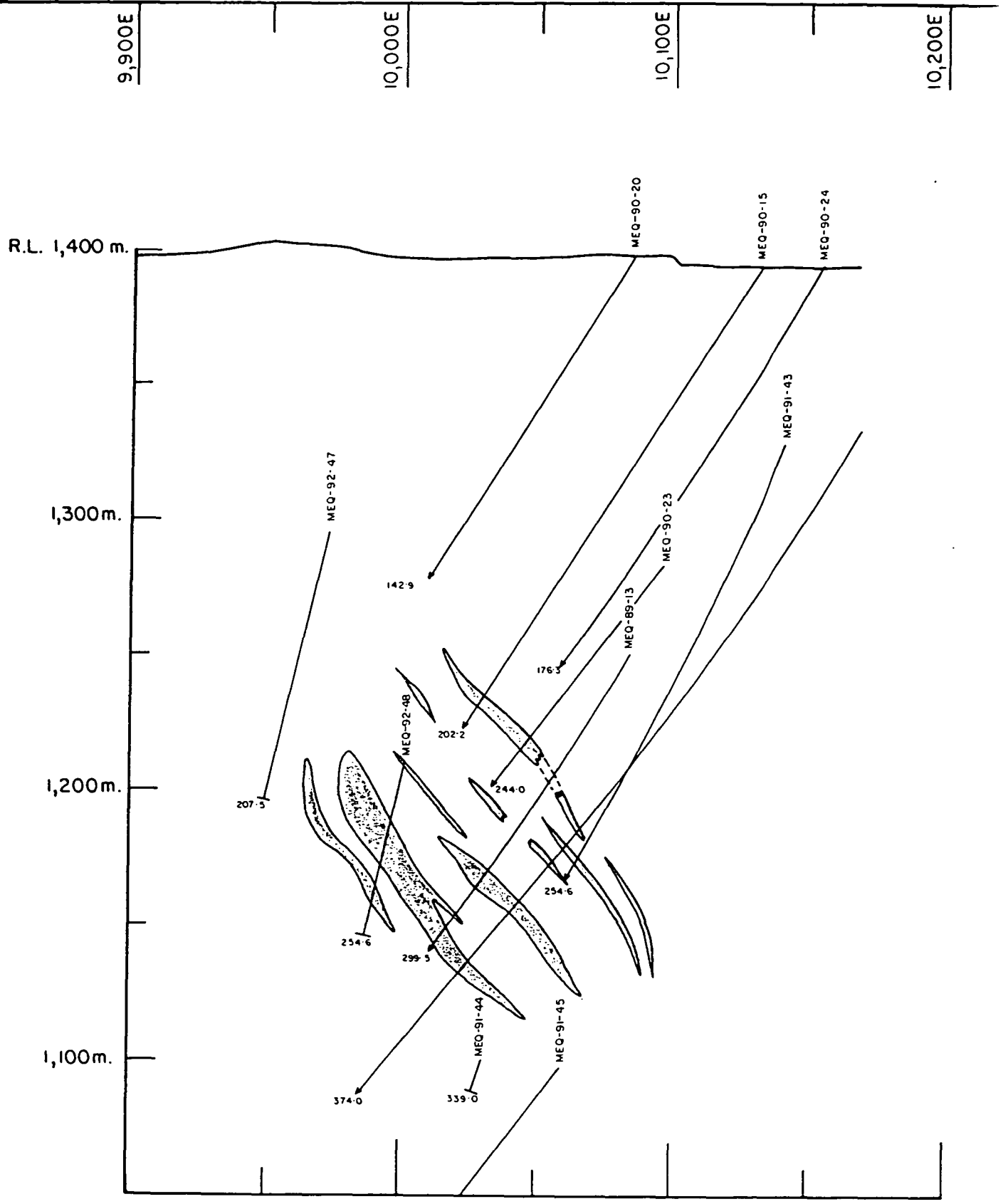

LEGEND

Drill hole trace

Cu - Au mineralization with cutoff of 3% Cu equivalent

0 50 100 m.

V = H

CYPRUS
Gold Australia Corporation

EPM 3370 SELWYN

MT ELLIOTT MINERALIZATION
(CUTOFF - 3 % Cu EQUIVALENT)

TRUE SECTION 10,025N

LOCATED ON MT MERLIN 1 100,000 SHEET				
COMPILED	S.GARRETT	MAY 92	SCALE 1:2000	FIG
DRAWN	K.J.CORRIE	MAY 92	SHEET 1 of 1	
REVISED			DWG NO -	

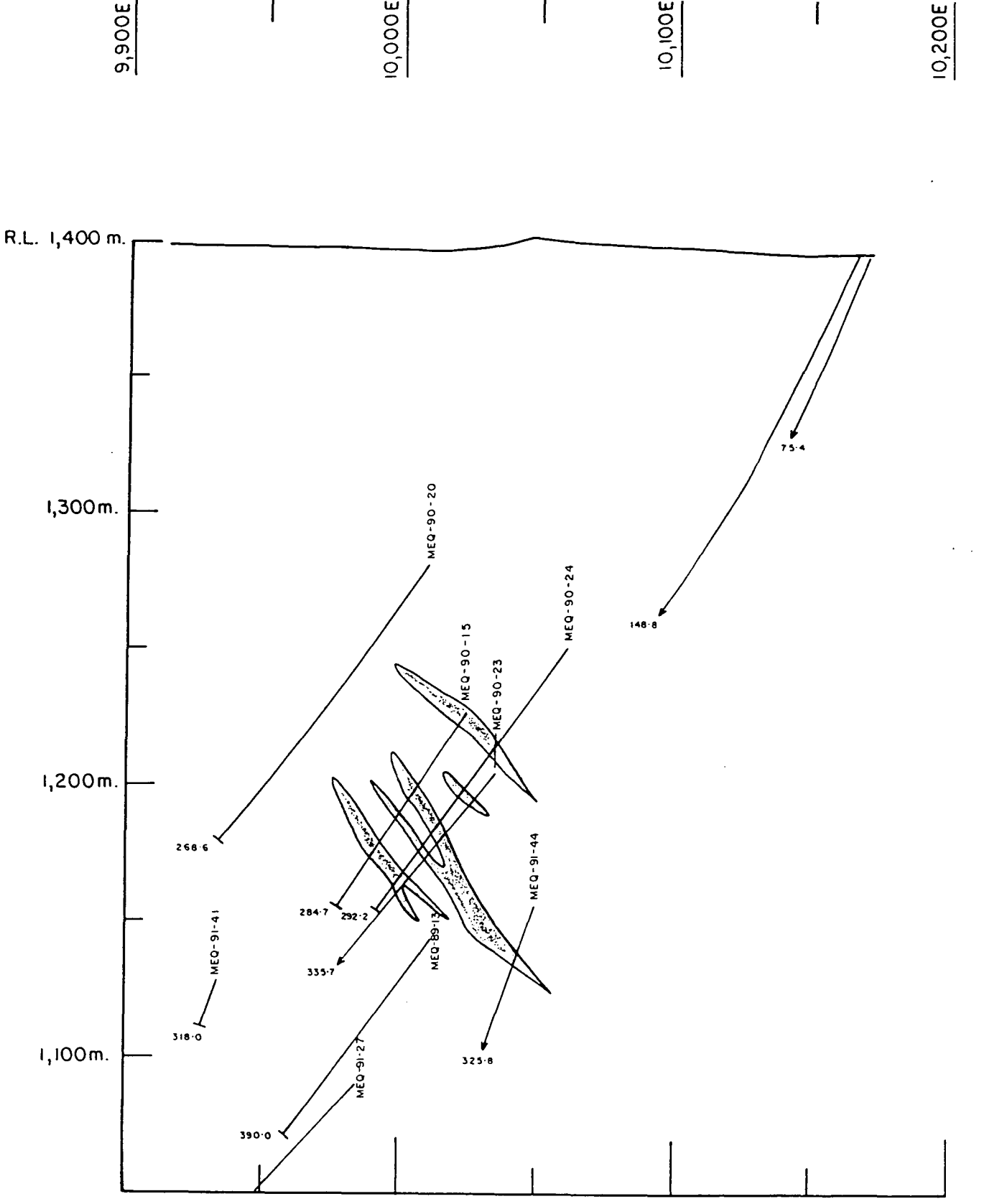

LEGEND

Drill hole trace

Cu - Au mineralization with cutoff of 3% Cu equivalent

0 50 100 m.

V = H

CYPRUS
Gold Australia Corporation

EPM 3370 SELWYN

MT ELLIOTT MINERALIZATION

(CUTOFF - 3% Cu EQUIVALENT)

TRUE SECTION 10,050N

LOCATED ON	MT MERLIN 1 100,000 SHEET			
COMPILED	S.GARRETT	MAY 92	SCALE 1:2000	FIG
DRAWN	K.J.CORRIE	MAY 92	SHEET 1 of 1	
REVISED			DWG NO -	

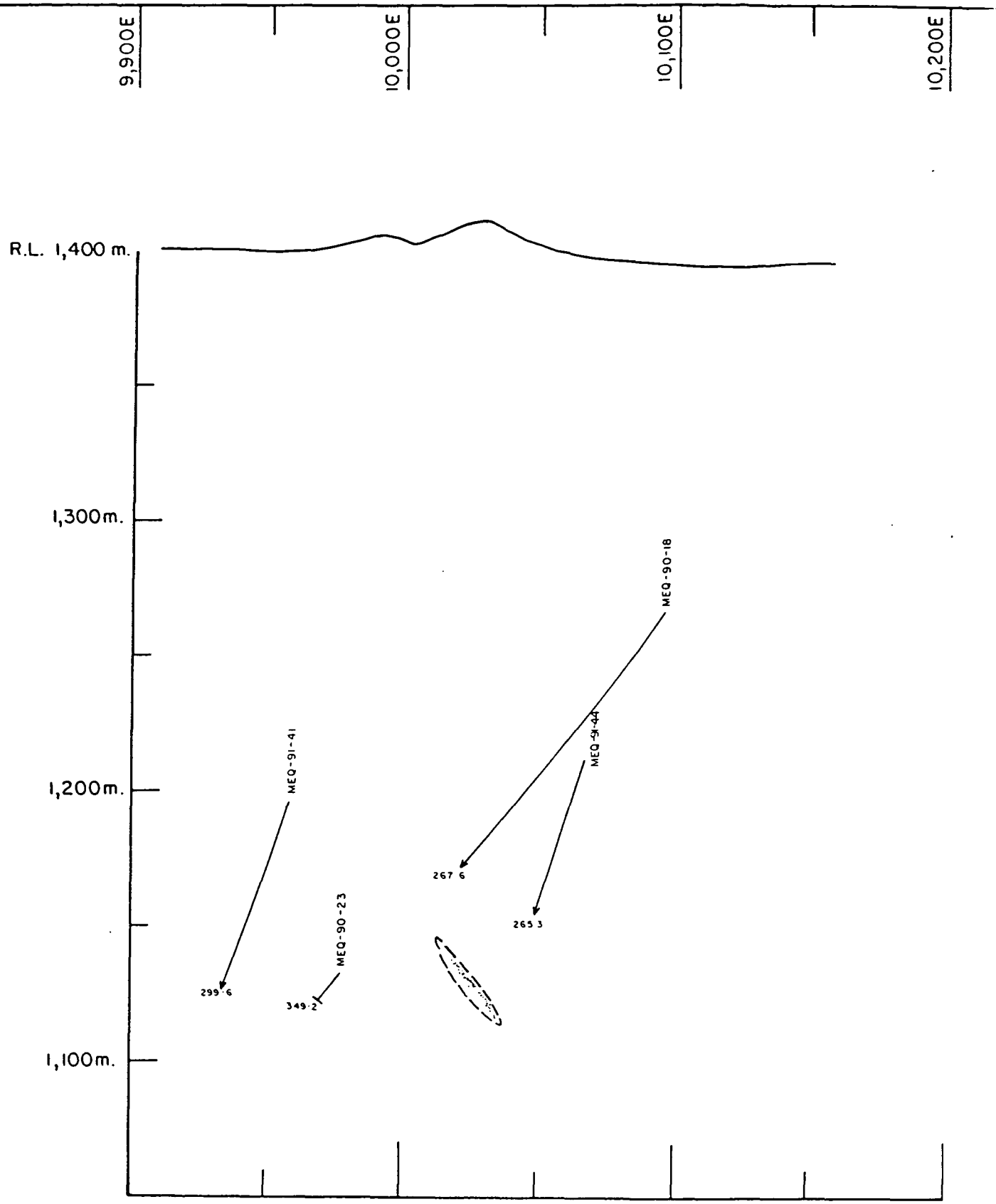

LEGEND

Drill hole trace

Cu - Au mineralization with cutoff of 3% Cu equivalent

0 50 100 m.

V = H

CYPRUS
Gold Australia Corporation

EPM 3370 SELWYN

MT ELLIOTT MINERALIZATION

(CUTOFF - 3% Cu EQUIVALENT)

TRUE SECTION 10,075N

LOCATED ON	MT MERLIN 1:100 000 SHEET		
COMPILED	S.GARRETT	MAY 92	SCALE 1:2000
DRAWN	K.J.CORRIE	MAY 92	SHEET 1 of 1

FIG

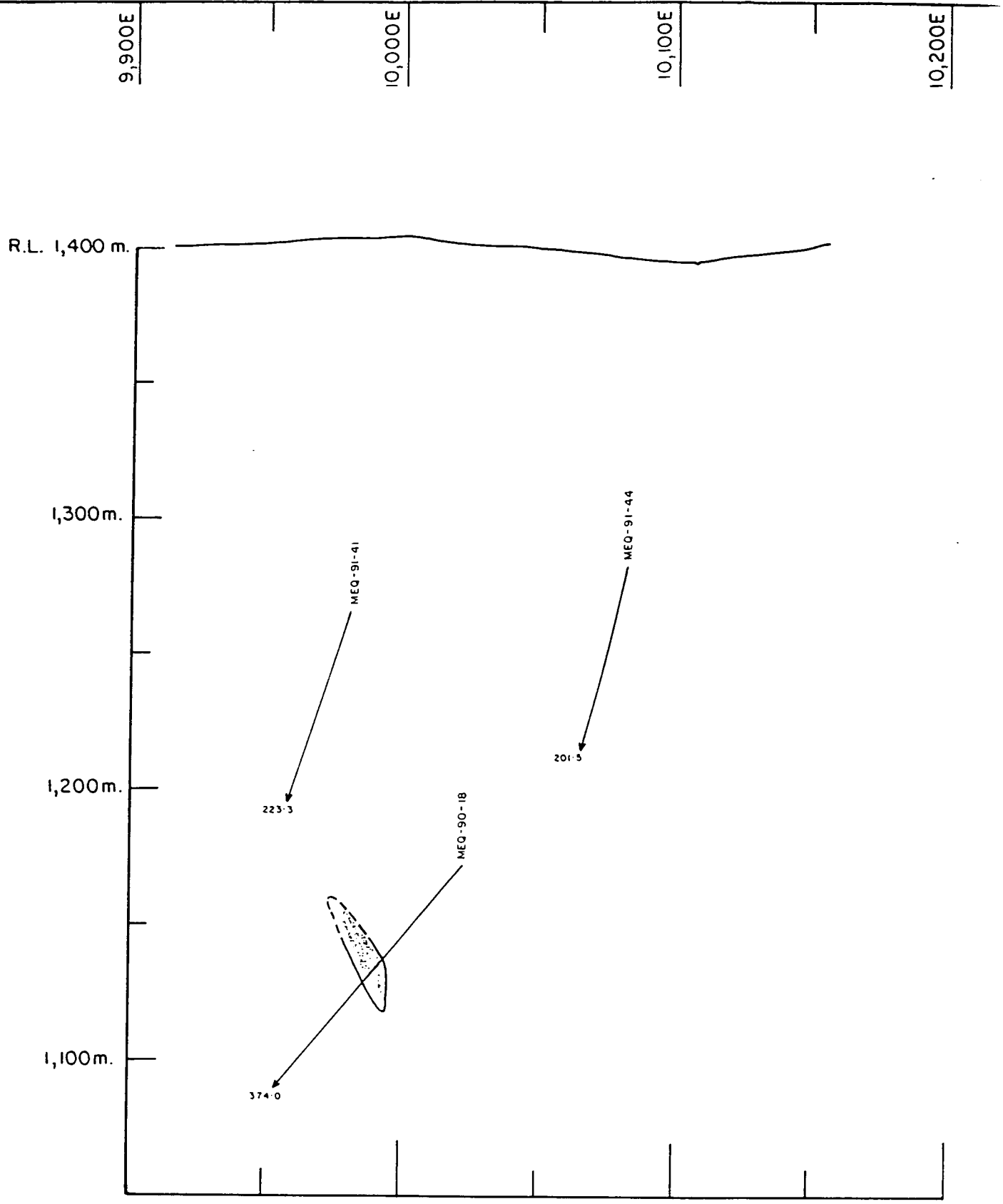

LEGEND

Drill hole trace

Cu - Au mineralization with cutoff of 3% Cu equivalent

0 50 100 m.

V = H

CYPRUS
Gold Australia Corporation

EPM 3370 SELWYN

MT ELLIOTT MINERALIZATION

(CUTOFF - 3% Cu EQUIVALENT)

TRUE SECTION 10,100 N

LOCATED ON	MT MERLIN 1:100 000 SHEET			
COMPILED	S.GARRETT	MAY 92	SCALE 1:2000	FIG
DRAWN	K.J.CORRIE	MAY 92	SHEET 1 of 1	
REVISED			DWG NO -	

APPENDIX 4

FREQUENCY DISTRIBUTION PLOTS

FOR CU AND AU GRADES

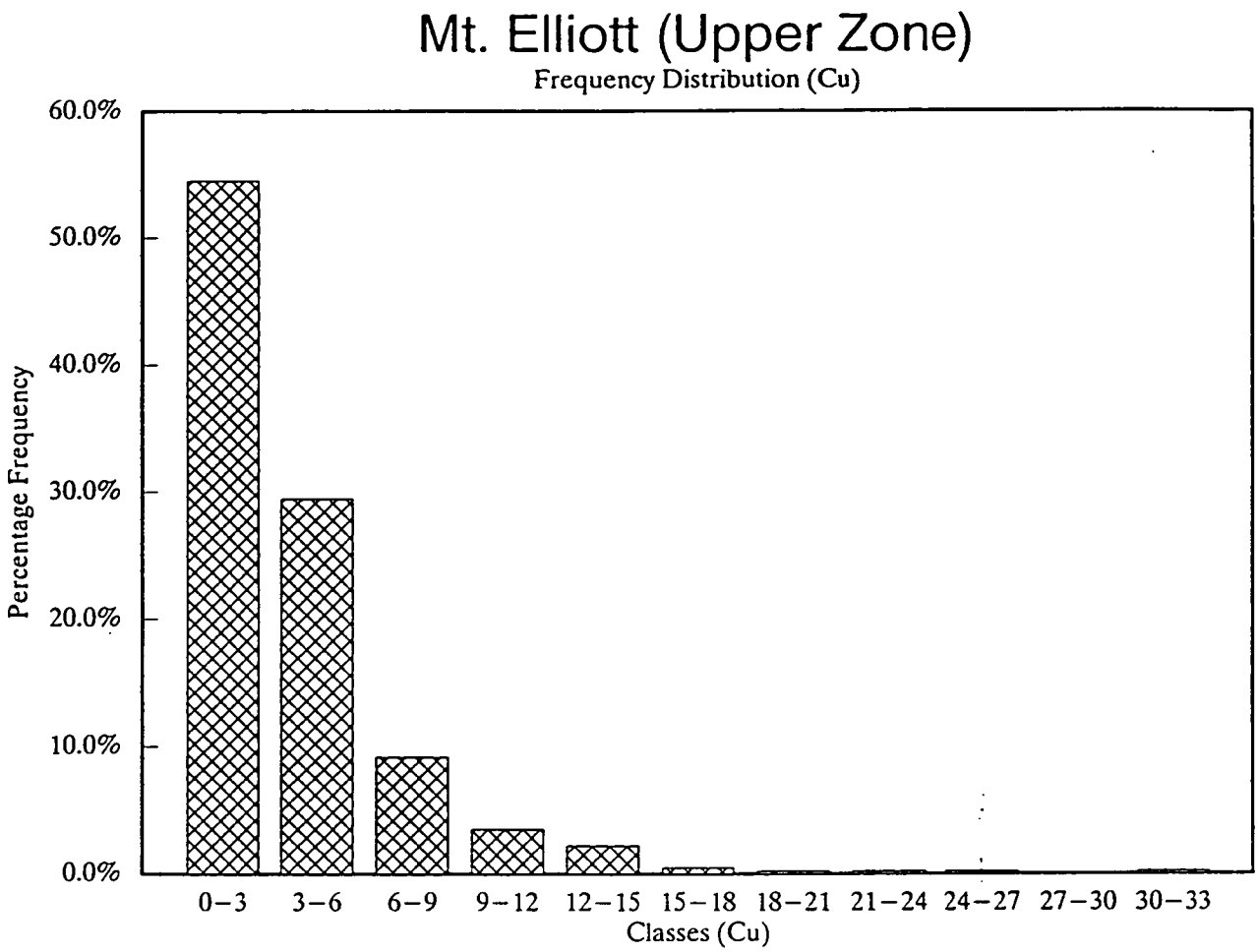
Mt. Elliott (Upper Zone)
Frequency Distribution (Cu)
60.0%
50.0%
40.0%
30.0%
20.0%
10.0%
0.0%
Percentage Frequency
0–3
3–6
6–9
9–12
12–15
15–18
18–21
21–24
24–27
27–30
30–33
Classes (Cu)

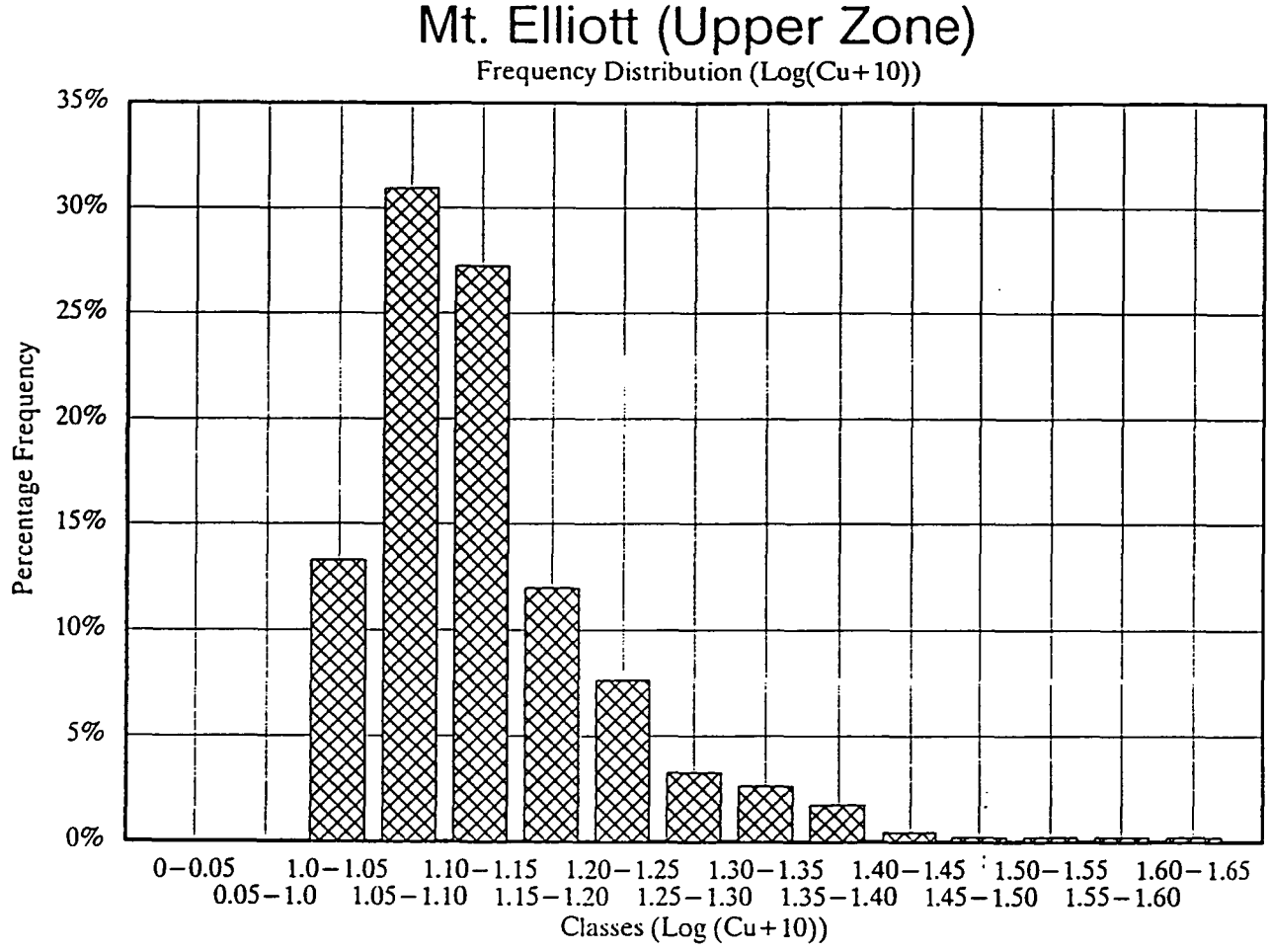
Mt. Elliott (Upper Zone)
Frequency Distribution (Log(Cu+10))
Percentage Frequency
35%
30%
25%
20%
15%
10%
5%
0%
0–0.05
0.05–1.0
1.0–1.05
1.05–1.10
1.10–1.15
1.15–1.20
1.20–1.25
1.25–1.30
1.30–1.35
1.35–1.40
1.40–1.45
1.45–1.50
1.50–1.55
1.55–1.60
1.60–1.65
Classes (Log (Cu+10))

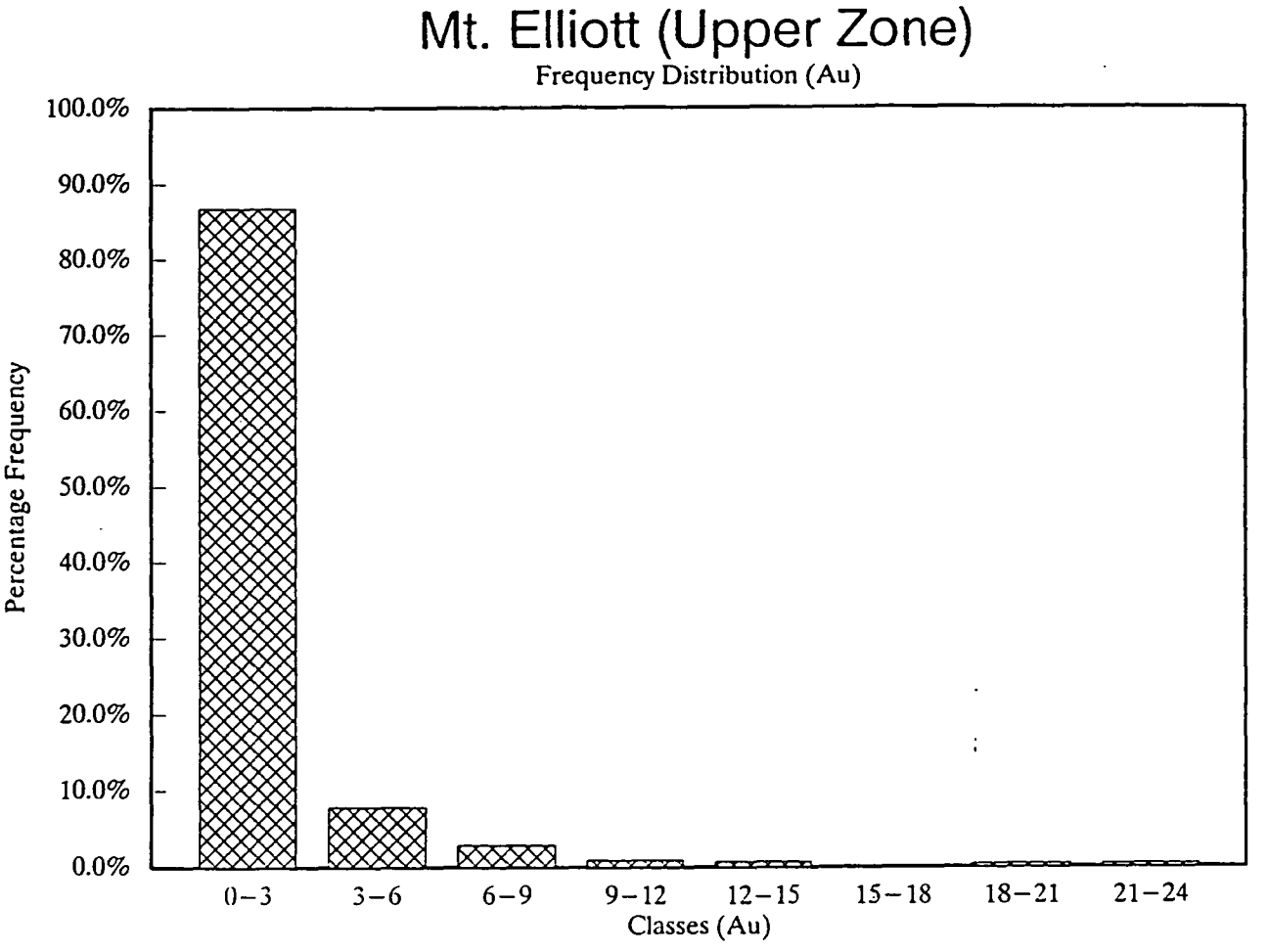
Mt. Elliott (Upper Zone)
Frequency Distribution (Au)
100.0%
90.0%
80.0%
70.0%
60.0%
50.0%
40.0%
30.0%
20.0%
10.0%
0.0%
Percentage Frequency
0–3
3–6
6–9
9–12
12–15
15–18
18–21
21–24
Classes (Au)

Mt. Elliott (Upper Zone)

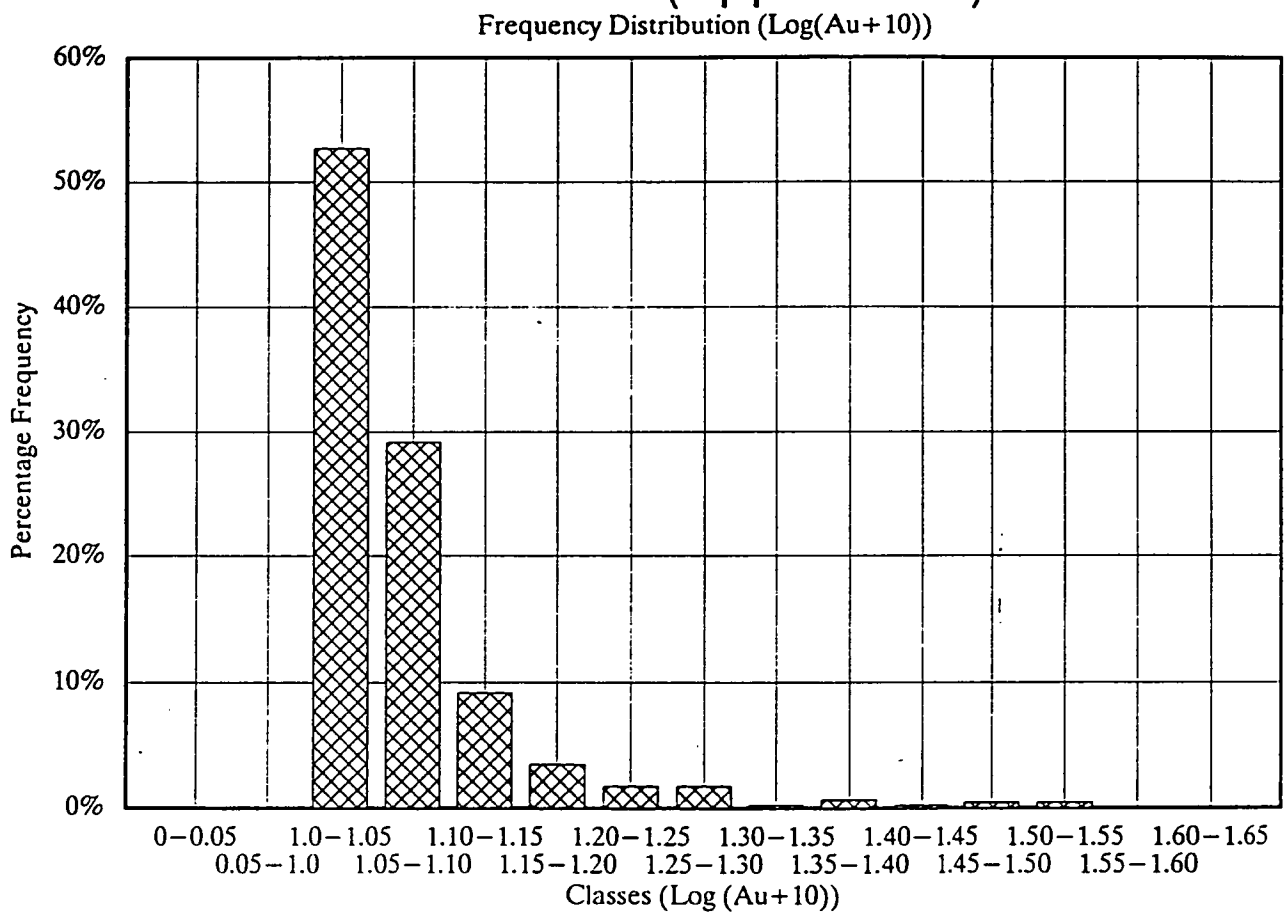

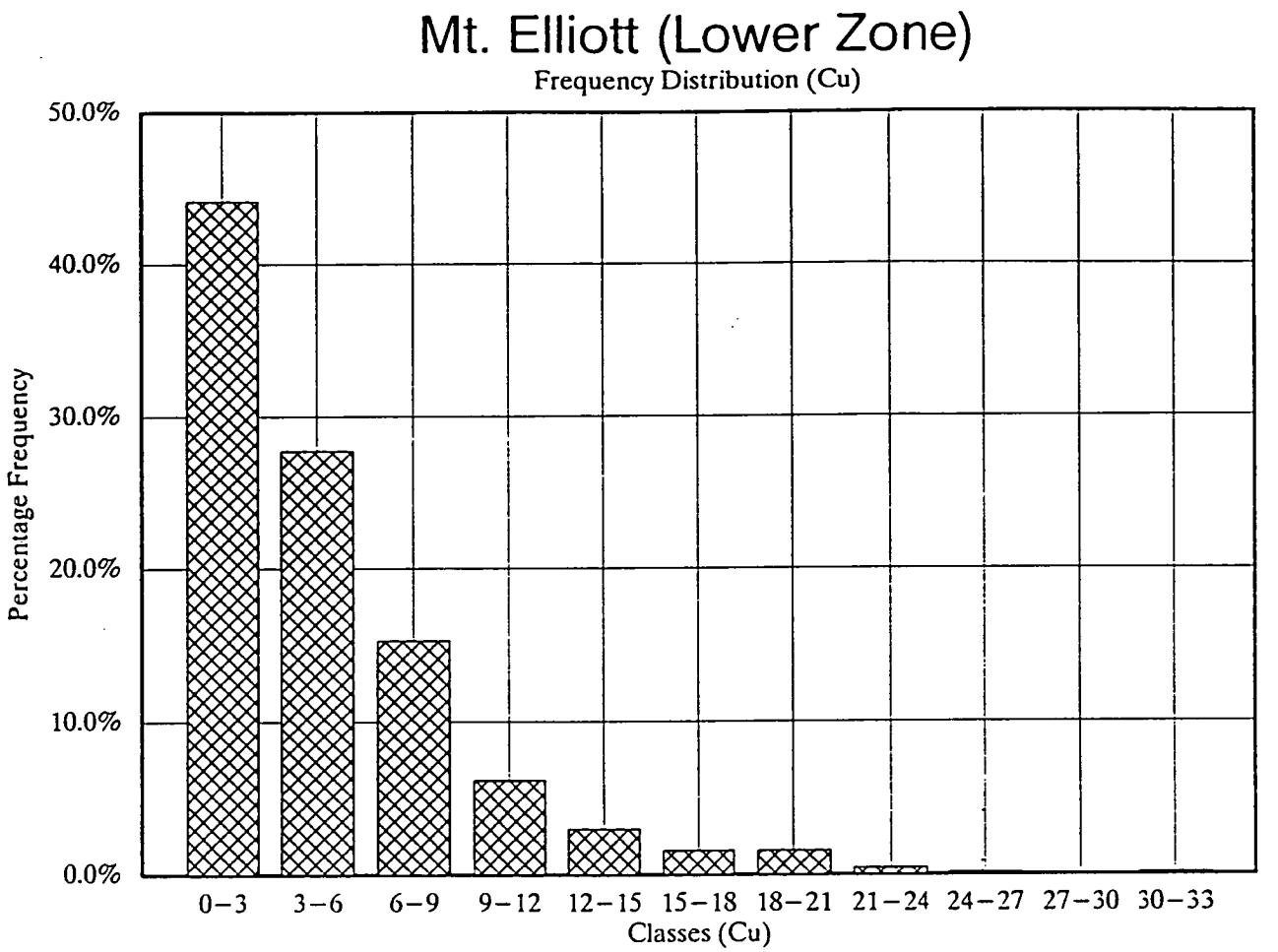
Mt. Elliott (Lower Zone)
Frequency Distribution (Cu)
50.0%
40.0%
30.0%
20.0%
10.0%
0.0%
Percentage Frequency
0–3
3–6
6–9
9–12
12–15
15–18
18–21
21–24
24–27
27–30
30–33
Classes (Cu)

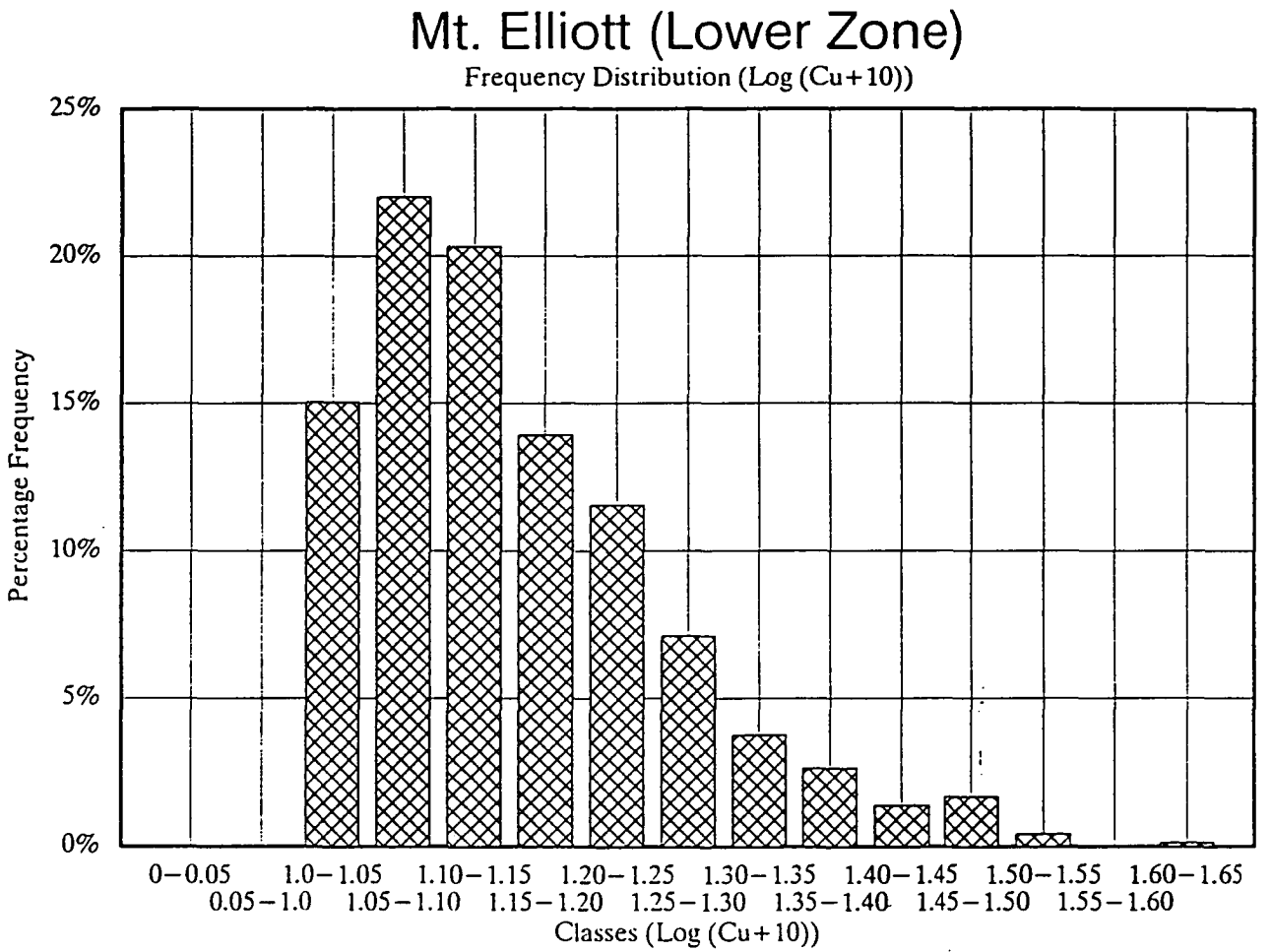
Mt. Elliott (Lower Zone)
Frequency Distribution (Log (Cu+10))
25%
20%
15%
10%
5%
0%
Percentage Frequency
0–0.05
0.05–1.0
1.0–1.05
1.05–1.10
1.10–1.15
1.15–1.20
1.20–1.25
1.25–1.30
1.30–1.35
1.35–1.40
1.40–1.45
1.45–1.50
1.50–1.55
1.55–1.60
1.60–1.65
Classes (Log (Cu+10))

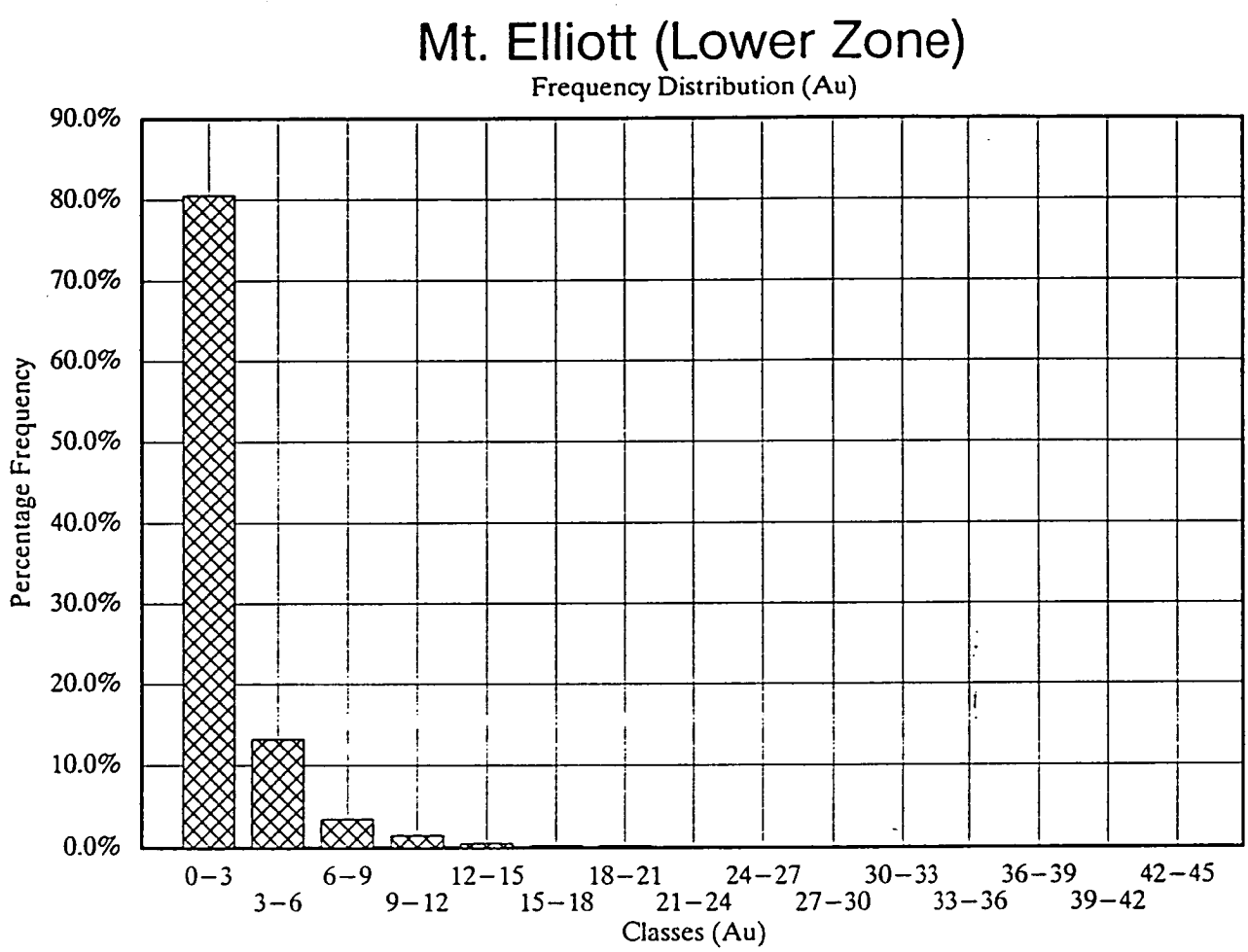
Mt. Elliott (Lower Zone)
Frequency Distribution (Au)
Percentage Frequency
90.0%
80.0%
70.0%
60.0%
50.0%
40.0%
30.0%
20.0%
10.0%
0.0%
0–3
3–6
6–9
9–12
12–15
15–18
18–21
21–24
24–27
27–30
30–33
33–36
36–39
39–42
42–45
Classes (Au)

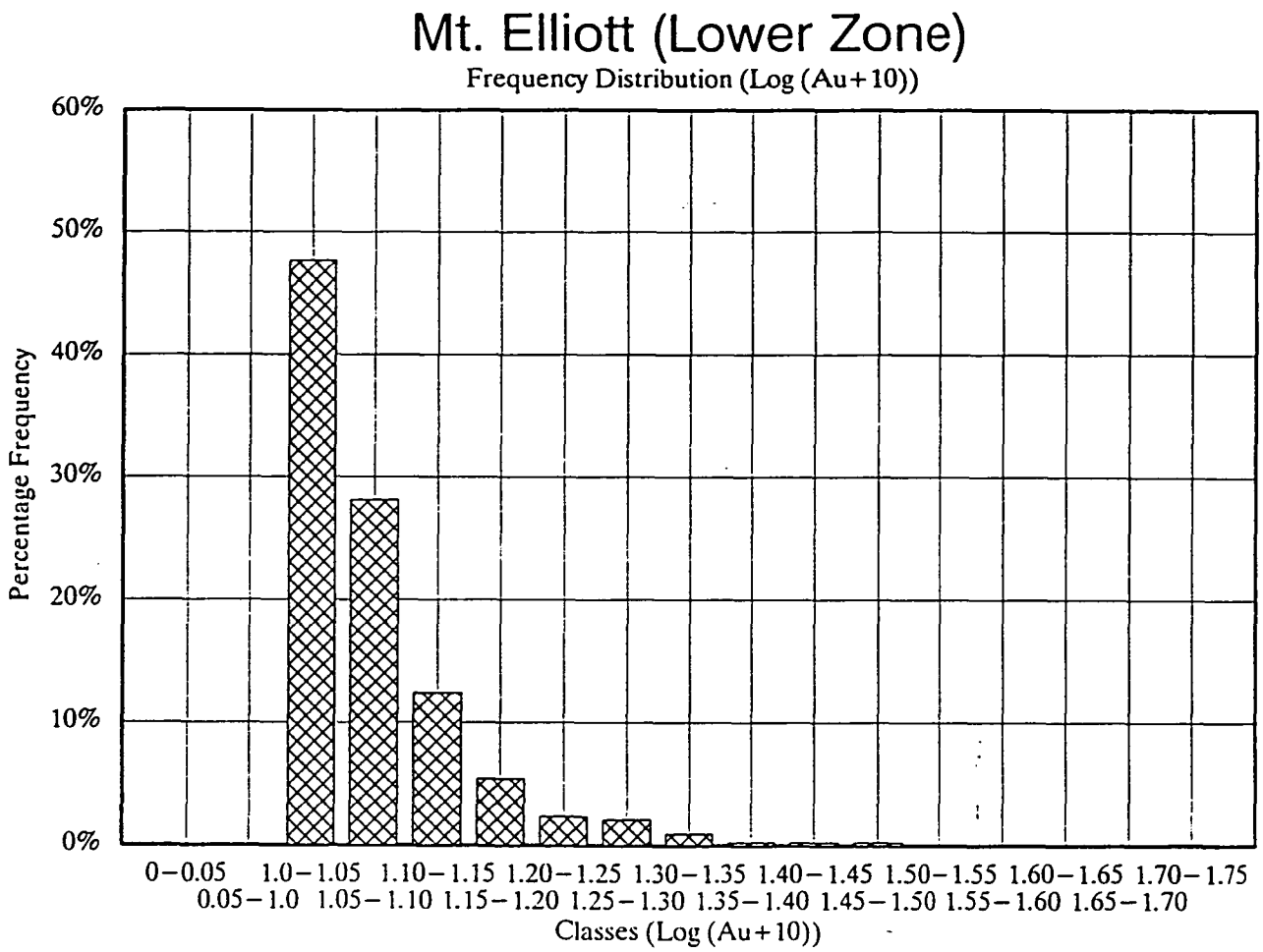
Mt. Elliott (Lower Zone)
Frequency Distribution (Log (Au+10))
60%
50%
40%
30%
20%
10%
0%
Percentage Frequency
0–0.05
0.05–1.0
1.0–1.05
1.05–1.10
1.10–1.15
1.15–1.20
1.20–1.25
1.25–1.30
1.30–1.35
1.35–1.40
1.40–1.45
1.45–1.50
1.50–1.55
1.55–1.60
1.60–1.65
1.65–1.70
1.70–1.75
Classes (Log (Au+10))

APPENDIX 5

Sulphur Isotope Sample Descriptions

S-Isotopes

1.	MEQ-14-310.9; CPY:	in footwall schist - elongate (sheared)
2.	MEQ-14-243.1; CPY:	coarse grained in coarse vein
3.	MEQ-21-232.1; CPY:	coarse grain vein breccia texture
4.	MEQ-21-232.1; PY:	adjacent to CPY
5.	MEQ-25-281.8; PY:	early pyrite in immature medium grained skarn
6.	MEQ-14-267.8; CPY	massive coarse grained in vein cross-cutting medium skarn
7.	MEQ-14-242.5; CPY:	coarse grained with foldspar in vein cross cutting outer carapace
8.	MEQ-14-242.5; PY:	cubic pyrite in contact with CPY
9.	MEQ-14-233; PY:	coarse pyrite in pyrite rich vein Py-cpx-cpy-mag
10.	MEQ-14-233; CPY:	interstitial, coarse grained
11.	MEQ-14-270; CPY:	interstitial in medium grained skarn
12.	MEQ-14-221.8; PY:	massive py vein
13.	MEQ-18-319.4; CPY:	vein cutting coarse schist (FW?)
14.	MEQ-12-189.3; PO:	breccia-texture hosted
15.	MEQ-11-373.7; CPY:	blebbygrains in mag-rich MG skarn
16.	MEQ-12-241.3; PY:	smeared PY cubes in fracture-vein cross cutting fine skarn or amphibolite
17.	MEQ-15-241.1; CPY:	coarse CPY in thin vein cross cutting outer carapace
18.	MEQ-15-241.1; PY:	Coarse PY grains in contact with CPY
19.	MEQ-11-302.6; CPY:	Coarse CPY in thin vein cross cutting outer carapace
20.	MEQ-10-213.8; PO:	coarse PO in scapolite-rich vein
21.	MEQ-10-315.8; CPY:	fine interstitial in medium grain skarn
22.	MEQ-10-315.8; PY:	fine interstitial in medium grain skarn (silicate, FeOx contamination

23.	MEQ-16-184.6; PY:	laminated pyrite (v-fine) in shale (possible Si contamination)
24.	MEQ-22-171.9; PO:	massive Po in coarse vein
25.	MEQ-22-164.6; PO:	Massive PO in coarse vein
26.	MEQ-22-164.6; CPY:	Adjacent to PO, finer grained
27.	MEQ-10-285.6; CPY:	CPY/PO mineralisation in coarse vein breccia texture
28.	MEQ-10-285.6; CPY:	CPY/PO mineralisation in coarse vein breccia texture
29.	MEQ-22-243.4; CPY:	CPY/PO mineralisation adjacent in coarse vein
30	MEQ-22-243.4; PO:	CPY/PO mineralisation adjacent in coarse vein